



Universidade do Minho
Escola de Engenharia

Paulo Renato da Silva Pereira

**Biomaterials based on natural
polymers and inspired by the sea**

Tese de Mestrado

Mestrado Integrado em Engenharia de Polímeros

Trabalho efetuado sob a orientação de:

Professora Doutora Natália Maria de Araújo Alves

Outubro de 2016

DECLARAÇÃO

Nome: Paulo Renato da Silva Pereira

Endereço eletrónico: paulovilar5@gmail.com Telefone: 962084547

Número do Bilhete de Identidade: 143214985

Título da dissertação: Biomaterials based on natural polymers and inspired by the sea

Orientador: Doutora Natália Maria de Araújo Alves

Ano de conclusão: 2016

Designação do Mestrado:

Ciclo de Estudos Integrados Conducentes ao Grau de Mestre em Engenharia

Área de Especialização: Mestrado Integrado em Engenharia de Polímeros

Escola: Escola de Engenharia

Nos exemplares das teses de doutoramento ou de mestrado ou de outros trabalhos entregues para prestação de provas públicas nas universidades ou outros estabelecimentos de ensino, e dos quais é obrigatoriamente enviado um exemplar para depósito legal na Biblioteca Nacional e, pelo menos outro para a biblioteca da universidade respetiva, deve constar uma das seguintes declarações:

1. DE ACORDO COM A LEGISLAÇÃO EM VIGOR, NÃO É PERMITIDA A REPRODUÇÃO DE QUALQUER PARTE DESTA TESE/TRABALHO

Universidade do Minho, 31/10/2016

Assinatura: Paulo Renato da Silva Pereira

Paulo Renato da Silva Pereira

ACKNOWLEDGEMENTS

To all concerned,

I wish to thank you to all that helped me to the conclusion of this stage. Firstly, I wish to thank you to my supervisor, Professor Natália Maria de Araújo Alves for giving me all the support during this master' thesis and the possibility to work at 3B's Research Group.

Also, I wish to thank you to Doctor Catarina Vale and Doctor Sofia Caridade for all the support during this work. Moreover, I wish to thank you to Department of Polymer Engineering, in particular to Engineer Maurício Malheiro for giving me all the support that I needed, in particular with FT-IR-ATR and TGA equipments, as well as to Support and Administration Staff, at 3B's Research Group, giving me all laboratorial material that I needed to perform my experiments.

I wish to thank you, also, to my course director, Professor António Manuel Cerqueira Gomes Brito, for all support and friendship during five years and to all my course and 3B's colleagues.

Finally, I wish to thank you very much to my family for their continuously support and motivation, in particular my parents and my brother! Without their support none of this would be possible.

Thank you to all!

“The whole is more than the sum of its parts”

Aristóteles

Biomaterials based on natural polymers and inspired by the sea

ABSTRACT

Marine mussels present an unusual amino acid, 3, 4-dihydroxy-L-phenylalanine (DOPA) obtained by postranslational modification of tyrosine which is used to stick in a various substrates, either inorganic or organic. The explanation for these adhesion properties is due to the presence of ortho-dihydroxyphenyl group, known as catechol group, present in DOPA and its analog dopamine.

Inspired by mussel adhesive proteins (MAPs) and its adhesive properties, many efforts have been carried out in order to mimic the incredible adhesive properties of these mussels, either in two-dimensional or three-dimensional materials.

In this present master' thesis, bioglass and silver doped bioglass nanoparticles were produced through the sol-gel technique. Bioglass nanoparticles (BGNPs) have much importance in the biomedical field, because they can interact with bone without creating a fibrous capsule. Furthermore, the silver presence in the bioglass network allows antibacterial properties. Eight different thermal treatments were done in order to study its influence on surface morphology and bioactivity properties. The result showed that all heat-treated and untreated nanoparticles showed similar surface morphology. Moreover, all studied samples induced the formation of hydroxyapatite, structurally and chemically similar to the mineral charge of bone, on its surface.

Moreover, free-standing films were developed using the layer-by-layer methodology. For that, chitosan was chosen as poly(cation) and hyaluronic acid and hyaluronic acid-dopamine conjugate were chosen as poly(anions). This modification was done in order to improve the films' adhesive properties. Also, silver doped bioglass nanoparticles were included as nanofiller to improve its mechanical properties. These nanocomposites were studied by different characterization techniques. The Ag-BG-NPs percentage present in the free-standing films was evaluated through thermogravimetric tests. Bioactivity tests were performed and revealed that these films induce the hydroxyapatite formation on its surface and the silver presence in the bioglass network allowed an effective antibacterial performance.

Biomaterials based on natural polymers and inspired by the sea

Finally, three-dimensional structures, hydrogels, were produced using chitosan and bioglass nanoparticles heat-treated at 700°C during three hours. The dynamic mechanical tests revealed that the bioglass nanoparticles addition led to higher mechanical properties. Also, different formulations of a catechol-chitosan-conjugate were successfully synthesized and studied by ultraviolet-visible spectroscopy.

The outcomes of this master' thesis revealed that the produced silver doped bioglass nanoparticles, free-standing films and hydrogels could be used in the orthopedic area or dental applications.

Biomateriais baseados em polímeros naturais e inspirados pelo mar

RESUMO

Os moluscos marinhos apresentam um aminoácido incomum, o 3, 4-dihidroxi-L-fenilalanina (DOPA) obtido através da modificação pós-traducional da tirosina que é usado para aderirem a vários substratos, quer inorgânicos, quer orgânicos. A explicação destas propriedades adesivas é devida à presença de grupos *orto*-di-hidróxifenis, conhecidos como catecóis, presentes na DOPA e na sua análoga dopamina.

Inspirado pelas proteínas adesivas dos moluscos (MAPs) e nas suas propriedades adesivas, muitos esforços tem sido feitos para mimetizar estas propriedades adesivas incríveis, quer em materiais bidimensionais quer tridimensionais.

Na presente tese de mestrado, nanopartículas de biovidro e de biovidro dopado com prata foram produzidos através da técnica sol-gel. As nanopartículas de biovidro (BGNPs) assumem um papel importante no campo biomédico, porque podem interagir com o osso sem a criação de uma cápsula fibrosa. Para além disso, a presença de prata na matriz do vidro bioactivo permite propriedades antibacterianas. Foram realizados oito tratamentos térmicos diferentes a fim de estudar a sua influência na morfologia da superfície e nas propriedades bioactivas. Os resultados mostraram que todas as nanopartículas tratadas e não tratadas termicamente mostraram morfologias da superfície similares. Além disso, todas as amostras estudadas induziram a formação de hidroxiapatite, estruturalmente e quimicamente semelhante à parte mineral do osso, na sua superfície.

Para além disso, foram desenvolvidas membranas *free-standing* usando a técnica camada-a-camada. Para tal, foi escolhido o quitosano como polícatião e o ácido hialurónico e ácido hialurónico conjugado com dopamina como polianiões. Esta modificação foi feita de forma a melhorar as propriedades adesivas das membranas. Mais, foram escolhidas nanopartículas de biovidro dopadas com prata como um nanomaterial de reforço por forma a melhorar as suas propriedades mecânicas. Estes nanocompósitos foram estudados por diversas técnicas de caracterização. A percentagem de nanopartículas de biovidro dopadas com prata presentes nas membranas *free-standing* foi avaliada através de testes

termogravimétricos. Foram realizados ainda testes de bioatividade que revelaram a formação de hidroxiapatite na sua superfície e a presença de prata na matriz do biovidro permitiu atestar as suas propriedades antibacterianas.

Finalmente, foram produzidas estruturas tridimensionais, hidrogéis, usando quitosano e nanopartículas de biovidro tratadas termicamente a 700°C durante três horas. Os testes de mecânica dinâmica revelaram que a adição de nanopartículas de biovidro levou a um melhoramento das propriedades mecânicas. Para além disso, foram sintetizadas com sucesso diferentes formulações de quitosano conjugado com grupos catecol e estudados pela espectroscopia ultravioleta-visível.

Os resultados desta tese de mestrado revelaram que a produção de nanopartículas de biovidro dopado com prata, as membranas *free-standing* e os hidrogéis poderão ser usados na área ortopédica ou para aplicações dentárias.

CONTENTS

Acknowledgements	iii
Abstract	v
Resumo	vii
Contents	ix
List of Abbreviators	xv
List of Figures	xvii
List of Tables	xxiv
Chapter 1 - General Introduction.....	1
1. General Introduction.....	3
1.1. Motivation.....	3
1.2. Structure and composition of marine mussel adhesive proteins (MAPs) and its adhesive properties	5
1.3. Studies of the adhesive properties of mussels	8
1.4. Layer-by-Layer (LbL) technique	9
1.5. Nanoparticles (NPs).....	11
1.6. Materials inspired by the structure of nacre.....	13
1.7. References.....	14
Chapter 2 - State of the Art	21
2. Natural-Based Biomaterials Inspired by Marine Mussel Adhesive Proteins	23
2.1. Introduction.....	24
2.2. Two-dimensional biomaterials produced by the LbL methodology based on MAPs	26
2.3. Three-dimensional biomaterials: hydrogels production based on MAPs	30
2.4. Polydopamine - based Biomaterials	34
2.4.1. PDA-coated Biomaterials	36
2.4.2. Hydrogels production based on PDA	42
2.5. Conclusions.....	44

2.6. References.....	44
Chapter 3 - Materials and Methods.....	55
3. Materials and Methods	57
3.1. Materials	57
3.1.1. Hyaluronic acid (HA)	57
3.1.2. Dopamine (DN)	58
3.1.3. Chitosan (CHT):	59
3.2. Methods	60
3.2.1. Processing techniques.....	60
3.2.1.1. Synthesis of hyaluronic acid-dopamine conjugate (HA-DN).....	60
3.2.1.2. Bioglass nanoparticles (BG-NPs) production	61
3.2.1.3. Silver doped bioglass nanoparticles (Ag-BG-NPs) production.....	62
3.2.2. Free-standing films production.....	63
3.2.3. Hydrogels production	65
3.2.3.1. Synthesis of chitosan hydrogel	65
3.2.3.3. Production of a poly(dimethylsiloxane) (PDMS) mold	65
3.2.4. Characterization techniques.....	66
3.2.4.1. Fourier transform infrared spectroscopy (FT-IR).....	66
3.2.4.2. Ultraviolet-visible spectroscopy (UV-vis)	67
3.2.4.3. Atomic force microscopy (AFM)	69
3.2.4.4. Scanning electron microscopy coupled with energy dispersive X-ray spectroscopy (SEM-EDS).....	70
3.2.4.5. Transmission electron microscopy (TEM)	71
3.2.4.6. X-ray diffraction (XRD).....	72
3.2.4.7. Water contact angle measurement.....	73
3.2.4.8. Bioactivity studies	75
3.2.4.9. Adhesion tests.....	76
3.2.4.10. Mechanical tests	77
3.2.4.11. Zeta potential tests	79
3.2.4.12. Thermogravimetry (TGA)	79
3.2.4.13. Dynamical Mechanical Analysis (DMA).....	81
3.3. References.....	82
Chapter 4 - Optimization of Silver Doped Bioglass Nanoparticles Synthesis Envisaging Biomedical Applications.....	89

4. Optimization of Silver Doped Bioglass Nanoparticles Synthesis Envisaging Biomedical Applications	91
4.1. Introduction.....	92
4.2. Experimental section:	93
4.2.1. Materials:	93
4.2.2. Methods	94
4.2.2.1. Synthesis of quaternary silver doped bioglass nanoparticles	94
4.2.3. Characterization techniques.....	95
4.3. Results and discussion	96
4.3.1. FT-IR analysis	96
4.3.2. Zeta-potential (ζ) analysis	97
4.3.3. Analysis of the nanoparticles morphology	99
4.3.4. Bioactivity tests	103
4.4. Conclusions.....	106
4.5. References:.....	107
Chapter 5 - Antibacterial Natural-Based Free-Standing Films Inspired by the Sea	111
5. Antibacterial Natural-Based Free-Standing Films Inspired by the Sea.....	113
5.1. Introduction.....	114
5.2. Experimental section.....	115
5.2.1. Materials	115
5.3. Methods	116
5.3.1. Synthesis of hyaluronic acid-dopamine conjugate (HA-DN).....	116
5.3.2. Free-standing films production.....	116
5.4. Characterization techniques	117
5.4.1. Fourier Transform Infrared (FT-IR) spectroscopy	117
5.4.2. Atomic force microscopy (AFM)	117
5.4.3. Scanning electron microscopy coupled with energy dispersive X-ray spectroscopy (SEM-EDS).....	117
5.4.4. X-ray diffraction (XRD).....	117
5.4.5. Thermogravimetric analysis (TGA)	118
5.4.6. Water contact angle (WCA) measurements	118

Biomaterials based on natural polymers and inspired by the sea

5.4.7.	Mechanical and adhesion tests	118
5.4.8.	In vitro bioactivity studies	119
5.4.9.	Swelling behavior	119
5.4.10.	Weight loss (WL).....	120
5.4.11.	Microbiological study:	120
5.4.12.	Statistical analysis	120
5.5.	Results and discussion	120
5.5.1.	FT-IR results.....	121
5.5.2.	Analysis of the free-standing films morphology	122
5.5.3.	Thermogravimetric analysis	126
5.5.4.	Mechanical properties of the crosslinked free-standing films.....	127
5.5.5.	Bioactivity tests	130
5.5.6.	Water contact angle measurements of the crosslinked free-standing films..	132
5.5.7.	Weight Loss (WL).....	134
5.5.8.	Microbiological analysis	135
5.6.	Conclusions.....	136
5.7.	References:.....	136
	Supporting information (SI).....	142

Chapter 6 - Hydrogels Development based on Natural Polymers and Inspired by the Sea

6.	Hydrogels Development based on Natural Polymers and Inspired by the Sea	145
6.1.	Introduction.....	146
6.2.	Experimental section.....	149
6.2.1.	Methods	149
6.2.1.1.	<u>Synthesis of ternary bioglass nanoparticles (BG-NPs)</u>	149
6.2.1.2.	<u>Production of a poly(dimethylsiloxane) (PDMS) mold</u>	149
6.2.1.3.	<u>Synthesis of chitosan and chitosan plus BG-NPs incorporation hydrogels</u>	149
6.2.1.4.	<u>Synthesis of chitosan-catechol conjugate (CHT-c)</u>	150
6.2.2.	Characterization techniques.....	150
6.2.2.1.	<u>Zeta potential analysis</u>	150
6.2.2.2.	<u>Ultraviolet-visible (UV-vis) spectroscopy</u>	150

6.2.2.3. <u>Scanning electron microscopy coupled with energy dispersive X-ray (SEM-EDS) spectroscopy</u>	151
6.2.2.4. <u>Bioactivity tests</u>	151
6.2.2.5. <u>Dynamic mechanical analysis (DMA)</u>	151
6.3. Results and Discussion	152
6.3.1. Bioglass nanoparticles (BG-NPs) production and characterization	152
6.3.2. Hydrogels production and characterization	153
6.3.3. Chitosan modified with catechol groups (CHT-cat) conjugate synthesis and characterization:.....	156
6.4. Conclusions and future work:	157
6.5. References:.....	158
Chapter 7 - Conclusions and Future Work	163
7. Conclusions and Future Work	165
Appendix	167
Appendix 1 - SEM-EDS micrographs before and after immersion in SBF solution (0 days and 7 days).....	168
Appendix 2 - Hyaluronic acid modified with dopamine (HA-DN) conjugate synthesis and characterization: UV-vis results	170
Appendix 3 - TGA results.....	172
Appendix 4 - AFM results	174
Appendix 5 - Analysis of the films morphology	176
Appendix 6 – Optimization work	177
1.1. Native films	177
1.1.1. FT-IR analysis of the native LbL free-standing films	177
1.1.2. Analysis of the native LbL free-standing films morphology	178
1.2. Crosslinked LbL free-standing films with EDC and NHS	179
1.2.1. FT-IR analysis of the crosslinked LbL free-standing films.....	180
1.2.2. Analysis of the crosslinked LbL free-standing films morphology	181
Conclusions	183
References.....	183

LIST OF ABBREVIATORS

A

AFM - Atomic force microscopy

Å – Angstrom

ASTM D1002 – Apparent Shear Strength of Single-Lap-Joint Adhesively Bonded Metal Specimens by Tension Loading

Ag-BG-NPs – Silver Doped Bioglass Nanoparticles

Ag – Silver

AgCO₃ – Silver Carbonate

AgO₂ – Silver Oxide

Ag₃PO₄ – Silver Phosphate

Au - Gold

B

BG-NPs – Bioglass Nanoparticles

C

°C - Celsius degrees

CaCO₃ – Calcium Carbonate

Ca-P – Calcium Phosphate

CHT – Chitosan

cm – Centimetre

D

DN – Dopamine

DOPA – 3, 4-dihydroxy-L-phenylalanine

DNA – Deoxyribonucleic acid

E

EDC – N-(3-Dimethylaminopropyl)-N'-ethylcarbodiimide hydrochloride

DNA – Deoxyribonucleic acid

ECM – Extracellular Matrix

F

Fe₃O₄ – Iron Oxide

G

g - Gram

H

HA – Hyaluronic acid

HA-DN – Hyaluronic acid-dopamine conjugate

HCA - Hydrocaffeic acid

HCl – Hydrochloric acid

h - Hours

L

LB – Langmuir-Blodgett

LbL – Layer-by-Layer

M

MAPs – Mussel Adhesive Proteins

m – Metre

µm – Micrometre

µL – Microlitre

Biomaterials based on natural polymers and inspired by the sea

mg – Milligram	R
min – Minute	Ra – Average Roughness
mfp – Mussel Foot Protein	Rq – Root Mean Square
mL – Mililitre	Rmax – Maximum Roughness
mm – Milimetre	RNA - Ribonucleic acid
m-SBF – Modified Simulated Body Fluid	S
M – Molar	SAM – Self-Assembled Monolayer
MPa - Megapascal	SEM - Scanning electron microscopy
N	SPIONs – Superparamagnetic iron-oxide nanoparticles
NaCl – Sodium Chloride	
NaOH – Sodium Hydroxide	T
N – Newton	tan (δ) – Loss factor
NHS – N-hydroxysuccinimide	T – Temperature
nm – Nanometre	t – Time
NPs – Nanoparticles	TEOS – Tetraethyl orthosilicate
P	TEM – Transmission electron microscopy
PBS – Phosphate Buffered Saline	TGA – Thermogravimetric analysis
PDA – Poly(dopamine)	U
PDDA – Poly(diallyldimethylammonium chloride)	UV-vis – Ultraviolet-visible spectroscopy
PDMS – Poly(dimethylsiloxane)	W
PEI – Poly(ethylenimine)	WCA – Water Contact Angle
PEG – Poly(ethylene glycol)	WL – Weight Loss
PEM – Poly(electrolyte) multilayer	wt. – Mass Fraction
PMMA – Poly(methyl methacrylate)	w/v – Mass/Volume
PS – Poly(styrene)	X
PTFE – Poly(tetrafluoroethylene)	XRD – X-ray Diffraction

LIST OF FIGURES

Figure 1. 1 - Natural-based polymers (chitosan and hyaluronic acid) can be conjugated with catechol groups in order to create natural-based polymers-catechol conjugates. These raw materials with either bioglass nanoparticles or silver doped bioglass nanoparticles, that presents bioactivity properties can be included in either 2D or 3D biomaterials. Finally these can be studied by different characterization techniques. This representative scheme allows understand better the mussel adhesive properties and its potential in the biomedical field. It can be seen the chemical structure of catechol group, chitosan, hyaluronic acid, chitosan-catechol conjugate and hyaluronic acid-dopamine conjugate..... 5

Figure 1. 2 - Marine mollusk *Mytilus Californianus* anatomy. 7

Figure 1. 3 - Simplified mechanism of layer-by-layer (LbL) technique. There is the formation of bilayers by addition of a polycation and a polyanion in a negatively charged substrate..... 10

Figure 2. 1 - LbL assembly. Formation of n bi-layers by the addition of a polycation and polyanion poly (electrolyte) molecules in a negatively charged substrate. This adsorption is made mainly through electrostatic interactions. 26

Figure 2. 2 - Building blocks (polymers, particles or cells) used in LbL assembly (2D and 3D) and their biomedical applications..... 27

Figure 2. 3- (A) Adhesive strength of four LbL film conditions. Statistically significant adhesive strength as compared with distinct conditions is shown (*p< 0.05), n = 5; mean ± standard deviation condition shown, (B) Photograph of Layer-by-Layer (LbL) coatings 16 h after being placed on top of a Mueller-Hinton agar plate with *E. coli* and *S. aureus* (1.5×10^8 CFU) incubated at 37 °C, (C) Representative SEM micrographs and respective quantitative EDS spectra analysis before and after SBF immersion for 7 days. The scale bar represents 1 µm. Condition 1: [CHT/HA–DN/CHT/AgBG]₅ + [CHT/HA–DN], control 1: [CHT/HA/CHT/AgBG]₅ + [CHT/HA], condition 2: [CHT/HA–DN/CHT/AgBG]₅, and control 2: [CHT/HA/CHT/AgBG]₅ 29

Figure 2. 4- (A) Conversion of catechol groups (un-oxidized) into quinone species (oxidized form) and complexation: Mono; Bis and Tris with metal ions, (B) Qualitative tests performed to study the self-healing properties of Al^{III}, Ga^{III} and In^{III} gels, and (C)

Storage modulus variation (G') in function of pH. The red line serves as a guide to the eye..... 31

Figure 2. 5- (A) Schematic representation of the Byssal thread of marine mussel with its adhesive plaque and its adhesive character, but also its cohesive character. The last one is responsible for hydrogels creation in basic pH through intermolecular catechol–catechol reactions, (B) Photograph of the HA-catechol (HA-DN) hydrogel. 33

Figure 2. 1- (A) Representation of multilayered films based on poly(dopamine)-modified carbon nanotubes (CNT@PDA) and poly(ethyleneimine) (PEI) and (B) The statistical histogram of the number of adhered platelets on different surfaces. * $p < 0.05$ versus silicon substrate, and * $p < 0.05$ versus (PEI–CNT@PDA)20.5 film (Student's t test). Data are expressed as mean \pm SD, $n = 3$37

Figure 2. 7- (A) Schematic representation of calcium phosphate (Ca-P) biominerals into a poly(dopamine) coating, a catecholamine, inspired by the adhesion mechanisms of mussels. (B) Material-independent hydroxyapatite formation via pHAF. The SEM images show that hydroxyapatites can cover any material surfaces by the enrichment of calcium ions on the polydopamine-coated surfaces. Hydroxyapatite was created on a wide range of flat solid substrates: noble metal and metal oxides [e.g., Ti, stainless steel (SUS 316L), Si, Au], ceramics (e.g., SiO₂ glass), and polymers [polystyrene, poly(methyl methacrylate), polydimethylsiloxane]. The scale bar represents 5 μm . and (C) The fabrication of organic–inorganic hybrid materials via pHAF. The SEM images demonstrate that the hydroxyapatite crystals can be integrated into 3D porous materials in a material-independent manner. The tested 3D materials of porous cellulose, polyester fiber, porous nylon, and PTFE membrane were hybridized with hydroxyapatites. All the materials were incubated in 1.5 x SBF for 2 days at 37 °C after polydopamine treatment 38

Figure 2. 8 - Schematic illustration of polydopamine-based cell patterning using microfluidics..... 38

Figure 2. 9 - (A) SEM images of adhered platelets, (B) inverted fluorescence microscopic images of attached L929 fibroblast cells, (C) CLSM fluorescence microscopic images of attached *E. coli* and *S. aureus* on PDA coatings with different thicknesses. The tested coatings were prepared by immersing clean glass substrates in 2 mg ml⁻¹ dopamine

Tris/HCl (pH 8.5) buffer for 30 min, 3 hours or 6 hours, and then thoroughly rinsed with Millipore water and dried with nitrogen before using 39

Figure 2. 10 – (A) TEM images of the Fe₃O₄@PDA microspheres with well-defined core shell nanostructure (PDA (shell) thickness - 15 nanometers (nm)), (B) TEM image of the Fe₃O₄@PDA microspheres based on 200 nm Fe₃O₄ sub-microspheres with different shell thicknesses: (B-a) 15 nm (B-b) 25 nm (the superficial roughness increases with higher DN concentration) and (C) The viability of cells (%) incubated with the Fe₃O₄@PDA microspheres at different concentrations (µg mL⁻¹h)..... 41

Figure 2. 11 – (A) Mechanism of poly(dopamine), obtained through its monomer (DN), incorporation into Gellan Gum (GG) hydrogel. The dark-brown color meaning the correct polymerization reaction of poly(dopamine), (B) Viability of MC3T3-E1 cells seeded on gellan gum hydrogels mineralized for 6 days. GG: 0 mg/ml ALP; GGALP: 2.5 mg/ml ALP; GGDAALP: 2.5 mg/ml ALP with 4 h incubation in DA solution pre-mineralization; tissue culture polystyrene (positive control). Error bars show standard deviation. (C- a) Influence of ALP concentration and sterilization by autoclaving (n = 5). Unmineralized hydrogels disintegrated during autoclaving. (C - b) Influence of incubation time in 2 mg/ml DA solution prior to mineralization (n = 3). Significances: *, **: p < 0.05, 0.01, respectively (Student's t-test)..... 43

Figure 3. 1 - Chemical structure of hyaluronic acid (HA)..... 57

Figure 3. 2 - Tyrosine, DOPA and dopamine chemical structure.. 59

Figure 3. 3 - Chemical structure 60

Figure 3. 4 - Synthesis of HA-DN conjugate 61

Figure 3. 5 - Dipping robot..... 64

Figure 3. 6 - UV-vis spectrophotometer..... 69

Figure 3. 7 - High-Resolution Field Emission Scanning Electron Microscope with Focused Ion Beam (FIB – SEM) 71

Figure 3. 8 - Bruker D8 Discover equipment, present in SEMAT labs 73

Figure 3. 9 - Contact angle goniometer equipment 75

Figure 3. 10 - Dimensions of the test panel (standard)..... 77

Figure 3. 11 - TGA equipment. 81

Figure 4. 1 – FT-IR- of Ag-BG-NPs (% 10 mol Ag) with different thermal treatments.	97
Figure 4. 2 - Zeta potential values of Ag-BG-NPs produced with different thermal treatments. (A) Ultra-pure water with 0.15 M NaCl; (B) Saline solution (0.15 M NaCl, pH = 5.5).....	99
Figure 4. 3 - SEM-EDS micrographs of the nanoparticles surface.	101
Figure 4. 4 - S-TEM micrographs of the all Ag-BG-NPs, (magnification of 200 000x).	103
Figure 4. 5 - XRD pattern of silver doped bioglass nanoparticles (A) without immersion in simulated body fluid (during 7 days) - Control and (B) with immersion in simulated body fluid (during 7 days).	104
Figure 4. 6 - SEM-EDS micrographs of Ag-BG-NPs before and after immersion in SBF (0 days-control and 7 days). Magnifications of 3 000 x.	106
Figure 5. 1 - Photographs of the macroscopic morphology of the native and crosslinked LbL films. (A) Formulation 1: [CHT/HA/CHT/HA] ₇₅ ; (B) Formulation 2: [CHT/HA-DN/CHT/HA-DN] ₇₅ ; (C) Formulation 3: [CHT/HA/CHT/Ag-BG-NPs] ₇₅ ; (D) Formulation 4: [CHT/HA-DN/CHT/Ag-BG-NPs] ₇₅	121
Figure 5. 2 - FT-IR results of the crosslinked free-standing films crosslinked with genipin (1 mg/mL) and the control (native film).	121
Figure 5. 3 - SEM-EDS micrographs. Top view of (A) Formulation 1: [CHT/HA/CHT/HA] ₇₅ ; (B) Formulation 2: [CHT/HA-DN/CHT/HA-DN] ₇₅ ; (C) Formulation 3: [CHT/HA/CHT/Ag-BG-NPs] ₇₅ ; (D) Formulation 4: [CHT/HA-DN/CHT/Ag-BG-NPs] ₇₅ ; Cross-section views of (E) Formulation 1: [CHT/HA/CHT/HA] ₇₅ ; (F) Formulation 2: [CHT/HA-DN/CHT/HA-DN] ₇₅ ; (G) Formulation 3: [CHT/HA/CHT/Ag-BG-NPs] ₇₅ and (H) Formulation 4: [CHT/HA-DN/CHT/Ag-BG-NPs] ₇₅	123
Figure 5. 4 - Atomic force microscopy (AFM) results (2D images). The bar next to all images is the Z-scale (nm). (A) Formulation 1: [CHT/HA/CHT/HA] ₇₅ (bottom view); (B) Formulation 1: [CHT/HA/CHT/HA] ₇₅ (top view); (C) Formulation 2: [CHT/HA-DN/CHT/HA-DN] ₇₅ (bottom view); (D) Formulation 2: [CHT/HA-DN/CHT/HA-DN] ₇₅ (top view); (E) Formulation 3: [CHT/HA/CHT/Ag-BG-NPs] ₇₅ (bottom view); (F)	

Formulation 3: [CHT/HA/CHT/Ag-BG-NPs]₇₅ (top view); **(G)** Formulation 4: [CHT/HA-DN/CHT/Ag-BG-NPs]₇₅ (bottom view); **(H)** Formulation 4: [CHT/HA-DN/CHT/Ag-BG-NPs]₇₅ (top view); **(I)** Column graphic with root mean square (Rq), average roughness (Ra) values and maximum roughness (Rmax), n = 3. Representative images four different free-standing films formulations: top and bottom views (10 μm x 10 μm)..... 125

Figure 5. 5 - Representative TGA results. Gray curve: Formulation 1-[CHT/HA/CHT/HA]₇₅; Dark yellow: Formulation 2-[CHT/HA-DN/CHT/HA-DN]₇₅; Orange curve: Formulation 3: [CHT/HA/CHT/Ag-BG-NPs]₇₅ (%10 mol Ag); Green curve: Formulation 4: [CHT/HA-DN/CHT/Ag-BG-NPs]₇₅ (%10 mol Ag). 126

Figure 5. 6 - Mechanical Properties-Dry samples. The data is presented as Mean ± SD, n = 5. **(A)** Tensile Young modulus (MPa) (one-way ANOVA, p< 0.01 [**], p< 0.0001 [****]) **(B)** Ultimate tensile strength (MPa) (non-parametric tests, Kruskal-Wallis statics), **(C)** Strain at break (%) (Non-parametric tests, Kruskal-Wallis statics), **(D)** Tensile stress (MPa) vs. tensile strain (%) - representative curves for each formulation. 127

Figure 5. 7 - Mechanical Properties-Wet samples. The data is presented as Mean ± SD. Formulation 1: [CHT/HA/CHT/HA]₇₅, Formulation 2: [CHT/HA-DN/CHT/HA-DN]₇₅, Formulation 3: [CHT/HA/CHT/Ag-BG-NPs]₇₅ and Formulation 4: [CHT/HA-DN/CHT/Ag-BG-NPs]₇₅. **(A)** Tensile Young modulus (MPa) (one-way ANOVA) **(B)** Ultimate tensile strength (MPa) (one-way ANOVA) **(C)** Strain at break (%) for (one-way ANOVA, p< 0.01 [**],p< 0.001 [***]) **(D)** Tensile stress (MPa) vs. tensile strain (%) curves for one of the representative curve for each formulation. 128

Figure 5. 8 - **(A)** All steps followed to prepare the samples to perform the adhesion tests, according to ASTM D1002 standard, as described in section Materials and Methods. **(B)** Adhesive strength of the free-standing films. Data shown is represented as Mean ± Standard Deviation (SD), n=5 at least. Statistical analysis performed using One-way ANOVA). Formulation 1-[CHT/HA/CHT/HA]₇₅; Formulation 2-[CHT/HA-DN/CHT/HA-DN]₇₅; Formulation 3: [CHT/HA/CHT/Ag-BG-NPs]₇₅; Formulation 4: [CHT/HA-DN/CHT/Ag-BG-NPs]₇₅. 129

Figure 5. 9 - XRD diffractograms. The black line corresponds to the XRD pattern before immersion in SBF solution (0 days) and the red line corresponds to the XRD pattern after immersion in SBF solution during 14 days. 130

Figure 5. 10 - SEM-EDS micrographs of the surface morphology of the free-standing films after, 14 days, of immersion in SBF solution..... 131

Figure 5. 11 - Water contact angle analysis of the free-standing films, top and bottom side. The top side corresponds to the hyaluronic acid (HA), hyaluronic acid dopamine conjugate (HA-DN) or silver doped bioglass nanoparticles (Ag-BG-NPs) and the bottom side corresponds to the layer composed by chitosan (CHT). Formulation 1: [CHT/HA/CHT/HA]₇₅; Formulation 2: [CHT/HA-DN/CHT/HA-DN]₇₅; Formulation 3: [CHT/HA/CHT/Ag-BG-NPs]₇₅ and Formulation 4: [CHT/HA-DN/CHT/Ag-BG-NPs]₇₅ The data is presented as Mean ± SD (non-parametric tests, Kruskal-Wallis test, p-value < 0,0001 [****]). 132

Figure 5. 12 - Swelling behavior of free-standing films when immersed in phosphate buffered saline (PBS) solution during different time-points. Formulation 1: [CHT/HA/CHT/HA]₇₅ (green line); Formulation 2: [CHT/HA-DN/CHT/HA-DN]₇₅ (orange line); Formulation 3: [CHT/HA/CHT/Ag-BG NPs]₇₅ (dark yellow line) and Formulation 4: [CHT/HA-DN/CHT/Ag-BG-NPs]₇₅ (blue line). The data is presented as Mean ± SD, n = 3. 133

Figure 5. 13 - Weight loss behavior of free-standing films when immersed in PBS solution during different time-points at T=37°C. Formulation 1: [CHT/HA/CHT/HA]₇₅ (green line); Formulation 2: [CHT/HA-DN/CHT/HA-DN]₇₅ (orange line); Formulation 3: [CHT/HA/CHT/Ag-BG-NPs]₇₅ (dark yellow line) and Formulation 4: [CHT/HA-DN/CHT/Ag-BG-NPs]₇₅ (blue line). The data is presented as Mean ± SD, n = 3. 134

Figure 5. 14 - Photograph of free-standing films after 16 hours after being placed on top of a Mueller-Hinton agar plate with gram-negative *E. coli* and gram-positive *S. aureus* (1.5×10^8 CFU) incubated at 37 °C. The antimicrobial behavior of the LbL coatings is demonstrated by the formation of an inhibitory zone surrounding of Formulation 3: [CHT/HA/CHT/AgBG NPs]₇₅ and Formulation 4: [CHT/HA-DN/CHT/AgBG NPs]₇₅..... 137

S 5. 1 - Comparison between (A) Tensile Young modulus (MPa) for the tensile tests performed in dry and wet conditions (n = 5, one-way ANOVA, p-value < 0.0001 [, ****]),

(B) Ultimate tensile strength (MPa) for the tensile tests performed in dry and wet conditions (n = 5, non-parametric tests, Kruskal-Wallis statics, p-value < 0.0001, [****])

(C) Strain at break (%) for the tensile tests performed in dry and wet conditions (n = 5, non-parametric tests, Kruskal-Wallis statics)..... 142

Figure 6. 1 - SEM-EDS micrographs of the surface of the ternary bioglass nanoparticles.

(A) BG-NPs before immersion in SBF solution; **(B)** BG-NPs after immersion SBF solution during 7 days and **(C)** Zeta potential value for BG-NPs with a thermal treatment at 700°C during 3 hours (n = 3). 152

Figure 6. 2 – Representative SEM micrographs of hydrogels production. **(A)** CHT hydrogel crosslinked with genipin, **(B)** CHT) + BG-NPs hydrogel crosslinked with genipin. The inset images are SEM micrographs with higher magnifications..... 153

Figure 6. 3 – SEM-EDS micrographs for hydrogels soaked in SBF solution for different time-points. **(A)** Cross-section view of CHT hydrogel crosslinked with genipin – 0 days (control), **(B)** Cross-section view of CHT+ BG-NPs hydrogel crosslinked with genipin – 0 days (control), **(C)** Cross-section view of CHT+BG-NPs hydrogel crosslinked with genipin – 3 days, **(D)** Cross-section view of CHT+BG-NPs hydrogel crosslinked with genipin – 7 days, **(E)** Cross-section view of CHT+BG-NPs hydrogel crosslinked with genipin – 14 days and **(F)** SEM-EDS micrographs for the bottom side of CHT+BG-NPs – 14 days..... 154

Figure 6. 4 - Dynamic mechanical analysis (DMA) results. **(A)** Modulus and tan (δ) results of the CHT hydrogel crosslinked with genipin; **(B)** Modulus and tan (δ) of the CHT + BG-NPs hydrogel crosslinked with genipin..... 155

Figure 6. 5 - **(A)** UV-vis spectrum of CHT (control) and CHT-catechol for Formulation 1, **(B)** UV-vis spectrum of CHT (control) and CHT-catechol for Formulation 2, **(C)** UV-vis spectrum of CHT (control) and CHT-catechol for Formulation 3 and **(D)** Overlay. 157

LIST OF TABLES

Table 5. 1 - Procedures for the formation of the freestanding films..... 118

Table 6. 1 - Different formulations tested to produce chitosan-catechol (CHT-c) conjugate..... 157

CHAPTER 1 GENERAL INTRODUCTION

1. GENERAL INTRODUCTION

1.1. Motivation

Marine mussels secrete specific proteins, which are used to stick onto different substrates and support harsh environmental conditions. These adhesive proteins have in their constitution an unusual amino acid, the 3, 4-dihydroxy-L-phenylalanine, known as DOPA [1-8]. Many efforts have been done in order to mimic these adhesive properties, even in wet conditions, shown by marine mussels, but unsuccessful for now [8].

Also, the layer-by-layer (LbL) technique has been the subject of much interest by the scientific community [9], since it allows obtaining nanostructured biomaterials, such as coatings [10], films [11] and free-standing films [12, 13]. For the LbL creation it is necessary at least two different charged species, called poly(electrolytes). The LbL assembly is driven, not only, but generally through electrostatic interactions between the negatively and positively poly(electrolyte) species [14]. It is a simple [10, 11, 14-20] and versatile [11, 13, 14, 16-19, 21] technique, which has applications in the biomedical field.

Nanoparticles also have been used in the biomedical field. In the present master' thesis bioglass nanoparticles were used, with a ternary formulation ($\text{SiO}_2/\text{CaO}/\text{P}_2\text{O}_5$ (mol %) = 50:45:5) as well as silver doped bioglass nanoparticles with a quaternary formulation ($\text{SiO}_2/\text{CaO}/\text{P}_2\text{O}_5/\text{Ag}_2\text{O}$ (mol %) = 56:30:4:10). Bioglass is used because it can induce the formation of hydroxyapatite with morphological and chemical structures similar to the mineral content of bone [22], after immersion in a simulated body fluid (SBF) solution (simulates the concentration of ionic species present in human body plasma) [23]. Furthermore, the presence of silver in the bioglass nanoparticles allows antibacterial properties, because silver ions released for the medium inhibit the bacterial cell wall creation, DNA and RNA synthesis [24], causing protein denaturation [24] and promoting the metabolic pathway disorder [25].

The layer-by-layer (LbL) assembly of polymeric chains and the presence of nanoparticles mimics the structure of nacre, also known as mother-of-pearl. It is constituted by a mineral phase, composed by aragonite with a percentage between 95 to 98 % [26], and organic phase, composed by polysaccharides and proteins [27], between 1 [28] to 5 % [27]. Furthermore, it presents a brick-and-mortar structure and it is studied because it

reveals exceptional mechanical properties [29] and the ability to dissipate high contents of energy [30].

Hydrogels are widely used for biomedical applications, because they present a 3D structure [31], mimic the extracellular matrix of the cells (ECM) [32], present high porosity [33] and have in their constitution great amounts of water [31]. Recently, hydrogels made through natural based polymers conjugated with catechol groups were reported in the literature [34-36]. It is also possible to develop hydrogels with the addition of nanoparticles, called hybrid or nanostructured hydrogels, for biomedical applications [37].

The goal of this master' thesis is the development of structures, either 2D or 3D, inspired in the marine mussel adhesive proteins potential. Free-standing films were created based on natural polymers, namely chitosan, hyaluronic acid, hyaluronic acid-dopamine conjugate and a mineral charge, silver doped bioglass nanoparticles. The last one was studied in detail and the best thermal treatment was chosen. These nanoparticles were incorporated in the layer-by-layer assembly. It is expected that the developed free-standing films have tissue-adhesive properties due to the presence of catechol groups, bioactivity properties and antibacterial performance. Also, an exploratory study of hydrogels development was done. The influence of bioglass nanoparticles in the mechanical and bioactivity properties of chitosan hydrogels crosslinked with a natural crosslinking agent, genipin was studied. Moreover, the synthesis of a chitosan-dopamine conjugate and the hybrid hydrogel production was tried.

In order to allow the overall comprehension of this master' thesis, it is divided in seven different chapters. Indeed, in Chapter 1, a brief introduction to marine mussel constitution, its adhesive proteins, nanoparticles, the layer-by-layer approach and nacre structure is depicted. Chapter 2 presents the state of the art on marine mussel adhesive proteins and natural-based biomaterials in the biomedical field. In Chapter 3, all materials and techniques used for realization of this master' thesis are described. Chapter 4, 5 and 6 present the experimental work developed during this thesis. Indeed, Chapter 4 describes the optimization work about silver doped bioglass nanoparticles obtained through the sol-gel technique. The same formulation was studied with eight different thermal treatments. The best thermal treatment was found and these silver doped bioglass nanoparticles were included in the free-standing films assembly, which is described in Chapter 5. Chapter 6 presents the exploratory work conducted on natural polymers-based hydrogels with the

incorporation of bioglass nanoparticles, and finally Chapter 7 presents the general conclusions of this master' thesis. The rationale of this master' thesis is summarized in Figure 1.1.

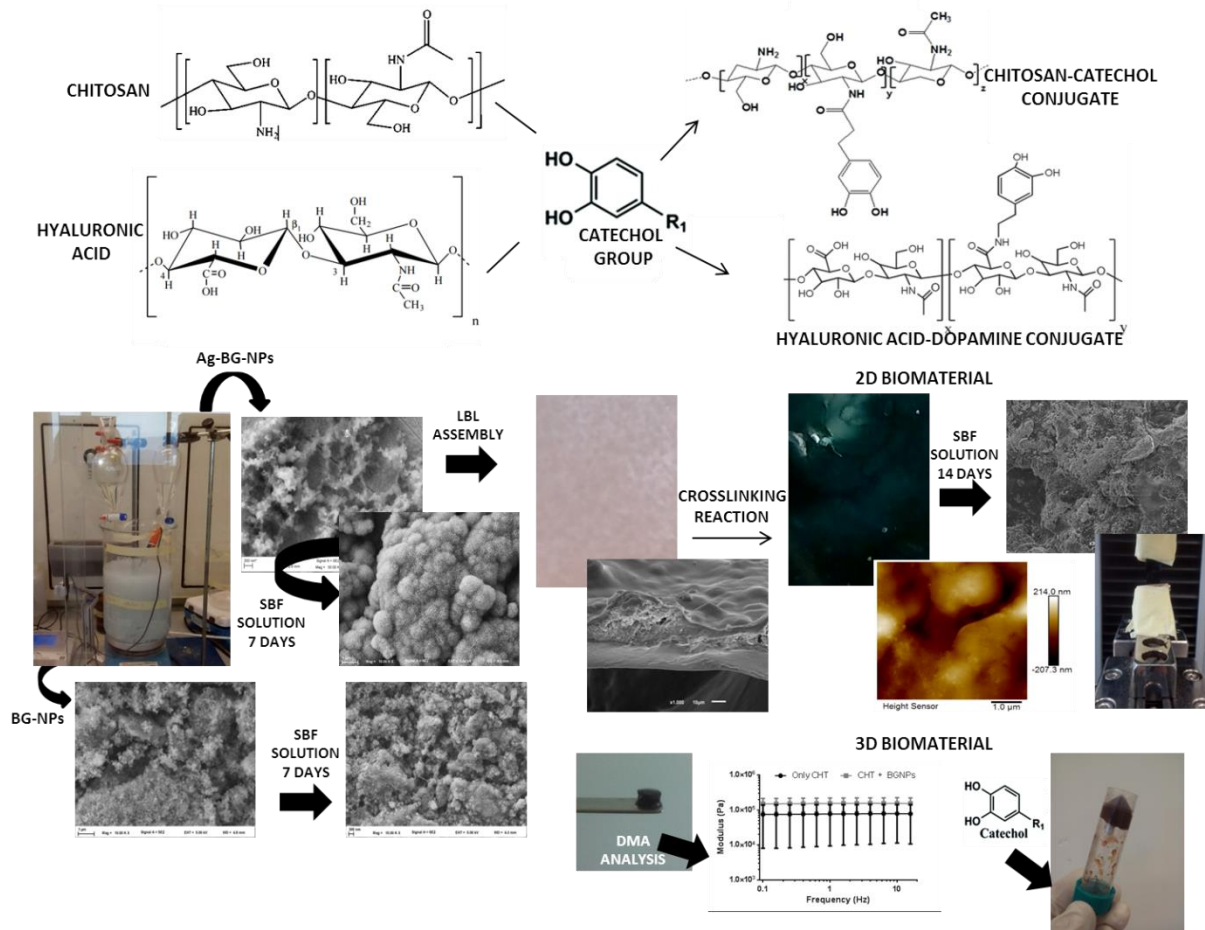


Figure 1.1 - Natural-based polymers (chitosan and hyaluronic acid) can be conjugated with catechol groups in order to create natural-based polymers-catechol conjugates. These raw materials with either bioglass nanoparticles or silver doped bioglass nanoparticles, that presents bioactivity properties can be included in either 2D or 3D biomaterials. Finally these can be studied by different characterization techniques. This representative scheme allows understand better the mussel adhesive properties and its potential in the biomedical field. It can be seen the chemical structure of catechol group, chitosan, hyaluronic acid, chitosan-catechol conjugate and hyaluronic acid-dopamine conjugate.

1.2. Structure and composition of marine mussel adhesive proteins (MAPs) and its adhesive properties

Recently the scientific community has showed interest in mussel adhesive proteins (MAPs) [3]. Marine mussels have been studied, as well as their secretion process. They are relevant to understand the adhesive bonds between the mussel and the substrate. According to Yamamoto [38], mussels and barnacles secreted marine adhesive proteins (MAPs) to stick to a variety of substrates. This secreted marine adhesive proteins with an unusual amino acid, 3, 4-dihydroxy-L-phenylalanine (DOPA) [1-8], obtained by

posttranslational modification of tyrosine [1-3, 8, 39], is used for the adhesion to various substrates [1, 3, 10, 40, 41] in wet environments [42]. According to Xu and co-workers [43] the bioadhesion is a phenomenon occurring between the natural macromolecule, natural or synthetic, and the substrate. When it comes to mollusks this bioadhesion is permanent [1], being due to the dihydroxyphenyl or catechol groups that form strong covalent and non-covalent bonds with many substrates [43] either creating hydrogen bonds [44], complex formation with metals or oxides [4, 44, 45], π - π interactions or crosslinking [44, 45]. Catechol groups present a strong adhesion of the respective coatings to substrates of complex geometries and chemical composition [46]. However, the physical and chemical mechanism of how this adhesion to the substrates is made is not yet fully explained [1, 42]. The explanation for mollusk adhesion to the rocks (inorganic substrate) will only be possibly due the Fe^{3+} complexes formation (present in the rocks) and the catechol groups present in MAPs and secreted by marine mussels [47-49]. According to Lee and co-workers [50] the rocks adhesion has advantages, such as a quickly elimination of wastes, gas exchange with sea water. However, disadvantages are present too, once the rocks adhesion entails the expenditure of 8 to 12% of metabolic energy [50].

Marine mussels present four constituents: plaques, byssus thread, stem and root [50], as it can be seen in Figure 1.2. According to Wilker [51], the plaque and thread (made almost by proteins) are extracellular. The mussel plaque architecture is varied due to the different proteins that form it. The mussels of *Mytilus* genus present twenty-five to thirty different proteins [39, 50], but only five are present only on the plaque [50]. It should be noted that all these proteins have in its constitution the amino acid DOPA [49, 50]. Indeed, and according to Lee and co-workers [50] plaques of mussels are specialists in substrate adhesion. The adhesive proteins mfp-3 and mfp-5 (20 % mol of DOPA [50] and 28 % mol of DOPA [50], respectively) are the ones in contact with the substrate, presenting high interactions with the surface to which they connect [50, 52], providing the water-resistant adhesion [52].

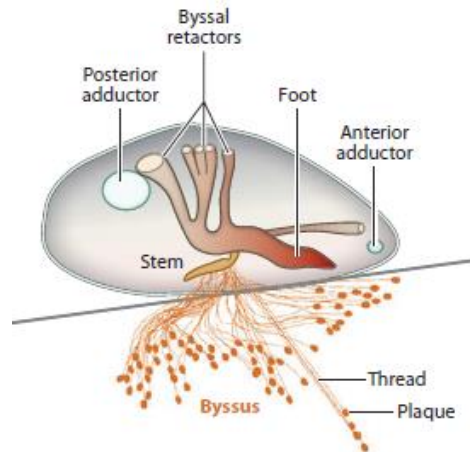


Figure 1. 2 - Marine mollusk *Mytilus Californianus* anatomy [1].

Catechol oxidase enzymes, namely tyrosinase [6, 42], are present in the secretion of mussel adhesive proteins (MAPs) that transform the catechol groups present in DOPA in highly reactive ortho-quinones [42]. Chemical oxidants, namely periodates, in aerobic conditions [6] also contribute to quinone formation. The oxidation process of DOPA originates semi-quinones, when it comes to an oxidation electron or DOPA-quinone, when it comes to an oxidation of two electrons [42]. Thereby, Xu et al. [43] found that DOPA and dopamine (DA) have similar oxidation mechanisms. First, they are oxidized to DOPA-o-quinone and DA-o-quinone, respectively, developing into dopacroma and dopaminacroma by cyclization and oxidation. Furthermore, the obtained quinones can self-crosslink by dismutations [43, 45]. The drawback of catechol compounds are the chemical instability of DOPA due to the oxidation at high pH's [43]. Oxidation of catechol groups that occurs in basic pH was investigated by Lee and co-workers [1]. For the purpose of that investigation it was used an inorganic surface as substrate, namely titanium (Ti). Indeed, strong reversible complexes with the inorganic substrate are formed with non-oxidized DOPA [1]. As far as oxidized DOPA is concerned in basic pH, covalent bonds are created [1, 3, 47]. An explanation for these bonds are not yet fully explained, there are currently two theories, the Michael addition theory and Schiff base reactions with primary amines [45, 50]. In summary, there is an equilibrium between DOPA or DOPA-quinone formation, just by changing the medium pH [1, 48]. MAPs can create bonds that resist the wet environment, in which they live, rocks with complex shapes and irregular forms [10, 47]. The created bonds are so resistant [47] and durable [2] that they can fulfill its function even when environmental factors change, for example, rip currents [2, 47], temperature changes [2, 47], choice of substrate [2],

presence or absence of moisture [2, 47], salinity [2, 47], season [2], but also biological factors, like age [2] and metabolic stage [2].

In fact, scientists have been developing efforts to create synthetic polymers with adhesive properties [8] equivalent to those shown by MAPs for biomedical applications [43, 53]. Thus, the study of materials and mechanisms such as marine mollusks adherence to substrates will be an asset for the creation of adhesives [42, 47], as well as, controlled drug delivery systems and hydrogels [43].

1.3. Studies of the adhesive properties of mussels

Sun and co-workers [45] developed a film constituted by poly(vinylpyrrolidone) (PVPON) and poly(acrylic acid) (PAA) modified with DOPA. When the pH was above 7, the color solution changed to brown, i.e. the oxidation of DOPA for ortho-quinone occurred. According to these authors, when the pH was below 7, the UV-vis spectrum of PAA-dopa showed the absorbance peak at 280 nm [45], characteristic of DOPA presence [10]. For a pH above 7, the absorbance peak was detected to 435 nm, due to o-quinone presence [45]. According to Lee and co-workers [50] studies have been carried out that allow the creation of synthetic polymers that mimic the adhesion of MAPs. In fact, researches have been carried out in order to create peptides and polymers that contain DOPA and catechol groups having adhesive and cohesive properties [50]. According to Kim and co-workers [39], adhesive bonds are made with either organic or inorganic substrates in underwater environment and cohesive bonds are made with amine, multivalent metal ions and thiol groups. According to Yamada and co-workers [54], non-oxidized DOPA is useful for adhesion. Hong and co-workers [55] demonstrated that in alkaline conditions, i.e., pH between 8 and 9, HA-DN revealed cohesive properties. These properties are useful, according to the same study, for gels [54] and hydrogels formation [55]. Polymers, peptides or other compounds with synthetic linear or branched DOPA will improve adhesion to various substrates [50]. For example, poly (ethylene glycol) (PEG) is used either in the polymeric chain or at the end of this [50]. PEG can be modified with DN because it is inert, biocompatible and have adhesive and cohesive characteristics, with further tissue adhesion [50]. Monomers combinations are also possible, for example, copolymers obtained by polymerization reactions of methacrylamide dopamine (DMAm) with 2-methoxyethyl acrylate (MEA) [50]. This potential of changing the constituents gives rise to polymers with different physical properties that can be used as adhesives

[50]. Podsiadlo and co-workers [3] built-up, for the first time, an artificial composite, which mimics the structure of nacre. According to these authors, DOPA presence improves the composite strength. Furthermore, the cross-linking process of DOPA has a high impact on the mechanical properties, once the results showed three times more strength and four times more toughness [3]. Lee and co-workers [56] resorted to MAPs, in particular the catechol and amine groups, for functionalizing synthetic polymers. They obtained poly(ethyleneimine) (PEI)-catechol by using PEI and 3-(3,4-dihydroxyphenyl)propionic acid. In order to use the LbL technique, they chose for substrate PTFE, PEI-catechol for cation and hyaluronic acid conjugated with catechol groups for anion. The obtained results showed that the contact angle decreased from 106° (PTFE unmodified) to 19.7° (PTFE with three cycles of PEI-catechol and HA-catechol), allowing the adhesion to various substrates. Furthermore, catechol groups improved the mechanical properties of the films created by the LbL technique [56]. Wang and co-workers [46] developed a composite coating based on MAPs and incorporated nanoparticles (NPs) using such technique. Thus, the LbL method is able to disperse nanoparticles in a substrate (organic matrix). These authors used hydroxyl-propylacrylamide for water solubility and catechol groups that are useful to adhere to a substrate, as well as to integrate silicon dioxide (SiO₂) and titanium dioxide (TiO₂) nanoparticles into coatings [46]. In conclusion, catechols groups present binder characteristic that are more favorable in acid and basic conditions to the assembly than without the presence of catechol groups [46]. Deming [47] conducted lap shear tensile adhesive measurements either with poly-L-lysine or co-polypeptides of L-lysine and DOPA. The results showed that the copolymer with 20% of DOPA presented ten times more adhesion values than the linked poly-L-lysine (control). Further, the copolymer showed a strong resistance to moisture, in the absence of oxidation.

1.4. Layer-by-Layer (LbL) technique

Layer-by-Layer (LbL) is a versatile technique that can be used in many applications, for example the creation of coatings [15, 57, 58], scaffolds for tissue engineering [17, 57], drug delivery systems [15, 17, 57-59], cells and proteins adhesion [59], intervention in cellular function [59], hepatic tissue engineering [17], antibacterial coatings [17, 18], micropatterning [58] and artificial cells [58].

The technique was introduced by Decker and co-workers in 1992 [15, 59] and distinct materials can be used, such as polysaccharides, polypeptides, proteins, nanoparticles and polyanions [58].

There are three techniques that can be used to produce thin films, namely Langmuir-Blodgett (LB) technique [14, 15, 59, 60], self-assembled monolayer (SAM) [14, 15, 59, 60] and layer-by-layer (LbL) technique [14, 15, 59, 60]. LbL technique is based on the addition of charged particles, polycations and polyanions by electrostatic interactions [14, 21, 60-62], as well as, hydrogen bonding [57, 59, 60, 62], covalent bonding [59, 60, 62], hydrophobic interactions [59, 60, 62], charge transfer [59, 60, 62], biological recognition [62] and coordination [60]. As far as materials that present charge in solution are concerned, multilayers films can occur by electrostatic interactions [14].

Physicochemical parameters, namely pH [12, 14, 20, 58, 63, 64], electrolyte species [14] and their concentration [12, 18], ionic strength [12, 14, 58, 64], solvent quality [14], added salt [18, 65], temperature [14], adsorption time [14, 18, 64], charge density [14, 63, 65], concentration [14], architecture [14], and molecular weight [14] strongly influence the stability [14, 58, 66], internal structure [14], dynamics [14], mechanical properties [66], swellability [66], thickness [18, 58] and growth [66].

According to Borges and Mano [14], any type of substrate or surface can be used in the LbL technique [14].

This process is typically based on the sequential deposition of a polycation and a polyanion onto a substrate and may be repeated until the desired number of bilayers is achieved, as depicted in Figure 1.3.

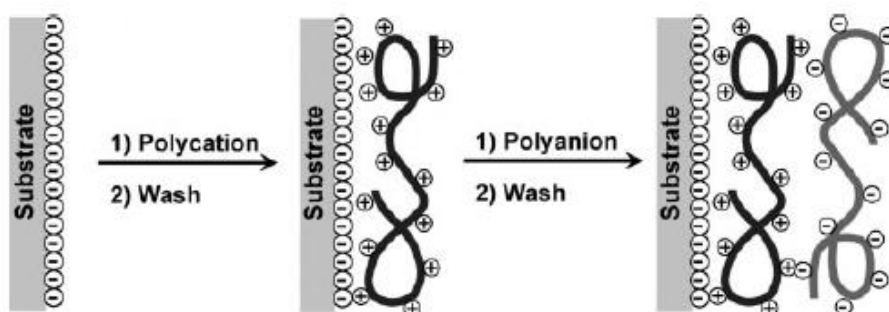


Figure 1. 3 - Simplified mechanism of layer-by-layer (LbL) technique. There is the formation of bilayers by addition of a polycation and a polyanion in a negatively charged substrate. Adapted from [59].

According to several authors [10, 11, 14-21, 57, 59] the LbL technique has many advantages. It's simple, cheap, versatile [11, 13, 14, 16-19, 21], efficient, flexible, and provides the union of different polymers without the need to create mixtures between them; It allows monitoring complex structures to nano-scale the formation of interconnected structures when there is molecular diffusion and thickness. According to Hammond [57], the main advantage of this technique is that the material is present in a charged solution, dispersed, not forming, therefore, agglomerates [57].

Multilayers films can grow linearly, exponentially or both forms. The systems that have at least one polypeptide or polysaccharide exhibit an exponential growth [14, 65, 67]. The strong polyelectrolytes pairs present a linear growth [14, 67]. According to Kujawa [67], the reason that weak polyelectrolytes have an exponential growth is most likely due to the fact that the quantity of polyelectrolyte adsorbed in each cycle is not constant, leading to a thickness increase [67]. When the thickness of each bilayer is higher than 100 or 200 nm a diffusion of polymer chains can occur in each cycle. This phenomenon can be disadvantageous for the construction of complex materials, for example, with the creation of selective permeability devices [57]. This can be minimized or eliminated with the introduction of barriers layers, i.e., one layer that prevent the interdiffusion between layers [57].

1.5. Nanoparticles (NPs)

Nanoparticles (NPs) have been the subject of much interest among scientists, since they have properties, such as physical, chemical and biologic [68] which are relevant for many applications, namely in the areas of physics, chemistry, engineering and biology area [16]. NPs have a small size and large surface to volume ratios and their addition to materials brings chemical and physical differences that would not exist without them. Nanoparticles are used due to enhancement of osteogenic cell differentiation and proliferation, angiogenic properties and bone-like apatite formation [69]. Furthermore, the presence of NP's has an antibacterial effect with Gram-negative and Gram-positive bacteria [68].

The first bioactive glass was invented by Hench in 1969 [70]. According to Vulpoi and co-workers [71], bioactive glasses allows the creation of hydroxyapatite (HA) and/or hydroxycarbonate apatite (HCA) [71]. According to Buckley and co-workers [72], hydroxyapatite, either $\text{Ca}_{10}(\text{PO}_4)_6(\text{OH})_2$ or HA, is a main component of bone. HA is used as medical support in surgical implants and tissue regeneration [72].

There are many types of bioactive glass, namely Bioglass 45S5 [73]; phosphate-based glasses [73]; and borate-based glasses [73].

According to Jones [73], “a bioactive material is defined as a material that stimulates a beneficial response from the body, particularly bonding to host tissue (usually bone)” [73].

Delben and co-workers [74] reported the physical properties of bioactive glasses doped with silver, prepared by the sol–gel method. This method was used because, according to Delben and co-workers [74], requires low temperatures, allows to control porosity and particle size and an homogeneous distribution of the components can be obtained. The results showed that an increase in silver implies an increase of quartz and metallic silver crystallization. This increase implies the reduction of hydroxyapatite crystallization [74]. According to Buckley and co-workers [72], if hydroxyapatite (HA) has a low surface area, consequently there is a poor dissolution of phosphate and/or metallic particles and that implies a reduction of microbiological action. When there is a high surface area of HA or less than 5 wt. % of Ag, there is a high dissolution rate of Ag⁺ ions and an enhancement of microbiological action [72]. If there is a bacterial adhesion to biomaterials, an infection occurs and poor tissue integration [75]. Bellantone and co-workers [75] incorporated 3wt% of Ag₂O into a SiO₂-CaO-P₂O₅ system, which showed antimicrobial properties without compromising its bioactivity [75]. In another work developed a bioactive glass system composed of SiO₂-CaO-P₂O₅ and Ag₂O was developed to reduce the potential microbial contamination. In this investigation three types of bacteria were used, namely *Escherichia coli*, *Pseudomonas aeruginosa* and *Staphylococcus aureus*. The results showed that for *Escherichia coli* (0.2 mg/mL) there was no growth in the cell population; for, *Pseudomonas aeruginosa* (0.05 mg/mL) a reduction of viability comparative to the inoculum was showed; for 0.1 mg/mL *Staphylococcus aureus* there was antibacteriostatic effect. To summarize, Bellantone and co-workers [76], estimated the MBCs values for *Escherichia coli*, *Pseudomonas aeruginosa* and *Staphylococcus aureus*. The values were 1 mg/mL for *Escherichia coli*; 0.5 mg/mL for *Pseudomonas aeruginosa* and 0.5 mg/mL for *Staphylococcus aureus*. Vulpoi and co-workers [71] investigated the silver species embedded into the BG before and after immersion in SBF. These authors used 56SiO₂(40-x)CaO·4P₂O₅·xAg₂O, where x assumed values of 0, 2 and 8 mol%. These nanoparticles were produced via sol-gel method. Afterwards, they were thermally treated at 580 °C for 30 minutes. The results

showed that silver addition promoted the formation of the hydroxyapatite and hydroxycarbonate apatite, as well as Ag_3PO_4 crystals when they are immersed in simulated body fluid. According to Vulpoi and co-workers [71], silver incorporation allows a slower ions release and an antibacterial effect of the bioactive glass for a longer period.

1.6. Materials inspired by the structure of nacre

In recent years a development of materials that have inorganic-organic components has stimulated research interests [62, 77]. Inorganic–organic nanocomposites have been created [27, 78, 79] based on biological materials, namely bone [77], mollusk shell [62, 77], teeth [62, 77], coccoliths [62], arthropods shells [77] and spider silk [77]. Inorganic-organic composites are constituted by calcite or aragonite and an organic phase [80]. Organic phase has 1 [28] to 5 wt% [28, 30, 77] and inorganic phase has 95-98 wt% [26, 81]. Organic phase has larger control of biomineral growth [82].

Nacre or “mother-of-pearl”, is constituted by polygonal aragonitic tablets, with 5 to 15 μm of diameter and a continuous laminae with 0.5 μm of thickness [83].

The nanocomposites can be homogeneous or heterogeneous [62]. The combination of organic and inorganic constituents could provide enhanced properties than one constituent only, namely optical [62, 84], electrical [62], magnetic [62], mechanical [62, 80, 84, 85] and catalytic [62] properties. To improve the aforementioned properties, both the two phases (organic and inorganic) as well as the interface between them must be accounted for [62]. Tang and co-workers [59] resorted to the LbL technique to create free-standings films with PDDA/clay prepared by chemical suppression of the interactions between the multilayer and the glass substrate [59]. The creation of an inspired nacre composite structure showed rupture stress values of 100 MPa and a tensile modulus of 10 GPa. The creation of composite organic-inorganic structure proves to be useful for the creation of biomaterials with high mechanical resistance [59]. According to Zhang and co-workers [86], these properties are attributed to the organic–inorganic alternating structure. Podsiadlo and co-workers [3] developed a natural composite with organic-inorganic structure, i.e., the poly(diallyldimethylammonium chloride) as the organic constituent and the Na^+ -Montmorillonite (C) as the inorganic constituent. The results showed that mechanical properties have similar values to nacre and bone, i.e., tensile

strength values of 11 ± 2 GPa and Young's modulus of 100 ± 10 MPa [3]. Summarizing, nacre structure has a combination of stiffness [87], strength [3, 87], and toughness [3, 87].

1.7. References

- [1] H. Lee, N. F. Scherer, and P. B. Messersmith, "Single-molecule mechanics of mussel adhesion," (in English), Proceedings of the National Academy of Sciences of the United States of America, Article vol. 103, no. 35, pp. 12999-13003, 2006.
- [2] H. G. Silverman and F. F. Roberto, "Understanding marine mussel adhesion," (in English), Marine Biotechnology, Review vol. 9, no. 6, pp. 661-681, 2007.
- [3] P. Podsiadlo, Z. Q. Liu, D. Paterson, P. B. Messersmith, and N. A. Kotov, "Fusion of seashell nacre and marine bioadhesive analogs: High-strength nanocomposite by layer-by-layer assembly of clay and L-3,4-dihydroxyphenylalanine polymer," (in English), Advanced Materials, Article vol. 19, no. 7, pp. 949- +, 2007.
- [4] S. K. Madhurakkat Perikamana et al., "Materials from Mussel-Inspired Chemistry for Cell and Tissue Engineering Applications," Biomacromolecules, vol. 16, no. 9, pp. 2541-55, 2015.
- [5] Y. C. Choi, J. S. Choi, Y. J. Jung, and Y. W. Cho, "Human gelatin tissue-adhesive hydrogels prepared by enzyme-mediated biosynthesis of DOPA and Fe³⁺ ion crosslinking," (in English), Journal of Materials Chemistry B, Article vol. 2, no. 2, pp. 201-209, 2014.
- [6] M. Cencer, Y. Liu, A. Winter, M. Murley, H. Meng, and B. P. Lee, "Effect of pH on the Rate of Curing and Bioadhesive Properties of Dopamine Functionalized Poly(ethylene glycol) Hydrogels," (in English), Biomacromolecules, Article vol. 15, no. 8, pp. 2861-2869, 2014.
- [7] Y. Lee et al., "Thermo-sensitive, injectable, and tissue adhesive sol-gel transition hyaluronic acid/pluronic composite hydrogels prepared from bio-inspired catechol-thiol reaction," (in English), Soft Matter, Article vol. 6, no. 5, pp. 977-983, 2010.
- [8] B. P. Lee, J. L. Dalsin, and P. B. Messersmith, "Synthesis and gelation of DOPA-Modified poly(ethylene glycol) hydrogels," (in English), Biomacromolecules, Article vol. 3, no. 5, pp. 1038-1047, 2002.
- [9] J. Borges, L. C. Rodrigues, R. L. Reis, and J. F. Mano, "Layer-by-Layer Assembly of Light-Responsive Polymeric Multilayer Systems," (in English), Advanced Functional Materials, Article vol. 24, no. 36, pp. 5624-5648, 2014.
- [10] A. I. Neto et al., "Nanostructured Polymeric Coatings Based on Chitosan and Dopamine-Modified Hyaluronic Acid for Biomedical Applications," (in English), Small, Article vol. 10, no. 12, pp. 2459-2469, 2014.
- [11] R. R. Costa and J. F. Mano, "Polyelectrolyte multilayered assemblies in biomedical technologies," Chemical Society Reviews, vol. 43, no. 10, pp. 3453-3479, 2014.
- [12] S. G. Caridade et al., "Myoconductive and osteoinductive free-standing polysaccharide membranes," Acta Biomaterialia, vol. 15, pp. 139-149, 2015.

- [13] S. G. Caridade, C. Monge, F. Gilde, T. Boudou, J. F. Mano, and C. Picart, "Free-Standing Polyelectrolyte Membranes Made of Chitosan and Alginate," (in English), *Biomacromolecules*, Article vol. 14, no. 5, pp. 1653-1660, 2013.
- [14] J. Borges and J. F. Mano, "Molecular Interactions Driving the Layer-by-Layer Assembly of Multilayers," (in English), *Chemical Reviews*, Review vol. 114, no. 18, pp. 8883-8942, 2014.
- [15] K. Ariga, J. P. Hill, and Q. M. Ji, "Layer-by-layer assembly as a versatile bottom-up nanofabrication technique for exploratory research and realistic application," (in English), *Physical Chemistry Chemical Physics*, Review vol. 9, no. 19, pp. 2319-2340, 2007.
- [16] Y. Zhou, M. J. Cheng, X. Q. Zhu, Y. J. Zhang, Q. An, and F. Shi, "A facile method for the construction of stable polymer-inorganic nanoparticle composite multilayers," (in English), *Journal of Materials Chemistry A*, Article vol. 1, no. 37, pp. 11329-11334, 2013.
- [17] A. L. Larkin, R. M. Davis, and P. Rajagopalan, "Biocompatible, Detachable, and Free-Standing Polyelectrolyte Multilayer Films," (in English), *Biomacromolecules*, Article vol. 11, no. 10, pp. 2788-2796, 2010.
- [18] C. S. Hajicharalambous, J. Lichter, W. T. Hix, M. Swierczewska, M. F. Rubner, and P. Rajagopalan, "Nano- and sub-micron porous polyelectrolyte multilayer assemblies: Biomimetic surfaces for human corneal epithelial cells," (in English), *Biomaterials*, Article vol. 30, no. 23-24, pp. 4029-4036, 2009.
- [19] P. Kujawa, G. Schmauch, T. Viitala, A. Badia, and F. M. Winnik, "Construction of viscoelastic biocompatible films via the layer-by-layer assembly of hyaluronan and phosphorylcholine-modified chitosan," (in English), *Biomacromolecules*, Article vol. 8, no. 10, pp. 3169-3176, 2007.
- [20] G. V. Martins, J. F. Mano, and N. M. Alves, "Nanostructured self-assembled films containing chitosan fabricated at neutral pH," (in English), *Carbohydrate Polymers*, Article vol. 80, no. 2, pp. 570-573, 2010.
- [21] S. Y. Yang and M. F. Rubner, "Micropatterning of polymer thin films with pH-sensitive and cross-linkable hydrogen-bonded polyelectrolyte multilayers," (in English), *Journal of the American Chemical Society*, Article vol. 124, no. 10, pp. 2100-2101, 2002.
- [22] N. M. Alves, I. B. Leonor, H. S. Azevedo, R. L. Reis, and J. F. Mano, "Designing biomaterials based on biomineralization of bone," (in English), *Journal of Materials Chemistry*, Article vol. 20, no. 15, pp. 2911-2921, 2010.
- [23] T. Kokubo and H. Takadama, "How useful is SBF in predicting in vivo bone bioactivity?," (in English), *Biomaterials*, Article vol. 27, no. 15, pp. 2907-2915, 2006.
- [24] A. A. Ahmed, A. A. Ali, D. A. R. Mahmoud, and A. M. El-Fiqi, "Study on the preparation and properties of silver-doped phosphate antibacterial glasses (Part I)," *Solid State Sciences*, vol. 13, no. 5, pp. 981-992, 2011.
- [25] Y.-F. Goh, A. Z. Alshemary, M. Akram, M. R. A. Kadir, and R. Hussain, "Bioactive Glass: An In-Vitro Comparative Study of Doping with Nanoscale Copper and Silver Particles," *International Journal of Applied Glass Science*, vol. 5, no. 3, pp. 255-266, 2014.

- [26] U. G. K. Wegst, H. Bai, E. Saiz, A. P. Tomsia, and R. O. Ritchie, "Bioinspired structural materials," *Nature Materials*, vol. 14, no. 1, pp. 23-36, 2015.
- [27] J. Y. Sun and B. Bhushan, "Hierarchical structure and mechanical properties of nacre: a review," *Rsc Advances*, vol. 2, no. 20, pp. 7617-7632, 2012.
- [28] C. M. Zaremba et al., "Critical transitions in the biofabrication of abalone shells and flat pearls," *Chemistry of Materials*, vol. 8, no. 3, pp. 679-690, 1996.
- [29] J. F. Wang, Q. F. Cheng, and Z. Y. Tang, "Layered nanocomposites inspired by the structure and mechanical properties of nacre," *Chemical Society Reviews*, vol. 41, no. 3, pp. 1111-1129, 2012.
- [30] Q. Chen and N. M. Pugno, "Bio-mimetic mechanisms of natural hierarchical materials: A review," *Journal of the Mechanical Behavior of Biomedical Materials*, vol. 19, pp. 3-33, 2013.
- [31] E. M. Ahmed, "Hydrogel: Preparation, characterization, and applications: A review," *Journal of Advanced Research*, vol. 6, no. 2, pp. 105-121, 2015.
- [32] J. L. Drury and D. J. Mooney, "Hydrogels for tissue engineering: scaffold design variables and applications," (in English), *Biomaterials, Review* vol. 24, no. 24, pp. 4337-4351, 2003.
- [33] L. Gasperini, J. F. Mano, and R. L. Reis, "Natural polymers for the microencapsulation of cells," (in English), *Journal of the Royal Society Interface, Article* vol. 11, no. 100, p. 19, 2014.
- [34] C. Lee et al., "Bioinspired, Calcium-Free Alginate Hydrogels with Tunable Physical and Mechanical Properties and Improved Biocompatibility," *Biomacromolecules*, vol. 14, no. 6, pp. 2004-2013, 2013.
- [35] J. H. Ryu, S. Hong, and H. Lee, "Bio-inspired adhesive catechol-conjugated chitosan for biomedical applications: A mini review," (in English), *Acta biomaterialia, ; Review* vol. 27, 2015.
- [36] J. Shin et al., "Tissue Adhesive Catechol-Modified Hyaluronic Acid Hydrogel for Effective, Minimally Invasive Cell Therapy," *Advanced Functional Materials*, vol. 25, no. 25, pp. 3814-3824, 2015.
- [37] A. K. Gaharwar, N. A. Peppas, and A. Khademhosseini, "Nanocomposite Hydrogels for Biomedical Applications," *Biotechnology and Bioengineering*, vol. 111, no. 3, pp. 441-453, 2014.
- [38] H. Yamamoto, "Marine adhesive proteins and some biotechnological applications," (in English), *Biotechnology and Genetic Engineering Reviews, Vol* 13, Review vol. 13, pp. 133-165, 1996.
- [39] B. J. Kim et al., "Mussel-Mimetic Protein-Based Adhesive Hydrogel," (in English), *Biomacromolecules, Article* vol. 15, no. 5, pp. 1579-1585, 2014.
- [40] J. J. Wilker, "The Iron-Fortified Adhesive System of Marine Mussels," (in English), *Angewandte Chemie-International Edition, Editorial Material* vol. 49, no. 44, pp. 8076-8078, 2010.
- [41] S. A. Burke, M. Ritter-Jones, B. P. Lee, and P. B. Messersmith, "Thermal gelation and tissue adhesion of biomimetic hydrogels," (in English), *Biomedical Materials, Article* vol. 2, no. 4, pp. 203-210, 2007.

- [42] M. E. Yu, J. Y. Hwang, and T. J. Deming, "Role of L-3,4-dihydroxyphenylalanine in mussel adhesive proteins," (in English), *Journal of the American Chemical Society*, Article vol. 121, no. 24, pp. 5825-5826, 1999.
- [43] J. K. Xu, G. M. Soliman, J. Barralet, and M. Cerruti, "Mollusk Glue Inspired Mucoadhesives for Biomedical Applications," (in English), *Langmuir*, Article vol. 28, no. 39, pp. 14010-14017, 2012.
- [44] B. Yang et al., "In Vivo Residue-Specific Dopa-Incorporated Engineered Mussel Bioglue with Enhanced Adhesion and Water Resistance," (in English), *Angewandte Chemie-International Edition*, Article vol. 53, no. 49, pp. 13360-13364, 2014.
- [45] J. X. Sun, C. Su, X. J. Zhang, W. J. Yin, J. Xu, and S. G. Yang, "Reversible Swelling-Shrinking Behavior of Hydrogen-Bonded Free-Standing Thin Film Stabilized by Catechol Reaction," (in English), *Langmuir*, Article vol. 31, no. 18, pp. 5147-5154, 2015.
- [46] C. X. Wang et al., "Catechol-based layer-by-layer assembly of composite coatings: a versatile platform to hierarchical nano-materials," (in English), *Soft Matter*, Article vol. 11, no. 31, pp. 6173-6178, 2015.
- [47] T. J. Deming, "Mussel byssus and biomolecular materials," (in English), *Current Opinion in Chemical Biology*, Review vol. 3, no. 1, pp. 100-105, 1999.
- [48] M. Krogsgaard, M. A. Behrens, J. S. Pedersen, and H. Birkedal, "Self-Healing Mussel-Inspired Multi-pH-Responsive Hydrogels," (in English), *Biomacromolecules*, Article vol. 14, no. 2, pp. 297-301, 2013.
- [49] J. Monahan and J. J. Wilker, "Specificity of metal ion cross-linking in marine mussel adhesives," (in English), *Chemical Communications*, Article no. 14, pp. 1672-1673, 2003.
- [50] B. P. Lee, P. B. Messersmith, J. N. Israelachvili, and J. H. Waite, "Mussel-Inspired Adhesives and Coatings," in *Annual Review of Materials Research*, Vol 41, vol. 41, D. R. Clarke and P. Fratzl, Eds. (Annual Review of Materials Research, Palo Alto: Annual Reviews, pp. 99-132, 2011.
- [51] J. J. Wilker, "Marine bioinorganic materials: mussels pumping iron," (in English), *Current Opinion in Chemical Biology*, Review vol. 14, no. 2, pp. 276-283, 2010.
- [52] J. Yang, M. A. C. Stuart, and M. Kamperman, "Jack of all trades: versatile catechol crosslinking mechanisms," (in English), *Chemical Society Reviews*, Review vol. 43, no. 24, pp. 8271-8298, 2014.
- [53] C. E. Brubaker and P. B. Messersmith, "The Present and Future of Biologically Inspired Adhesive Interfaces and Materials," *Langmuir*, vol. 28, no. 4, pp. 2200-2205, 2012.
- [54] K. Yamada, T. H. Chen, G. Kumar, O. Vesnovsky, L. D. T. Topoleski, and G. F. Payne, "Chitosan based water-resistant adhesive. Analogy to mussel glue," (in English), *Biomacromolecules*, Article vol. 1, no. 2, pp. 252-258, 2000.
- [55] S. Hong et al., "Hyaluronic Acid Catechol: A Biopolymer Exhibiting a pH-Dependent Adhesive or Cohesive Property for Human Neural Stem Cell Engineering," (in English), *Advanced Functional Materials*, Article vol. 23, no. 14, pp. 1774-1780, 2013.

- [56] H. Lee, Y. Lee, A. R. Statz, J. Rho, T. G. Park, and P. B. Messersmith, "Substrate-independent layer-by-layer assembly by using mussel-adhesive-inspired polymers," (in English), *Advanced Materials*, Article vol. 20, no. 9, pp. 1619-+, 2008.
- [57] P. T. Hammond, "Engineering Materials Layer-by-Layer: Challenges and Opportunities in Multilayer Assembly," (in English), *Aiche Journal*, Editorial Material vol. 57, no. 11, pp. 2928-2940, 2011.
- [58] H. Ai, S. A. Jones, and Y. M. Lvov, "Biomedical applications of electrostatic layer-by-layer nano-assembly of polymers, enzymes, and nanoparticles," (in English), *Cell Biochemistry and Biophysics*, Review vol. 39, no. 1, pp. 23-43, 2003.
- [59] Z. Y. Tang, Y. Wang, P. Podsiadlo, and N. A. Kotov, "Biomedical applications of layer-by-layer assembly: From biomimetics to tissue engineering," (in English), *Advanced Materials*, Review vol. 18, no. 24, pp. 3203-3224, 2006.
- [60] M. Matsusaki, H. Ajiro, T. Kida, T. Serizawa, and M. Akashi, "Layer-by-Layer Assembly Through Weak Interactions and Their Biomedical Applications," *Advanced Materials*, vol. 24, no. 4, pp. 454-474, 2012.
- [61] C. Y. Jiang and V. V. Tsukruk, "Freestanding nanostructures via layer-by-layer assembly," (in English), *Advanced Materials*, Review vol. 18, no. 7, pp. 829-840, 2006.
- [62] H. P. Cong and S. H. Yu, "Self-assembly of functionalized inorganic-organic hybrids," (in English), *Current Opinion in Colloid & Interface Science*, Review vol. 14, no. 2, pp. 71-80, 2009.
- [63] S. Boddohi, C. E. Killingsworth, and M. J. Kipper, "Polyelectrolyte multilayer assembly as a function of pH and ionic strength using the polysaccharides chitosan and heparin," (in English), *Biomacromolecules*, Article vol. 9, no. 7, pp. 2021-2028, 2008.
- [64] P. Podsiadlo et al., "Layer-by-layer assembly of nacre-like nanostructured composites with antimicrobial properties," (in English), *Langmuir*, Article vol. 21, no. 25, pp. 11915-11921, 2005.
- [65] R. von Klitzing, "Internal structure of polyelectrolyte multilayer assemblies," (in English), *Physical Chemistry Chemical Physics*, Review vol. 8, no. 43, pp. 5012-5033, 2006.
- [66] C. Picart, "Polyelectrolyte multilayer films: From physico-chemical properties to the control of cellular processes," (in English), *Current Medicinal Chemistry*, Review vol. 15, no. 7, pp. 685-697, 2008.
- [67] P. Kujawa, P. Moraille, J. Sanchez, A. Badia, and F. M. Winnik, "Effect of molecular weight on the exponential growth and morphology of hyaluronan/chitosan multilayers: A surface plasmon resonance spectroscopy and atomic force microscopy investigation," (in English), *Journal of the American Chemical Society*, Article vol. 127, no. 25, pp. 9224-9234, 2005.
- [68] M. A. Shenashen, S. A. El-Safty, and E. A. Elshehy, "Synthesis, Morphological Control, and Properties of Silver Nanoparticles in Potential Applications," (in English), *Particle & Particle Systems Characterization*, Review vol. 31, no. 3, pp. 293-316, 2014.

- [69] U. Rottensteiner et al., "In vitro and in vivo Biocompatibility of Alginate Dialdehyde/Gelatin Hydrogels with and without Nanoscaled Bioactive Glass for Bone Tissue Engineering Applications," (in English), *Materials*, Article vol. 7, no. 3, pp. 1957-1974, 2014.
- [70] J. R. Jones, "Review of bioactive glass: From Hench to hybrids," *Acta Biomaterialia*, vol. 9, no. 1, pp. 4457-4486, 2013.
- [71] A. Vulpoi et al., "Bioactivity and protein attachment onto bioactive glasses containing silver nanoparticles," *Journal of Biomedical Materials Research Part A*, vol. 100A, no. 5, pp. 1179-1186, 2012.
- [72] J. J. Buckley, A. F. Lee, L. Olivi, and K. Wilson, "Hydroxyapatite supported antibacterial Ag₃PO₄ nanoparticles," (in English), *Journal of Materials Chemistry*, Article vol. 20, no. 37, pp. 8056-8063, 2010.
- [73] J. R. Jones, "Reprint of: Review of bioactive glass: From Hench to hybrids," (in English), *Acta biomaterialia*, ; Review vol. 23 Suppl, pp. S53-82, 2015.
- [74] J. R. J. Delben et al., "Synthesis and thermal properties of nanoparticles of bioactive glasses containing silver," *Journal of Thermal Analysis and Calorimetry*, vol. 97, no. 2, pp. 433-436, 2009.
- [75] M. Bellantone, N. J. Coleman, and L. L. Hench, "Bacteriostatic action of a novel four-component bioactive glass," (in English), *Journal of Biomedical Materials Research*, Article vol. 51, no. 3, pp. 484-490, 2000.
- [76] M. Bellantone, H. D. Williams, and L. L. Hench, "Broad-spectrum bactericidal activity of Ag₂O-doped bioactive glass," (in English), *Antimicrobial Agents and Chemotherapy*, Article vol. 46, no. 6, pp. 1940-1945, 2002.
- [77] F. Barthelat, "Designing nacre-like materials for simultaneous stiffness, strength and toughness: Optimum materials, composition, microstructure and size," (in English), *Journal of the Mechanics and Physics of Solids*, Article vol. 73, pp. 22-37, 2014.
- [78] Z. Y. Tang, N. A. Kotov, S. Magonov, and B. Ozturk, "Nanostructured artificial nacre," (in English), *Nature Materials*, Article vol. 2, no. 6, pp. 413-U8, 2003.
- [79] A. Sellinger et al., "Continuous self-assembly of organic-inorganic nanocomposite coatings that mimic nacre," *Nature*, vol. 394, no. 6690, pp. 256-260, 1998.
- [80] A. G. Checa and A. B. Rodriguez-Navarro, "Self-organisation of nacre in the shells of Pterioidea (Bivalvia : Mollusca)," (in English), *Biomaterials*, Article vol. 26, no. 9, pp. 1071-1079, 2005.
- [81] B. Bar-On and H. D. Wagner, "Structural motifs and elastic properties of hierarchical biological tissues - A review," (in English), *Journal of Structural Biology*, Review vol. 183, no. 2, pp. 149-164, 2013.
- [82] A. M. Belcher, X. H. Wu, R. J. Christensen, P. K. Hansma, G. D. Stucky, and D. E. Morse, "Control of crystal phase switching and orientation by soluble mollusc-shell proteins," (in English), *Nature*, Article vol. 381, no. 6577, pp. 56-58, 1996.
- [83] F. Nudelman, "Nacre biomineralisation: A review on the mechanisms of crystal nucleation," *Seminars in Cell & Developmental Biology*.

- [84] W. Zhang, G. Xu, R. Ding, K. Duan, and J. Qiao, "Nacre biomimetic design—A possible approach to prepare low infrared emissivity composite coatings," *Materials Science and Engineering: C*, vol. 33, no. 1, pp. 99-102, 2013.
- [85] G. M. Luz and J. F. Mano, "Biomimetic design of materials and biomaterials inspired by the structure of nacre," (in English), *Philosophical Transactions of the Royal Society a-Mathematical Physical and Engineering Sciences, Review* vol. 367, no. 1893, pp. 1587-1605, 2009.
- [86] S. Zhang, J. Zhang, Z. Zhang, H. Dang, W. Liu, and Q. Xue, "Preparation and characterization of self-assembled organic–inorganic nacre-like nanocomposite thin films," *Materials Letters*, vol. 58, no. 17–18, pp. 2266-2269, 2004.
- [87] F. Barthelat and R. Rabiei, "Toughness amplification in natural composites," (in English), *Journal of the Mechanics and Physics of Solids*, Article vol. 59, no. 4, pp. 829-840, 2011.

CHAPTER 2 STATE OF THE ART

2. NATURAL-BASED BIOMATERIALS INSPIRED BY MARINE MUSSEL ADHESIVE PROTEINS

Abstract:

In recent years, natural-based materials have been the subject of much interest by many researchers, because they present several advantages, namely its biocompatibility and small toxicity. Also, marine mussels have been studied because they present an incredible ability to stick to various substrates in harsh environments, either organic or inorganic. This capacity is due to specific proteins secreted by marine mussels, known as marine mussel adhesive proteins (MAPs). These proteins have in their constitution an unusual amino acid, 3, 4-dihydroxyphenylalanine, known as DOPA. For that reason, many biomaterials, either with two-dimensional or three-dimensional structures, have been developed trying to mimic this incredible performance.

In this review, an overview of the application of MAPs and its adhesive properties on the development of distinct biomaterials will be presented, namely on coatings, free-standing films and hydrogels production. The variety of applications of these bioinspired materials will be discussed.

Keywords: natural-based materials, DOPA, poly(dopamine), hydrogels, biomedical applications.

2.1. Introduction

The marine mussels can stick onto various substrates [1-4], organic and inorganic substrates, even in wet environments [4, 5], such as: polymeric surfaces [6], rocks [7], metal oxides [6], metals [6] and biomacromolecules [6]. This adhesion is tough, durable and fast [8], can resist against a wide temperature range, namely - 40°C to + 40°C, to the presence of humidity/moisture, currents, tides, waves and salinities changes [9]. This incredible ability is due to the marine mussel adhesive proteins (MAPs) secreted by marine mussels, that have in their constitution an unusual amino acid, 3, 4-dihydroxyphenylalanine, known as DOPA [2-7, 10-21], which is obtained by the post-translational modification of tyrosine [4, 7, 8, 10, 16, 20]. In particular, this adhesive property is due to the catechol groups present in DOPA and its analog dopamine (DN). This one has been subject of much interest by scientists, because it presents a similar chemical structure of combined DOPA and lysine. DN is a catecholamine present in our body as neurotransmitter and hormone [5]. DOPA is present in two distinct forms, the non-oxidized and oxidized forms [8, 19]. The non-oxidized form is important in inorganic substrates adhesion. The mussels glues have in their constitution transition-metal ions, namely zinc, copper and iron, with a concentration up to 100 000 times those ocean water has [20]. In fact, the inorganic substrate adhesion is due to metal complexation, the iron ions, Fe^{III}, and the catechol groups form coordination complexes. The second one is important in organic substrates adhesion [8, 19]. The ortho-quinone is responsible for moisture-free resistance of mussels in wet environments [22]. The oxidative species can react with themselves [23, 24] via aryl-aryl bonds [23] or Michael-type addition with proteins that contain amine groups [23, 25] to form a tough cohesive composite [24]. The un-oxidized and oxidized forms are formed by two different manners: the first is due to the change to an alkaline pH [8, 26], metal binding and further redox reactions [4] and the presence of enzymes [4, 8]. According to Yu and co-workers [13], catechol groups and ortho-quinone forms are responsible by adhesive bonds and crosslinker bonds creation, respectively [13]. The adhesive properties are created through irreversible covalent bonds with natural substrates or reversible π - π interactions between synthetic polymers and coordination with metal oxides [27] whereas the cohesive bonds are created with multivalent metal ions or amine and thiol functional groups present in amino acids of byssal thread [28]. As far as mussel attachment to the substrate is concerned, there are foot proteins, namely mfp-3 and mfp-5 that have high concentrations in DOPA (between

15 and 30%), having a crucial importance in substrate adhesion [8], because they are in contact with it [23], and protein crosslinking [8].

Scientists have been developing efforts to create synthetic polymers with adhesive properties [29] equivalent to those shown by MAPs for biomedical applications [18, 30]. According to Shafiq and co-workers [19], it is possible to chemically functionalize the catechol groups present in mussels to produce adhesive thin films and coatings [11, 13] on all substrates, creating anchors to metal oxide surfaces [19], to produce hydrogels [18, 19] and to incorporate catechol groups in the polymer backbone, acting as a crosslinker or self-healing agent [19].

It's possible to produce two-dimensional or three-dimensional structures based on MAPs, namely coatings and hydrogels. It is well known that to nanofabricate thin and ultrathin films different techniques have been used, namely the Langmuir-Blodgett (LB) technique, the self-assembled (SAM) monolayer method and the Layer-by-Layer (LbL) technique [31-34]. The LbL approach was discovered by Decker and co-workers in 1992 [31, 35]. It is a cheap [31, 36, 37], effective [34], flexible [34, 37, 38], reproducible [34], simple [12, 31, 34, 36-42], versatile [34, 36, 37, 39-45] and efficient [37, 45] methodology. Furthermore, it allows the union of different polymers without the need to create mixtures between them [46] and the creation of complex structures [37, 41] to a nano-scale level [12].

Many hydrogels have been produced with natural-based polymers, including chitosan [47-50], hyaluronic acid [48-51], alginate [48-51], elastin [48, 49], fibrin [49-51], collagen [48-51], cellulose [47], heparin [48], dextran [47, 49], gelatin [47, 48, 51], chondroitin sulfate [48] and agarose [49-51], because natural polymers present advantages, such as biocompatibility and small toxicity [50], but there are only few papers in the literature regarding hydrogels that combine natural-based polymers and based in MAPs either using DN or poly(dopamine). Recently, the scientific community has shown interest in PDA [5]. It has similar chemical structure than DN and has different functional groups in its composition, namely the imine, amine and catechol groups [52].

Herein, with this review, we want to demonstrate the huge potential of using MAPs and its adhesive properties to produce distinct bioadhesive biomaterials. First, the main works on coatings and free-standing films produced through the LbL technique based on MAPs will be discussed. Then, an overview about natural-based hydrogels inspired by MAPs will be presented. The biomedical applications of these materials will be examined. The

importance of PDA-based coatings, films, fibers and hydrogels in the biomedical field will also be analysed.

2.2. Two-dimensional biomaterials produced by the LbL methodology based on MAPs

Beyond the LbL technique, there are two more techniques typically used to create micro- or nano-assemblies, namely the LB and SAM [33] techniques. Although these techniques are useful, the higher assembly time [33, 35, 37], the expensive equipment [31, 33, 37], the low stability on physiological environment [33, 35, 37] and the reduced types of biomolecules that can be used (amphiphilic molecules are needed) [31, 33] are the major disadvantages of these techniques.

The LbL technique allows the creation of nanostructured structures with polymers and the construction of nanostructured thin films that have been the subject of attention by the scientific community [34]. To obtain a poly(electrolyte) multilayer are needed poly(cation) and poly(anion) solutions, as well as washing solutions, shown in Figure 2.1. The first one forms cations, whereas the second one forms anions in solution [37]. Regarding the washing steps, they are needed to stabilize the adsorbed chains and not contaminate the followed poly(electrolyte) solutions [53]. Furthermore, the multilayer integrity is guaranteed by electrostatic and non-electrostatic interactions between the poly(anionic) and poly(cationic) chains [37, 53].

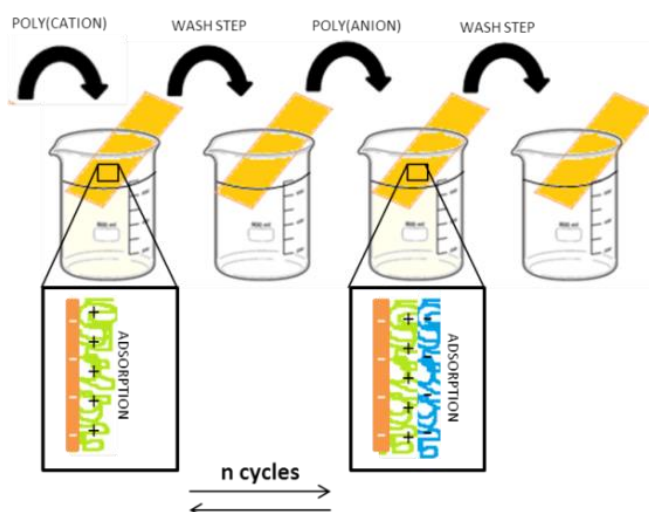


Figure 2. 2 - LbL assembly. Formation of n bi-layers by the addition of a polycation and polyanion poly (electrolyte) molecules in a negatively charged substrate. This adsorption is made mainly through electrostatic interactions.

These interactions are regulated by the ionic strength, polymer charge densities and pH [53]. LbL assembly can be performed on all types of substrates [54], with any size [37] or shape [37], such as porous [37], colloidal [37], planar [37] and cylindrical structures [37], as it can be seen in Figure 2.2. The LbL assembly allows including filler charge, such as carbon nanotubes [35, 37, 40], clays [37, 40], inorganic dyes [35, 37], metal oxides [37], particles [37] and nanoparticles [35, 40]. Also, it is possible to include polymers [37], poly(peptides) [37, 40], poly(saccharides) [40], dendrimers [35, 40], nucleic acids [37, 40], proteins [37], enzymes [37], and viral constituents [37, 40] in the multilayer assembly - Figure 2.2. Beyond the electrostatic interactions, there are many other types of interactions that can allow the film production, such as covalent bonding [35], hydrogen bonding [35], hydrophobic interactions [35], biological recognition [35] and charge transfer [35]. Moreover, beyond the poly(electrolyte) molecules complementarity (needed to assure the film production), internal and external parameters can alter the physicochemical properties of the poly(electrolyte) multilayer film. The internal parameters depend on the polymer properties, such as ionic strength [40, 55], polyion solution concentration [55] and solvent quality [37], among others. The external parameters are changes in pH [40, 55] and temperature [40, 55], among others. Both can affect the swelling or shrinking ability [37], stability [55], wettability [37], stiffness [37], as well as their structure [37] and thickness [37, 55] of the created PEM film. More information can be found in detail in [37, 40, 55].

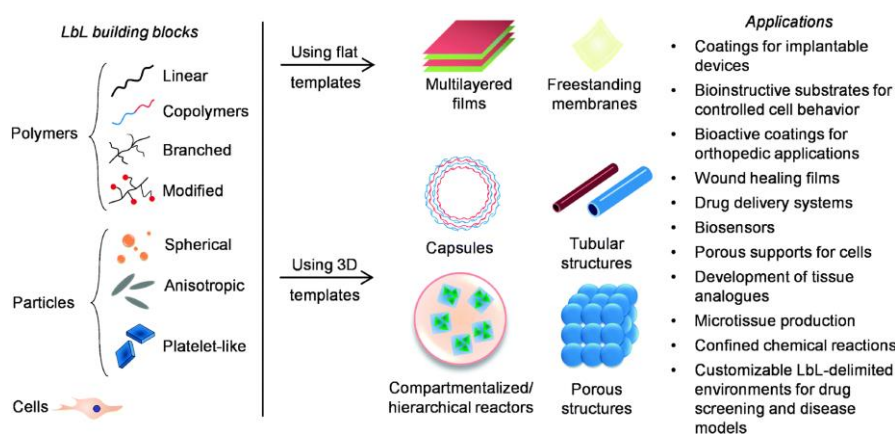


Figure 2. 3 - Building blocks (polymers, particles or cells) used in LbL assembly (2D and 3D) and their biomedical applications [40].

There are many applications for films produced by the LbL technique in the biomedical field, such as coatings production for enhanced cell and protein adhesion [35], drug delivery systems [31, 35, 39, 46, 55], films for hepatic tissue engineering [39] and

antibacterial coatings [39, 41]. Herein only two-dimensional biomaterials based on natural polymers will be showed, although, the creation of coatings and adhesives using synthetic polymers for biomedical applications is also possible and can be found in [56, 57]. By using MAPs, which have amine and catechol functional groups, it is possible to create an LbL assembly using these proteins as primers or substrate on all types of surfaces [54]. Indeed, Lee and co-workers [54] used the LbL technology to produce a poly(electrolyte) multilayer film using poly(ethyleneimine) (PEI) functionalized with catechol groups and HA-DN on different substrates. First, LbL assembly using PEI-DN/HA-DN was done upon a poly(tetrafluoroethylene) substrate. The results showed that the wettability significantly decreased after PEI-DN/HA-DN adsorptions. Also, different substrates, such as noble metals, polymers and oxides were used and the results showed that the catecholamine polymers simplify the LbL assembly. Neto and co-workers [12] developed a thin film using chitosan (CHT) and HA-DN. The results showed that the produced film through the LbL process with HA-DN, had higher adhesion strength, 2.32 ± 2.20 MPa compared to those who did not contain DN, CHT / HA, 0.75 ± 0.14 MPa. Furthermore, films with DN presented higher cellular adhesion, proliferation, viability and could be used as adhesives of implants [12]. Zhang and co-workers [58] developed multilayer coatings of CHT and HA-DN on an inorganic substrate, a titanium alloy, namely Ti-24Nb-2Zr. DN was used to the detriment of either PEI or poly-L-lysine, to improve the adhesion between CHT and HA and titanium alloy, since PEI and poly-L-lysine are cytotoxic and their use in biomedical applications is limited [58]. The obtained results showed that the addition of CHT and HA-DN multilayers caused a decrease in surface roughness. Cell studies revealed that catechol groups enhanced the osteoblast proliferation and the LbL methodology can be used as implant modifier [58].

Neto and co-workers [4] developed a film containing a superhydrophobic character of lotus leaf and the adhesive performance of MAPs, just in one material. The water contact angle (WCA) measurements results showed the correct modification of the poly(styrene) to a superhydrophobic surface, because the WCA increased to $156.2^\circ \pm 0.3^\circ$, comparing with the control one, $98.9^\circ \pm 1.1^\circ$. On the other hand, the surface which contained poly(3,4-dihydroxystyrene-co-styrene) (75%/25% mol, respectively) showed a WCA value of $73.8^\circ \pm 1.05^\circ$. Furthermore, the adhesion tests performed to poly(3,4-dihydroxystyrene-co-styrene) with oxidant revealed that it adheres to all studied surfaces, namely steel, glass, PTFE and porcine skin. Neto and co-workers [59] produced HA-DN and HA with excess of DN (HA-4DN). They used a poly(styrene) superhydrophobic

surface patterned with wettable regions to study different assemblies (5, 10 and 15 bi-layers). The results revealed that the adhesive strength was higher for multilayers films with higher concentration of dopamine (4DN) comparing with the control one (1DN) and this adhesion strength increased with the increase of the number of bi-layers. Moreover, coatings containing DN ([CHT/HA-DN]_{5,10,15} and [CHT/HA-4DN]_{5,10,15}) revealed enhanced cell adhesion (SaOs-2 and L929) than the control ones. These coatings are useful for the biomedical field, to develop wound healing bandages, coatings for optimized cell–substrate interaction or surgical sealants [59]. Recently, coatings that are simultaneously inspired by MAPS and that mimic the structure of nacre were developed [60, 61]. First, a coating containing ternary bioglass nanoparticles, HA-DN and CHT was proposed. The results showed that the produced coatings containing HA-DN led to an enhancement of adhesion strength [61]. Moreover, cell studies performed with L929 cells line showed higher viability, adhesion and proliferation for the formulations containing DN. [61]. A coating containing silver doped bioglass nanoparticles, CHT) and HA-DN was also produced [60], with an antibacterial action combined with enhanced adhesion strength - Figure 2.3 – A and B.

The LbL technique also allows the free-standing films processing [62]. There are few papers in the literature about free-standing films production which contain DN and natural-based biopolymers with a nacre-like structure. However, in general, we can conclude that the nanofiller incorporation into a free-standing film leads to better mechanical properties. Tang and co-workers [35] showed that the nanofiller, Na⁺-Montmorillonite clay, with the addition of poly(ethylene glycol), lysine and DOPA led to better mechanical properties. These properties were due to the crosslinking process with iron ions that formed complexes with DOPA.

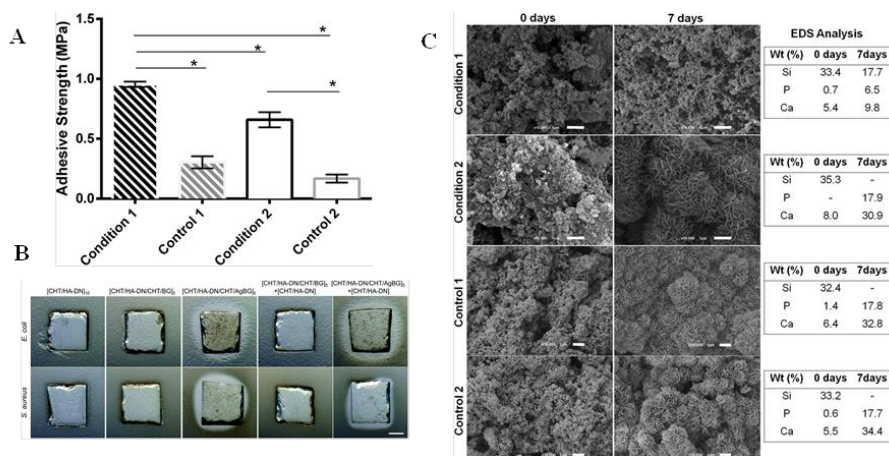


Figure 2. 4- (A) Adhesive strength of four LbL film conditions. Statistically significant adhesive strength as compared with distinct conditions is shown (*p< 0.05), n = 5; mean ± standard deviation condition

shown, **(B)** Photograph of Layer-by-Layer (LbL) coatings 16 h after being placed on top of a Mueller-Hinton agar plate with *E. coli* and *S. aureus* (1.5×10^8 CFU) incubated at 37 °C, **(C)** Representative SEM micrographs and respective quantitative EDS spectra analysis before and after SBF immersion for 7 days. The scale bar represents 1 μm . Condition 1: [CHT/HA–DN/CHT/AgBG]₅ + [CHT/HA–DN], control 1: [CHT/HA/CHT/AgBG]₅ + [CHT/HA], condition 2: [CHT/HA–DN/CHT/AgBG]₅, and control 2: [CHT/HA/CHT/AgBG]₅ [60].

2.3. Three-dimensional biomaterials: hydrogels production based on MAPs

The necessity to create biomaterials that could be used in several applications, such as tissue adhesives, drug delivery systems, bandages or bleeding barriers that can act as wound healings has been felt for long [8]. Hydrogels have a three-dimensional structure [47-49, 63-65] and are used because they are biocompatible [48, 66, 67], biodegradable [7], and present flexibility [66], softness [66], high porosity [65], extracellular matrix (ECM) likeness [48, 49, 68] and high water content [66]. They are made with hydrophilic polymers [65] and can swell in contact with body fluids or water [47-49, 63, 64]. Furthermore, the capability of either synthetic or natural polymers crosslinking, by either physical or chemical way, is indispensable for hydrogels production [48, 66]. Hydrogels that can respond to pH or temperature stimulus are called stimuli-responsive hydrogels [69]. Furthermore, with pH variation there is swelling or deswelling behaviour, presenting an advantage for the biomedical field, whereas hydrogels that changes their properties according to the temperature are called temperature reversible hydrogels [69]. They are useful for biomedical applications, such as film cleaning/separation, drug delivery systems and tissue regeneration [69]. According to Li and co-workers [7], injectable adhesive tissue and hemostatic hydrogels have been used, because they present easy manipulation and mimic the extracellular matrix of the cells. The biological tissue adhesives present several advantages, namely biodegradability and biocompatibility, but they also present great disadvantages, such as poor mechanical properties and low adhesion strength [70].

There can be found in literature two kinds of hydrogels inspired by MAPs: i) made through complexation between metal ions, usually iron metals (Fe^{I} , Fe^{II} and Fe^{III}) and the catechol moiety, known as stereo-complexed hydrogels, and ii) covalent crosslinked hydrogels. As far as the stereo-complexed hydrogel creation is concerned, mussels have in their constitution iron ions present in their byssus coating [71]. Moreover, there is the formation of stereo-complexes between the Fe^{III} ions and catechol groups present in DOPA, shown in Figure 2.4-A. This complexation is pH-dependent, allowing self-healing and higher strength properties [71], such as extensibility and high hardness [72]).

Krogsgaard and co-workers [71] developed a chitosan-catechol conjugated hydrogel with Fe^{III} . The results showed that the storage modulus increased until the pH reached the physiological pH. After that, at basic pH, the storage modulus backed down. The maximum storage modulus for Fe^{III} -chitosan-catechol hydrogel was near to 30 kPa, near to its pKa value, shown in Figure 2.4-C. Furthermore, the maximum storage modulus decreased along the coordination metals group, $\text{Al}^{\text{III}} < \text{Ga}^{\text{III}} < \text{In}^{\text{III}}$ [8]. Moreover, and according to the same author [71], for diverse applications the uncolored hydrogels are preferred. Accordingly, the influence of the coordinating metal choice (Al^{III} , Ga^{III} and In^{III} gels) in the hydrogel color and self-healing capacity was studied - Figure 2.4-B. It was found that the color can be tuned changing the metal and the antioxidant agent (oxygen or nitrogen) [71].

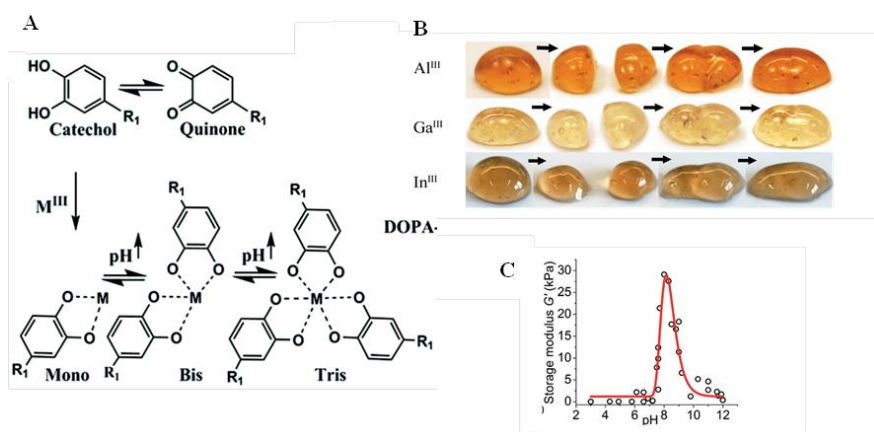


Figure 2. 5- (A) Conversion of catechol groups (un-oxidized) into quinone species (oxidized form) and complexation: Mono; Bis and Tris with metal ions, (B) Qualitative tests performed to study the self-healing properties of Al^{III} , Ga^{III} and In^{III} gels, and (C) Storage modulus variation (G') in function of pH. The red line serves as a guide to the eye. Adapted from [71].

Holten-Andersen and co-workers [73] studied the stereo-complex formation between the iron ions and the $\text{PEG}-(\text{N-Boc-dopa})_4$ and two different crosslinking agents. The first one was the pH change and the second one was the sodium periodate addition. The results revealed for the first one, that the Fe^{I} -DOPA is present when the pH values are below 5.6, whereas Fe^{II} -DOPA and Fe^{III} -DOPA are present, overall, at pH between 5.6 and 9.1 and above the last value, respectively. Moreover, the Fe^{III} - $\text{PEG}-(\text{N-Boc-dopa})_4$ hydrogel recovered its storage modulus and cohesiveness after shear strain failure. As far as the second one is concerned, $\text{PEG}-(\text{N-Boc-dopa})_4$ crosslinked with sodium periodate, it did not recover. Summarizing, Fe^{III} - $\text{PEG}-(\text{N-Boc-dopa})_4$ presented an advantage when compared with the covalent crosslinked one, because it presented self-healing ability. In another work, developed by Krogsgaard and co-workers [17], the self-healing capacity of

hydrogels made by DOPA-functionalized with a synthetic polymer, namely polyallylamine was studied. The influence of iron addition and the complex formation depending to the pH variation was studied. It was found that catechol-Fe^I complex was dominant in a pH range from 1 to 5, catechol-Fe^{II} in a pH range from 5 to 10.8 and, finally, catechol-Fe^{III} in a pH ranges from 10.8 to 12. The created hydrogels showed self-healing properties, once the obtained storage modulus value ($G' = 4700$ Pa) after the experience (dynamic oscillatory rheology) had had a similar value to the initial one ($G' = 3800$ Pa). Furthermore, the pH variation showed the reversible character of the studied hydrogel. This kind of hydrogels is advantageous in drug delivery systems. Furthermore, beside the coordinative complexes, the Fe^{III} ions are responsible for the oxidative character in the catechol moieties present in CHT-catechol hydrogel under acidic pH (with 5 % acetic acid) [72]. In this study, another crosslinking agent, sodium periodate, was tried. The results showed that when increasing the molar ratio of IO⁴⁻ and catechol between 1:1; 1:2 and 1:3, a decrease of the gelation time happened with an increase of the catechol ratio. Instead, for Fe^{III}-CHT-catechol crosslinking, the gelation time increased with the increase of molar ratio between Fe^{III} and catechol: 2:3 to 3:3, inducing the formation of mono-catecholate species, preventing the coordination complexes. In another study, Choi and co-workers [70] developed an in-situ crosslinkable hydrogel made by gelatin from human adipose tissue, modified by tyrosinase and crosslinked by Fe^{III} ions. Gelatin was used, because it was biocompatible and biodegradable [70] and many hydrogels have been produced, and reported in the literature, based on natural polymers, including gelatin [47, 48, 51]. DOPA molecules were formed with tyrosinase from gelatin and put in contact with FeCl₃ solution at 37 °C. The hydrogel was produced mixing the solution with the metal ions by coordination and oxidation of the catechol moieties. An adhesive, biocompatible and hemostatic hydrogel was produced, which showed hemostatic properties in rat liver, evidencing the ability to be used as a tissue adhesive for surgical applications. The main conclusion of these works is that the iron ions and its complexes formed with catechol moieties were responsible for the mechanical properties shown by hydrogels.

Regarding the covalent crosslinked hydrogels, different natural-based polymers were used in order to produce hydrogels with DN and its analogues, such as alginate [74], chitosan [14] and hyaluronic acid [27, 75]. Hong and co-workers [27] developed a hydrogel made with HA-DN that presented either adhesive or cohesive properties. The second one is important for hydrogels creation, due to the oxidation of catechol groups,

originating quinone species (highly reactive). The results showed that an hydrogel was formed in an accelerated manner when the ratio between the oxidizing agent, sodium periodate, and the catechol content present in the hyaluronic acid was 1.5:1, shown in Figure 2.5. Moreover, the rheometric analysis revealed a storage modulus near to 550 Pa and a loss modulus with value of 200 Pa. Cell studies performed with human Neural Stem Cells (hNSC) revealed viability and stability, showing that this hydrogel had applications in neural tissues, especially for cells encapsulation.

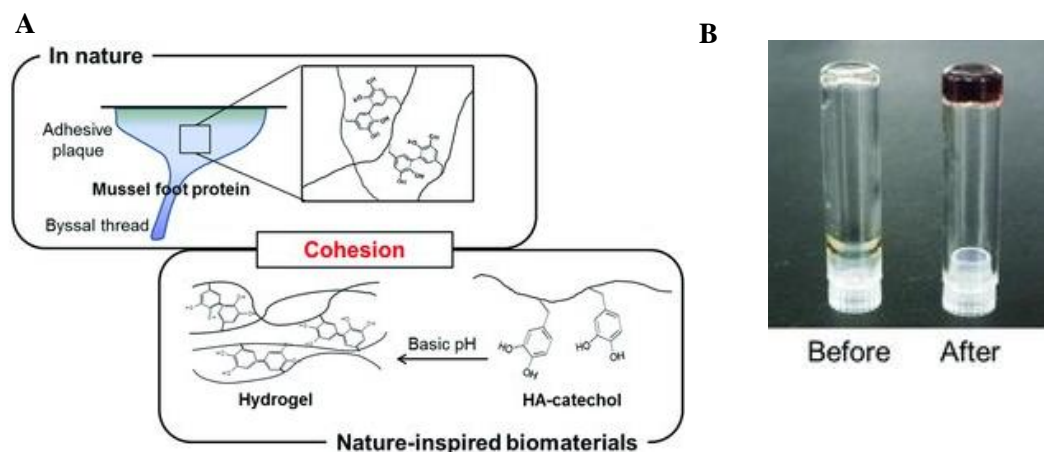


Figure 2. 6- (A) Schematic representation of the Byssal thread of marine mussel with its adhesive plaque and its adhesive character, but also its cohesive character. The last one is responsible for hydrogels creation in basic pH through intermolecular catechol-catechol reactions, (B) Photograph of the HA-catechol (HA-DN) hydrogel. Adapted from [27].

The catechol conjugation with natural-polymers is possible as it is shown above. Alginate is a linear polysaccharide composed by β -(1-4)-D-mannuronic acid and α -1-4-L-guluronic and it is originated from brown seaweed and bacteria [68]. Alginate is a copolymer made from mannuronic (M) and guluronic (G) monomers [68]. Commonly for alginate gels formation divalent cations, such as, Ba^{2+} , Sr^{2+} and Ca^{2+} are used. Ionic bridges are formed between G monomers dispersed around polymer chains [68]. However, Lee and co-workers [74] used a different approach. A gel made with alginate inspired by MAPs was produced, using sodium periodate as oxidizing agent with an equimolar ratio between IO_4^- and catechol. The hydrogel was formed after 3 to 4 minutes, due to the quinone-quinone bonds creation. The rheological analysis showed a storage modulus (G') value of 378.9 ± 38.9 and 5445.3 ± 666.6 Pa for alginate-catechol conjugate hydrogel with two different concentration (2 % w/v and 4% w/v), respectively. The obtained result was 10 times higher than the control one (hydrogel made through divalent cations). Release studies were done using alginate-catechol hydrogel obtained through sodium periodate as oxidizing agent, alginate-catechol hydrogel obtained through calcium ions and alginate crosslinked with Ca^{2+} ions, as a control. The results showed

that the first one didn't release basic fibroblast growth factor (bFGF) but the second one released 10% of bFGF. It was revealed that the oxidizing agent had impact in the released profile of alginate-catechol hydrogel. These hydrogels can be used in several biomedical applications, such as cell therapy and tissue engineering. Another work developed by Lee and co-workers [6] showed a temperature-reversible and injectable hydrogel made by HA-DN and thiol-Pluronic F127 composite. The results showed that the developed hydrogel was adhesive and its adhesion was due to the covalent interactions formed between the unreacted and oxidized catechol groups and the thiol groups of the surrounding tissues. Ryu and co-workers [14] developed a chitosan-dopamine conjugate (CHT-C) thermosensitive composite hydrogel with thiol-terminated Pluronic F-127. The CHT-C/Plu-SH nanocomposite hydrogel showed excellent tissue adhesiveness, with an adhesion force of 15.0 ± 3.5 kPa, revealing to be advantageous when used in tissue regeneration and tissue adhesives for drug delivery systems. Cencer and co-workers [76] developed hydrogel made using a 4-armed-PEG end-capped with DN and studied the influence of pH variation on adhesive properties. The results showed that the curing rate was lower for low pH. For higher pH values, pH=8, the average molecular weight between crosslinking was higher implying lower mechanical properties and higher crosslinking density. The compression tests performed in all studied conditions showed that the hydrogel produced in pH = 7.4 presented the highest compressive stress and toughness. At this pH, a good equilibrium with curing rate and mechanical properties was achieved [76].

2.4. Polydopamine - based Biomaterials

PDA is a pigment of melamine, called eumelanin. It has a chemical structure similar to DN and it has different functional groups in its composition, namely the imine, amine and catechol groups [52]. PDA can be formed by the oxidative polymerization of DN [52, 77, 78], usually with a concentration above 2 mg/mL [52, 77], as well as norepinephrine and L-DOPA [78] solutions. This oxidation is done under aerobic conditions and at a pH > 7.5 [52, 77-79].

The formation of PDA has been explained through a covalent polymerization, when there is the oxidation of the catechol groups to dopaminequinone [80]. The oxidation and further polymerization, i.e., deprotonation and intermolecular Michael addition reaction of dopaminequinone leads to the formation of PDA. This process is done under alkaline

and aerobic conditions. The formation of PDA has also been explained as a self-assembly process. However, according to Hong and co-workers [81], PDA can be formed by a covalent reaction and also by non-covalent self-assembly. The last one is due to the self-assembly between unpolymerized DN and 5, 6-dihydroxyindole, due to cation- π , quadrupole-quadrupole, π - π , ionic and hydrogen bonding interactions. Covalent and non-covalent assemblies are important to PDA formation, because the oxidation and self-polymerization are simultaneous. The DN oxidation and the formation of PDA induces a color change from pale brown to deep brown, meaning that polymerization occurred. Unlike DN, PDA is highly stable [82]. Various substrates can be coated with PDA, namely distinct ceramics such as silica and aluminum oxide, metals such as stainless steel, synthetic polymers, including PTFE, and magnetic and gold nanoparticles [79]. Furthermore, the coating thickness is dependent of the concentration, reaction time, solvent, additives and pH [79]. PDA presents strong adhesion to virtually all types of substrates [52, 83]. PDA adhesion on diverse substrates is done through chelation bonding (Fe^{III} [20] or TiO_2), covalent bonding (thiol or amine groups) and hydrogen bonding (SiO_2) [84]. The successful or unsuccessful deposition of PDA in a substrate can be evaluated by its hydrophilicity [5]. According to d'Ischia and co-workers [85], PDA presents high adhesiveness due to the combination of different functional groups present in lysine and DOPA. Moreover, their adhesiveness can also be justified by non-covalent or covalent binding [52, 83]. Non-covalent adhesion is justified by non-covalent bonding with metal oxides or metal substrates, using metal coordination or chelating, π - π interactions, hydrogen bonding, covalent bonds and charge-transfer [5, 52, 83]. These interactions are made by amino, quinone, carboxyl, phenol and imine functional groups present in PDA [5]. Covalent adhesion is also possible and relies on the covalent bonding between the amine and thiol groups, via Schiff base reactions or Michael addition, when the pH value is above 7 [52, 83].

PDA has several advantages when used in the biomedical field, such as: it is biocompatible [86-88], it is hydrophilic [86] and it has the facility to functionalize different substrates [86, 87]. Moreover, it has low cytotoxicity and it presents high adhesion and proliferation of cells [88]. Besides, it is used in the biomedical area for several applications, such as in drug protein purification [87], delivery systems [87], enzyme immobilization [87] and chemo/biosensing [87]. It has been used to produce coatings and films, fibers, capsules and spheres (hollow and/or dense) and hydrogels. In the next sections their applications in the biomedical field will be discussed.

2.4.1. PDA-coated Biomaterials

As it is said above, PDA is used to produce coatings which allows a big range of possible applications in the biomedical field, namely in the tissue engineering area such as nerve/neural tissue regeneration [89-91], in devices to be in contact with blood [92-94], in the orthopedic area [89, 95], drug delivery systems [96], control material-cells interactions [89, 97, 98], anti-fouling surfaces [99] and biosensors [100], as well as in the prevention of protein adsorption [84] and separation [101].

As far as the neural tissue generation is concerned, Ku and co-workers [89] studied the influence of cell viability and adhesion. Mouse osteoblast MC3T3-E1 and rat pheochromocytoma PC12 cell lines were used on various substrates modified and unmodified with PDA. Different surfaces were studied, such as poly(tetrafluoroethylene), poly(ethylene), poly(dimethyl-siloxane), silicone rubber and glass (control). The results revealed that the modified surfaces allowed a good cell adhesion on all substrates. Furthermore, the projected area of the cultured cells on un-modified and modified substrates was studied. 1600 to 2000 μm^2 per cell was obtained for cell on modified surfaces, whereas for the control ones only 600 μm^2 of projected area per cell (mouse osteoblast MC3T3-E1) was obtained. This study allowed the inference that the PDA ad-layer is non-toxic for cells. For PC12 cell lines, the projected area of the cultured cells revealed higher values for the modified substrates too. In another study, Bhang and co-workers [91] studied the influence of PDA-gelatin-poly(styrene) coating on pheochromocytoma 12 cells. The results revealed that the studied condition increased the viability and cell adhesion. The authors explained these results through three different ways. 1) the PDA coating can be useful for material-cells interactions, because it enhances the PC12 cells adjusting its surface energy; 2) the WCA result for PDA coating was 40.2° and this could enhance the PC12 cell proliferation; and 3) The amine groups present in PDA coating (positively charged) and glycoproteins present on cells membrane (negatively charged) could enhance the adhesion through electrostatic interactions. Also, PDA can be useful as a coating or “priming” agent which can be used in devices for blood compatibility. Accordingly, Wei and co-workers [93] developed a coating inspired in MAPs with different materials, namely polyethersulfone (PES), nylon and cellulose. Bovine serum albumin (BSA) was immobilized on the PDA layer in order to enhance the blood compatibility. The results showed that the platelet adhesion was lower for PES-PDA-BSA and this system showed better results in blood compatibility. In another work,

Wang and co-workers [92] developed a superhydrophobic assembly using modified carbon nanotubes (CNT) with PDA and PEI. The modification with PDA was done because it is useful in CNT dispersion. Furthermore, the catechol groups of PDA form covalent bonds with primary amino groups of PEI, stabilizing the film. Moreover, the developed film has applications in medical devices, proving to be adequate to stay in contact with blood. In fact, it revealed low platelet adhesion and antibacterial performance, after silane deposition, against *Escherichia coli* bacterial over 4 hours at 37°C - Figure 2.6.

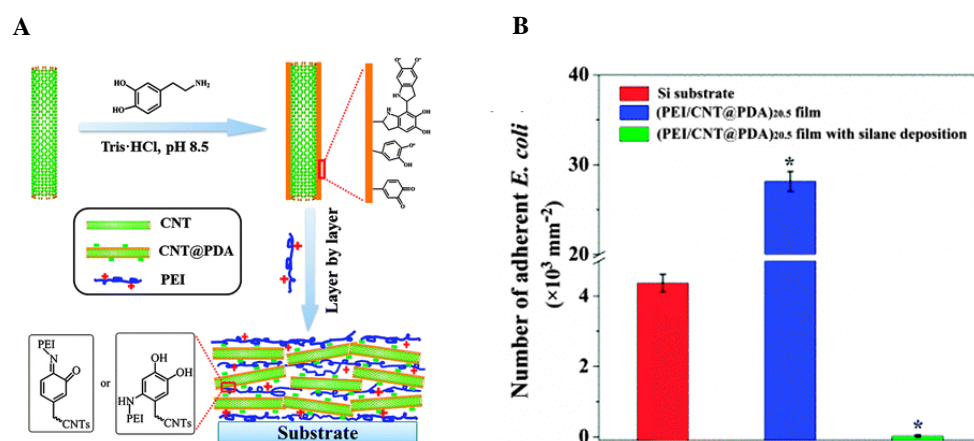


Figure 2. 7- (A) Representation of multilayered films based on poly(dopamine)-modified carbon nanotubes (CNT@PDA) and poly(ethyleneimine) (PEI) and (B) The statistical histogram of the number of adhered platelets on different surfaces. * $p < 0.05$ versus silicon substrate, and * $p < 0.05$ versus (PEI–CNT@PDA)_{20.5} film (Student's t test). Data are expressed as mean \pm SD, $n = 3$ [92].

Regarding the orthopedic area, Nardo and co-workers [95] coated a PTFE membrane using PDA and hydroxyapatite nanoparticles. The results showed that the PDA/hydroxyapatite composite exhibited hydrophilicity and higher surface roughness that is useful for osteoblast cell adhesion. Cell studies performed with pre-osteoblast MC3T3-E1 showed proliferation, due to the synergetic effect of DOPA and hydroxyapatite nanoparticles. In another work, Park and co-workers [102] developed a PDA coating functionalized with hydroxyapatite, known as PDA-assisted hydroxyapatite formation. To produce this coating different substrates were tested, namely titanium, semiconductors, stainless steel, Si, Au, ceramics (SiO_2), and polymers, such as PDMS, PS, PMMA, nylon, cellulose, PTFE and polyester. The substrates were then immersed in PDA solution and simulated body fluid during 2 days. The results showed that the surfaces were completely covered by a calcium-phosphate layer - Figure 2.7. According to the results, the catecholamine moieties present in PDA acts like a binder.

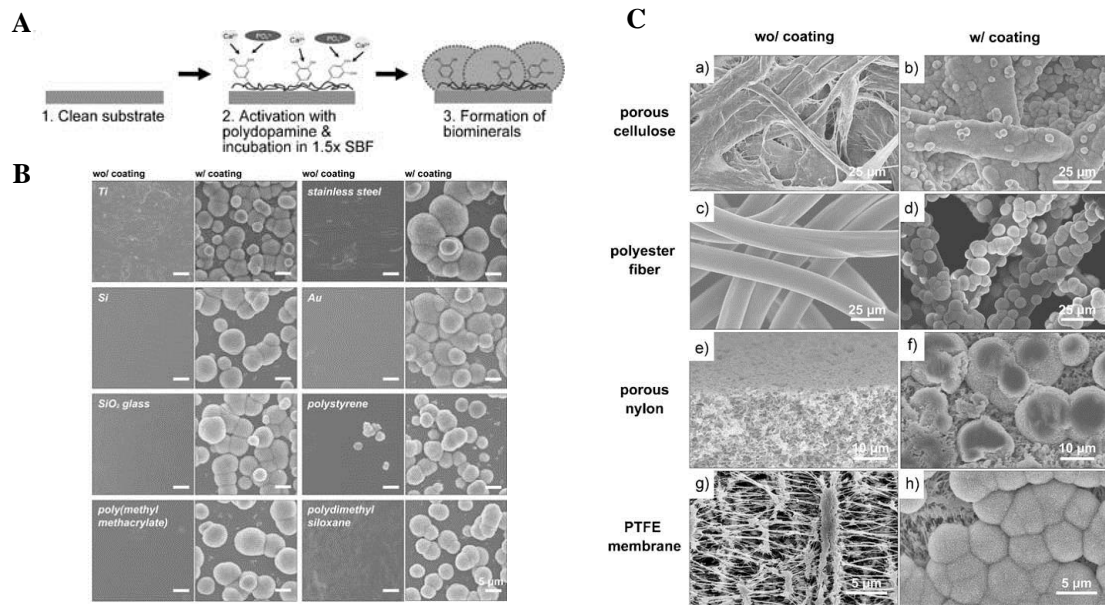


Figure 2. 8- (A) Schematic representation of calcium phosphate (Ca-P) biominerals into a poly(dopamine) coating, a catecholamine, inspired by the adhesion mechanisms of mussels. (B) Material-independent hydroxyapatite formation via pHAF. The SEM images show that hydroxyapatites can cover any material surfaces by the enrichment of calcium ions on the polydopamine-coated surfaces. Hydroxyapatite was created on a wide range of flat solid substrates: noble metal and metal oxides [e.g., Ti, stainless steel (SUS 316L), Si, Au], ceramics (e.g., SiO₂ glass), and polymers [polystyrene, poly(methyl methacrylate), polydimethylsiloxane]. The scale bar represents 5 μm. and (C) The fabrication of organic–inorganic hybrid materials via pHAF. The SEM images demonstrate that the hydroxyapatite crystals can be integrated into 3D porous materials in a material-independent manner. The tested 3D materials of porous cellulose, polyester fiber, porous nylon, and PTFE membrane were hybridized with hydroxyapatites. All the materials were incubated in 1.5× SBF for 2 days at 37 °C after polydopamine treatment [102].

PDA allows the production of micropatterns which can be used as a control of material–cells interactions. Ku and co-workers [98] developed a biomimetic stable, versatile and simple cell-adhesive micropatterns surface based on MAPs, using PDA. The studied cell lines were put in contact with the poly(dimethylsiloxane) substrates - Figure 2.8. Different cell densities were used, such as fibrosarcoma HT1080, used to screen anticancer drugs, mouse fibroblast NIH-3T3, used as a model cell line for cell-based devices, and mouse preosteoblast MC3T3-E1, relevant to study cell–material interaction and for bone tissue engineering. The results revealed that the studied cell-lines only adhered to PDMS-PDA substrate, showing well-organized cytoskeletons.

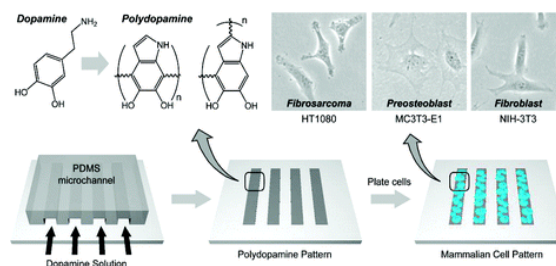


Figure 2. 9 - Schematic illustration of polydopamine-based cell patterning using microfluidics. Adapted from [98].

Another interesting application of PDA coatings is related with inhibition of protein adhesion into a substrate due to their antifouling characteristics. For example, Dang and co-workers [83] showed that the functional groups present in PDA can serve as a biofouling. They studied the effect of platelet, L929, *Escherichia coli* and *Staphylococcus aureus* bacteria adhesion - Figure 2.9. The results showed that the attached biofoulings are higher for higher PDA thickness, because the available surface area increased when the coating thickness increased too. The biofouling property showed by PDA is due to its $-NH$, $-OH$ and $-NH_2$ functional groups. There are different treatments to overcome this drawback, such as oxidation, thermal treatment, coordination and grafting.

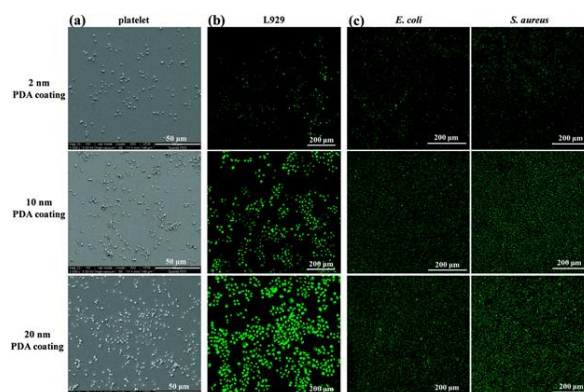


Figure 2. 10 - (A) SEM images of adhered platelets, (B) inverted fluorescence microscopic images of attached L929 fibroblast cells, (C) CLSM fluorescence microscopic images of attached *E. coli* and *S. aureus* on PDA coatings with different thicknesses. The tested coatings were prepared by immersing clean glass substrates in 2 mg ml^{-1} dopamine Tris/HCl (pH 8.5) buffer for 30 min, 3 hours or 6 hours, and then thoroughly rinsed with Millipore water and dried with nitrogen before using [83].

In another work, Huang and co-workers [84] developed a gold substrate with a surface modification with PDA and hyaluronic acid. The results revealed that this surface modification led to a WCA decrease (84.9° - only Au) to 42.5° (Au-PDA) and 24.8° (Au-PDA/HA), allowing the inference of the correct surface modification. Moreover, the authors studied the nonspecific protein adsorption with BSA on its surface. The Au-PDA film had similar results than the control one (only Au - 207.8 ng/cm^2), but for the co-deposited PDA/HA film, the obtained value was less than 5 ng/cm^2 . This can probably be explained by the electrostatic repulsion between HA and PDA, allowing adsorption protein resistance. Other proteins were chosen, namely lysozyme, β -lactoglobulin (β -LG), fibrinogen, blood serum and soybean milk. The results revealed low adsorption values for β -LG, BSA and lysozyme, but higher values for the other proteins in study. Furthermore, the produced films could be re-used, being, therefore, useful for diverse applications.

PDA can also be used to produce coatings not only on 2D, but also on 3D biomaterials. To this end, PDA can coat 3D spheres and capsules (hollow or dense) and fibers. Currently, there are two different solvents used to produce a PDA layer on iron oxide nanoparticles surfaces: water with the addition of a base in aerobic conditions and water-ethanol with a buffer solution (Tris) [87]. The last one allows the reduction of the self-polymerization rate of DN, implying a surface modification more controllable [82, 87]. Hollow capsules made by PDA can be produced and have applications in drug delivery systems [103]. It's possible to produce hollow capsules using PDA films deposited on colloidal surfaces, presenting several advantages in the biomedical field, because PDA acts as biomineralization agents. Furthermore, this surface modification can be used in microfluidics [78]. The hollow capsules are formed after the dissolution of the core. Hollow capsules have a pH dependent permselectivity, thanks to their negative surface charge, i.e., for pH above 4, they permeate cations, whereas, they permeate anions in pH below 7. This capacity is useful, for instance, for drug delivery systems.

PDA can be used to coat Fe₃O₄ magnetic nanoparticles, in detriment of Au [104] or SiO₂ [105] coatings in order to allow NPs dispersability. Superparamagnetic iron oxide nanoparticles, known as SPIONs, present superparamagnetic properties. They can and have been used in magnetic resonance imaging, being useful for disease diagnosis and treatment monitoring, namely cancer therapy. The great advantage of SPIONs is acting as tumor targeting and drug delivery systems for its therapy [106]. Not only Fe₃O₄ magnetic nanoparticles are produced and surface modified with PDA, gold nanoparticles [88] have also been used in the biomedical field. Fe₃O₄ magnetic nanoparticles have been used due to its physical and chemical properties [103, 107, 108] in biomedical applications [107, 108], such as in drug delivery systems [103, 107, 109-111], in magnetic resonance imaging [107, 112], in molecular detector and separator [86, 112], at immunoassay analyzer [107] and cancer therapy [106, 107, 113]. Si and Yang developed [110] Fe₃O₄@PDA core/shell spheres. They could tune the size and the shell thickness of spheres. A PDA coating was obtained through self-polymerization of DN, its monomer, and the obtained shell thickness was 15 nanometers, shown in Figure 2.10. The authors studied the possibility of changing the Fe₃O₄@PDA nanoparticles size, either modifying the shell or the core. The shell thickness can be easily tuned changing the concentration of monomer used to produce PDA. There was 10 nanometers (15 to 25 nm) difference on shell thickness changing the DN concentration from 8×10^{-4} to 12×10^{-4} M.

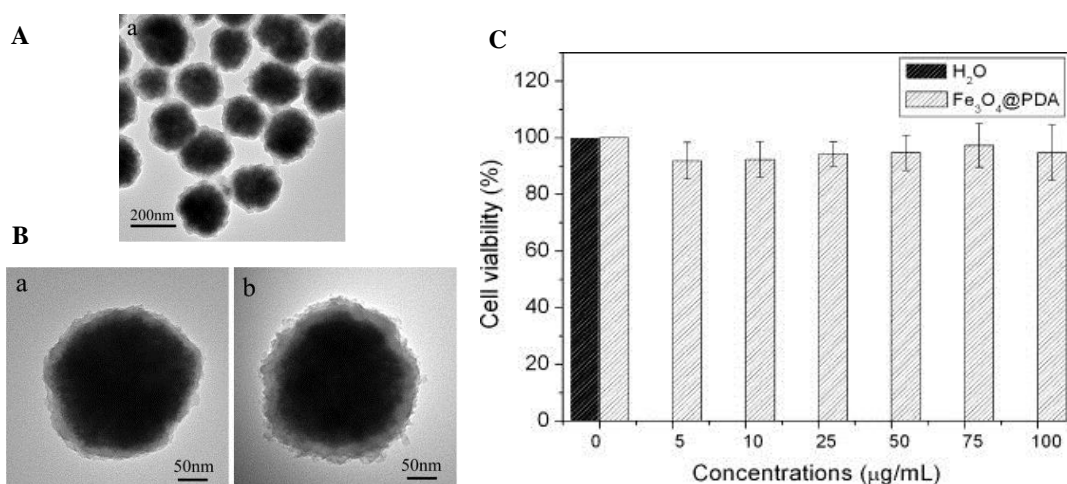


Figure 2. 11 – (A) TEM images of the Fe₃O₄@PDA microspheres with well-defined core shell nanostructure (PDA (shell) thickness - 15 nanometers (nm)), (B) TEM image of the Fe₃O₄@PDA microspheres based on 200 nm Fe₃O₄ sub-microspheres with different shell thicknesses: (B-a) 15 nm (B-b) 25 nm (the superficial roughness increases with higher DN concentration) and (C) The viability of cells (%) incubated with the Fe₃O₄@PDA microspheres at different concentrations (µg mL^{-h}). Adapted from [110].

Regarding the Fe₃O₄ magnetic nanoparticles, Zhou and co-workers [86] developed superparamagnetic Fe₃O₄ nanoparticles with a PDA coating. The TEM results showed that the surface modification with PDA was correctly done and had 10 nm of thickness. The created nanoparticles showed superparamagnetic properties, which could be separated just by a strong magnetic action. Moreover, hemoglobin protein was embedded in the PDA layer. After removing the imprinted sites, forms with complementary shapes to the hemoglobin were obtained. The results revealed that the produced imprinted Fe₃O₄ nanoparticles bonded preferentially to hemoglobin, equine myoglobin and horseradish peroxidase. This imprinted ferromagnetic revealed to be an interesting tool to recognize proteins. Moreover, PDA coatings present big advantages since it can be used in diverse biomedical applications. Hang and co-workers [113] produced PDA core-shell nanoparticles that can be used for tumor therapy applications. The core is constituted by PDA and the shell is composed by a photo-activator of photosensitizers conjugated with hyaluronic acid (PS-HA). The shell is responsible for energy transfer from the shell to the core, implying the creation of singlet oxygen generation and fluorescence emissions when the laser beam is acting. The results revealed excellent anti-tumor properties, being useful for a new generation of photodynamic tumour therapy.

PDA is also useful to coat nanofibers obtained through electrospinning [114]. PDA allows better biomaterial-cell interactions [115] and has several biomedical applications, namely vascular [116], cardiac [115, 117] and bioengineering [118] area, as well as for drug delivery systems and tissue engineering [114]. Although the processing of nanofibers is

made using synthetic polymers, such as poly- ϵ -caprolactone, among others, PDA is used as a surface modifier. In our opinion, it is relevant to show PDA potential, because many efforts have been made to create synthetic polymers with the same adhesive properties shown by marine mussels [29]. For this reason, Ku and Park [116] developed polycaprolactone (PCL) nanofibers with a PDA ad-layer. To the purpose of their study, in order to increase the attachment and proliferation of endothelial cells for vascular applications, a PDA ad-layer was used. For that, three different conditions were studied: unmodified PCL as a control, PCL-gelatin and PCL-PDA. The water contact angle (WCA) measurements results corroborated the successful incorporation of PDA, because the surface became completely hydrophilic. Furthermore, the cell culturing results of the three different samples with human umbilical vein endothelial cells (HUVECs) showed that PDA coated-PCL nanofibers presented an enhanced adhesion, proliferation and viability, even in non-adherent substrates, such as poly(dimethylsiloxane), polyethylene, silicone rubber and poly(tetrafluoroethylene).

2.4.2. Hydrogels production based on PDA

Douglas and co-workers [119] produced a gellan gum hydrogel incorporated with alkaline phosphatase (ALP), in order to induce mineralization after immersion in calcium glycerophosphate (CaGP) solution. Also, PDA was incorporated on its constitution. It was found that the hydrogel changed its color to dark-brown, meaning that the self-polymerization reaction occurred, shown in Figure 2.11 - A. After immersion in CaGP solution, mechanical tests were done, showing that the increase of the alkaline phosphatase concentration resulted in an increase in Young's modulus-Figure 2.11 - C.a. Moreover, the autoclaving process led to hydrogel disintegration, when it was not in contact with CaGP solution. The PDA presence led to an increase in Young's modulus when the hydrogels were immersed from 0 to 4 hours. After that time, the hydrogel were saturated with PDA, shown in Figure 2.11-C.b. Cell studies performed with osteoblastic cell line MC3T3-E1 seeded onto hydrogel samples revealed that the best results were achieved for the formulation composed by alkaline phosphatase and PDA, because there was cells proliferation and viability, shown in Figure 2.11-B. Summarizing, PDA bind calcium ions present in CaGP solution, acting as a Ca-P nucleation agent. This hydrogel could be used in the orthopedic area.

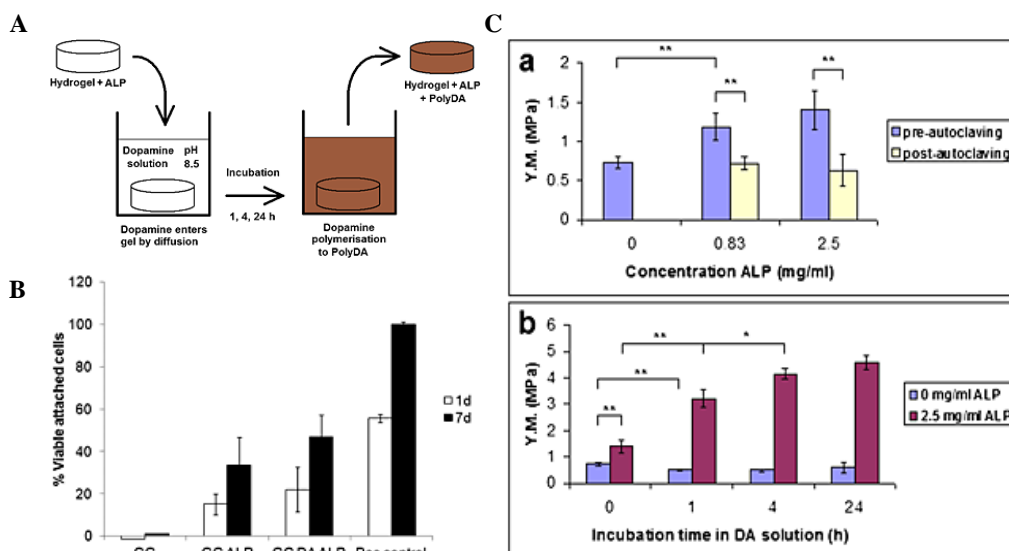


Figure 2.12 – (A) Mechanism of poly(dopamine), obtained through its monomer (DN), incorporation into Gellam Gum (GG) hydrogel. The dark-brown color meaning the correct polymerization reaction of poly(dopamine), (B) Viability of MC3T3-E1 cells seeded on gellan gum hydrogels mineralized for 6 days. GG: 0 mg/ml ALP; GGALP: 2.5 mg/ml ALP; GGDAALP: 2.5 mg/ml ALP with 4 h incubation in DA solution pre-mineralization; tissue culture polystyrene (positive control). Error bars show standard deviation and (C- a) Influence of ALP concentration and sterilization by autoclaving (n = 5). Unmineralized hydrogels disintegrated during autoclaving, (C - b) Influence of incubation time in 2 mg/ml DA solution prior to mineralization (n = 3). Significances: *, **: p < 0.05, 0.01, respectively (Student's t-test) [119].

In another recent work, Zhu and co-workers [120], developed a PDA and collagen hydrogel via collagen self-assembly. Six different formulations with different concentrations of DN (0.5 mg/mL, 1 mg/mL, 2 mg/mL, 5 mg/mL, 10 mg/mL and the pristine) were studied. The PDA-COL hydrogel was formed using 10 mg/mL of collagen with a pH adjusted to 7.4. The degradation assays revealed that the degradation properties presented higher values for lower DN concentrations. It was suggested that higher concentrations of DN formed stronger collagen fibrils inhibiting the enzymatic degradation. Moreover, AFM images revealed that when the DN concentration was increased there was a surface modification to fine and loose fibrils. This result showed that the collagen fibrils self-assembly are limited by higher concentrations of DN, corroborated by DSC analysis. Furthermore, cell studies performed with L929 fibroblasts revealed that for lower DN concentrations (0.5 and 1 mg/mL) there was higher cell proliferation and adhesion rates. Summarizing, appropriate DN concentrations can promote cell adhesion, proliferation and higher elasticity. These hydrogels creation can be used as adhesive to cells, being able to be used in the biomedical field.

2.5. Conclusions

Nature is an inspiration for scientists worldwide to create biomaterials for different biomedical applications. Herein, we present the recent developments of 2D or 3D development of biomaterials inspired by MAPs in the biomedical field. Despite of the scientific interest demonstrated by researchers worldwide about MAPs, there are few systematic studies about films or free-standing membranes. Furthermore, works about nanostructured coatings mimicking the nacre structure using MAPs and nanoparticles have been recently proposed. It is known that with the incorporation of nanofillers better mechanical properties can be obtained. Free-standing membranes based on natural polymers conjugated with MAPs and nanofillers could be tried in order to improve the mechanical and adhesive properties when compared with biodegradable polymers only. The development of such hybrid materials can be performed using the LbL technique which allows the creation of films or free-standings with complex structures. Also, hydrogels have been made based on natural polymers, for instance alginate, hyaluronic acid or chitosan conjugated with catechol groups, in order to improve their adhesive properties. However, the poor mechanical properties and the pH-dependence are the major drawbacks of these biomaterials. The addition of nanofillers could be tried in order to obtain better mechanical properties and superior tissue-adhesive properties.

Also, PDA is the subject of much interesting since it was discovered. It has a high stability when compared with DOPA and the possibility to adhere to all substrates is an advantage, which could be useful in different biomedical applications, as discussed here. The development of 3D structures using PDA is also possible as it was shown by some relevant examples in this review.

Acknowledgments

The authors acknowledge the Portuguese Foundation for Science and Technology (FCT) and the European program FEDER/COMPETE for the financial support through project LA ICVS/3Bs - 2015-2017.

2.6. References

- [1] S. K. Madhurakkat Perikamana et al., "Materials from Mussel-Inspired Chemistry for Cell and Tissue Engineering Applications," *Biomacromolecules*, vol. 16, no. 9, pp. 2541-55, 2015.

- [2] S. M. Kang et al., "One-Step Modification of Superhydrophobic Surfaces by a Mussel-Inspired Polymer Coating," *Angewandte Chemie-International Edition*, vol. 49, no. 49, pp. 9401-9404, 2010.
- [3] Y. H. Lee et al., "Bioinspired Surface Immobilization of Hyaluronic Acid on Monodisperse Magnetite Nanocrystals for Targeted Cancer Imaging," (in English), *Advanced Materials*, Article vol. 20, no. 21, pp. 4154-+, 2008.
- [4] A. I. Neto, H. J. Meredith, C. L. Jenkins, J. J. Wilker, and J. F. Mano, "Combining biomimetic principles from the lotus leaf and mussel adhesive: polystyrene films with superhydrophobic and adhesive layers," (in English), *Rsc Advances*, Article vol. 3, no. 24, pp. 9352-9356, 2013.
- [5] S. K. M. Perikamana et al., "Materials from Mussel-Inspired Chemistry for Cell and Tissue Engineering Applications," *Biomacromolecules*, vol. 16, no. 9, pp. 2541-2555, 2015.
- [6] Y. Lee et al., "Thermo-sensitive, injectable, and tissue adhesive sol-gel transition hyaluronic acid/pluronic composite hydrogels prepared from bio-inspired catechol-thiol reaction," (in English), *Soft Matter*, Article vol. 6, no. 5, pp. 977-983, 2010.
- [7] L. Li, W. Smitthipong, and H. B. Zeng, "Mussel-inspired hydrogels for biomedical and environmental applications," (in English), *Polymer Chemistry, Review* vol. 6, no. 3, pp. 353-358, 2015.
- [8] M. Krogsgaard, V. Nue, and H. Birkedal, "Mussel-Inspired Materials: Self-Healing through Coordination Chemistry," *Chemistry-a European Journal*, vol. 22, no. 3, pp. 844-857, 2016.
- [9] M. E. Yu and T. J. Deming, "Synthetic polypeptide mimics of marine adhesives," (in English), *Macromolecules*, Article vol. 31, no. 15, pp. 4739-4745, 1998.
- [10] J. Sedo, J. Saiz-Poseu, F. Busque, and D. Ruiz-Molina, "Catechol-Based Biomimetic Functional Materials," (in English), *Advanced Materials, Review* vol. 25, no. 5, pp. 653-701, 2013.
- [11] T. J. Deming, "Mussel byssus and biomolecular materials," (in English), *Current Opinion in Chemical Biology, Review* vol. 3, no. 1, pp. 100-105, 1999.
- [12] A. I. Neto et al., "Nanostructured Polymeric Coatings Based on Chitosan and Dopamine-Modified Hyaluronic Acid for Biomedical Applications," (in English), *Small*, Article vol. 10, no. 12, pp. 2459-2469, 2014.
- [13] M. E. Yu, J. Y. Hwang, and T. J. Deming, "Role of L-3,4-dihydroxyphenylalanine in mussel adhesive proteins," (in English), *Journal of the American Chemical Society*, Article vol. 121, no. 24, pp. 5825-5826, 1999.
- [14] J. H. Ryu, Y. Lee, W. H. Kong, T. G. Kim, T. G. Park, and H. Lee, "Catechol-Functionalized Chitosan/Pluronic Hydrogels for Tissue Adhesives and Hemostatic Materials," (in English), *Biomacromolecules*, Article vol. 12, no. 7, pp. 2653-2659, 2011.
- [15] B. Yang et al., "In Vivo Residue-Specific Dopa-Incorporated Engineered Mussel Bioglue with Enhanced Adhesion and Water Resistance," (in English), *Angewandte Chemie-International Edition, Article* vol. 53, no. 49, pp. 13360-13364, 2014.

- [16] P. Podsiadlo, Z. Q. Liu, D. Paterson, P. B. Messersmith, and N. A. Kotov, "Fusion of seashell nacre and marine bioadhesive analogs: High-strength nanocomposite by layer-by-layer assembly of clay and L-3,4-dihydroxyphenylalanine polymer," (in English), *Advanced Materials*, Article vol. 19, no. 7, pp. 949-+, 2007.
- [17] M. Krogsgaard, M. A. Behrens, J. S. Pedersen, and H. Birkedal, "Self-Healing Mussel-Inspired Multi-pH-Responsive Hydrogels," (in English), *Biomacromolecules*, Article vol. 14, no. 2, pp. 297-301, 2013.
- [18] J. K. Xu, G. M. Soliman, J. Barralet, and M. Cerruti, "Mollusk Glue Inspired Mucoadhesives for Biomedical Applications," (in English), *Langmuir*, Article vol. 28, no. 39, pp. 14010-14017, 2012.
- [19] Z. Shafiq et al., "Bioinspired Underwater Bonding and Debonding on Demand," *Angewandte Chemie-International Edition*, vol. 51, no. 18, pp. 4332-4335, 2012.
- [20] M. J. Sever, J. T. Weisser, J. Monahan, S. Srinivasan, and J. J. Wilker, "Metal-mediated cross-linking in the generation of a marine-mussel adhesive," (in English), *Angewandte Chemie-International Edition*, Article vol. 43, no. 4, pp. 448-450, 2004.
- [21] P. Wilke, N. Helfricht, A. Mark, G. Papastavrou, D. Faivre, and H. G. Borner, "A Direct Biocombinatorial Strategy toward Next Generation, Mussel-Glue Inspired Saltwater Adhesives," *Journal of the American Chemical Society*, vol. 136, no. 36, pp. 12667-12674, 2014.
- [22] H. G. Silverman and F. F. Roberto, "Understanding marine mussel adhesion," (in English), *Marine Biotechnology*, Review vol. 9, no. 6, pp. 661-681, 2007.
- [23] H. Lee, N. F. Scherer, and P. B. Messersmith, "Single-molecule mechanics of mussel adhesion," (in English), *Proceedings of the National Academy of Sciences of the United States of America*, Article vol. 103, no. 35, pp. 12999-13003, 2006.
- [24] J. A. Callow and M. E. Callow, "Trends in the development of environmentally friendly fouling-resistant marine coatings," *Nature Communications*, vol. 2, 2011, Art. no. 244.
- [25] D. E. Fullenkamp et al., "Mussel-inspired silver-releasing antibacterial hydrogels," (in English), *Biomaterials*, Article vol. 33, no. 15, pp. 3783-3791, 2012.
- [26] J. X. Sun, C. Su, X. J. Zhang, W. J. Yin, J. Xu, and S. G. Yang, "Reversible Swelling-Shrinking Behavior of Hydrogen-Bonded Free-Standing Thin Film Stabilized by Catechol Reaction," (in English), *Langmuir*, Article vol. 31, no. 18, pp. 5147-5154, 2015.
- [27] S. Hong et al., "Hyaluronic Acid Catechol: A Biopolymer Exhibiting a pH-Dependent Adhesive or Cohesive Property for Human Neural Stem Cell Engineering," (in English), *Advanced Functional Materials*, Article vol. 23, no. 14, pp. 1774-1780, 2013.
- [28] B. J. Kim et al., "Mussel-Mimetic Protein-Based Adhesive Hydrogel," (in English), *Biomacromolecules*, Article vol. 15, no. 5, pp. 1579-1585, 2014.
- [29] B. P. Lee, J. L. Dalsin, and P. B. Messersmith, "Synthesis and gelation of DOPA-Modified poly(ethylene glycol) hydrogels," (in English), *Biomacromolecules*, Article vol. 3, no. 5, pp. 1038-1047, 2002.

- [30] C. E. Brubaker and P. B. Messersmith, "The Present and Future of Biologically Inspired Adhesive Interfaces and Materials," *Langmuir*, vol. 28, no. 4, pp. 2200-2205, 2012.
- [31] K. Ariga, J. P. Hill, and Q. M. Ji, "Layer-by-layer assembly as a versatile bottom-up nanofabrication technique for exploratory research and realistic application," (in English), *Physical Chemistry Chemical Physics*, Review vol. 9, no. 19, pp. 2319-2340, 2007.
- [32] D. S. Couto, N. M. Alves, and J. F. Mano, "Nanostructured Multilayer Coatings Combining Chitosan with Bioactive Glass Nanoparticles," (in English), *Journal of Nanoscience and Nanotechnology*, Article vol. 9, no. 3, pp. 1741-1748, 2009.
- [33] M. Matsusaki, H. Ajiro, T. Kida, T. Serizawa, and M. Akashi, "Layer-by-Layer Assembly Through Weak Interactions and Their Biomedical Applications," *Advanced Materials*, vol. 24, no. 4, pp. 454-474, 2012.
- [34] J. Borges, L. C. Rodrigues, R. L. Reis, and J. F. Mano, "Layer-by-Layer Assembly of Light-Responsive Polymeric Multilayer Systems," (in English), *Advanced Functional Materials*, Article vol. 24, no. 36, pp. 5624-5648, 2014.
- [35] Z. Y. Tang, Y. Wang, P. Podsiadlo, and N. A. Kotov, "Biomedical applications of layer-by-layer assembly: From biomimetics to tissue engineering," (in English), *Advanced Materials*, Review vol. 18, no. 24, pp. 3203-3224, 2006.
- [36] Y. Zhou, M. J. Cheng, X. Q. Zhu, Y. J. Zhang, Q. An, and F. Shi, "A facile method for the construction of stable polymer-inorganic nanoparticle composite multilayers," (in English), *Journal of Materials Chemistry A*, Article vol. 1, no. 37, pp. 11329-11334, 2013.
- [37] J. Borges and J. F. Mano, "Molecular Interactions Driving the Layer-by-Layer Assembly of Multilayers," (in English), *Chemical Reviews*, Review vol. 114, no. 18, pp. 8883-8942, 2014.
- [38] G. V. Martins, J. F. Mano, and N. M. Alves, "Nanostructured self-assembled films containing chitosan fabricated at neutral pH," (in English), *Carbohydrate Polymers*, Article vol. 80, no. 2, pp. 570-573, 2010.
- [39] A. L. Larkin, R. M. Davis, and P. Rajagopalan, "Biocompatible, Detachable, and Free-Standing Polyelectrolyte Multilayer Films," (in English), *Biomacromolecules*, Article vol. 11, no. 10, pp. 2788-2796, 2010.
- [40] R. R. Costa and J. F. Mano, "Polyelectrolyte multilayered assemblies in biomedical technologies," *Chemical Society Reviews*, vol. 43, no. 10, pp. 3453-3479, 2014.
- [41] C. S. Hajicharalambous, J. Lichter, W. T. Hix, M. Swierczewska, M. F. Rubner, and P. Rajagopalan, "Nano- and sub-micron porous polyelectrolyte multilayer assemblies: Biomimetic surfaces for human corneal epithelial cells," (in English), *Biomaterials*, Article vol. 30, no. 23-24, pp. 4029-4036, 2009.
- [42] P. Kujawa, G. Schmauch, T. Viitala, A. Badia, and F. M. Winnik, "Construction of viscoelastic biocompatible films via the layer-by-layer assembly of hyaluronan and phosphorylcholine-modified chitosan," (in English), *Biomacromolecules*, Article vol. 8, no. 10, pp. 3169-3176, 2007.

- [43] S. G. Caridade, C. Monge, F. Gilde, T. Boudou, J. F. Mano, and C. Picart, "Free-Standing Polyelectrolyte Membranes Made of Chitosan and Alginate," (in English), *Biomacromolecules*, Article vol. 14, no. 5, pp. 1653-1660, 2013.
- [44] S. Y. Yang and M. F. Rubner, "Micropatterning of polymer thin films with pH-sensitive and cross-linkable hydrogen-bonded polyelectrolyte multilayers," (in English), *Journal of the American Chemical Society*, Article vol. 124, no. 10, pp. 2100-2101, 2002.
- [45] P. H. Chua, K. G. Neoh, E. T. Kang, and W. Wang, "Surface functionalization of titanium with hyaluronic acid/chitosan polyelectrolyte multilayers and RGD for promoting osteoblast functions and inhibiting bacterial adhesion," (in English), *Biomaterials*, Article vol. 29, no. 10, pp. 1412-1421, 2008.
- [46] P. T. Hammond, "Engineering Materials Layer-by-Layer: Challenges and Opportunities in Multilayer Assembly," (in English), *Aiche Journal, Editorial Material* vol. 57, no. 11, pp. 2928-2940, 2011.
- [47] L. Klouda and A. G. Mikos, "Thermoresponsive hydrogels in biomedical applications," *European Journal of Pharmaceutics and Biopharmaceutics*, vol. 68, no. 1, pp. 34-45, 2008.
- [48] N. Annabi et al., "25th Anniversary Article: Rational Design and Applications of Hydrogels in Regenerative Medicine," *Advanced Materials*, vol. 26, no. 1, pp. 85-124, 2014.
- [49] N. Annabi, S. M. Mithieux, E. A. Boughton, A. J. Ruys, A. S. Weiss, and F. Dehghani, "Synthesis of highly porous crosslinked elastin hydrogels and their interaction with fibroblasts in vitro," *Biomaterials*, vol. 30, no. 27, pp. 4550-4557, 2009.
- [50] N. A. Peppas, J. Z. Hilt, A. Khademhosseini, and R. Langer, "Hydrogels in biology and medicine: From molecular principles to bionanotechnology," *Advanced Materials*, vol. 18, no. 11, pp. 1345-1360, 2006.
- [51] K. Y. Lee and D. J. Mooney, "Hydrogels for tissue engineering," *Chemical Reviews*, vol. 101, no. 7, pp. 1869-1879, 2001.
- [52] Y. Liu, K. Ai, and L. Lu, "Polydopamine and Its Derivative Materials: Synthesis and Promising Applications in Energy, Environmental, and Biomedical Fields," *Chemical Reviews*, vol. 114, no. 9, pp. 5057-5115, 2014.
- [53] N. G. Hoogeveen, M. A. C. Stuart, G. J. Fleer, and M. R. Bohmer, "Formation and stability of multilayers of polyelectrolytes," *Langmuir*, vol. 12, no. 15, pp. 3675-3681, 1996.
- [54] H. Lee, Y. Lee, A. R. Statz, J. Rho, T. G. Park, and P. B. Messersmith, "Substrate-independent layer-by-layer assembly by using mussel-adhesive-inspired polymers," (in English), *Advanced Materials*, Article vol. 20, no. 9, pp. 1619+, 2008.
- [55] H. Ai, S. A. Jones, and Y. M. Lvov, "Biomedical applications of electrostatic layer-by-layer nano-assembly of polymers, enzymes, and nanoparticles," (in English), *Cell Biochemistry and Biophysics*, Review vol. 39, no. 1, pp. 23-43, 2003.
- [56] B. P. Lee, P. B. Messersmith, J. N. Israelachvili, and J. H. Waite, "Mussel-Inspired Adhesives and Coatings," in *Annual Review of Materials Research*, Vol 41, vol.

- 41, D. R. Clarke and P. Fratzl, Eds. (Annual Review of Materials Research, Palo Alto: Annual Reviews, pp. 99-132, 2011.
- [57] S. Moulay, "Dopa/Catechol-Tethered Polymers: Bioadhesives and Biomimetic Adhesive Materials," (in English), *Polymer Reviews*, Review vol. 54, no. 3, pp. 436-513, 2014.
- [58] X. M. Zhang, Z. Y. Li, X. B. Yuan, Z. D. Cui, and X. J. Yang, "Fabrication of dopamine-modified hyaluronic acid/chitosan multilayers on titanium alloy by layer-by-layer self-assembly for promoting osteoblast growth," (in English), *Applied Surface Science*, Article vol. 284, pp. 732-737, 2013.
- [59] A. I. Neto, N. L. Vasconcelos, S. M. Oliveira, D. Ruiz-Molina, and J. F. Mano, "High-Throughput Topographic, Mechanical, and Biological Screening of Multilayer Films Containing Mussel-Inspired Biopolymers," *Advanced Functional Materials*, vol. 26, no. 16, pp. 2745-2755, 2016.
- [60] A. L. Carvalho et al., "Antibacterial bioadhesive layer-by-layer coatings for orthopedic applications," *Journal of Materials Chemistry B*, 10.1039/C6TB00841K 2016.
- [61] S. J. Rego, A. C. Vale, G. M. Luz, J. F. Mano, and N. M. Alves, "Adhesive Bioactive Coatings Inspired by Sea Life," (in English), *Langmuir*, Article vol. 32, no. 2, pp. 560-568, 2016.
- [62] J. M. Silva, A. R. C. Duarte, S. G. Caridade, C. Picart, R. L. Reis, and J. F. Mano, "Tailored Freestanding Multi layered Membranes Based on Chitosan and Alginate," (in English), *Biomacromolecules*, Article vol. 15, no. 10, pp. 3817-3826, 2014.
- [63] T. R. Hoare and D. S. Kohane, "Hydrogels in drug delivery: Progress and challenges," (in English), *Polymer*, Review vol. 49, no. 8, pp. 1993-2007, 2008.
- [64] L. Yu and J. Ding, "Injectable hydrogels as unique biomedical materials," *Chemical Society Reviews*, vol. 37, no. 8, pp. 1473-1481, 2008.
- [65] L. Gasperini, J. F. Mano, and R. L. Reis, "Natural polymers for the microencapsulation of cells," (in English), *Journal of the Royal Society Interface*, Article vol. 11, no. 100, p. 19, 2014, Art. no. Unsp 20140817.
- [66] E. Caló and V. V. Khutoryanskiy, "Biomedical applications of hydrogels: A review of patents and commercial products," *European Polymer Journal*, vol. 65, pp. 252-267, 2015.
- [67] J. B. Park, "The use of hydrogels in bone-tissue engineering," (in English), *Medicina Oral Patologia Oral Y Cirugia Bucal*, Article vol. 16, no. 1, pp. E115-E118, 2011.
- [68] J. L. Drury and D. J. Mooney, "Hydrogels for tissue engineering: scaffold design variables and applications," (in English), *Biomaterials*, Review vol. 24, no. 24, pp. 4337-4351, 2003.
- [69] M. C. Koetting, J. T. Peters, S. D. Steichen, and N. A. Peppas, "Stimulus-responsive hydrogels: Theory, modern advances, and applications," *Materials Science and Engineering: R: Reports*, vol. 93, pp. 1-49, 2015.
- [70] Y. C. Choi, J. S. Choi, Y. J. Jung, and Y. W. Cho, "Human gelatin tissue-adhesive hydrogels prepared by enzyme-mediated biosynthesis of DOPA and Fe³⁺ ion

- crosslinking," (in English), *Journal of Materials Chemistry B*, Article vol. 2, no. 2, pp. 201-209, 2014.
- [71] M. Krogsgaard, M. R. Hansen, and H. Birkedal, "Metals & polymers in the mix: fine-tuning the mechanical properties & color of self-healing mussel-inspired hydrogels," *Journal of Materials Chemistry B*, vol. 2, no. 47, pp. 8292-8297, 2014.
- [72] Z. W. Guo, K. F. Ni, D. Z. Wei, and Y. H. Ren, "Fe³⁺-induced oxidation and coordination cross-linking in catechol-chitosan hydrogels under acidic pH conditions," *Rsc Advances*, vol. 5, no. 47, pp. 37377-37384, 2015.
- [73] N. Holten-Andersen et al., "pH-induced metal-ligand cross-links inspired by mussel yield self-healing polymer networks with near-covalent elastic moduli," (in English), *Proceedings of the National Academy of Sciences of the United States of America*, Article vol. 108, no. 7, pp. 2651-2655, 2011.
- [74] C. Lee et al., "Bioinspired, Calcium-Free Alginate Hydrogels with Tunable Physical and Mechanical Properties and Improved Biocompatibility," *Biomacromolecules*, vol. 14, no. 6, pp. 2004-2013, 2013.
- [75] J. Shin et al., "Tissue Adhesive Catechol-Modified Hyaluronic Acid Hydrogel for Effective, Minimally Invasive Cell Therapy," *Advanced Functional Materials*, vol. 25, no. 25, pp. 3814-3824, 2015.
- [76] M. Cencer, Y. Liu, A. Winter, M. Murley, H. Meng, and B. P. Lee, "Effect of pH on the Rate of Curing and Bioadhesive Properties of Dopamine Functionalized Poly(ethylene glycol) Hydrogels," (in English), *Biomacromolecules*, Article vol. 15, no. 8, pp. 2861-2869, 2014.
- [77] H. Lee, S. M. Dellatore, W. M. Miller, and P. B. Messersmith, "Mussel-inspired surface chemistry for multifunctional coatings," (in English), *Science*, Article vol. 318, no. 5849, pp. 426-430, 2007.
- [78] V. Ball, D. D. Frari, V. Toniazzo, and D. Ruch, "Kinetics of polydopamine film deposition as a function of pH and dopamine concentration: Insights in the polydopamine deposition mechanism," *Journal of Colloid and Interface Science*, vol. 386, no. 1, pp. 366-372, 2012.
- [79] R. Mrówczyński, R. Markiewicz, and J. Liescher, "Chemistry of polydopamine analogues," *Polymer International*, 2016.
- [80] Q. Liu, N. Y. Wang, J. Caro, and A. S. Huang, "Bio-Inspired Polydopamine: A Versatile and Powerful Platform for Covalent Synthesis of Molecular Sieve Membranes," *Journal of the American Chemical Society*, vol. 135, no. 47, pp. 17679-17682, 2013.
- [81] S. Hong, Y. S. Na, S. Choi, I. T. Song, W. Y. Kim, and H. Lee, "Non-Covalent Self-Assembly and Covalent Polymerization Co-Contribute to Polydopamine Formation," *Advanced Functional Materials*, vol. 22, no. 22, pp. 4711-4717, 2012.
- [82] X. L. Gu, Y. C. Zhang, H. W. Sun, X. F. Song, C. H. Fu, and P. X. Dong, "Mussel-Inspired Polydopamine Coated Iron Oxide Nanoparticles for Biomedical Application," (in English), *Journal of Nanomaterials*, Review p. 12, 2015, Art. no. 154592.
- [83] Y. Dang et al., "Substrate independent coating formation and anti-biofouling performance improvement of mussel inspired polydopamine," (in English), *Journal of Materials Chemistry B*, Article vol. 3, no. 20, pp. 4181-4190, 2015.

- [84] R. L. Huang et al., "Conjugation of Hyaluronic Acid onto Surfaces via the Interfacial Polymerization of Dopamine to Prevent Protein Adsorption," *Langmuir*, vol. 31, no. 44, pp. 12061-12070, 2015.
- [85] M. d'Ischia, A. Napolitano, V. Ball, C. T. Chen, and M. J. Buehler, "Polydopamine and Eumelanin: From Structure-Property Relationships to a Unified Tailoring Strategy," *Accounts of Chemical Research*, vol. 47, no. 12, pp. 3541-3550, 2014.
- [86] W. H. Zhou, C. H. Lu, X. C. Guo, F. R. Chen, H. H. Yang, and X. R. Wang, "Mussel-inspired molecularly imprinted polymer coating superparamagnetic nanoparticles for protein recognition," *Journal of Materials Chemistry*, vol. 20, no. 5, pp. 880-883, 2010.
- [87] Q. Yue, M. H. Wang, Z. K. Sun, C. Wang, Y. H. Deng, and D. Y. Zhao, "A versatile ethanol-mediated polymerization of dopamine for efficient surface modification and the construction of functional core-shell nanostructures," *Journal of Materials Chemistry B*, vol. 1, no. 44, pp. 6085-6093, 2013.
- [88] Y. S. Lee, J. Y. Bae, H. Y. Koo, Y. B. Lee, and W. S. Choi, "A remote-controlled generation of gold@polydopamine (core@shell) nanoparticles via physical-chemical stimuli of polydopamine/gold composites," *Scientific Reports*, vol. 6, 2016, Art. no. 22650.
- [89] S. H. Ku, J. Ryu, S. K. Hong, H. Lee, and C. B. Park, "General functionalization route for cell adhesion on non-wetting surfaces," *Biomaterials*, vol. 31, no. 9, pp. 2535-2541, 2010.
- [90] C. J. Bettinger, J. P. Bruggeman, A. Misra, J. T. Borenstein, and R. Langer, "Biocompatibility of biodegradable semiconducting melanin films for nerve tissue engineering," *Biomaterials*, vol. 30, no. 17, pp. 3050-3057, 2009.
- [91] S. H. Bhang et al., "Enhanced neuronal differentiation of pheochromocytoma 12 cells on polydopamine-modified surface," *Biochemical and Biophysical Research Communications*, vol. 430, no. 4, pp. 1294-1300, 2013.
- [92] J. L. Wang, K. F. Ren, H. Chang, S. M. Zhang, L. J. Jin, and J. Ji, "Facile fabrication of robust superhydrophobic multilayered film based on bioinspired poly(dopamine)-modified carbon nanotubes," *Physical Chemistry Chemical Physics*, vol. 16, no. 7, pp. 2936-2943, 2014.
- [93] Q. Wei et al., "Improving the blood compatibility of material surfaces via biomolecule-immobilized mussel-inspired coatings," *Journal of Biomedical Materials Research Part A*, vol. 96A, no. 1, pp. 38-45, 2011.
- [94] Y. Liu et al., "Tailoring of the dopamine coated surface with VEGF loaded heparin/poly-L-lysine particles for anticoagulation and accelerate in situ endothelialization," *Journal of Biomedical Materials Research Part A*, vol. 103, no. 6, pp. 2024-2034, 2015.
- [95] T. Nardo, V. Chiono, G. Ciardelli, and M. Tabrizian, "PolyDOPA Mussel-Inspired Coating as a Means for Hydroxyapatite Entrapment on Polytetrafluoroethylene Surface for Application in Periodontal Diseases," (in English), *Macromolecular Bioscience*, Article vol. 16, no. 2, pp. 288-298, 2016.
- [96] A. Perez-Anes et al., "Bioinspired Titanium Drug Eluting Platforms Based on a Poly-beta-cyclodextrin-Chitosan Layer-by-Layer Self-Assembly Targeting

- Infections," *Acs Applied Materials & Interfaces*, vol. 7, no. 23, pp. 12882-12893, 2015.
- [97] K. Wang and Y. Luo, "Defined Surface Immobilization of Glycosaminoglycan Molecules for Probing and Modulation of Cell-Material Interactions," *Biomacromolecules*, vol. 14, no. 7, pp. 2373-2382, 2013.
- [98] S. H. Ku, J. S. Lee, and C. B. Park, "Spatial Control of Cell Adhesion and Patterning through Mussel-Inspired Surface Modification by Polydopamine," *Langmuir*, vol. 26, no. 19, pp. 15104-15108, 2010.
- [99] H. J. Ye et al., "Dopamine-assisted deposition and zwitteration of hyaluronic acid for the nanoscale fabrication of low-fouling surfaces," *Journal of Materials Chemistry B*, vol. 4, no. 23, pp. 4084-4091, 2016.
- [100] X. Liu, R. L. Huang, R. X. Su, W. Qi, L. B. Wang, and Z. M. He, "Grafting Hyaluronic Acid onto Gold Surface to Achieve Low Protein Fouling in Surface Plasmon Resonance Biosensors," *Acs Applied Materials & Interfaces*, vol. 6, no. 15, pp. 13034-13042, 2014.
- [101] J. Luo, S. S. Jiang, and X. Y. Liu, "Efficient One-Pot Synthesis of Mussel-Inspired Molecularly Imprinted Polymer Coated Graphene for Protein-Specific Recognition and Fast Separation," *Journal of Physical Chemistry C*, vol. 117, no. 36, pp. 18448-18456, 2013.
- [102] J. Ryu, S. H. Ku, H. Lee, and C. B. Park, "Mussel-Inspired Polydopamine Coating as a Universal Route to Hydroxyapatite Crystallization," *Advanced Functional Materials*, vol. 20, no. 13, pp. 2132-2139, 2010.
- [103] J. W. Cui et al., "Immobilization and Intracellular Delivery of an Anticancer Drug Using Mussel-Inspired Polydopamine Capsules," *Biomacromolecules*, vol. 13, no. 8, pp. 2225-2228, 2012.
- [104] N. Pazos-Perez, B. Rodriguez-Gonzalez, M. Hilgendorff, M. Giersig, and L. M. Liz-Marzan, "Gold encapsulation of star-shaped FePt nanoparticles," *Journal of Materials Chemistry*, vol. 20, no. 1, pp. 61-64, 2010.
- [105] R. Y. Hong, H. P. Fu, G. Q. Di, Y. Zheng, and D. G. Wei, "Facile route to γ -Fe₂O₃/SiO₂ nanocomposite used as a precursor of magnetic fluid," *Materials Chemistry and Physics*, vol. 108, no. 1, pp. 132-141, 2008.
- [106] M. Q. Zhang and F. M. Kievit, "Surface engineering of iron oxide nanoparticles for targeted cancer therapy," *Abstracts of Papers of the American Chemical Society*, vol. 243, 2012.
- [107] Y. Yuan, D. Rende, C. L. Altan, S. Bucak, R. Ozisik, and D. A. Borca-Tasciuc, "Effect of Surface Modification on Magnetization of Iron Oxide Nanoparticle Colloids," *Langmuir*, vol. 28, no. 36, pp. 13051-13059, 2012.
- [108] E. Amstad, T. Gillich, I. Bilecka, M. Textor, and E. Reimhult, "Ultrastable Iron Oxide Nanoparticle Colloidal Suspensions Using Dispersants with Catechol-Derived Anchor Groups," *Nano Letters*, vol. 9, no. 12, pp. 4042-4048, 2009.
- [109] M. Talelli et al., "Superparamagnetic Iron Oxide Nanoparticles Encapsulated in Biodegradable Thermosensitive Polymeric Micelles: Toward a Targeted Nanomedicine Suitable for Image-Guided Drug Delivery," *Langmuir*, vol. 25, no. 4, pp. 2060-2067, 2009.

- [110] J. Si and H. Yang, "Preparation and characterization of bio-compatible Fe₃O₄@Polydopamine spheres with core/shell nanostructure," *Materials Chemistry and Physics*, vol. 128, no. 3, pp. 519-524, 2011.
- [111] R. Liu, Y. L. Guo, G. Odusote, F. L. Qu, and R. D. Priestley, "Core-Shell Fe₃O₄ Polydopamine Nanoparticles Serve Multipurpose as Drug Carrier, Catalyst Support and Carbon Adsorbent," *Acs Applied Materials & Interfaces*, vol. 5, no. 18, pp. 9167-9171, 2013.
- [112] M. D. Shultz, J. U. Reveles, S. N. Khanna, and E. E. Carpenter, "Reactive nature of dopamine as a surface functionalization agent in iron oxide nanoparticles," *Journal of the American Chemical Society*, vol. 129, no. 9, pp. 2482-2487, 2007.
- [113] J. Han, W. Park, S. J. Park, and K. Na, "Photosensitizer-Conjugated Hyaluronic Acid-Shielded Polydopamine Nanoparticles for Targeted Photomediated Tumor Therapy," *Acs Applied Materials & Interfaces*, vol. 8, no. 12, pp. 7739-7747, 2016.
- [114] J. W. Xie, P. L. Michael, S. P. Zhong, B. Ma, M. R. MacEwan, and C. T. Lim, "Mussel inspired protein-mediated surface modification to electrospun fibers and their potential biomedical applications," *Journal of Biomedical Materials Research Part A*, vol. 100A, no. 4, pp. 929-938, 2012.
- [115] Y. M. Shin, H. Park, and H. Shin, "Enhancement of Cardiac Myoblast Responses onto Electrospun PLCL Fibrous Matrices Coated with Polydopamine for Gelatin Immobilization," *Macromolecular Research*, vol. 19, no. 8, pp. 835-842, 2011.
- [116] S. H. Ku and C. B. Park, "Human endothelial cell growth on mussel-inspired nanofiber scaffold for vascular tissue engineering," *Biomaterials*, vol. 31, no. 36, pp. 9431-9437, 2010.
- [117] Y. M. Shin, I. Jun, Y. M. Lim, T. Rhim, and H. Shin, "Bio-inspired Immobilization of Cell-Adhesive Ligands on Electrospun Nanofibrous Patches for Cell Delivery," *Macromolecular Materials and Engineering*, vol. 298, no. 5, pp. 555-564, 2013.
- [118] S. R. Nielsen, F. Besenbacher, and M. Chen, "Mussel inspired surface functionalization of electrospun nanofibers for bio-applications," *Physical Chemistry Chemical Physics*, vol. 15, no. 40, pp. 17029-17037, 2013.
- [119] T. E. L. Douglas et al., "Enzymatic mineralization of gellan gum hydrogel for bone tissue-engineering applications and its enhancement by polydopamine," *Journal of Tissue Engineering and Regenerative Medicine*, vol. 8, no. 11, pp. 906-918, 2014.
- [120] S. C. Zhu et al., "Fabrication of a novel bio-inspired collagen-polydopamine hydrogel and insights into the formation mechanism for biomedical applications," (in English), *Rsc Advances*, Article vol. 6, no. 70, pp. 66180-66190, 2016.

CHAPTER 3

METHODS

MATERIALS

AND

3. MATERIALS AND METHODS

In this chapter, all materials used for realization of this thesis, as well as the techniques used for their characterization will be described.

3.1. Materials

3.1.1. Hyaluronic acid (HA)

Hyaluronic acid (HA) [1, 2], also known as hyaluronan [1-3] or hyaluronate [2, 3], is an anionic glycosaminoglycan (GAGs) [1] that has received a lot of attention from the scientific community. HA is a linear polymer [1, 4, 5], non-sulfated [5-7] constituted by a disaccharide repeating units, N-acetyl-D-glucosamine and D-glucuronate, with β 1-4 and β 1-3 linkages [1, 4, 5, 7, 8], as it can be seen in Figure 3.1. Dissacharides units can be at least 10 000 per chain, corresponding to a length of 10 μ m [9] and they have a molecular mass of 4 million Dalton (Da) [1], $8 \cdot 10^6$, 10^7 or 10^8 Da [10]. It is a major carbohydrate component of ECM [2, 11]. According to Mano and co-workers [3], when hyaluronic acid is a rigid molecule and in solution it occupies a volume approximately 1000 times higher than in its dry state [3].

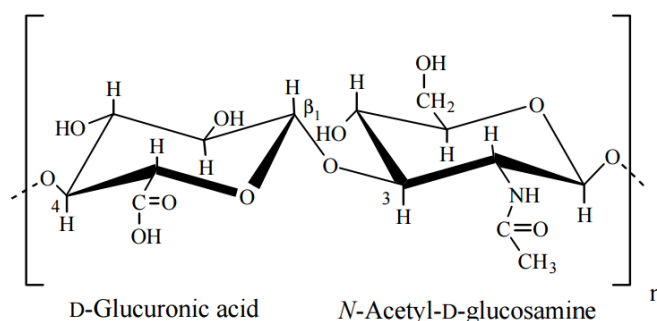


Figure 3. 1 - Chemical structure of hyaluronic acid (HA) [3].

HA is present in bacteria [5, 10], organs [11], tissues [5, 7, 11] and body fluids [5] of vertebrates [5, 10], namely skin [2, 10, 11], synovial fluid [2, 3, 10] in joints [11], cartilage [2, 7], connective tissue [3, 7], vitreous humour of the eye [2, 3, 10, 11], muscles [2], brain [2] and umbilical tissue [3]. HA affects cellular behavior, namely by changing the micro and macroenvironment around cells by complex interactions with cells and other extracellular matrix components [11].

According to Morra [1], HA is a molecule that is important for numerous cellular and biological processes. Furthermore, HA is present in many physiological and pathological processes, namely tissue damage [1], cell migration and proliferation [1, 10, 11], immune

regulation [9], fertilization [9], angiogenesis [11] inflammation [1, 4, 9, 11], tumor metastasis [4, 10] and development [1, 4, 9, 10], osteoarthritis [9], and atherosclerosis [9]. Furthermore, HA presents hygroscopic, rheological and viscoelastic properties [11]. According to Schanté and co-workers [10], high molecular weight HA (>100 kDa) has anti-angiogenic¹ and anti-inflammatory properties, but low M_w HA presents the opposite results [10].

HA presents many advantages, such as the fact that it is soluble in water [3], it is biocompatible [6-9], it is biodegradable [7, 8] (through the action of hyaluronidase (Hyal) enzymes) [9], non-immunogenic [7, 8, 13], non-adhesive [13], non-toxicity [8] and non-inflammatory [2, 7, 8]. It presents many applications, for example, in biomaterials and bionanotechnology [9], and medical applications, namely drug delivery materials [6-10, 14], tissue repair [11], eye/ ophthalmic surgery [8, 10], wound healing [6, 8, 10], post-surgical anti-adhesion materials [6] and viscosupplementation [10]. HA can be chemically modified in two different ways: cross-linking or conjugation [10].

For this thesis hyaluronic acid salt from *Streptococcus equi* was used, from Sigma-Aldrich.

3.1.2. Dopamine (DN)

Dopamine hydrochloride (DN) (Sigma-Aldrich) has received attention and been a target of ongoing investigations since its discovery [15] in chemistry and biomedical research [16]. Dopamine is a catecholamine and it is present in the human body, as a hormone or a neurotransmitter [16]. In the human body, depleted dopamine levels can originate physical symptoms connected with Parkinson's disease (PD) [17], namely bradykinesia², rigidity and tremors [19]. The PD symptoms are attenuating the depletion of dopamine in the brain after administration of L-DOPA [17].

Dopamine, according to Perikamana and co-workers [16], has a similar chemical structure to lysine and DOPA [16]. DOPA and lysine form strong adhesive bonds with numerous substrates [20]. DN, Figure 3.2, is an adhesive molecule, which contains the

Chapter 3. Materials and Methods

¹**Anti-angiogenic:** "Angiogenesis is a physiological process that allows the formation of new blood vessels, either from the local vascular structures, or from circulating endothelial progenitor cells, mobilized from the bone marrow, and attracted to the neovascularization site. This mechanism is controlled by pro-angiogenic molecules. It is crucial to supply oxygen and nutrients to tissues during growth, embryonic development or tissue regeneration in response to injuries. Thus, the dermis part of the skin is highly vascularized by a dense network of small and medium arteries and of capillaries and venules. In case of injury, rapid tissue repair is possible through this vascular network. However, once the vascularization is restored in tissue repair, the process of angiogenesis is negatively regulated by anti-angiogenic molecules". [12] J. J. Lataillade, P. Albanese, and G. Uzan, "Implication of hyaluronic acid in normal and pathological angiogenesis. Application for cellular engineering," (in French), *Annales De Dermatologie Et De Venereologie*, Article vol. 137, pp. S15-S22, Apr 2010.

²**Bradykinesia:** is difficulty with walking, speaking, or getting into and out of chairs. [18] V. Cutsuridis and S. Perantonis, "A neural network model of Parkinson's disease bradykinesia," *Neural Networks*, vol. 19, no. 4, pp. 354-374, 5// 2006.

catechol functional group [21]. Interfacial adhesion between plaques and the substrates influences the adhesion to a surface and its cohesive interactions promote the integrity of threads and byssal plaques [22]. In polar polymer substrates there is the hydrogen bonding or formation of covalent bond. When, there is a hydrophobic polymer as a substrates, an π - π interaction between polymer and the surface [23] occurs. DOPA is a component in the adhesive structure of mussels [24] and is produced via hydroxylation of tyrosine by tyrosine hydroxylase. DOPA catechol oxidation to quinone happens at alkaline pH [25].

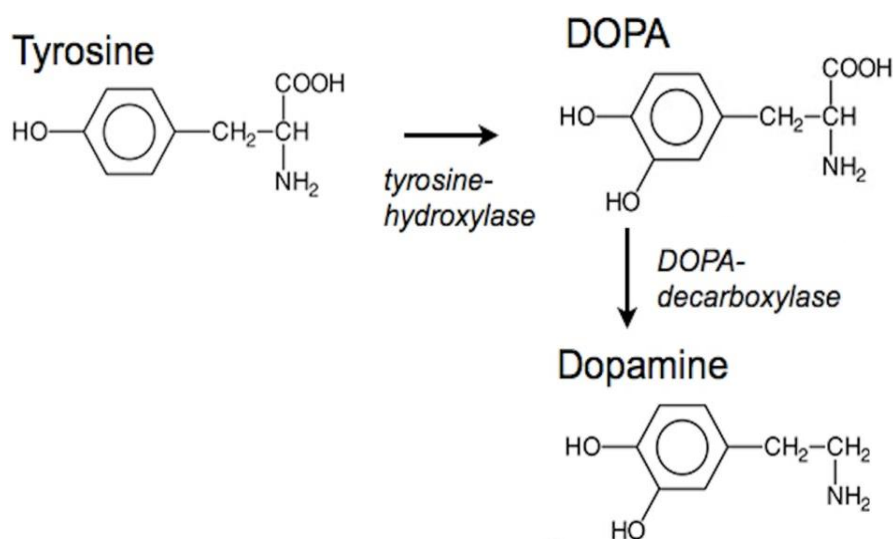


Figure 3. 2 - Tyrosine, DOPA and dopamine chemical structure. Adapted from [26].

3.1.3. Chitosan (CHT):

Chitin was discovered in 1984 [27]. This is one of the most abundant organic materials, being second only to cellulose [27-29]. Chitin is a component of the exoskeleton in animals [28], namely insects [28-31], crustaceans [28-31], cell wall of certain fungi [14, 28, 31], yeast [14, 29], green algae cell walls [29] and mollusks [28].

For this study we used chitosan medium molecular weight (purchased on Sigma-Aldrich Company) which was purified according to [32] protocol. Chitosan is a linear polysaccharide [28]. It's constituted by glucosamine and N-acetyl glucosamine units linked by β -(1-4) glycosidic bonds [28], as it can be seen in Figure 3.3.

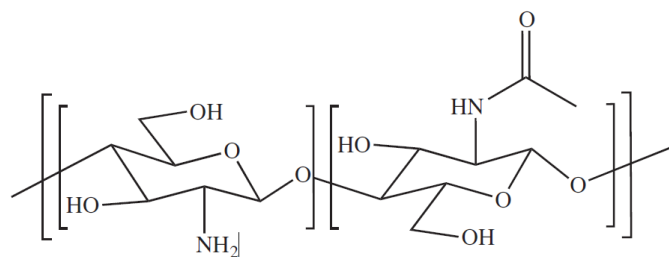


Figure 3. 3 - Chemical structure [29].

Through deacetylation, over alkaline conditions [28], that vary between 60 and 100% [29], chitin becomes soluble in aqueous acidic solutions [27], (pH < 6) [29]. When deacetylation takes place, a protonation of NH₂ group (present in C₂ position in D-glucosamine repeat unit) occurs [27]. Depending on the source and preparation, chitosan molecular weight ranges from 300 to 1000 kDa [29].

Chitosan is biodegradable [14, 29, 31, 33, 34], biocompatible [14, 29, 31, 33, 34], bioadhesive [14], osteoconductive [33], non-toxic [14, 29], antimicrobial [28, 29], antifungal [14], antibacterial [14, 34], it participates in the enhancement of immunogenicity [34], it is a hydrating agent [14, 29], it is hemostat [35], it is hydrophilic [3], it has antitumor activity [34], it has reactivity [3], it is non-allergenic [14], and it is wound healing (stimulates the improvement level of natural hyaluronic acid synthesis [35]) [29, 33, 35].

Chitosan can be processed into membranes [35], hydrogels [29, 31, 34, 35], beads [14, 35], fibers [14], films [14], nanofibers [14, 29, 35], sponges [14, 29, 35] micro/nanoparticles [31, 35], and gels [14] and it presents many applications, specifically drug delivery [28, 30, 31, 35], gene delivery [35] and therapy [31], bioimaging [31], wound healing [35], artificial skin [30], ophthalmology [30] and tissue engineering [28, 31, 35].

3.2. Methods

3.2.1. Processing techniques

3.2.1.1. Synthesis of hyaluronic acid-dopamine conjugate (HA-DN)

The synthesis of hyaluronic acid-dopamine conjugate was produced using N-(3-Dimethylaminopropyl)-N'-ethylcarbodiimide hydrochloride (EDC) as the activation agent. This synthesis was based on Lee and co-workers procedure [6].

Thus, 1g of hyaluronic acid (HA) was dissolved in 100 mL of phosphate buffered saline (PBS) solution (Laborspirit Company). Under magnetic stirring, the pH was adjusted to 5.5 using sodium hydroxide (NaOH) or hydrochloric acid (HCl) aqueous solutions (0.5 M) [6]. Then, during thirty minutes, the solution was purged with nitrogen.

Afterwards, 338 mg of N-(3-Dimethylaminopropyl)-N'-ethylcarbodiimide hydrochloride (EDC) (purchased on Sigma-Aldrich Company) and 447 mg of dopamine (DN) (purchased on Sigma-Aldrich Company) were weighed and added to the previous solution. The synthesis of HA-DN was done in pH of 5.5 a 4°C, for 2 hours, as it can be seen in Figure 3.4 below.

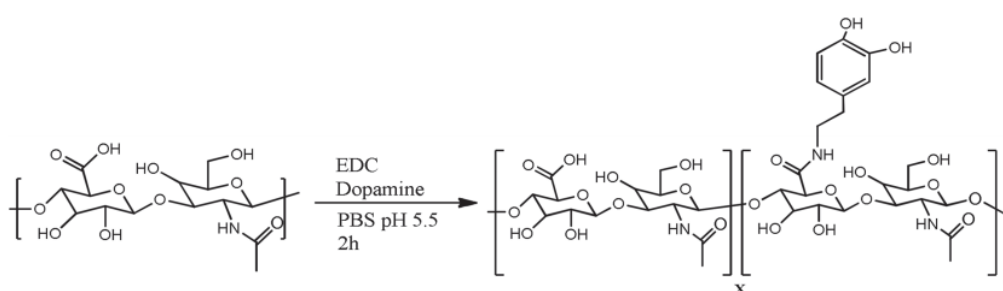


Figure 3. 4 - Synthesis of HA-DN conjugate [5].

During a week, dialysis was made in order to remove all unreacted chemicals using distilled water. Afterwards, the HA-DN conjugate was lyophilized for 4 days. To avoid the oxidation of HA-DN conjugate [5] in the presence of light and air, this was stored at 4°C with an aluminum film.

3.2.1.2. Bioglass nanoparticles (BG-NPs) production

Bioglass nanoparticles (BG-NPs) were prepared using the protocol present in [36], using the sol-gel method. This method is optimized for our group to obtain the ternary system of BG (SiO_2 ; CaO ; P_2O_5 (mol %) = 50:45:5). Briefly, at room temperature, 7.639 g of calcium nitrate tetrahydrate was dissolved in 120 mL of deionized water. After that, using 60 mL of ethanol absolute and 9.8353 mL of tetraethyl orthosilicate were added to the calcium nitrate solution. The pH was adjusted to 2 with a citric acid solution (30 mL, 10%), and the reaction was left to agitation for 3 h to produce solution A. For the solution B, 1.078 g of ammonium phosphate dibasic was dissolved in deionized water, and ammonium hydroxide solution was used to adjust the pH to 11.5.

Then, solution A was added drop-by-drop to solution B. Ammonium hydroxide solution was used to maintained the pH value at 11.5. This mixture was left to dissolve under

magnetic stirring during 48 h, and then a resting period of 24 h followed. The precipitate was washed three times with distilled water and was stored for 24 h at the ultra-low freezer ($T = -80\text{ }^{\circ}\text{C}$). The precipitate was subsequently freeze dried for 7 days. The gel was calcinated at $700\text{ }^{\circ}\text{C}$ during 3 h. Zeta (ζ) (Nano ZS) from Malvern Instruments with a Dispersion Technology Software (DTS) potential analysis were performed to order to evaluate its stability using the laser Doppler velocimetry mode of the Nano-ZS instrument (Malvern).

3.2.1.3. Silver doped bioglass nanoparticles (Ag-BG-NPs) production

Based on Delben and co-workers [37] protocol, the Ag-BG-NPs, with % 10 mol of silver (Ag), i.e., nanoparticles composed by $\text{SiO}_2\text{-CaO-P}_2\text{O}_5\text{-Ag}_2\text{O}$ (mol % = 56:30:4:10) was prepared. Briefly, ammonium phosphate dibasic, calcium nitrate tetra hydrate 99%, ethanol absolute, ammonia water (ammonium hydrogen phosphate 98%, maximum of 33% NH_3), and hydrochloric acid (HCl) were purchased on Sigma-Aldrich company. Also, tetraethyl orthosilicate (TEOS) 99.90% was purchased by Merck Chemicals, nitric acid monohydrate 69% was obtained by VWR. Silver Nitrate (AgNO_3) was obtained by VWR. To produce these nanoparticles was necessary firstly, at room temperature, add osmotized water to tetraethyl orthosilicate (TEOS), and then added together ethanol absolute. It's necessary take in account the pH value, and it should has a value of 2 with addition of nitric acid (2M). The reaction mixture was kept stirring for 60 min to produce a solution A. Then, for producing the solution B, calcium nitrate tetrahydrate, ammonium phosphate dibasic and silver nitrate were added to 1500 mL of osmotized water and the pH value was adjusted to 11.5 with ammonium hydroxide solution. The reaction mixture was kept under stirring for 60 min. Under smooth stirring, the solution A was slowly added to the solution B drop-by-drop. During this step, the pH value of solution B was maintained at 11.5 using ammonia hydroxide solution. Then, the final solution was kept under stirring for 48h.

Eight different thermal treatment of nanoparticles were done, to be precise 1 day on 50°C , 1h at 100°C , 2h at 100°C , 2h at 90°C plus $\frac{1}{2}$ h at 100°C , $100^{\circ}\text{C}/\text{h}$ plus $\frac{1}{2}$ h at 400°C , $100^{\circ}\text{C}/\text{h}$ plus $\frac{1}{2}$ h at 500°C , $100^{\circ}\text{C}/\text{h}$ plus $\frac{1}{2}$ h at 580°C and $100^{\circ}\text{C}/\text{h}$ plus $\frac{1}{2}$ h at 700°C . Using a concentration of 0.3 mg/mL, Ag-BG-NPs were suspended in ultra-pure water (UPW) with 0.15 M NaCl and saline (0.15 M NaCl, pH = 5.5) solutions under magnetic stirring during 30 minutes and further ultrasonic dispersion at 25°C during 15 minutes. Moreover, the Zetasizer equipment (Nano ZS) from Malvern Instruments with a

Dispersion Technology Software (DTS) was used to perform this analysis. Moreover, to study their morphology the High-Resolution Field Emission Scanning Electron Microscope with Focused Ion Beam (FIB-SEM) (AURIGA COMPACT, ZEISS) and the Scanning Electron Microscope (SEM) with EDS (JSM-6010 LV, JEOL, Japan) coupled with dispersive X-ray spectroscopy (INCAx-Act, PentaFET Precision, Oxford Instruments) equipment were used. Also, Fourier Transform infrared spectroscopy was used to analyze the nanoparticles powder in order to know their characteristic functional groups. The results in this article were obtained using the FT-IR (infrared spectrum-Jasco), in attenuated total reflectance (ATR), transmission mode. The FT-IR spectra were recorded from 400 to 4000 cm^{-1} . To the purpose of this paper the Bruker AXS D8 Discover, USA equipment was used, which is present in SEMAT labs, Physics Department, Science Scholl, University of Minho to analyze the chemical elements in quaternary silver doped bioglass nanoparticles and hydroxyapatite characteristics peaks after 7 days immersed in modified-simulated body fluid (m-SBF 1.5 x). The Cu-K α radiation ($\lambda=1,54060\text{\AA}$), scanning from 15° to 60° at a speed of 0,04°/1s was used. The analysis for phase identification was performed using analytical software EVA. The crystalline phases were indexed using the ICDD-2015 database (International Center for Diffraction Data).

3.2.2. Free-standing films production

Medium molecular weight chitosan (CHT) purchased on Sigma-Aldrich Company, which was purified by recrystallization with an N-deacetylation degree of 80% and a molecular weight obtained by viscosimetry of 770 kDa, silver bioglass nanoparticles heat treated at 2 hours at 90°C and ½ hour at 100°C, hyaluronic acid-dopamine conjugate (HA-DN) and hyaluronic acid from *Streptococcus equi.*, purchase on Sigma-Aldrich, with a molecular weight of 595 kDa were used to produce free-standings films).

Briefly, fresh chitosan solutions in 1% of acetic acid (CH_3COOH), hyaluronic acid (HA) and hyaluronic acid-dopamine conjugate (HA-DN) solutions were prepared, with a final concentration of 2 mg/mL. Silver doped bioglass nanoparticles (Ag-BG-NPs) solutions, with 0.15 M of NaCl as solvent were done. The final concentration was 2.5 mg/mL. Furthermore, as washing/rinsed step solutions, with distilled water and 0.15 M of NaCl, were prepared. In another works of our group were used a pH of 5.5 [38, 39]. Poly(propylene) (PP) films were used as a substrate. Different formulations were done, namely:

Formulation 1: [CHT/HA/CHT/HA]₇₅;

Formulation 2: [CHT/HA-DN/CHT/HA-DN]₇₅;

Formulation 3: [CHT/HA/CHT/Ag-BG-NPs]₇₅;

Formulation 4: [CHT/HA-DN/CHT/Ag-BG-NPs]₇₅.

The multilayers films were built-up with 10 minutes immersed in HA, HA-DN or CHT solutions, 5 minutes in a washing solution and 20 minutes in Ag-BG-NPs solution. The films were built-up with 75 tetralayers using a dipping robot (University of Minho), shown in Figure 3.5.

Two different crosslinking processes were done, with two different concentrations. Regarding the first crosslinking process: firstly, N-(3-Dimethylaminopropyl)-N'-ethylcarbodiimide hydrochloride (EDC) (30 and 50 mg/mL) and N-hydroxysuccinimide (NHS) (11 mg/mL) were dissolved in distilled water with a pH of 5.5. The free-standing films were put in contact at 4°C overnight. Then, the films were washed with phosphate buffered saline (PBS) solution and were left to dry during 1 day at room temperature. This protocol was based on Caridade and co-workers' [40] work. As far as the second crosslinking process is concern, free-standing films were put in contact with 1 mg/mL of genipin (Sigma-Aldrich), dissolved DMSO/sodium acetate buffer (0.15 M NaCl) overnight at 37°C. The resulting crosslinked freestanding films were then washed with sodium acetate buffer (0.15 M NaCl, pH 5.5) during 30 minutes and then with DW during 1 hour. Finally, the FS films were dried during 1 day at room temperature. This crosslinking process was based on Silva and co-workers' [41] work.



Figure 3. 5 - Dipping robot [42].

3.2.3. Hydrogels production

3.2.3.1. Synthesis of chitosan hydrogel

Based on Oliveira and co-workers [43] work, solutions of purified medium molecular weight chitosan (CHT) (Sigma-Aldrich) was prepared in acetic acid (2% v/v) in concentrations of 2% (w/v) of CHT. Also, 12.5% w/v of bioglass nanoparticles relative to the total mass of CHT were incorporated. 80 μ L of each solution was dropped in a PDMS mold well (5 millimeters of diameter and 4 millimeters of height). 40 μ L of genipin with concentrations of 1 v/v % and dissolved in a 10 ethanol–90 water mixture were dropped on the top of each well. The crosslinking reaction occurred overnight at 37 °C and it was stopped by immersing the hydrogels in ethanol (to clean the genipin residues), and afterwards in PBS at 37 °C for 1 hour.

3.2.3.2. Synthesis of chitosan dopamine conjugate (CHT-c)

Chitosan chemically modified with catechol groups (CHT-cat) was synthesized using EDC chemistry, where the catechols were conjugated to the amine groups of chitosan, based on the procedure proposed by Ryu and co-workers [44].

Briefly, 60 mL of 1% (w/v) low molecular weight chitosan (CHT) solution was prepared in hydrochloric acid (HCl) at pH 2.5. Then, 0.145 g of hydrocaffeic acid (HCA) was dissolved in 15 mL of ethanol to prevent precipitation and 0.356 g of EDC was dissolved in 15 mL of deionized water. These two solutions were mixed and added to chitosan solution under intensive stirring at room temperature for 18 h and the pH of the reaction solution was maintained to 5.5. The resulting products were purified by dialysis in acidic deionized water solution (pH 5.0, HCl) for typically 2 days, in PBS buffer for 4 h and in deionized water for 4 h. The final product was lyophilized and kept in a moisture-free desiccator. Characterization of the conjugate was performed UV-vis spectrophotometry, in order to confirm the correct modification of the modification of chitosan with the catechol groups present in hydrocaffeic acid, and also to determine the degree of substitution of hydrocaffeic acid in the modified chitosan.

3.2.3.3. Production of a poly(dimethylsiloxane) (PDMS) mold

In order to create a poly(dimethylsiloxane) (PDMS) mold, Sylgard(r) 184 silicone elastomer kit was purchased from Dow Corning (Seneffe, Belgium). The curing agent was added to the silicone in a proportion of 1:9. After mixing vigorously the resultant mixture was put into Petri dishes. Then, the samples were stored under vacuum for 30

minutes in order to remove the air bubbles. Finally, to accelerate the gelation of the PDMS mold, the samples were left at 60°C until complete crosslinking. After that, the PDMS mold was punched (5 mm of diameter and 4 mm of height).

3.2.4. Characterization techniques

The various characterizations techniques used to develop this experimental work will be presented in this section.

3.2.4.1. Fourier transform infrared spectroscopy (FT-IR)

Firstly, it is important to understand what spectroscopy is. This is based on the interaction between matter and electromagnetic radiation [45]. The latter is defined by its frequency (ν) and velocity of light in vacuum, $3 \times 10^{10} \text{ cms}^{-1}$ [45]. The wavelength (λ) is obtained by division of velocity by frequency, equation 1 [45].

$$\lambda = c / \nu, \text{ in } \mu\text{m} \quad (1)$$

However, it is used the reciprocal of wavelength, ν^* in cm^{-1} , equation 2 [45].

$$\nu^* = \nu / c, \text{ in } \text{cm}^{-1} \quad (2)$$

The identification of characteristic functional groups is possible due to the characteristic absorption bands at well determined frequencies [45]. FT-IR provides molecular-level information [45, 46], namely chemical changes [45], functional groups [47], molecular conformations [46, 47], crystallinity [45], bonds [47] and orientation [45]. Spectral bands provide the identification of biochemical composition [47]. Each polymer has an unique vibrational mode [45].

A molecule is detectable through infrared if their dipole moment ($\vec{\mu}$) alters during its molecular vibration [46].

The energy of a molecule is similarly divided between all types of motion or degrees of freedom. Each molecule with N atoms presents three translational degrees of freedom, namely 3N, rotation, vibration and translational degrees. Three angles are needed to define the rotation of the molecule about the three perpendicular axes through its center mass (x, y and z). Three degrees of freedom belong to translational movement of molecule, so it obtains 3N-3 independent degrees of freedom. For rotational movement, there are 3 movements too. In summary, there are 3N-6, independent degrees of freedom [45, 48], for non-linear molecules [46].

In this technique, soluble and insoluble materials can be studied, namely films [45], fibers [45], bulk samples [45] or powders [45]. Soluble materials are normally studied in solution [45], for films the normal thickness used is 5 to 20 μm . As for powders, palletization is used before mixing in an infrared transparent powder, normally KBr [45]. This technique is simple [47], reproducible [47] and requires minimum sample preparation [47].

In regard to the equipment, infrared spectrometers have a wavenumber range 4000 to 200 cm^{-1} . The components of FT-IR are infrared source, namely Ever-Glo ceramic, Michelson interferometer and IR detector, that measure the intensity of the IR radiation passing through the sample [49]. The spectra can be obtained by reflection method or transmission (most commonly used).

As far as the attenuated total reflectance is concerned, when an electromagnetic radiation reach to an interface of two media refraction, reflection and refraction occurs. In ATR equipment, and according to Snell law, once the crystal is higher refractive index than air, then there is a critical angle (α_c) wherein the angle β is zero on media 2, and therefore the sine of that angle is 1, because when electromagnetic radiations reach to another medium, there is a different physical density. In this situation, internal reflection occurs. It is mandatory that there is contact between the crystal surface and sample, to obtain good-quality spectra [50].

Fourier Transform infrared spectroscopy was used to analyze the functional groups of silver doped bioglass nanoparticles powder heat-treated and without thermal treatment, see Chapter 4. Also, this equipment was used to analyze the uncrosslinked and crosslinked free-standing films - see Chapter 5. The results were obtained using the FT-IR (infrared spectrum-Jasco), in attenuated total reflectance (ATR), transmission mode. The FT-IR spectra were recorded from 400 to 4000 cm^{-1} .

3.2.4.2. Ultraviolet-visible spectroscopy (UV-vis)

Molecules have electrons that participate in bonds (π -electrons) or non-bonding electrons (n-electrons) [51]. The electrons were excited to higher anti-bonding molecular orbitals, after absorbing UV-vis radiation. Using the Beer–Lambert law (equation 3), it's possible to determinate the concentration, quantitatively, in a solution [51]. UV-vis technique allows the identification of electrons transfer into bands of atoms, orbitals, ions and molecules in solids, liquids and gases.

$$A = \log_{10} (I_0/I) = \epsilon c L \quad (3)$$

Where:

A: absorbance [51];

I_0 : intensity of the incident light [51];

I: transmitted intensity [51];

L: length of sample (cm) [51, 52];

c: concentration of the absorbing species (mol/L) [51, 52];

ϵ : molar absorptivity for each species and wavelength (L/mol·cm)[51, 52].

Ultraviolet and visible radiation (UV-vis) include a small part of the electromagnetic spectrum. The UV-vis technique offers reduced qualitative information. Various chromophores exhibit a wavelength where they have absorbance maxima (intensity and wavelength of absorbance maximum alters with solvent, pH and temperature). The UV-vis technique isn't an absolute technique. The obtained spectra is analyzed through comparison with a reference spectrum [53].

With regard to sample preparation, for powders samples, diffuse reflection is used (DRS) [54]. For samples in solution, it is mandatory that a pure sample of the solvent (blank) is used [53]. The spectrophotometer is used to measure the absorbance (A) or transmittance of a given sample depends on the wavelength of electromagnetic radiation. This is made by two source lamps (deuterium and a tungsten), and a monochromator, which transmits a thin band of light that passes through the sample and ends in a detector. Measuring the intensity of light, I_0 , and the intensity of light detected by the detector, I the absorbance can be calculated (see equation (3)).

Different solutions with different concentrations of hyaluronic acid-dopamine conjugate (HA-DN) (0.5 mg/mL, 1 mg/mL, 1.5 mg/mL and 2 mg/mL) and hyaluronic acid (HA) (0.5 mg/mL, 1 mg/mL, 1.5 mg/mL and 2 mg/mL) were made in order to investigate the correct modification of HA - see Appendixes 2.1 to 2.3. Also, the UV-vis spectrophotometer (Shimadzu UV - 1601), shown in Figure 3.6, was used to investigate the correct modification of medium molecular weight chitosan with catechol groups - see Chapter 6. 1 cm quartz cells were used (because quartz cells are transparent to UV light). The UV-vis data were recorded from 200 to 4000 nanometers (nm).



Figure 3. 6 - UV-vis spectrophotometer.

3.2.4.3. Atomic force microscopy (AFM)

Atomic force microscopy is a topographic technique [55]. This is used for direct measurements of micro-structural parameters [56] on a nanometer scale [57]. AFM is used to measure surface roughness [55], as well as to investigate surface properties, namely measuring adhesion forces [55], friction [55], viscoelastic properties [55]. Atomic force microscopy is also useful to identify the intermolecular forces at nanoscale [56]. The drawback of this technique is the sample conductivity [52].

AFM system consists of a cantilever [51] probe [51, 56]. The cantilever is made of silicon nitride or silicon, with 100–200 mm long and 1 mm of thickness and a tip radius. In regard to the functioning mechanism, if the tip is brought close to the sample surface, then there is a deflection of the cantilever according to Hooke's law, because the force between the tip and sample leads to a deflection of the cantilever [51]. AFM scans the sample surface with feedback mechanisms. A piezoelectric scanner maintains the tip at a constant force, or constant height above the sample surface. The up and down movement with the contour, the laser beam deflected from the cantilever offers measurements of the difference in light intensities between the photo detectors. There are two modes: constant force mode, and constant height mode. In the first case, the transducer monitors real time height deviation and in the second case, the deflection force is registered [56].

Three different modes are possible in AFM, namely the intermittent contact mode, non-contact mode and contact mode [51]. As far as the intermittent contact mode is concerned, the cantilever moves up and down at a small distance and its movement is equal to a resonant frequency [51]. The tip of the cantilever, in the non-contact mode, doesn't make direct contact with the sample surface, because the cantilever moves at a low frequency (above its resonant frequency). Finally, with regard to the contact mode, the AFM tip

scans across the surface at a very low force. The deflection is due to the repulsive force between the surface atoms and the tip [51].

To the purpose surface roughness analysis was used the Atomic Force Microscope (AFM). For the characterization of the samples, AFM Dimension Icon (Bruker, USA) was used in PeakForce Tapping (ScanAsyst) in air. Moreover, the AFM cantilevers (ScanAsyst-Air, Bruker) made of silicon nitride with a spring constant of 0.4 N/m and frequency of 70 kHz were used – see Chapter 5 and Appendix 4.

3.2.4.4. Scanning electron microscopy coupled with energy dispersive X-ray spectroscopy (SEM-EDS)

Scanning electron microscopy (SEM) is an electron microscopic technique. This allows us to obtain images of a sample surface by scanning a focused energetic electron beam, since it allows a study of the surface morphology and identifies small areas. The functional mechanism is based on primary electrons (emitted by an electron gun) that interact with atoms, in the sample surface [51]. When this lose energy collides on the sample, it implies a loss of energy, since they “repeated random scattering and absorption within a volume of the specimen known as the interaction volume, which resembles a tear drop or balloon with a depth of 1–5 mm into the surface depending on the electron energy. Various signals originate from different depths of the interaction volume and secondary electrons are emitted from the top 5–10 nm of the sample surface and contain topographical information” [51]. The electron beam passes through scanning coils deflector plates or deflector plates in the electron column. This passing is necessary in order to have a deflection and to scan the studied area, which, normally is-rectangular [51]. Then, the emitted signals are perceived by detectors and then amplified and displayed on a cathode ray tube, which, by its turn, is synchronized with the rastering of the electron beam. Finally, the obtained image can be considered an intensity map of the signals emitted [51]. It is mandatory the existence of vacuum in the system, i.e., 933 to 1.333 Pa [52].

With regard to SEM-EDS, this has an energy-dispersive X-ray spectroscopy (EDS) detector. This equipment is used for chemical characterization or elemental analysis. Since x-rays are produced by primary electrons and the emitted energy is specific of the element from which it is emitted, the composition of the sample in study can be determined just by measuring the energy emitted by the sample [51].

For sample preparation, it is normally required for it to be dry. Furthermore, the sample should be electrically conductive. In case of hydrated and non-conductive materials, it is mandatory a range of pre-treatments [51].

The High-Resolution Field Emission Scanning Electron Microscope with Focused Ion Beam (FIB–SEM) (AURIGA COMPACT, ZEISS), shown in Figure 3.7, and the Scanning Electron Microscope (SEM) with EDS (JSM-6010 LV, JEOL, Japan) coupled with dispersive X-ray spectroscopy (INCAx-Act, PentaFET Precision, Oxford Instruments) equipment were used to evaluate the surface morphology and the chemical elements present on the samples surface.



Figure 3. 7 - High-Resolution Field Emission Scanning Electron Microscope with Focused Ion Beam (FIB – SEM) [58] .

3.2.4.5. Transmission electron microscopy (TEM)

TEM is used to understand the morphology of polymers. In order to use this technique it is mandatory that the sample in study has at least 10^{-7} to 10^{-8} m to avoid the degradation of samples. For samples with more thickness and no contrast, to obtain electron diffraction it is necessary that an electron beam passes on established points of the sample. For that reason, no knowledge exists about bulk materials [45].

As far as the scanning transmission electron microscopy (S-TEM) is concerned, “high atomic-number contrast may be obtained”, because “[...] the diffracted beams emerging from the sample are recombined on the viewing screen of the microscope. The resultant contrast depends on the relative phases of the diffracted beams, which is sensitive to microscope and sample parameters [59].”

Scanning transmission electron microscopy (S-TEM): the NanoSEM-FEI Nova 200 (FEG/SEM); EDAX - Pegasus X4M (EDS/EBSD) equipment was used to analyze eight

different thermal treatment of nanoparticles, to be precise 1 day on 50°C, 1h at 100°C, 2h at 100°C, 2h at 90°C plus 1/2h at 100°C, 100°C/h plus ½ at 400°C, 100°C/h plus ½ at 500°C, 100°C/h plus ½ at 580°C, 100°C/h plus ½ at 700°C and the powder gel in SEMAT labs, Physic Department, Science Scholl, University of Minho, Guimarães, Portugal.

3.2.4.6. X-ray diffraction (XRD)

According to Guinebretière [60], a material emits an x-ray beam with a wavelength equal to the x-ray beam that it was used to irradiate it [60]. The utilization of X-ray diffraction XRD method provides much information, namely on nanostructured materials, phase identification, nanoparticles orientation, nanowires and tubes. Regarding the functional mechanism, when a monochromatic X-ray beam radiates on the crystalline material, there is a diffracted beam due to the arrangement of atoms in the sample [49].

The Bragg's law allows the calculation of the interplanar spacing between atomic planes, d , as it can be seen on equation 4. The calculation of d allows the knowledge of structural parameters, namely cell volume and unit cell dimensions [49]. Miller indices characterize the atomic planes. These indices show the interception of the crystallographic axes with a plane and they are associated with the unit cell dimension [45].

$$2 d \sin(\theta) = n \lambda \quad (4)$$

Where:

d = the interplanar spacing between atomic planes [49];

2θ = angle between the primary beam and the diffracted beam;

θ = angle between the crystalline domains and the diffracted beam;

n = order of reflection;

λ = the wavelength of the X-rays [49].

When an electron bombards the sample its electron moves to the excited state. They return to the minimum state of energy emitting x-rays photons with the equal energy of the different electron shells [61]. It is mandatory that the incident waves have wavelengths similar to the distance between atoms [62].

In the Bragg-Brentano diffractometers the distance between the sample and the detector is constant. According to Guinebretière [60] there are two devices with equal distance sample-detector: θ - 2θ detector and θ - θ detector. Regarding the first, the x-ray source

is static and the sample moves at a velocity ω and the detector moves a velocity 2ω . The detector measure the diffraction peaks relative to the angle θ . As to the second type of detector, the sample is static, but the x-ray source and detector moves in contrary directions at a velocity ω [60].

The Bruker AXS D8 Discover, USA equipment, shown in Figure 3.8, was used, which is present in SEMAT labs, Physic Department, Science Scholl, University of Minho, to analyze the chemical elements in quaternary silver doped bioglass nanoparticles before and after immersion in m-SBF 1.5 x during 7 days and the hydroxyapatite characteristics peaks on the free-standing films after 14 days immersed in m-SBF 1.5 x solution. The Cu-K α radiation ($\lambda = 1,54060\text{\AA}$), scanning from 15° to 60° at a speed of $0,04^\circ/1s$ was used. The analysis for phase identification was performed using analytical software EVA. The crystalline phases were indexed using the ICDD-2015 database (International Center for Diffraction Data). The results are shown in Chapters 4 and 5.

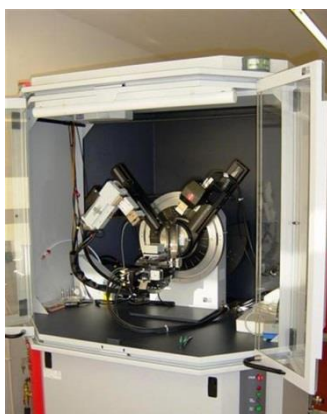


Figure 3. 8 - Bruker D8 Discover equipment, present in SEMAT labs [63].

3.2.4.7. Water contact angle measurement

The contact angle of a liquid drop with the biomaterial surface (substrate) is defined as the angle formed by the liquid and the phase boundary, i.e., gas and solid interacting phases [49]. The functional mechanism of contact angle measurement is the tangent of a liquid drop with a solid surface at the base [49, 64]. This technique is useful to estimate the solid–vapor and solid–liquid interfacial tensions [64]. The definition of surface tension is the energy necessary to create a unit area of an interface. Using the Young’s equation, equation 5, the surface energy can be calculated by measuring the surface tension of the liquid and the contact angle [49].

$$\gamma_s = \gamma_{sl} + \gamma_l \cos(\theta) \quad (5)$$

Where:

γ_s = surface tension components of the solid phase [49];

γ_{sl} = interfacial tension between the two phases [49];

γ_l = surface tension components of the liquid phase [49];

θ = Young contact angle [64] .

The spreading parameter, S , is also used. This measures the difference between the surface energy of the sample under dry or wet conditions, as can be seen on equation (6).

$$S = \gamma_s - (\gamma_l + \gamma_{sl}) \quad (6)$$

There are three types of solid surfaces: high-energy surfaces and low-energy surfaces and materials with high-surface energy. If low-energy materials have negative surface tension (< 0)-the liquid does not spread. When surface tension is bigger than zero, then the liquid spreads completely with zero θ to lower its surface [49]. To summarize, if $\theta < 90^\circ$, then the liquid wets the surface. When $\theta > 90^\circ$, the liquid doesn't wet the surface. Both hypotheses occur if surface tension is lower than zero [49]. Contact angle measurement has advantages, such as the evaluation of interactions occurring between gas, liquid, and solid phases. Furthermore, it is sensitive, simple, and inexpensive. This technique allows the characterization of the surface and it also allows the knowledge of physical properties of the studied material.

In order to analyze the wettability of films was used using an OCA15 plus goniometer equipment (DataPhysics, Germany), shown in Figure 3.9. The contact angle measurement were performed on both sides of the films, i.e., “top” corresponds to the top of the film, i.e., hyaluronic acid, hyaluronic acid-dopamine conjugate and/or silver doped bioglass nanoparticles and “bottom” surface corresponds to the film in contact with the substrate (poly(propylene), PP), chitosan (CHT). A drop of 3 μL of ultra-pure water (UPW) was used to measure the WCA values. The measurements were performed at room temperature ($T = 25^\circ\text{C}$) and the pictures were taken after the drop contact the surface. To assess the WCA values were used the SCA20 software – see Chapter 5.



Figure 3. 9 - Contact angle goniometer equipment [65].

3.2.4.8. Bioactivity studies

When artificial materials are implanted into bone, normally defects are encapsulated by a fibrous tissue. This fibrous tissue causes their isolation from the bone [66]. According to Kokubo and co-worker [66], Hench and co-workers developed a Bioglass ® and “showed that a SiO₂-rich layer and calcium phosphate film are formed on the surface of Bioglass when implanted in the body environment” [66]. Bioglass ®, when analyzed by Fourier transform infrared spectroscopy, x-ray diffraction, transmission electron microscopy and scanning electron microscopy and transmission electron microscopy after the presence in simulated body fluid (SBF) showed that the layer created was comparable to mineral bone in structure and composition [66].

Simulated body fluid (SBF) is a solution with a similar pH and ion concentrations to human blood plasma [68]. A kinetic of precipitation of Ca-P was made by many authors, however Ca-P precipitation analysis in SBF remains rare, because of its complexity and of its chemical composition. The precipitation analysis is also difficult due to all the association/dissociation between ions and ion groups [68]. To accelerate apatite nucleation, elevated degrees of saturation are needed, which is called supersaturation. Apatite nucleation is guaranteed by adsorption of silicate and calcium ions that are released [67].

These studies were conducted by immersion the four different formulations of free-standing films into the modified-simulated body fluid solution (m-SBF 1.5 x). This solution was prepared following the Oyane and co-workers [69] and Oyane and co-workers [70] procedures. This solution was prepared dissolving sodium chloride (NaCl, Merck), sodium sulphate (Na₂SO₄, Panreac), magnesium chloride hexahydrate

($\text{MgCl}_2 \cdot 6\text{H}_2\text{O}$, Merck), di-Potassium hydrogen phosphate trihydrate ($\text{K}_2\text{HPO}_4 \cdot 3\text{H}_2\text{O}$, Merck), calcium chloride (CaCl_2 , Merck), potassium chloride (KCl, Merck), sodium hydrogen carbonate (NaHCO_3 , Merck), sodium carbonate (Na_2CO_3 , Merck), sodium hydroxide (NaOH, Panreac) and 2-(4-(2-hydroxyethyl)-1-piperazinyl) ethanesulfonic acid (HEPES, $\text{C}_8\text{H}_{18}\text{N}_2\text{O}_4\text{S}$, Sigma) in ultra-pure water (UPW) at 36.5°C . The final pH was adjusted to 7.4.

All the nine samples in study in Chapter 4 were put in contact with a carbon tape (to stick) and immersed in 25 mL of m-SBF 1.5 x during 7 days at 37°C . After that time, they were washed with distilled water and were put under air drying during 1 day. The results are shown in Chapter 4 and Appendix 1. Moreover, in Chapter 5, the free-standings films were put into a substrate of poly(propylene) holders with a window of 7 mm x 7 mm and immersed, during 14 days in 10 mL of SBF solutions at 37°C . After being removed from m-SBF 1.5 x solution, the films were washed with distilled water (DW) and were put under air drying overnight. These films were characterized by diverse characterization techniques, namely Scanning Electron Microscope (SEM) with EDS (JSM-6010 LV, JEOL, Japan) coupled with dispersive X-ray spectroscopy (INCAx-Act, PentaFET Precision, Oxford Instruments) (see Chapter 5 and Appendix 5) and Bruker AXS D8 Discover, USA equipment, with Cu-K α radiation ($\lambda=1,54060\text{\AA}$), scanning from 15° to 60° at a speed of $0.04^\circ/\text{s}$. The analysis for phase identification was performed using analytical software EVA. The crystalline phases were indexed using the ICDD-2015 database (International Center for Diffraction Data). The results are shown in Chapters 4 and 5.

3.2.4.9. Adhesion tests

In adhesive bonding, the adhesive serves as an intermediate for load transmission [71]. There are two different methods in adhesive tests, namely quantitative and qualitative methods. Quantitative methods are used for producing property data for design purposes and qualitative methods are used to obtain results about the performance of bonded systems. In regard to adhesive joints tests there are factors that are necessary to have in mind, because they can alter the reproducibility and repeatability, namely processing variables, specimen and machine alignment, adhesive storage and joint ageing and surface treatment [72]. Adhesion joint tests are peel [72], tensile [72], shear [72], cleavage [72] and toughness [72].

According to ASTM D1002 standard [73], the test method has “applications in controlling surface preparations, primer, and adhesive systems for determining strength properties of tested systems [...] The recommended thickness of the sheets is 1.62 ± 0.125 mm (0.064 ± 0.005 in.). The recommended length of overlap for most metals of 1.62 mm (0.064 in.) in thickness is 12.7 ± 0.25 mm (0.5 ± 0.01 in.)” and it is “[...] recommended that test specimens be made up in multiples of at least five specimens, and then cut into individual test specimens” [73], as can it be seen in Figure 3.10. The adhesion tests were performed according the ASTM D1002 standard. The adhesive strength was evaluated through the lap-shear adhesive stress tests. Briefly, the free-standing films were cut with 5 mm width and 15 mm length and with an overlapping area of 3.75×5 mm². Then, they were put between two lamellae and soaked in phosphate buffered saline (PBS) solution overnight. They were tested in the referred universal testing machine under the same conditions with a load speed of 5 mm/min). The lap shear strength was determined from the maximum of the stress-strain curve. The data is presented as Mean \pm SD using at least five specimens.

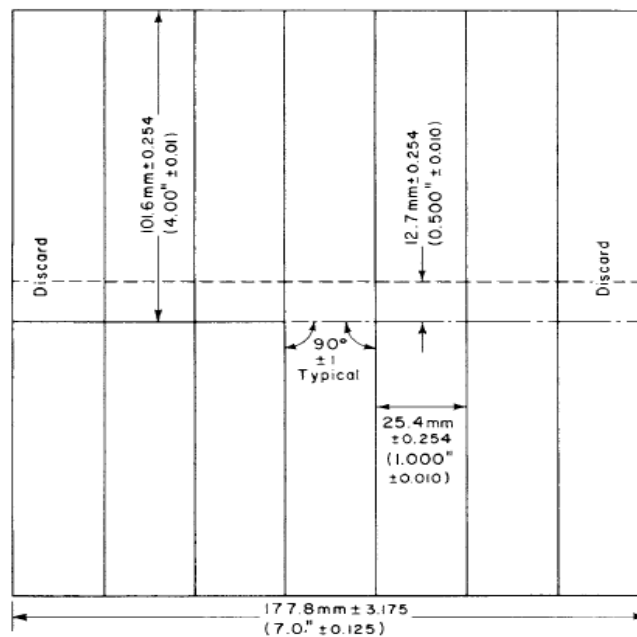


Figure 3. 10 - Dimensions of the test panel (standard) [60]

3.2.4.10. Mechanical tests

According to D. W. Van Krevelen [74], the mechanical properties of polymers are important for applications where polymers are used as structural materials. Furthermore, mechanical tests provide the knowledge of the chemical resistance or ageing of materials [75]. Indeed, much information can be gathered, but the most important mechanical

property of polymers is the modulus [74]. There are three types of deformations, namely the shear, tension and hydrostatic pressure. In this dissertation only the tensile test is explored, used for films, but there is also the compression test for hydrogels. In the first case, the specimen is submitted to an uniaxial load until the material fractures [76]. According to Aklonis [77], the tensile modulus (E) is defined as, equation (7).

$$E = \sigma/\varepsilon = (F/A)/(\Delta L/L) \quad (7)$$

Where:

E : tensile modulus [MPa] [75, 77];

σ : tensile stress [MPa] [75, 77];

A : cross sectional area [mm²] [75, 77];

ε : tensile strain [%] [75, 77];

ΔL : length between gauge marks minus the original gauge length (L) [mm] [75, 77].

The properties of polymers are dependent on humidity [75], temperature [75] and timescale or speed of test [75], because polymers are viscoelastic materials. The mechanical test results will have variability due to variations in sample preparation [75], sample material [75], machine accuracy [75] and test procedure, that are designed to minimize errors [75].

The Young modulus, also called as modulus of elastic or tensile modulus, per definition is the “ratio of the applied stress to the strain it produces in the region where strain is proportional to stress, i.e., in the initial straight-line portion of the stress-strain curve. [75]” The Young modulus provides information about the stiffness of the material in study [75].

Regarding the mechanical universal testing machine equipment, these, normally, are vertical machines. These are constituted by load cells, that measure forces values. To do the mechanical tests the use of grips are required. There are various types of grips, namely wedge, Gavin, pneumatic and eccentric grips. They may ensure the alignment of the specimen and not allow shearing, bending or twisting [75].

Tensile strength tests were performed using a universal electromechanical testing machine equipment (Instron 5543, USA), equipped with a 1 kN load cell, using the tensile mode. The samples for mechanical tests were cut with 0.6 cm width, 3.0 cm length and

with a gauge length equal to 1.2 cm. The thickness of the dried samples was measured three times ($n = 3$) for each sample. The same dimensions and the same gauge length were chosen for the wet tensile tests, but the samples were previously immersed in PBS during 60 min. The measurements were taken under a loading speed of 1.5 mm/min. for the dry samples and 0.5 mm/min. for the wet samples. The values were calculated through analysis of the stress-strain curves, such as the ultimate tensile strength (UTS, in MPa), tensile Young modulus (MPa) and the strain at break (ϵ , in %).

3.2.4.11. Zeta potential tests

There is a formation of an interfacial charge when there is a solid surface in contact with an aqueous solution. A nonzero net charge region with density near the interface exists due to the interfacial charge that implies the reorganization of the free ions in the solution. This reorganization and the complementary counterions in the liquid is mentioned as electrical double layer [78].

As Sze and co-workers [78] mentioned, there is a thin layer of counterions immediately next to the charged solid surface, called the compact layer. The counterions in the compact layer are immobile due to the strong electrostatic attraction. Counterions outside the compact layer are mobile. This part of the EDL is called the diffuse layer. The zeta (ζ) potential is the electrostatic potential at the boundary dividing the compact layer and the diffuse layer [78].

The zeta potential analysis to the Ag-BG-NPs with eight different thermal treatments produced in Chapter 4 were done using the Zetasizer equipment (Nano ZS) from Malvern Instruments with a Dispersion Technology Software (DTS). 0.3 mg/mL of all samples in study were suspended in ultrapure water (UPW) with 0.15 M NaCl and saline solution (0.15 M NaCl, pH = 5.5). They were kept on the ultrasonic bath 15 minutes before the measurement to avoid nanoparticle agglomeration.

3.2.4.12. Thermogravimetry (TGA)

According to Level and co-workers [79], TGA is defined as “a technique where the mass of the sample is measured [...]” According to Canevarolo [80] the thermogravimetric technique allows the thermal analysis of samples. In fact, this technique is based on mass variation in function of temperature or time. Furthermore, TGA allows to know the impact of temperature on samples mass, i.e., the range of temperatures that the samples

keep stable and with constant parameters, namely the chemical composition and temperature that does not happen [80].

There are three types of TGA techniques, namely, the isothermal TGA, TGA-quasi-isothermal and dynamic of conventional TGA. The first is defined as the mass change of the sample as a function of time at a constant temperature; the second is based on the increase of the sample temperature. This increase is linear allowing to know when there is no weight change of the sample; and finally, the latter type is characterized in that the temperature variation (increase or decrease) in a predetermined temperature range, preferably linear. The latter, the mass change of the sample occurs according to the temperature or time, as can be seen in equation (8) [80]:

$$m = f(t \text{ or } T) \quad (8)$$

According to the book *Thermal characterization of polymeric materials* [81], in multilayer films, as the case study, the stability and the chemistry of each component of the multilayer film can be evaluated [81].

Regarding the mechanism functioning there is a thermobalance. It is used to obtain a thermogravimetric curve. The results obtained by TGA experiences can be, namely a curve of mass against temperature or time. Thus, when a mass loss takes place, there is a minimum of heating rate. As Dunn [82] mentioned, “this gives mass losses over very narrow temperature ranges and sometimes enables two close reactions to be resolved. This method has the advantage of using fast heating rates when no thermal event is taking place and then slowing down the heating rate when a mass change is in progress” [82].

To evaluate the filler percentage (silver doped bioglass nanoparticles (Ag-BG-NPs) heat-treated during 2 hours at 90°C and ½ hour at 100°C) present in the free-standings films, the Q500 TGA equipment (TA Instruments, USA), present in Department of Polymer Engineering, University of Minho and shown in Figure 3.11, was used. The tests were performed using a temperature range of 40°C to 800°C at a rate of 10°C/min. The results are shown in Chapter 5 and Appendix 3.



Figure 3. 11 - TGA equipment.

3.2.4.13. Dynamical Mechanical Analysis (DMA)

The dynamical mechanical analysis (DMA) is a non-destructive technique [83] and is used because and according to Roeder [84], to study the viscoelastic behavior of biomaterials. In fact, the viscoelastic materials have a phase delay between the stimulus solicitation (stress) and their response (strain response) [84]. Indeed, the stress has a sinusoidal curve, as it can be seen on equation 9.

$$\sigma = \sigma_0 \cdot \sin(\omega t + \delta) \quad (9)$$

Where:

σ : Final sinusoidal stress ($\sigma_f = E_f / \epsilon_f$) [84];

σ_0 : Initial sinusoidal stress ($\sigma_0 = E_0 / \epsilon_0$) [84];

ω : $2 \pi f$ [rad/s] [84];

f : ordinary frequency [Hz] [84];

t : time [s] [84];

δ : phase angle between stress and strain [84].

Also, the stress can be divided in two factors, the elastic and a viscous phase [84]. The storage and loss modulus are obtained as shown on equations 10 and 11 [84]. Also, the phase angle (δ) is obtained through equation 12 [84]. $\tan(\delta)$ gives us information about the damping competency of the biomaterial [83]. E' and E'' can change with the temperature or frequency ranges [83].

$$E' = \sigma_0 \cdot \cos(\delta) \quad (10)$$

$$E'' = \sigma_0 \cdot \sin(\delta) \quad (11)$$

$$\delta = \arctan (E'' / E') \quad (12)$$

Dynamical mechanical analysis technique is useful to determinate the relaxation times, creep, glass transition temperature and stress relaxation [84]. According to Silva and co-workers [41], the dynamic mechanical analysis technique can be used to study the mechanical properties of biomaterials and simulates, closely, the physiological conditions. Furthermore, and according to Caridade and co-workers [85], DMA analysis performed in wet environment have different results than in dry ones. According to Ghosh and co-workers [83], polymeric biomaterials have viscoelastic properties, which allows dissipation of mechanical energy and they are responsible for time-dependence properties. These viscoelastic properties are relevant for tissue engineering area, once the living tissues have a viscoelastic behavior [83].

To study the compression properties at physiological-like conditions the produced hydrogels, chitosan crosslinked with genipin (CHT + genipin) and chitosan hydrogel with bioglass nanoparticles incorporation and crosslinked with genipin (CHT + BG-NPs + genipin), DMA analysis were performed using a TRITEC 2000 DMA equipment (Trinton Technology, UK), using a range of frequencies scan between 0.1 and 15.849 Hz. The studied hydrogels were immersed in phosphate buffered saline (PBS) solution at 37°C placed in a Teflon reservoir. Phosphate buffered saline solution mimics, closely, the physiological environment. Data shown represented the Mean \pm Standard Deviation with a population of $n = 5$.

3.3. References

- [1] M. Morra, "Engineering of biomaterials surfaces by hyaluronan," (in English), *Biomacromolecules*, Review vol. 6, no. 3, pp. 1205-1223, 2005.
- [2] N. B. Zhao, X. Wang, L. Qin, Z. Z. Guo, and D. H. Li, "Effect of molecular weight and concentration of hyaluronan on cell proliferation and osteogenic differentiation in vitro," *Biochemical and Biophysical Research Communications*, vol. 465, no. 3, pp. 569-574, 2015.
- [3] J. F. Mano et al., "Natural origin biodegradable systems in tissue engineering and regenerative medicine: present status and some moving trends," (in English), *Journal of the Royal Society Interface*, Review vol. 4, no. 17, pp. 999-1030, 2007.
- [4] P. Kujawa, P. Moraille, J. Sanchez, A. Badia, and F. M. Winnik, "Effect of molecular weight on the exponential growth and morphology of hyaluronan/chitosan multilayers: A surface plasmon resonance spectroscopy and

- atomic force microscopy investigation," (in English), *Journal of the American Chemical Society*, Article vol. 127, no. 25, pp. 9224-9234, 2005.
- [5] A. I. Neto et al., "Nanostructured Polymeric Coatings Based on Chitosan and Dopamine-Modified Hyaluronic Acid for Biomedical Applications," (in English), *Small*, Article vol. 10, no. 12, pp. 2459-2469, 2014.
- [6] Y. Lee et al., "Thermo-sensitive, injectable, and tissue adhesive sol-gel transition hyaluronic acid/pluronic composite hydrogels prepared from bio-inspired catechol-thiol reaction," (in English), *Soft Matter*, Article vol. 6, no. 5, pp. 977-983, 2010.
- [7] Y. Li, J. Rodrigues, and H. Tomas, "Injectable and biodegradable hydrogels: gelation, biodegradation and biomedical applications," *Chemical Society Reviews*, vol. 41, no. 6, pp. 2193-2221, 2012.
- [8] A.-M. Vasi, M. I. Popa, M. Butnaru, G. Dodi, and L. Verestiuc, "Chemical functionalization of hyaluronic acid for drug delivery applications," *Materials Science & Engineering C-Materials for Biological Applications*, vol. 38, pp. 177-185, 2014.
- [9] F. Bano, M. Carril, P. Di Gianvincenzo, and R. P. Richter, "Interaction of Hyaluronan with Cationic Nanoparticles," (in English), *Langmuir*, Article vol. 31, no. 30, pp. 8411-8420, 2015.
- [10] C. E. Schante, G. Zuber, C. Herlin, and T. F. Vandamme, "Chemical modifications of hyaluronic acid for the synthesis of derivatives for a broad range of biomedical applications," (in English), *Carbohydrate Polymers*, Review vol. 85, no. 3, pp. 469-489, 2011.
- [11] W. Y. J. Chen and G. Abatangelo, "Functions of hyaluronan in wound repair," (in English), *Wound Repair and Regeneration*, Review vol. 7, no. 2, pp. 79-89, Mar-1999.
- [12] J. J. Lataillade, P. Albanese, and G. Uzan, "Implication of hyaluronic acid in normal and pathological angiogenesis. Application for cellular engineering," (in French), *Annales De Dermatologie Et De Venereologie*, Article vol. 137, pp. S15-S22, 2010.
- [13] J. B. Leach, K. A. Bivens, C. W. Patrick, and C. E. Schmidt, "Photocrosslinked hyaluronic acid hydrogels: Natural, biodegradable tissue engineering scaffolds," *Biotechnology and Bioengineering*, vol. 82, no. 5, pp. 578-589, 2003.
- [14] M. Rinaudo, "Main properties and current applications of some polysaccharides as biomaterials," *Polymer International*, vol. 57, no. 3, pp. 397-430, 2008.
- [15] J. M. Beaulieu and R. R. Gainetdinov, "The Physiology, Signaling, and Pharmacology of Dopamine Receptors," (in English), *Pharmacological Reviews*, Review vol. 63, no. 1, pp. 182-217, 2011.
- [16] S. K. M. Perikamana et al., "Materials from Mussel-Inspired Chemistry for Cell and Tissue Engineering Applications," *Biomacromolecules*, vol. 16, no. 9, pp. 2541-2555, 2015.
- [17] F. R. F. Leite, C. M. Maroneze, A. B. de Oliveira, W. T. P. dos Santos, F. S. Damos, and R. D. S. Luz, "Development of a sensor for L-Dopa based on Co(DMG)(2)ClPy/multi-walled carbon nanotubes composite immobilized on

- basal plane pyrolytic graphite electrode," (in English), *Bioelectrochemistry*, Article vol. 86, pp. 22-29, 2012.
- [18] V. Cutsuridis and S. Perantonis, "A neural network model of Parkinson's disease bradykinesia," *Neural Networks*, vol. 19, no. 4, pp. 354-374, 2006.
- [19] P. J. Barrett and J. Timothy Greenamyre, "Post-translational modification of α -synuclein in Parkinson's disease," *Brain Research*.
- [20] H. Wei, J. Ren, B. Han, L. Xu, L. Han, and L. Jia, "Stability of polydopamine and poly(DOPA) melanin-like films on the surface of polymer membranes under strongly acidic and alkaline conditions," *Colloids and Surfaces B: Biointerfaces*, vol. 110, pp. 22-28, 2013.
- [21] X. M. Zhang, Z. Y. Li, X. B. Yuan, Z. D. Cui, and X. J. Yang, "Fabrication of dopamine-modified hyaluronic acid/chitosan multilayers on titanium alloy by layer-by-layer self-assembly for promoting osteoblast growth," (in English), *Applied Surface Science*, Article vol. 284, pp. 732-737, 2013.
- [22] W. Wei, J. Yu, C. Broomell, J. N. Israelachvili, and J. H. Waite, "Hydrophobic Enhancement of Dopa-Mediated Adhesion in a Mussel Foot Protein," (in English), *Journal of the American Chemical Society*, Article vol. 135, no. 1, pp. 377-383, 2013.
- [23] H.-C. Yang, J. Luo, Y. Lv, P. Shen, and Z.-K. Xu, "Surface engineering of polymer membranes via mussel-inspired chemistry," *Journal of Membrane Science*, vol. 483, pp. 42-59, 2015.
- [24] Y.-T. Liu, T.-M. Lee, and T.-S. Lui, "Enhanced osteoblastic cell response on zirconia by bio-inspired surface modification," *Colloids and Surfaces B: Biointerfaces*, vol. 106, pp. 37-45, 2013.
- [25] C. E. Brubaker and P. B. Messersmith, "The Present and Future of Biologically Inspired Adhesive Interfaces and Materials," *Langmuir*, vol. 28, no. 4, pp. 2200-2205, 2012.
- [26] A. B. Barron, E. Sovik, and J. L. Cornish, "The roles of dopamine and related compounds in reward-seeking behavior across animal phyla," (in English), *Frontiers in Behavioral Neuroscience*, Review vol. 4, p. 9, 2010, Art. no. 163.
- [27] M. Rinaudo, "Chitin and chitosan: Properties and applications," (in English), *Progress in Polymer Science*, Review vol. 31, no. 7, pp. 603-632, 2006.
- [28] N. M. Alves and J. F. Mano, "Chitosan derivatives obtained by chemical modifications for biomedical and environmental applications," (in English), *International Journal of Biological Macromolecules*, Review vol. 43, no. 5, pp. 401-414, 2008.
- [29] F. Croisier and C. Jerome, "Chitosan-based biomaterials for tissue engineering," *European Polymer Journal*, vol. 49, no. 4, pp. 780-792, 2013.
- [30] M. Kumar, "A review of chitin and chitosan applications," (in English), *Reactive & Functional Polymers*, Review vol. 46, no. 1, pp. 1-27, 2000.
- [31] M. Dash, F. Chiellini, R. M. Ottenbrite, and E. Chiellini, "Chitosan-A versatile semi-synthetic polymer in biomedical applications," *Progress in Polymer Science*, vol. 36, no. 8, pp. 981-1014, 2011.
- [32] R. Signini and S. P. Campana, "On the preparation and characterization of chitosan hydrochloride," *Polymer Bulletin*, vol. 42, no. 2, pp. 159-166, 1999.

- [33] M. R. Leedy, H. J. Martin, P. A. Norowski, J. A. Jennings, W. O. Haggard, and J. D. Bumgardner, "Use of Chitosan as a Bioactive Implant Coating for Bone-Implant Applications," in *Chitosan for Biomaterials II*, vol. 244, R. Jayakumar, M. Prabakaran, and R. A. A. Muzzarelli, Eds. (Advances in Polymer Science, Berlin: Springer-Verlag Berlin, pp. 129-165, 2011).
- [34] K. Kim, J. H. Ryu, D. Y. Lee, and H. Lee, "Bio-inspired catechol conjugation converts water-insoluble chitosan into a highly water-soluble, adhesive chitosan derivative for hydrogels and LbL assembly," (in English), *Biomaterials Science*, Article vol. 1, no. 7, pp. 783-790, 2013.
- [35] R. Jayakumar, M. Prabakaran, P. T. S. Kumar, S. V. Nair, and H. Tamura, "Biomaterials based on chitin and chitosan in wound dressing applications," *Biotechnology Advances*, vol. 29, no. 3, pp. 322-337, 2011.
- [36] G. M. Luz and J. F. Mano, "Chitosan/bioactive glass nanoparticles composites for biomedical applications," (in English), *Biomedical Materials*, Article vol. 7, no. 5, p. 9, 2012, Art. no. 054104.
- [37] J. R. J. Delben et al., "Synthesis and thermal properties of nanoparticles of bioactive glasses containing silver," *Journal of Thermal Analysis and Calorimetry*, vol. 97, no. 2, pp. 433-436, 2009.
- [38] A. L. Carvalho et al., "Antibacterial bioadhesive layer-by-layer coatings for orthopedic applications," *Journal of Materials Chemistry B*, 10.1039/C6TB00841K 2016.
- [39] S. J. Rego, A. C. Vale, G. M. Luz, J. F. Mano, and N. M. Alves, "Adhesive Bioactive Coatings Inspired by Sea Life," (in English), *Langmuir*, Article vol. 32, no. 2, pp. 560-568, 2016.
- [40] S. G. Caridade et al., "Myoconductive and osteoinductive free-standing polysaccharide membranes," *Acta Biomaterialia*, vol. 15, pp. 139-149, 2015.
- [41] J. M. Silva, S. G. Caridade, N. M. Oliveira, R. L. Reis, and J. F. Mano, "Chitosan-alginate multilayered films with gradients of physicochemical cues," *Journal of Materials Chemistry B*, vol. 3, no. 22, pp. 4555-4568, 2015.
- [42] (2015, 02/12/2015). Equipment info. Available: <http://www.3bs.uminho.pt/researchers/equipmentview/58>
- [43] M. B. Oliveira, G. M. Luz, and J. F. Mano, "A combinatorial study of nanocomposite hydrogels: on-chip mechanical/viscoelastic and pre-osteoblast interaction characterization," (in English), *Journal of Materials Chemistry B*, Article vol. 2, no. 34, pp. 5627-5638, 2014.
- [44] J. H. Ryu, Y. Lee, W. H. Kong, T. G. Kim, T. G. Park, and H. Lee, "Catechol-Functionalized Chitosan/Pluronic Hydrogels for Tissue Adhesives and Hemostatic Materials," (in English), *Biomacromolecules*, Article vol. 12, no. 7, pp. 2653-2659, 2011.
- [45] G. Bodor, *Structural investigation of polymers*. New York : Ellis Horwood, 1991. (Ellis Horwood series in polymer science and technology).
- [46] R. A. Niquist, A. Press, Ed. *The handbook of infrared and Raman spectra of inorganic compounds and organic salts*. San Diego, cop. 1997.

- [47] Z. Movasaghi, S. Rehman, and I. U. Rehman, "Fourier transform infrared (FTIR) spectroscopy of biological tissues," *Applied Spectroscopy Reviews*, vol. 43, no. 2, pp. 134-179, 2008.
- [48] M. Born, "Kinetic Theory of Gases," in *The Restless Universe* 2nd ed. Dover, New York, pp. 37-124, 1951.
- [49] T. S. Sampath Kumar, "Chapter 2 - Physical and Chemical Characterization of Biomaterials," in *Characterization of Biomaterials*, A. B. Bose, Ed. Oxford: Academic Press, pp. 11-47, 2013.
- [50] M. W. Urban, *Attenuated total reflectance spectroscopy of polymers : theory and practice*. Washington : ACS, cop. 1996., 1953.
- [51] H. Wang and P. K. Chu, "Chapter 4 - Surface Characterization of Biomaterials," in *Characterization of Biomaterials*, A. B. Bose, Ed. Oxford: Academic Press, pp. 105-174, 2013.
- [52] R. Lambert Oréfice, M. d. M. Pereira, and H. S. Mansur, O. R.L., P. M.M., and M. H.S., Eds. *Biomateriais-Fundamentos e Aplicações*. Cultura Médica, 2006.
- [53] T. Owen, *Fundamentals of modern UV-visible spectroscopy*. Agilent Technologies, 2000.
- [54] M. Hunger and J. Weitkamp, "In situ IR, NMR, EPR, and UV/Vis spectroscopy: Tools for new insight into the mechanisms of heterogeneous catalysis," *Angewandte Chemie-International Edition*, vol. 40, no. 16, pp. 2954-2971, 2001.
- [55] S. Vahabi, B. Nazemi Salman, and A. Javanmard, "Atomic force microscopy application in biological research: a review study," *Iranian journal of medical sciences*, vol. 38, no. 2, pp. 76-83, 2013.
- [56] N. Jalili and K. Laxminarayana, "A review of atomic force microscopy imaging systems: application to molecular metrology and biological sciences," *Mechatronics*, vol. 14, no. 8, pp. 907-945, 2004.
- [57] M. Göken and M. Kempf, "Microstructural properties of superalloys investigated by nanoindentations in an atomic force microscope," *Acta Materialia*, vol. 47, no. 3, pp. 1043-1052, 1999.
- [58] (2015, 02/12/2015). Equipment. Available: <http://www.3bs.uminho.pt/equipment-list>
- [59] S. J. Pennycook and L. A. Boatner, "Chemically sensitive structure-imaging with a scanning transmission electron microscope," *Nature*, 10.1038/336565a0 vol. 336, no. 6199, pp. 565-567, 1988.
- [60] R. Guinebretière, "- Kinematic and Geometric Theories of X-Ray Diffraction," pp. - 38, 2010.
- [61] R. Guinebretière, "- Instrumentation used for X-ray Diffraction," pp. - 126, 2010.
- [62] B. Fultz and J. Howe, "Diffraction and the X-Ray Powder Diffractometer," in *Transmission Electron Microscopy and Diffractometry of Materials*(Graduate Texts in Physics: Springer Berlin Heidelberg, pp. 1-57, 2013.
- [63] (2010, 02/12/2015). Difracção de Raios-X (XRD) - Bruker D8 Discover. Available: http://www.semat.lab.uminho.pt/Equipamento_2.htm

- [64] D. Y. Kwok and A. W. Neumann, "Contact angle measurement and contact angle interpretation," *Advances in Colloid and Interface Science*, vol. 81, no. 3, pp. 167-249, 1999.
- [65] (02/12/2015). Facility info. Available: <http://www.3bs.uminho.pt/researchers/equipmentview/6>
- [66] T. Kokubo and H. Takadama, "How useful is SBF in predicting in vivo bone bioactivity?," (in English), *Biomaterials*, Article vol. 27, no. 15, pp. 2907-2915, 2006.
- [67] I. B. Leonor, S. Gomes, P. C. Bessa, J. F. Mano, and R. L. Reis, "New biomineralization strategies for the use of natural-based polymeric materials in bone-tissue engineering," in *Natural-based polymers for biomedical applications*: Woodhead Publishing Limited, pp. 193-230, 2008.
- [68] X. Lu and Y. Leng, "Theoretical analysis of calcium phosphate precipitation in simulated body fluid," *Biomaterials*, vol. 26, no. 10, pp. 1097-1108, 2005.
- [69] A. Oyane, H. M. Kim, T. Furuya, T. Kokubo, T. Miyazaki, and T. Nakamura, "Preparation and assessment of revised simulated body fluids," *Journal of Biomedical Materials Research Part A*, vol. 65A, no. 2, pp. 188-195, 2003.
- [70] A. Oyane, K. Onuma, A. Ito, H. M. Kim, T. Kokubo, and T. Nakamura, "Formation and growth of clusters in conventional and new kinds of simulated body fluids," *Journal of Biomedical Materials Research Part A*, vol. 64A, no. 2, pp. 339-348, 2003.
- [71] S.-C. Her, "Stress analysis of adhesively-bonded lap joints," *Composite Structures*, vol. 47, no. 1-4, pp. 673-678, 1999.
- [72] B. Broughton and M. Gower, *Measurement Good Practice Guide No. 47-Preparation and Testing of Adhesive Joints*. Teddington, Middlesex, United Kingdom, TW11 0LW, 2001.
- [73] ASTM D 1002-05 Standard Test Method for Apparent Shear Strength of Single-Lap-Joint Adhesively Bonded Metal Specimens by Tension Loading (Metal-to-Metal) 2005.
- [74] D. W. Van Krevelen, *Properties of polymers : their correlation with chemical structure, their numerical estimation and prediction from additive group contributions.* , 3rd rev. ed . Amsterdam : Elsevier ed. 1990.
- [75] B. A. Professional, Ed. *Polymer characterisation* / ed. B. J. Hunt, M. I. James. London, 1993.
- [76] C. A. G. d. M. Branco, *Mecânica dos materiais*, 2ª ed. Lisboa : Fundação Calouste Gulbenkian ed. 1994.
- [77] J. J. Aklonis, "MECHANICAL-PROPERTIES OF POLYMERS," *Journal of Chemical Education*, vol. 58, no. 11, pp. 892-897, 1981.
- [78] A. Sze, D. Erickson, L. Q. Ren, and D. Q. Li, "Zeta-potential measurement using the Smoluchowski equation and the slope of the current-time relationship in electroosmotic flow," (in English), *Journal of Colloid and Interface Science*, Article vol. 261, no. 2, pp. 402-410, 2003.

- [79] T. Lever, P. Haines, J. Rouquerol, E. L. Charsley, P. Van Eckeren, and D. J. Burlett, "ICTAC nomenclature of thermal analysis (IUPAC Recommendations 2014)," *Pure and Applied Chemistry*, vol. 86, no. 4, pp. 545-553, 2014.
- [80] S. V. Canevarolo Jr., A. Editora, Ed. *Técnicas de caracterização de polímeros*. São Paulo, 2003.
- [81] *Thermal characterization of polymeric materials*, 2nd ed. San Diego : Academic Press ed. (no. 1 : 1529 p., pag. var. vol.2 : 1192 p., pag. var.). cop.1997.
- [82] J. G. Dunn, "Thermogravimetric Analysis," in *Characterization of Materials*: John Wiley & Sons, Inc., 2002.
- [83] S. Ghosh et al., "Dynamic mechanical behavior of starch-based scaffolds in dry and physiologically simulated conditions: Effect of porosity and pore size," *Acta Biomaterialia*, vol. 4, no. 4, pp. 950-959, 2008.
- [84] R. K. Roeder, "Chapter 3 - Mechanical Characterization of Biomaterials A2 - Bandyopadhyay, Amit," in *Characterization of Biomaterials*, S. Bose, Ed. Oxford: Academic Press, pp. 49-104, 2013.
- [85] S. G. Caridade, E. G. Merino, N. M. Alves, and J. F. Mano, "Bioactivity and Viscoelastic Characterization of Chitosan/Bioglass (R) Composite Membranes," *Macromolecular Bioscience*, vol. 12, no. 8, pp. 1106-1113, 2012.

CHAPTER 4 **OPTIMIZATION** **OF**
SILVER DOPED BIOGLASS NANOPARTICLES
SYNTHESIS ENVISAGING BIOMEDICAL
APPLICATIONS

Chapter 4. Silver Doped Bioglass Nanoparticles Synthesis Envisaging Biomedical Applications

4. OPTIMIZATION OF SILVER DOPED BIOGLASS NANOPARTICLES SYNTHESIS ENVISAGING BIOMEDICAL APPLICATIONS

Abstract:

Bioglass nanoparticles (BG-NPs) are of outmost importance in the biomedical field, because they can interact with bone without creating a fibrous capsule. Furthermore, they can induce apatite formation and bond to living hard tissue. In this work, novel silver doped bioglass nanoparticles (Ag-BG-NPs) were synthesized by the sol-gel method, adopting different thermal treatments. This is the first time that a systematic study of the effect of the chosen thermal treatment on the properties of the Ag-BG-NPs was analysed. The effect of the studied thermal treatments on the properties of the synthesized nanoparticles was analysed by several characterization techniques: FT-IR, XRD, S-TEM, SEM-EDS and Zeta potential. FT-IR allows the identification of the characteristic peaks of the nanoparticles and XRD revealed the presence of the characteristic peaks of calcium carbonate and silver carbonate. By S-TEM analysis it was found that the produced nanoparticles are dense and have a diameter less than 200 nm. The SEM micrographs showed the surface morphology and zeta potential measurements were performed to study their stability. Bioactivity tests confirmed their bioactivity properties. It was also shown that the developed nanoparticles had an antibacterial effect against two different types of bacteria.

The developed nanoparticles can be incorporated either in 2D or 3D structures and could be used for several biomedical applications, namely in the orthopedic or dental area.

Keywords: Nanoparticles (NPs), bioglass® (BG), silver (Ag), antibacterial activity.

4.1. Introduction

Nanoparticles have been the subject of much interest by the scientific community [1, 2]. This interest is due to their large surface and small size to volume ratios. Silver nanoparticles and ions have been used in many applications, namely in antibacterial among others [1, 3]. Changing the feeding ratio of reagents or the production apparatus can result in a change of the nanoparticles' morphology and shape [3]. Furthermore, the micro- and nanoparticles can be incorporated with polymers to create composite materials, for instance to produce bioactive coatings with enhanced mechanical properties [3]. Many bioglass nanoparticles have been created since 1969 [6]. Bioactive glasses present many advantages, namely their biocompatibility and bioactivity in vitro and in vivo [4], being used in a variety of applications, namely in the orthopedic area, in tissue engineering and in dental applications. Bioglass is generally composed by SiO_2 - CaO - P_2O_5 and Na_2O and can be obtained by two processes: melting or sol-gel process [2, 5]. The silica quantity present in the bioglass obtained by the sol-gel methodology or melt process, both with the same composition, can be much higher in the sol-gel methodology [6]. Furthermore, this method allows the synthesis of nanoparticles with a higher surface area, implying faster dissolution rate and faster formation of hydroxycarbonated apatite [6, 7]. The sol-gel technique allows the production of particles with a specific surface area and a pore volume two orders higher than the ones derived from the melting technique [5]. According to Simchi and co-workers [8], after a surgery, when an implant is put in our body, bacterial infections can happen, because there is an adherence and because of the colonization of bacteria on the surfaces of implants. Bellantone and co-workers developed SiO_2 - CaO - P_2O_5 - Ag_2O nanoparticle systems [9] and these nanoparticles present antimicrobial properties without affecting their bioactivity. In fact, Ag reduces the risk of microbial infections, although it is not yet fully explained through which mechanism silver ions have toxicity in bacteria. El-Kady and co-workers [5] also developed silver doped bioglass nanoparticles by a sol-gel method. The silver dissolution rate was evaluated and the results showed that with higher silver content, the dissolution rate is also higher. Furthermore, all nanoparticles in study showed antibacterial effect against *Staphylococcus aureus* and *E. coli* bacteria. Catauro and co-workers [10] developed nanoparticles with $\text{Na}_2\text{O}\cdot\text{CaO}\cdot 2\text{SiO}_2$ composition and with and without silver, obtained through the sol-gel methodology, using methyl ethyl ketone as solvent. The antibacterial tests showed that after 2 hours the completely inhibition in *Escherichia coli*

and *Staphylococcus mutans* occurred. According to Vernè and co-workers [11], it is well known that silver doped biomaterials are important in preventing bacterial development, however, the connection between silver content, released ions profile and their toxic effects are still unknown [11]. Goh and co-workers [2] produced silver and copper doped bioglass nanoparticles by quick alkali-mediated sol-gel method with different concentrations, to study the relation of their ion release profile with their antibacterial performances. The results showed that the morphology of doped and non-doped nanoparticles were similar. Furthermore, XRD and UV-vis analysis showed copper and silver in bioglass, which allowed to corroborated the successful incorporation in bioglass nanoparticles. All nanoparticles formulations were put in PBS solution during 14 days. The results showed that silver doped bioglass have much higher dissolution profiles than Copper (Cu) doped BG during the first day. In conclusion, silver doped bioglass nanoparticles are better antibacterial agents than copper doped BG nanoparticles against *Escherichia coli* bacteria.

In the present work, novel Ag-BG-NPs were synthesized by the sol-gel method, adopting different thermal treatments. It should be pointed that, as far as we know, this is the first time that a systematic study of the effect of the chosen thermal treatment on the properties of the Ag-doped bioglass nanoparticles was analysed. The following treatments were adopted: 1 day at 50°C, 1 and 2 hours at 100 °C, 2 hours at 90°C plus ½ hour at 100°C, 100°C/h plus ½ h at 400°C, 100°C/h plus ½ h at 500°C, 100°C/h plus ½ h at 580°C, 100°C/h plus ½ h at 700°C, and also, the powder gel, i.e., NPs without thermal treatment. The main aim of this work was to analyse the effect of such thermal treatments on the properties of the synthesized nanoparticles. The distinct nanoparticles were analysed by FT-IR, XRD, S-TEM, SEM-EDS and Zeta potential. Antibacterial tests against *Staphylococcus aureus* and *Escherichia coli* bacteria were also performed.

4.2. Experimental section:

4.2.1. Materials:

Several reagents were used to produce this quaternary system. In this case, nitric acid monohydrate 69% was obtained by VWR and tetraethyl orthosilicate (TEOS) 99.90% was purchased by Merck Chemicals. Calcium nitrate tetra hydrate 99%, ammonia water (ammonium hydrogen phosphate 98%, maximum of 33% NH₃), ammonium phosphate

Chapter 4. Silver Doped Bioglass Nanoparticles Synthesis Envisaging Biomedical Applications

dibasic, ethanol absolute, and hypochloric acid (HCl) were acquired from Sigma-Aldrich. Furthermore, silver nitrate (AgNO_3) was obtained by VWR.

4.2.2. Methods

4.2.2.1. Synthesis of quaternary silver doped bioglass nanoparticles

Based on Delben and co-workers [12] protocol, the Ag-BG-NPs, with % 10 mol of Ag, i.e., nanoparticles composed by $\text{SiO}_2\text{-CaO-P}_2\text{O}_5\text{-Ag}_2\text{O}$ (56:30:4:10) was prepared. Briefly, ammonium phosphate dibasic, calcium nitrate tetra hydrate 99%, ethanol absolute, ammonia water (ammonium hydrogen phosphate 98%, maximum of 33% NH_3), and hydrochloric acid (HCl) were purchased on Sigma-Aldrich company. Also, tetraethyl orthosilicate (TEOS) 99.90% was purchased by Merck Chemicals, nitric acid monohydrate 69% was obtained by VWR. Silver Nitrate (AgNO_3) was obtained by VWR. To produce these nanoparticles was necessary firstly, at room temperature, to add osmotized water to tetraethyl orthosilicate (TEOS), and then added together to ethanol absolute. It's necessary to take in account the pH value, it should have a value of 2 with addition of nitric acid (2M). The reaction mixture was kept stirring for 60 min to produce a solution A. Then, for producing the solution B, calcium nitrate tetrahydrate, ammonium phosphate dibasic and silver nitrate were added to 1500 mL of osmotized water and the pH value was adjusted to 11.5 with ammonium hydroxide solution. The reaction mixture was kept under stirring for 60 min. Under smooth stirring, the solution A was slowly added to the solution B drop-by-drop. During this step, the pH value of solution B was maintained at 11.5 using ammonia hydroxide solution. Then, the final solution was kept under stirring for 48h. Eight different thermal treatment of nanoparticles were produced, such as 1 day at 50°C, 1h at 100°C, 2h at 100°C, 2h at 90°C plus ½ h at 100°C, 100°C/h plus ½ at 400°C, 100°C/h plus ½ at 500°C, 100°C/h plus ½ at 580°C, 100°C/h plus ½ at 700°C and the powder gel. To the purpose of studying the stability of the produced nanoparticles, and using a concentration of 0.3 mg/mL, Ag-BG-NPs were suspended in ultra-pure water (UPW) with 0.15 M NaCl and saline (0.15 M NaCl, pH = 5.5) solutions under magnetic stirring during 30 minutes and further ultrasonic dispersion at 25°C during 15 minutes. Moreover, the Zetasizer equipment (Nano ZS) from Malvern Instruments with a Dispersion Technology Software (DTS) was used to perform this analysis. Moreover, to study their morphology the High-Resolution Field Emission Scanning Electron Microscope with Focused Ion Beam (FIB-SEM) (AURIGA COMPACT, ZEISS) equipment was used. Also, Fourier Transform infrared spectroscopy was used to

analyze the nanoparticles powder in order to know their characteristic functional groups. The results were obtained using the FT-IR (infrared spectrum-Jasco), in attenuated total reflectance (ATR), transmission mode. The FT-IR spectra were recorded from 400 to 4000 cm^{-1} . The Bruker AXS D8 Discover, USA equipment was used to analyze the chemical elements of Ag-BG-NPs before and after immersion in modified-simulated body fluid (m-SBF 1.5 x) during 7 days. The Cu-K α radiation ($\lambda=1,54060\text{\AA}$), scanning from 15° to 60° at a speed of 0,04°/1s was used. The analysis for phase identification was performed using analytical software EVA. The crystalline phases were indexed using the ICDD-2015 database (International Center for Diffraction Data).

4.2.3. Characterization techniques

Fourier Transform infrared spectroscopy was used to analyze the silver doped bioglass nanoparticles powder heat-treated and without thermal treatment. The results in this article were obtained using the FT-IR (infrared spectrum-Jasco), in attenuated total reflectance (ATR), transmission mode. The FT-IR spectra were recorded from 400 to 4000 cm^{-1} . The zeta potential analysis to the created Ag-BG-NPs with eight different thermal treatments were done using the Zetasizer equipment (Nano ZS) from Malvern Instruments with a Dispersion Technology Software (DTS) was used to perform this analysis. 0.3 mg/mL of all samples in study were suspended in ultrapure water (UPW) with 0.15 M NaCl and saline solution (0.15 M NaCl, pH = 5.5). They were kept on the ultrasonic bath during 15 minutes before the measurement to avoid nanoparticle agglomeration. The morphology and composition of the glass powders were analysed using SEM coupled with EDS. The elemental composition of the glass powders was determined by EDS using the High-Resolution Field Emission Scanning Electron Microscope with Focused Ion Beam (FIB-SEM) (AURIGA COMPACT, ZEISS) and the Scanning Electron Microscope (SEM) with EDS (JSM-6010 LV, JEOL, Japan) coupled with dispersive X-ray spectroscopy (INCAx-Act, PentaFET Precision, Oxford Instruments) equipments. Scanning transmission electron microscopy was performed using the NanoSEM-FEI Nova 200 (FEG/SEM); EDAX - Pegasus X4M (EDS/EBSD) equipment to analyze eight different thermal treatment of nanoparticles, to be precise 1 day on 50°C, 1h at 100°C, 2h at 100°C, 2h at 90°C plus 1/2h at 100°C, 100°C/h plus ½ at 400°C, 100°C/h plus ½ at 500°C, 100°C/h plus ½ at 580°C, 100°C/h plus ½ at 700°C and the powder gel. Also, X-ray diffraction (XRD) experiments were performed on a Bruker AXS D8 Discover with Cu-K α radiation ($\lambda =1.54060\text{\AA}$), scanning from 15° to 60° at a

Chapter 4. Silver Doped Bioglass Nanoparticles Synthesis Envisaging Biomedical Applications

speed of 0.04°/s. The analysis for phase identification was performed using analytical software EVA. The crystalline phases were indexed using the ICDD 2015 database (International Center for Diffraction Data). Bioactivity test was carried out using the modified-simulated body fluid solution (m-SBF 1.5 x) following the Oyane and co-workers [13] and Oyane and co-workers [14] procedures. This solution was prepared dissolving sodium chloride (NaCl, Merck), sodium sulphate (Na₂SO₄, Panreac), magnesium chloride hexahydrate (MgCl₂.6H₂O, Merck), di-Potassium hydrogen phosphate trihydrate (K₂HPO₄.3H₂O, Merck), calcium chloride (CaCl₂, Merck), potassium chloride (KCl, Merck), sodium hydrogen carbonate (NaHCO₃, Merck), sodium carbonate (Na₂CO₃, Merck), sodium hydroxide (NaOH, Panreac) and 2-(4-(2-hydroxyethyl)-1-piperazinyl) ethanesulfonic acid (HEPES, C₈H₁₈N₂O₄S, Sigma) in ultra-pure water (UPW) at 36.5°C. The final pH was adjusted to 7.4. All the nine samples in study were put in contact with a carbon tape (to stick) and immersed in 25 mL of m-SBF 1.5 x during 7 days at 37°C. After that, washing steps were done and the nanoparticles were left drying at room temperature during 1 day.

4.3. Results and discussion

4.3.1. FT-IR analysis

Silver doped bioglass nanoparticles (Ag-BG-NPs), with 10 % mol of Ag, were synthesized by the sol-gel method and adopting different thermal treatments, as described at the experimental section. The FT-IR spectrum of Ag-BG-NPs is shown in Figure 4.1 - A to I. The intention of this study was to identify various vibrational modes, namely O-H stretching vibration at 3430 cm⁻¹, as well as at 1630 cm⁻¹ by O-H flex vibration due to the presence of water [2, 4]. Furthermore, it can be seen that, around 1045 and 1051 cm⁻¹ there is the Si-O-Si asymmetric stretching vibration [2, 4, 5, 15]. According to Goh and co-workers [2], for wavenumbers around 1000 and 1100 cm⁻¹ there is the P-O antisymmetric stretching. Through the analysis of this spectrum, it is not possible to corroborate its existence. However, and according to the same author [2], the Si-O-Si asymmetric stretching vibration can be overlapped with P-O antisymmetric stretching. Also, it can be possible to see the Si-O symmetric stretching approximately at 800 cm⁻¹ [4, 5], and around 950 cm⁻¹ it we can be seen the vibration of Si-O-Si groups [15]. The band at 600 cm⁻¹ indicates the presence of phosphorus in thee nanoparticles, that are under the form of orthophosphate [2]. According to Luz and Mano [16], the existence of bands

on $1400\text{-}1300\text{ cm}^{-1}$ is related with calcium nitrate precursor. It can also be seen that the band at 1350 cm^{-1} tends to disappear with higher temperatures, which is related to the decomposition of the $\text{Ca}(\text{NO}_3)_2$ [16].

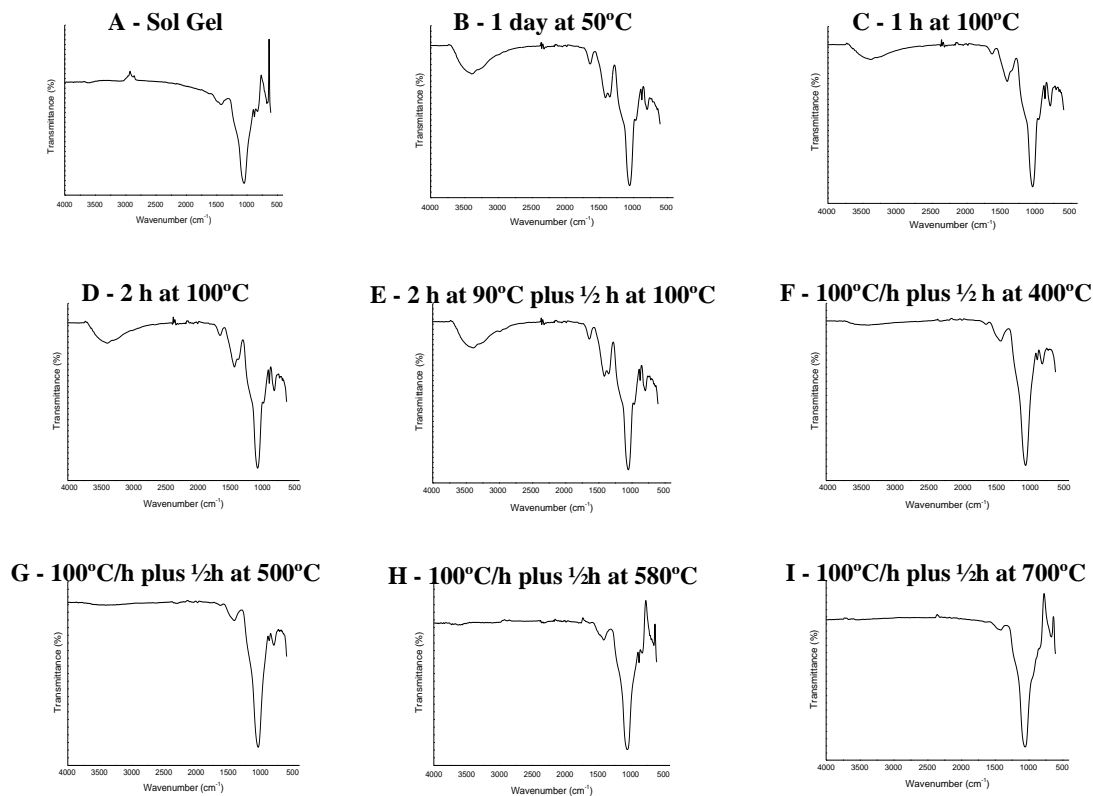


Figure 4. 1 – FT-IR- of Ag-BG-NPs (% 10 mol Ag) with different thermal treatments.

4.3.2. Zeta-potential (ζ) analysis

Zeta potential analysis was performed to analyse the stability of the produced nanoparticles in ultra-pure water with 0.15M of NaCl and saline solution (0.15M NaCl, pH = 5.5) shown in Figure 4.2 – A and B. The ζ potential was performed in order to understand the electrostatic interactions between nanoparticles. All particles in suspension have an electrical potential difference between the stationary layer of fluid and the dispersion of the medium. Consequently, this gives us the degree of repulsion between adjacent similarly charged particles. The zeta potential value is obtained through the electrophoretic mobility of the particles. If the obtained value for zeta potential is above $\pm 30\text{ mV}$, the repulsive charges present in the nanoparticles will avoid their agglomeration and, consequently, ensure their stability in a solution [17]. According to Lu and co-workers [18] a negative value of zeta potential experiences engages the bioactive character of bioglass nanoparticles. Furthermore, apatite formation is favored by negative surfaces [18].

Chapter 4. Silver Doped Bioglass Nanoparticles Synthesis Envisaging Biomedical Applications

Through the analysis of Figure 4.2 – A, the zeta potential of the nanoparticles subjected to a thermal treatment of 2 days at 75°C, 3 hours at 400°C and 3 hours at 700°C, obtained in a previous work from our group, is also included in this figure for the sake of comparison. It is possible to conclude that the thermal treatment of 2 days at 75°C originates lower zeta potential values than the treatments of 2h at 90°C plus ½ h at 100°C and 3 h at 400°C. So these values showed that such nanoparticles will have a higher tendency to agglomerate than the ones subjected to the thermal treatment of 2 days at 75°C. Furthermore, it's preferable to choose a thermal treatment of 2 days at 75°C than 1 day at 50°C, 1h at 100°C or 2h at 100°C because the obtained zeta potential is higher (more stable). When it comes to higher temperatures, nanoparticles heat-treated during 100°C/h plus ½h at 580°C present higher zeta potential results than 2h at 90°C plus 1/2h at 100°C, 100°C/hour plus ½ hour at 400°C, 100°C/hour plus ½ hour at 500°C, 100°C/hour plus ½ hour at 580°C and 100°C/hour plus ½ hour at 700°C, 3h at 400°C and 3h at 700°C. Comparing the zeta potential values of BGNPs (obtained in a previous work from our group), -15.7 ± 0.5 mV, with the values obtained for these Ag-BG-NPs, with thermal treatments of 2h at 90°C plus 1/2h at 100°C, of 100°C/hour plus ½ hour at 400°C, 3h at 400°C, 100°C/hour plus ½ hour at 500°C, 100°C/hour plus ½ hour at 580°C and 100°C/hour plus ½ hour at 700°C, it can be concluded that Ag-BG-NPs present lower aggregation and, consequently, higher stability.

As far as Figure 4.2 – B is concerned, the tests performed in saline solution (0.15 M NaCl, pH = 5.5). The results showed that for higher thermal treatments (above 400°C) the zeta potential values were lower than the values at lower temperatures (below 400°C). The best result was achieved with the sample heat-treated during 2 hours at 90°C plus ½ hour at 100°C.

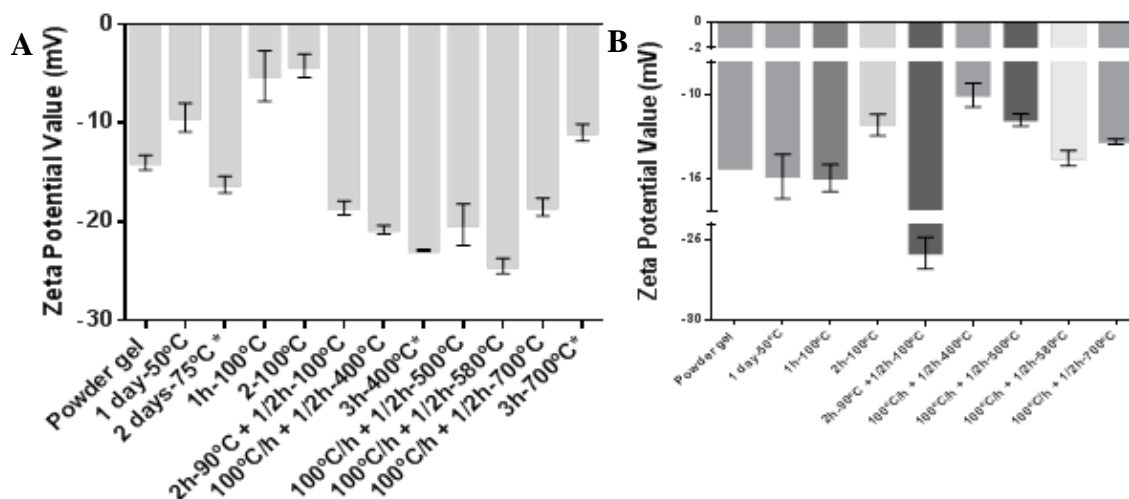


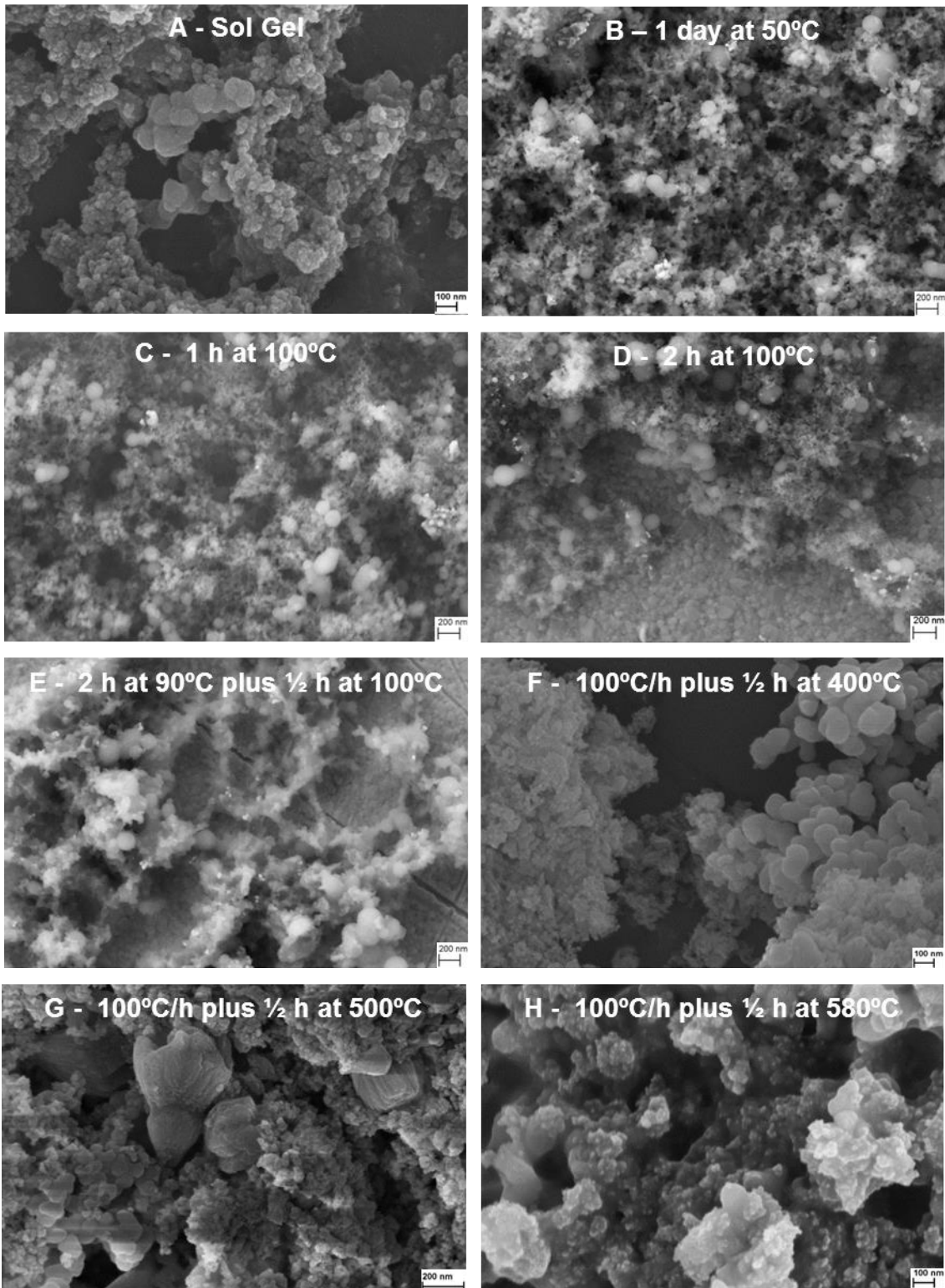
Figure 4. 2 - Zeta potential values of Ag-BG-NPs produced with different thermal treatments. (A) Ultra-pure water with 0.15 M NaCl; (B) Saline solution (0.15 M NaCl, pH = 5.5).

4.3.3. Analysis of the nanoparticles morphology

The nanoparticles morphology are shown in Figure 4.3. It can be seen that the micrograph A do not present a spherical form. In fact, they have unconsolidated spheroids, because the obtained structures had no thermal treatment and present a very big range of diameters. Moreover, these nanoparticles demonstrated a tendency to aggregate. Indeed, this occurs because there is a reduction of the energy on the surface when van der Waals forces actuate in these particles. The final diameter of these nanoparticles is due to the competition process between repulsive and attraction forces [19]. Also, it can be seen that for the thermal treatments at lower temperatures (4.3 - B to E), the nanoparticles have a more spherical form than those produced at higher temperatures. Spheroids with very small diameter and an aggregated structure can be observed both in micrographs B and C. The spheroids in micrograph D present a wide range of diameters with an aggregated structure. Few spheroids are observed in micrograph E, but in this case they have more uniformity in their diameters. The nanoparticles depicted in Micrographs F, G, H and I, do not present a spherical structure at all, but a flake-like structure. Also, comparing the aggregation of the thermal treatment either at lower or higher temperatures, the morphology is different and the nanoparticles thermal treated with higher temperatures are much more aggregated. Comparing this quaternary nanoparticles composed by SiO₂-CaO-P₂O₅-Ag₂O (56:30:4:10 % mol) with binary (SiO₂:CaO) (70:30 % mol) and ternary (SiO₂:CaO:P₂O₅ =55:40:5 % mol) nanoparticles created by Luz and Mano's [20] work, the results showed a spherical form with thermal treatments of 700°C, but in this case that

Chapter 4. Silver Doped Bioglass Nanoparticles Synthesis Envisaging Biomedical Applications

didn't happen, probably because silver disrupt the bioglass network structure at higher temperatures.



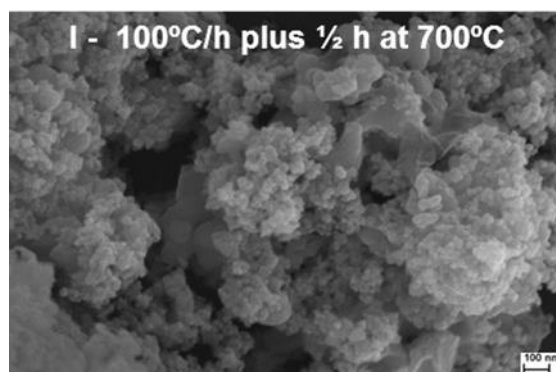
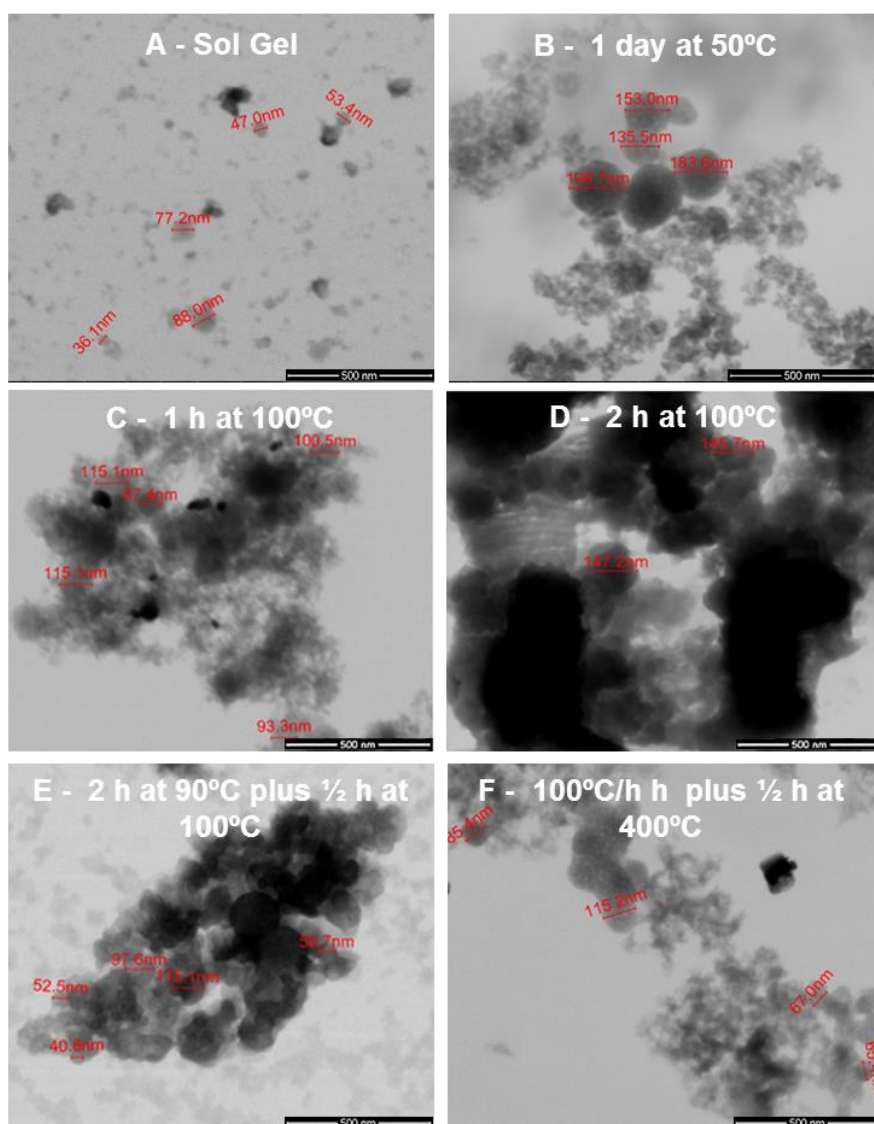


Figure 4. 3 - SEM-EDS micrographs of the nanoparticles surface.

In order to obtain further information of the morphology of the distinct nanoparticles systems, S-TEM analysis was also performed and shown in Figure 4.4. Through the analysis of Figure 4.4-A it's possible to see that the non-thermally treated silver doped bioglass nanoparticles (powder gel) show a less aggregated structure than all thermally treated samples. In fact, and according to the SEM micrographs results (Figure 4.3), probably, the thermal treatment induces the aggregation of these nanoparticles, changing their morphology. According to zeta potential values obtained for Micrograph A, -14.0 ± 0.737 mV, nanoparticles avoid agglomeration when their zeta potential value is above ± 30 mV, which is not the case [17]. We can see that the nanoparticles show diameters between 36.1 and 97.6 nm. As to Figure 4.4- B, Ag-BG-NPs show a very aggregated structure, according to the zeta potential results (-9.41 ± 1.44 mV). Also, spheroids present a diameter range between 150 and 200 nm. According to Luz and Mano's [17] results, if there is a strong contrast between the dark edge and the pale center of the particles, the nanoparticles are hollow. If not, they are dense. The result shows that all thermally and non-thermally treated nanoparticles are dense. As far as Ag-BG-NPs with thermal treatment of 100°C during an hour is concerned (Figure 4.4- C), it presents an aggregated structure more aggregated than the one with 1 day to 50°C, coincident with the zeta potential results (-5.21 ± 2.55 mV), presenting a big range of diameters with an average of 116 nm. Regarding the Ag-BG-NPs with thermal treatment of 100°C during two hours, 4.4-D, they also show an agglomerated structure. Through it analysis, it's possible to see that the nanoparticles don't have a spherical form, instead they present a morula-like structure [17]. Indeed, these figures have a different morphology than those from the SEM micrographs and present much aggregated structures, which are according to the zeta potential values (-4.18 ± 1.19 mV). In Figure 4.4-E an aggregated structure (-18.6 ± 0.7 mV) is shown, but not as aggregated as Figure 4.4-D. It can be seen, through the analysis of S-TEM images, that these nanoparticles have a diameter between 35 and

Chapter 4. Silver Doped Bioglass Nanoparticles Synthesis Envisaging Biomedical Applications

115.1 nm and have more uniform diameters than the others (comparing to Figure 4.4-A to D), but have similar diameters comparing to Figure 4.4-F to I and a similar aggregated structure to samples thermally-treated with higher temperatures. Through the analysis of Figure 4.4-F it's possible to see that it presents a similar aggregated structure (-20.8 ± 0.436 mV) than the samples thermally treated at $100^\circ\text{C}/\text{h}$ plus $\frac{1}{2}$ h at 500°C , 580°C and 700°C , with a zeta potential value of -20.3 ± 2.08 mV, -24.5 ± 0.8 mV and -18.5 ± 0.9 mV, respectively. Taking into account zeta potential and S-TEM results, it can be concluded that the nanoparticles with higher stability are Ag-BG-NPs thermally treated at 2h at 90°C plus $\frac{1}{2}$ h at 100°C , $100^\circ\text{C}/\text{h}$ plus $\frac{1}{2}$ h at 400°C , 500°C , 580°C and 700°C , because they present higher zeta potential values and, consequently, higher stability in solution.



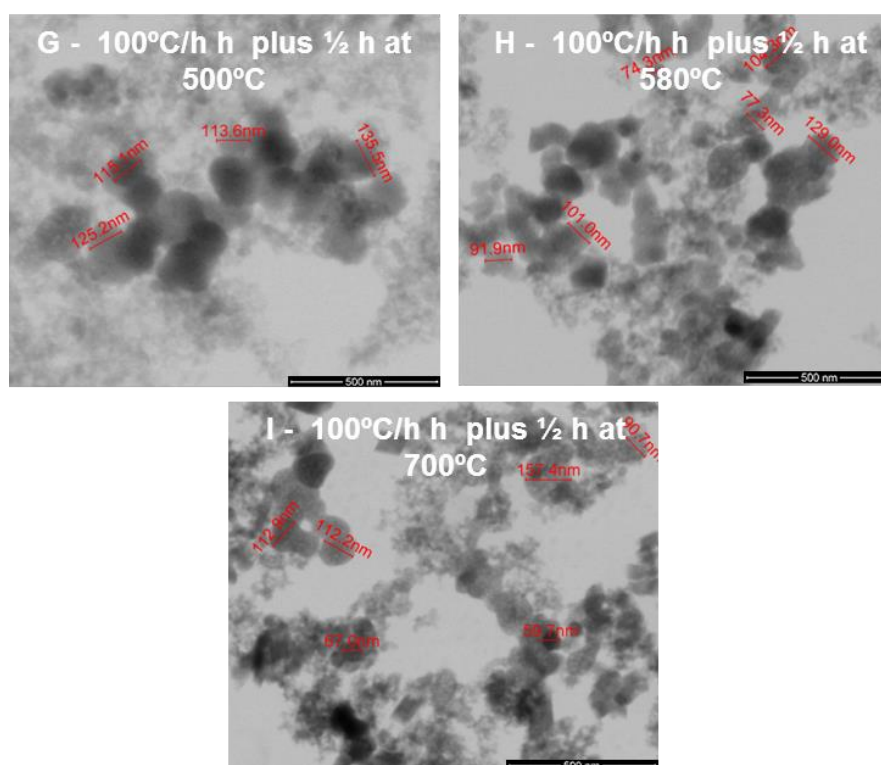


Figure 4. 4 - S-TEM micrographs of the all Ag-BG-NPs, (magnification of 200 000x).

4.3.4. Bioactivity tests

In order to investigate if the developed Ag-BG-NPs presented a bioactive character they were immersed in SBF during 7 days. Figures 4.5 – A and B show the XRD pattern with and without immersion in SBF after 7 days, respectively. Figure 4.5 - A shows the characteristic peaks of calcium carbonate (CaCO_3). This appearance is due to the insufficient ammonium hydroxide (NH_4OH) added during the nanoparticles synthesis, since it was not sufficient to increase the gelation time in order to prevent the reaction of Ca^{2+} ions with the oxygen present in the air and consequently, the formation of CaCO_3 [21]. Moreover, the CaCO_3 -Rhombohedral, pattern: 00-005-0586) is present in all XRD patterns and it was detected the characteristic peaks of hydroxyapatite- $(\text{Ca}_5(\text{PO}_4)_3(\text{OH}))$, Hexagonal, pattern: 01-089-4405) for the samples heat treated with $100^\circ\text{C}/\text{hour}$ plus $\frac{1}{2}$ hour at 580°C and $100^\circ\text{C}/\text{hour}$ plus $\frac{1}{2}$ hour at 700°C . Silver carbonate (AgCO_3 , Hexagonal, Pattern: 00-031-1237) for the samples heat treated with 1 day at 50°C , 1 hour at 100°C , 2 hour at 100°C and 2 hour at 90°C plus $\frac{1}{2}$ hour at 100°C , is also detected Figure 4.5 – B shows an amorphous halo where it's possible to detect the presence of hydroxyapatite ($\text{Ca}_5(\text{PO}_4)_3(\text{OH})$) in all samples, corroborating its bioactivity character useful for the envisaged applications.

Chapter 4. Silver Doped Bioglass Nanoparticles Synthesis Envisaging Biomedical Applications

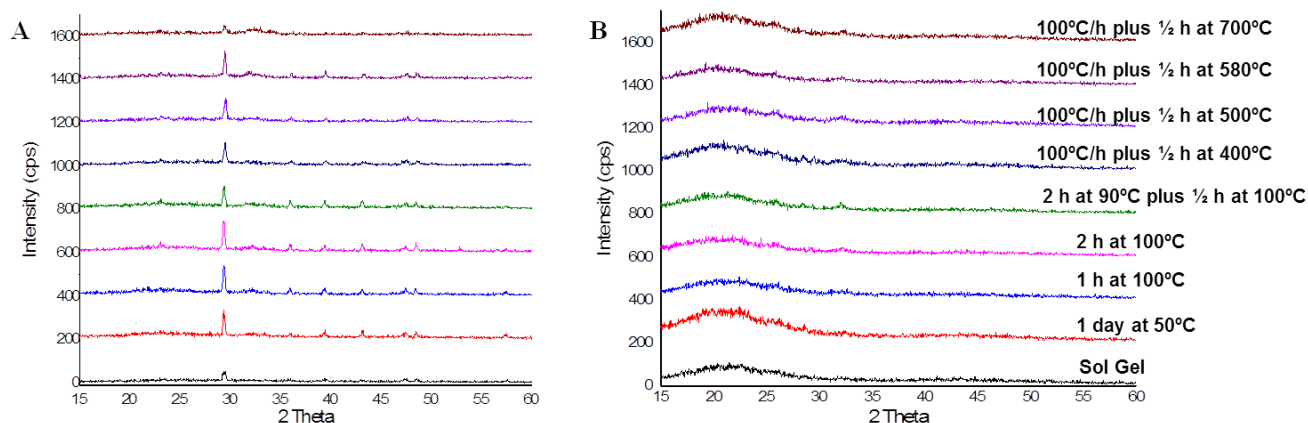


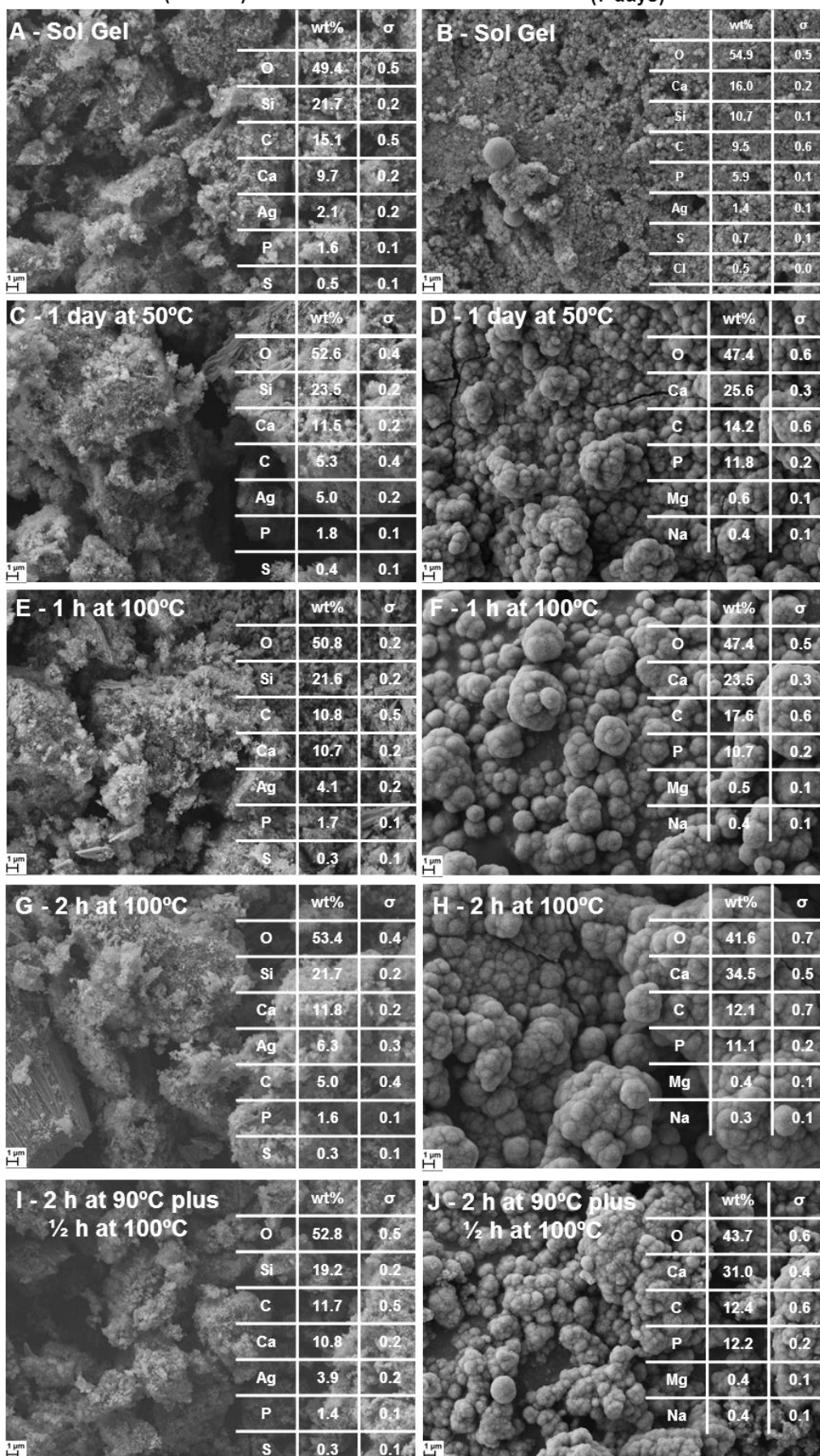
Figure 4.5 - XRD pattern of silver doped bioglass nanoparticles (A) without immersion in simulated body fluid (during 7 days) - Control and (B) with immersion in simulated body fluid (during 7 days).

The capability of these nanoparticles to induce hydroxyapatite formation upon immersion in SBF was further investigated by SEM-EDS shown in Figure 4.6. Comparing the EDS before and after immersion, it can be seen that there is a decrease of Si and an increase of Ca and P weight percentages. Furthermore, after the corresponding SEM micrographs reveals the presence of hydroxyapatite, with its typical cauliflower structure. In fact, an ion exchange occurs when bioglass nanoparticles are soaked in SBF. The presence of H_3O^+ in solution with Ca^{2+} and Na^+ ions implies a pH increase of the solution and the formation of hydrated titania or silica [22, 23]. The formation of a crystalline calcium phosphate (Ca-P) layer has place after this hydrated titania or silica (Si-OH or Ti-OH) formation [22], because it serves as nucleation sites [23]. All the produced nanoparticles have the Si component has a critical importance in the mineralization of materials [4]. Phosphorus also plays an important role in bioactivity [17]. Nanoparticles composed by bioglass present an advantage. Indeed, these nanoparticles have an important capability to replace damaged mineralized tissues like bone [17]. Summarizing, SEM-EDS results are in agreement with XRD data, confirming that both non-treated and thermally treated nanoparticles are bioactive (induces the formation of a calcium-phosphate layer on its surface).

Chapter 4. Silver Doped Bioglass Nanoparticles Synthesis Envisaging Biomedical Applications

Without immersion in SBF solution
(Control)

After immersion in SBF solution
(7 days)



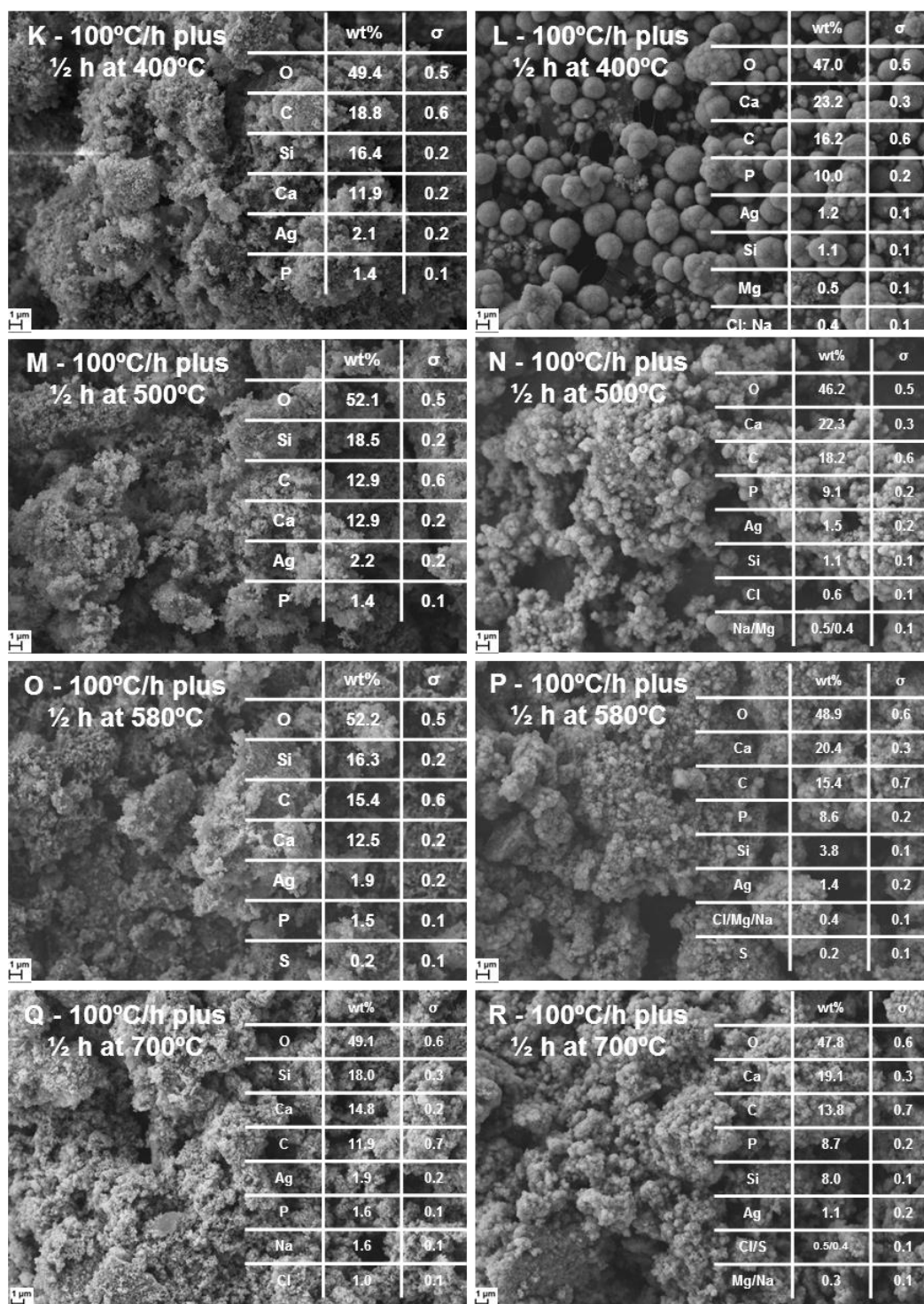


Figure 4. 6 - SEM-EDS micrographs of Ag-BG-NPs before and after immersion in SBF (0 days-control and 7 days). Magnifications of 3 000 x.

4.4. Conclusions

Silver doped bioglass nanoparticles [SiO₂-CaO-P₂O₅-Ag₂O (mol %):56-30-4-10] were successfully produced through an optimized sol-gel technique. Moreover, SEM micrographs and EDS spectra showed the correct production of nano-sized nanoparticles

(diameters between 50 and 200 nm) as well as the silver incorporation in the bioglass matrix. The effect of the chosen thermal treatment on the properties of the Ag-BG-NPs for the first time was studied. Comparing the zeta potential and S-TEM results, the samples with better stability were 2h at 90°C plus ½ h at 100°C, 100°C/h plus ½ h at 400°C, 500°C, 580°C and 700°C. In order to evaluate their bioactive character, in vitro bioactivity studies were made. The results showed (SEM-EDS and XRD analysis) the presence of hydroxyapatite on its surface. Summarizing, these silver doped bioglass nanoparticles could be used in the biomedical fields for instance in free-standing films build-up and/or hydrogels production for the orthopedic area or dental applications.

Acknowledgements:

The authors acknowledge the Portuguese Foundation for Science and Technology (FCT) and the European program FEDER/COMPETE for the financial support through project LA ICVS/3Bs - 2015-2017.

4.5. References:

- [1] M. A. Shenashen, S. A. El-Safty, and E. A. Elshehy, "Synthesis, Morphological Control, and Properties of Silver Nanoparticles in Potential Applications," (in English), *Particle & Particle Systems Characterization*, Review vol. 31, no. 3, pp. 293-316, 2014.
- [2] Y.-F. Goh, A. Z. Alshemary, M. Akram, M. R. A. Kadir, and R. Hussain, "Bioactive Glass: An In-Vitro Comparative Study of Doping with Nanoscale Copper and Silver Particles," *International Journal of Applied Glass Science*, vol. 5, no. 3, pp. 255-266, 2014.
- [3] A. R. Boccaccini, M. Erol, W. J. Stark, D. Mohn, Z. K. Hong, and J. F. Mano, "Polymer/bioactive glass nanocomposites for biomedical applications: A review," (in English), *Composites Science and Technology*, Article; Proceedings Paper vol. 70, no. 13, pp. 1764-1776, 2010.
- [4] Z. K. Hong et al., "Mono-dispersed bioactive glass nanospheres: Preparation and effects on biomechanics of mammalian cells," (in English), *Journal of Biomedical Materials Research Part A*, Article vol. 95A, no. 3, pp. 747-754, 2010.
- [5] A. M. El-Kady, A. F. Ali, R. A. Rizk, and M. M. Ahmed, "Synthesis, characterization and microbiological response of silver doped bioactive glass nanoparticles," (in English), *Ceramics International*, Article vol. 38, no. 1, pp. 177-188, 2012.
- [6] S. Lin, C. Ionescu, K. J. Pike, M. E. Smith, and J. R. Jones, "Nanostructure evolution and calcium distribution in sol-gel derived bioactive glass," (in English), *Journal of Materials Chemistry*, Article vol. 19, no. 9, pp. 1276-1282, 2009.

Chapter 4. Silver Doped Bioglass Nanoparticles Synthesis Envisaging Biomedical Applications

- [7] C. Vichery and J.-M. Nedelec, "Bioactive Glass Nanoparticles: From Synthesis to Materials Design for Biomedical Applications," *Materials*, vol. 9, no. 4, Apr 2016, Art. no. 288.
- [8] A. Simchi, E. Tamjid, F. Pishbin, and A. R. Boccaccini, "Recent progress in inorganic and composite coatings with bactericidal capability for orthopaedic applications," *Nanomedicine: Nanotechnology, Biology and Medicine*, vol. 7, no. 1, pp. 22-39, 2011.
- [9] M. Bellantone, N. J. Coleman, and L. L. Hench, "Bacteriostatic action of a novel four-component bioactive glass," (in English), *Journal of Biomedical Materials Research*, Article vol. 51, no. 3, pp. 484-490, 2000.
- [10] M. Catauro, M. G. Raucci, F. De Gaetano, and A. Marotta, "Antibacterial and bioactive silver-containing Na₂O center dot CaO center dot 2SiO(2) glass prepared by sol-gel method," (in English), *Journal of Materials Science-Materials in Medicine*, Article vol. 15, no. 7, pp. 831-837, 2004.
- [11] E. Vernè et al., "Surface characterization of silver-doped bioactive glass," *Biomaterials*, vol. 26, no. 25, pp. 5111-5119, 2005.
- [12] J. R. J. Delben et al., "Synthesis and thermal properties of nanoparticles of bioactive glasses containing silver," *Journal of Thermal Analysis and Calorimetry*, vol. 97, no. 2, pp. 433-436, 2009.
- [13] A. Oyane, H. M. Kim, T. Furuya, T. Kokubo, T. Miyazaki, and T. Nakamura, "Preparation and assessment of revised simulated body fluids," *Journal of Biomedical Materials Research Part A*, vol. 65A, no. 2, pp. 188-195, 2003.
- [14] A. Oyane, K. Onuma, A. Ito, H. M. Kim, T. Kokubo, and T. Nakamura, "Formation and growth of clusters in conventional and new kinds of simulated body fluids," *Journal of Biomedical Materials Research Part A*, vol. 64A, no. 2, pp. 339-348, 2003.
- [15] A. Vulpoi et al., "Bioactivity and protein attachment onto bioactive glasses containing silver nanoparticles," *Journal of Biomedical Materials Research Part A*, vol. 100A, no. 5, pp. 1179-1186, 2012.
- [16] G. M. Luz and J. F. Mano, "Preparation and characterization of bioactive glass nanoparticles prepared by sol-gel for biomedical applications," (in English), *Nanotechnology*, Article vol. 22, no. 49, p. 11, 2011, Art. no. 494014.
- [17] G. M. Luz and J. F. Mano, "Nanoengineering of bioactive glasses: hollow and dense nanospheres," (in English), *Journal of Nanoparticle Research*, Article vol. 15, no. 2, p. 11, 2013, Art. no. 1457.
- [18] H. H. Lu, S. R. Pollack, and P. Ducheyne, "Temporal zeta potential variations of 45S5 bioactive glass immersed in an electrolyte solution," *Journal of Biomedical Materials Research*, vol. 51, no. 1, pp. 80-87, 2000.
- [19] M. Tirrell, E. Kokkoli, and M. Biesalski, "The role of surface science in bioengineered materials," *Surface Science*, vol. 500, no. 1-3, pp. 61-83, 2002.
- [20] G. M. Luz and J. F. Mano, "Preparation and characterization of bioactive glass nanoparticles prepared by sol-gel for biomedical applications," *Nanotechnology*, vol. 22, no. 49, 2011, Art. no. 494014.

Chapter 4. Silver Doped Bioglass Nanoparticles Synthesis Envisaging Biomedical Applications

- [21] H. W. Kim, H. E. Kim, and J. C. Knowles, "Improvement of hydroxyapatite sol-gel coating on titanium with ammonium hydroxide addition," *Journal of the American Ceramic Society*, vol. 88, no. 1, pp. 154-159, 2005.
- [22] H. M. Kim, "Ceramic bioactivity and related biomimetic strategy," *Current Opinion in Solid State & Materials Science*, vol. 7, no. 4-5, pp. 289-299, 2003.
- [23] N. M. Alves, I. B. Leonor, H. S. Azevedo, R. L. Reis, and J. F. Mano, "Designing biomaterials based on biomineralization of bone," (in English), *Journal of Materials Chemistry*, Article vol. 20, no. 15, pp. 2911-2921, 2010.

Chapter 4. Silver Doped Bioglass Nanoparticles Synthesis Envisaging Biomedical Applications

CHAPTER 5

ANTIBACTERIAL

NATURAL-BASED FREE-STANDING FILMS

INSPIRED BY THE SEA

5. ANTIBACTERIAL NATURAL-BASED FREE-STANDING FILMS INSPIRED BY THE SEA

Abstract

Marine mussels present an unusual amino acid, 3, 4-dihydroxy-L-phenylalanine (DOPA), which is used to stick to various substrates, either inorganic or organic. This adhesion is due to the presence of the catechol group, present in DOPA and its analog dopamine. In this study, novel free-standing films, based on natural polymers, namely chitosan (CHT), hyaluronic acid (HA), hyaluronic acid-dopamine conjugate (HA-DN) were developed. Also, silver doped bioglass nanoparticles (Ag-BG-NPs) were incorporated in their constitution. Characterization techniques were performed to study their surface morphology and topography, wettability, as well as, weight loss, swelling, mechanical, adhesion and bioactivity tests. Bioactivity tests revealed that upon immersion in simulated body fluid during 14 days there was the formation of a bone-like apatite layer. The produced films also exhibited an antibacterial effect against *Staphylococcus aureus* and *Escherichia coli* cultures. Such free-standing films could be used in biomedical applications, namely in the orthopedic or dental areas.

Keywords: MAPs, catechol, free-standing films, genipin, silver doped bioglass nanoparticles.

5.1. Introduction

Recently the scientific community has showed interest in mussel adhesive proteins, known as MAPs [1]. These marine adhesive proteins contains an unusual amino acid, 3, 4-dihidroxy-L-phenyalanine (DOPA) [1-7], which presents the catechol group that is responsible for their outstanding adhesion to various substrates [1, 2, 8-10], either in dry or wet environments. In this work we used only natural-based polymers, namely chitosan (CHT) and hyaluronic acid (HA). Chitosan is a linear polysaccharide made by glucosamine and N-acetyl glucosamine units linked by β -1, 4 glycosidic bonds [11]. Chitosan is soluble in acidic solution, because there is the protonation of the amine (NH₂) functional group present in the second carbon in the D-glucosamine repeat unit [12], in weak acids solutions, i.e. pH below 6 [13]. CHT is used in biomedical fields, because it is biodegradable [14, 15], it is biocompatible [15], non-toxic [14], antimicrobial [15], has low immunogenicity [15], it has an anti-tumor effect [14] and it presents fungistatic characteristics [14]. HA is made of N-acetyl-D-glucosamine and D-glucuronate, with β 1-4 and β 1-3 linkages [8, 16, 17]. It is a glycosaminoglycan present in the synovial fluid, vitreous humour of the human eye, connective tissues [18] and bacteria [19]. Furthermore, HA has influence in cell migration, adhesion and proliferation. HA is useful in the biomedical field, because it plays an important role in wound healing and lubricity [20]. The LbL technique was also chosen in the present work, because it has many advantages, such as simplicity [21, 22], cost-effectivity [21], versatility [21], flexibility [21-23], efficiency [23], reproducibility [23] and it has structural precision [22]. LbL is based on different charged species (poly(electrolytes)) that can be sequently deposited on a substrate [24]. Free-standing films have received large attention by researchers [25]. This development from LbL technique is useful to create materials for biomedical applications [26, 27], such as membranes [28], scaffolds [28], among others, and are useful for many applications, namely wound healing [27, 29], drug delivery [27, 28] and biosensors creation [25]. In a previous work of our group [8] a LbL coating using CHT and hyaluronic acid modified with dopamine (HA-DN) was produced. The results showed that this film produced by LbL had higher adhesion strength, compared with the one that did not contain dopamine [8]. Furthermore, these coatings with dopamine presented high cellular adhesion, proliferation and viability [8]. Zhang and co-workers [30] also developed multilayer coatings of CHT with HA-DN and found that the catechol groups enhanced the osteoblast proliferation [30].

Chapter 5. Antibacterial Natural-Based Free-Standing Films Inspired by the Sea

For the purpose of the present paper, a quaternary formulation [SiO₂-CaO-P₂O₅-Ag₂O =56:30:4:10] % mol of silver doped bioglass nanoparticles was incorporated in the free-standing films' build-up. Nanoparticles composed by SiO₂,CaO and P₂O₅ induce an apatite layer formation [31]. Furthermore, the presence of silver ions allows antimicrobial activity and a reduction of microbial infection [31]. As far as we know, this is the first time that a nanostructured free-standing film made by natural-based biopolymers, such as HA, HA-DN and CHT and, as nanofiller, Ag-BG-NPs was developed. These free-standing films were crosslinked with genipin which also has a natural origin [21], in order to obtain LbL films systems with reinforced stability and better mechanical properties. These films were morphologically, topographically and mechanically studied in detail.

5.2. Experimental section

5.2.1. Materials

Hyaluronic acid from *Streptococcus equi*. (Sigma-Aldrich) with a molecular weight of 595 kDa, was used. CHT with a medium molecular weight (Sigma-Aldrich), obtained by viscosimetry of 770 kDa, was purified by recrystallization with an N-deacetylation degree of 80%. Also, genipin, dimethyl sulfoxide ACS reagent $\geq 99.9\%$ and dopamine hydrochloride were from Sigma-Aldrich.

Sodium chloride (NaCl), di-Potassium hydrogen phosphate trihydrate (K₂HPO₄.3H₂O), magnesium chloride hexahydrate (MgCl₂.6H₂O, calcium chloride (CaCl₂), potassium chloride (KCl), sodium hydrogen carbonate (NaHCO₃), sodium carbonate (Na₂CO₃) from Merck, sodium sulphate (Na₂SO₄) and sodium hydroxide (NaOH) from Panreac and 2-(4-(2-hydroxyethyl)-1-piperazinyl) ethanesulfonic acid (HEPES, C₈H₁₈N₂O₄S) were from Sigma-Aldrich.

5.3. Methods

5.3.1. Synthesis of hyaluronic acid-dopamine conjugate (HA-DN)

This synthesis was based on Lee and co-workers procedure [7]. The synthesis of HA-DN was produced using N-(3-Dimethylaminopropyl)-N'-ethylcarbodiimide hydrochloride (EDC) as the activation agent. Briefly, 1g of hyaluronic acid (HA) was dissolved in 100 mL of phosphate buffered saline solution (PBS) (purchased on Laborspirit Company). Under magnetic stirring, the pH was adjusted to 5.5 using sodium hydroxide (NaOH) or hydrochloric acid (HCl) aqueous solutions (0.5 M) [7]. Then, during 30 minutes, the solution was purged with nitrogen. Afterwards, 338 mg of N-(3-Dimethylaminopropyl)-N'-ethylcarbodiimide hydrochloride (EDC) (purchased on Sigma-Aldrich Company) and 447 mg of dopamine (DN) (Sigma-Aldrich) were weighed and added to the previous solution. The synthesis of HA-DN was done at pH of 5.5 a 4°C, for 2 hours. Dialysis was made in order to remove all unreacted chemicals using distilled water. Afterwards, the HA-DN conjugate was lyophilized for 4 days.

5.3.2. Free-standing films production

Fresh CHT, HA and HA-DN and Ag-BG-NPs solutions were prepared. As washing solutions, 0.15 M of NaCl was used. For the CHI solution it was added 1% (v/v) of acetic acid (CH₃COOH) to the NaCl solution. The solutions were prepared under stirring and left dissolving overnight. The build-up pH chosen was 5.5, taking into account the results of our previous works [32, 33]. Poly(propylene) (PP) films were used as a substrate. Different formulations were prepared, as is shown in Table 5.1. The films were built-up with 75 tetralayers using a home-made dipping robot.

Table 5.1. - Procedures for the formation of the freestanding films

Formulations	Poly(electrolyte) concentration
1: [CHT/HA/CHT/HA] ₇₅	CHT (+): 2 mg/mL
	HA (-): 2mg/mL
2: [CHT/HA-DN/CHT/HA-DN] ₇₅	CHT (+): 2 mg/mL
	HA-DN (-): 2mg/mL
3: [CHT/HA/CHT/Ag-BG-NPs] ₇₅	CHT (+): 2 mg/mL
	HA (-): 2mg/mL
	Ag-BG-NPs (-): 2.5 mg/mL
4: [CHT/HA-DN/CHT/Ag-BG-NPs] ₇₅	CHT (+): 2 mg/mL
	HA-DN (-): 2mg/mL
	Ag-BG-NPs (-): 2.5 mg/mL

Chapter 5. Antibacterial Natural-Based Free-Standing Films Inspired by the Sea

Furthermore, Ag-BG-NPs [$\text{SiO}_2\text{-CaO-P}_2\text{O}_5\text{-Ag}_2\text{O}$ (56:30:4:10)] thermally treated during 2 hours at 90°C and $\frac{1}{2}$ h at 100°C were chosen, because the obtained zeta potential was higher in the construction build-up parameter (0.15 M NaCl solution, $\text{pH}=5.5$). As far as the crosslinking process is concerned, free-standing films were put in contact with 1 mg/mL of genipin (Sigma-Aldrich), dissolved in DMSO/sodium acetate buffer (0.15M NaCl) overnight at 37°C . The resulting films were then washed with sodium acetate buffer (0.15 M NaCl, pH 5.5) during 30 minutes and then with DW during 1 hour. Finally, the free-standing films were dried during 1 day at room temperature. This crosslinking process was based on Silva and co-workers' work [34].

5.4. Characterization techniques

5.4.1. Fourier Transform Infrared (FT-IR) spectroscopy

Fourier Transform infrared spectroscopy was used to analyze the crosslinked free-standing films. The results were obtained using the FT-IR (infrared spectrum-Jasco), in the attenuated total reflectance (ATR), transmission mode. The FT-IR spectra were recorded from 600 to 4000 cm^{-1} .

5.4.2. Atomic force microscopy (AFM)

An AFM Dimension Icon (Bruker, USA) was used in PeakForce Tapping (ScanAsyst) in air. Moreover, the AFM cantilevers (ScanAsyst-Air, Bruker) made of silicon nitride with a spring constant of 0.4 N/m and frequency of 70 kHz were used.

5.4.3. Scanning electron microscopy coupled with energy dispersive X-ray spectroscopy (SEM-EDS)

The High-Resolution Field Emission Scanning Electron Microscope with Focused Ion Beam (FIB-SEM) (AURIGA COMPACT, ZEISS) and the Scanning Electron Microscope (SEM) with EDS (JSM-6010 LV, JEOL, Japan) coupled with dispersive X-ray spectroscopy (INCAx-Act, PentaFET Precision, Oxford Instruments) equipment were used to characterize the films.

5.4.4. X-ray diffraction (XRD)

A Bruker AXS D8 Discover, USA equipment was used for this characterization. The $\text{Cu-K}\alpha$ radiation ($\lambda=1.54060\text{ \AA}$) was chosen, scanning from 15° to 60° at a speed of $0.04^\circ/1\text{ s}$. The analysis for phase identification was performed using analytical software EVA. The

crystalline phases were indexed using the ICDD-2015 database (International Center for Diffraction Data).

5.4.5. Thermogravimetric analysis (TGA)

To evaluate the filler percentage (Ag-BG-NPs thermally treated during 2h at 90°C plus ½ h at 100°C) present in the free-standing films, the Q500 TGA equipment (TA Instruments, USA) was used. The tests were performed using a temperature range of 40°C to 800°C at a rate of 10°C/min.

5.4.6. Water contact angle (WCA) measurements

A OCA15 plus goniometer equipment (DataPhysics, Germany) was used. The contact angle measurements were performed on both sides of the films, i.e., “top” corresponds to the top of the film, i.e., HA, HA-DN and/or Ag-BG-NPs and “bottom” surface corresponds to the film in contact with the substrate, which was always a CHT layer. A drop of 3 µL of ultra-pure water was used to measure the WCA values. The measurements were performed at 25°C and the pictures were taken after the drop contacted the surface. The SCA20 software was used.

5.4.7. Mechanical and adhesion tests

Tensile strength and also lap-shear adhesive strength tests were performed using a universal electromechanical testing machine equipment (Instron 5543, USA), equipped with a 1 kN load cell, under the tensile mode. For this mechanical characterization, all samples were cut with 0.6 cm width, 3.0 cm length and with a gauge length equal to 1.2 cm. The thickness of the dried samples was measured three times ($n = 3$) for each sample. The same dimensions and the same gauge length were chosen for the wet tensile tests, but the samples were previously immersed in PBS during 60 min. The measurements were taken under a loading speed of 1.5 mm/min. for the dry samples and 0.5 mm/min. for the wet samples. The values were calculated through analysis of the stress-strain curves, such as the ultimate tensile strength (UTS, MPa), tensile Young modulus (MPa) and the strain at break (ϵ , %). Additionally, the adhesion test were performed according to the ASTM D1002 standard. The adhesive strength was evaluated through the lap-shear adhesive stress tests. Briefly, the free-standing films were cut with 5 mm width and 15 mm length and with an overlapping area of $3.75 \times 5 \text{ mm}^2$. Then, they were put between two lamellae and soaked in phosphate buffered saline (PBS) solution overnight. They were tested in the referred universal testing machine under the same conditions with a load speed of 5

mm/min. The lap shear strength was determined from the maximum of the stress-strain curves. The data is presented as Mean \pm SD using at least five specimens.

5.4.8. *In vitro* bioactivity studies

The four different formulations of free-standing films were immersed in a modified-simulated body fluid solution (m-SBF 1.5 x). This solution was prepared following the Oyane and co-workers [35] and Oyane and co-workers [36] procedures. This solution was prepared dissolving sodium chloride (NaCl, Merck), sodium sulphate (Na₂SO₄, Panreac), magnesium chloride hexahydrate (MgCl₂.6H₂O, Merck), di-Potassium hydrogen phosphate trihydrate (K₂HPO₄.3H₂O, Merck), calcium chloride (CaCl₂, Merck), potassium chloride (KCl, Merck), sodium hydrogen carbonate (NaHCO₃, Merck), sodium carbonate (Na₂CO₃, Merck), sodium hydroxide (NaOH, Panreac) and 2-(4-(2-hydroxyethyl)-1-piperazinyl) ethanesulfonic acid (HEPES, C₈H₁₈N₂O₄S, Sigma) in ultra-pure water (UPW) at 36.5°C. The final pH was adjusted to 7.4. SBF is used because it simulates the concentration of ionic species present in human body plasma. The free-standing films were put into a substrate of poly(propylene) holders with a window of 7 mm x 7 mm and immersed, during 14 days in 10 mL of SBF at 37 °C. After being removed from m-SBF 1.5 x, the films were washed with DW and left to dry at room temperature overnight. These films were characterized by diverse characterization techniques, namely Scanning Electron Microscope (SEM) with EDS (JSM-6010 LV, JEOL, Japan) coupled with dispersive X-ray spectroscopy (INCAx-Act, PentaFET Precision, Oxford Instruments) and Bruker AXS D8 Discover, USA equipment, with Cu-K α radiation ($\lambda = 1,54060\text{\AA}$), scanning from 15° to 60° at a speed of 0.04°/1s. The analysis in order to determinate the phase was performed using analytical software EVA. The crystalline phases were indexed using the ICDD-2015 database (International Center for Diffraction Data).

5.4.9. Swelling behavior

To determine the swelling behavior of the produced free-standing films, equation 13 was used. Firstly, the films, $n = 3$, were weighted. The films, with previously determined weight, were soaked in PBS at pH = 7.4. The excess of solution was removed from the samples using filter paper and the swollen films were weighted at $t = 0, 5 \text{ min}, 15 \text{ min}, 30 \text{ min}$ and 1h to 7 h.

$$\text{Swelling (\%)} = ((W_s - W_d) / W_d) * 100 \quad (13)$$

Where: W_s = weight of swollen films and W_d = weight of dried films.

5.4.10. Weight loss (WL)

In order to determine the degradation behavior of these free-standing films ($n = 3$), they were soaked in PBS for different time points, namely $t = 7, 14, 21$ and 28 days at $T = 37^\circ\text{C}$. The films were weighted before and after each time point. After using different solutions with different percentages of ethanol, to dehydrate the sample, and after drying at 37°C overnight, the samples were weighed. To evaluate the weight loss (WL) of the freestanding films, equation 14 was used.

$$\text{WL (\%)} = ((W_i - W_f) / W_i) \times 100\% \quad (14)$$

Where: W_i = initial dry weight of the sample and W_f = final dry weight after each time point.

5.4.11. Microbiological study:

To study the inhibition of bacterial growth, the LbL films were placed in a Mueller-Hinton agar plate inoculated with 1.5×10^8 CFU of a standard culture of *Staphylococcus aureus* and *Escherichia coli* (OD600 of approximately 0.1) and incubated during 16 hours at 37°C . The formation of inhibition zone surrounding the free-standing film was used as indicator of antibacterial behavior.

5.4.12. Statistical analysis

All experiments were performed in triplicate. The results were presented as a mean \pm standard deviation (SD). Statistical analyses were made using one-way ANOVA followed by Turkey test (Graph Pad Prism 6.0 for Windows), otherwise it was mentioned.

5.5. Results and discussion

Free-standing films build-up was correctly done for the four formulations. Photographs of the macroscopic morphology of the native and crosslinked LbL films are shown in Figure 5.1. The native films were not stable after immersion in distilled water and PBS solution. To overcome this drawback, the films were crosslinked with genipin with a concentration of 1 mg/mL.

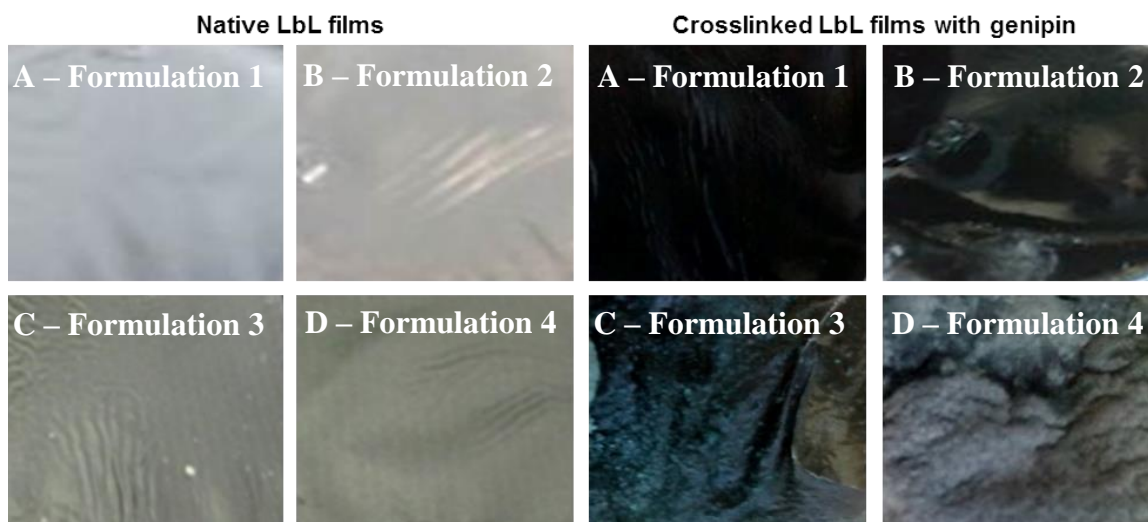


Figure 5. 1 - Photographs of the macroscopic morphology of the native and crosslinked LbL films. (A) Formulation 1: [CHT/HA/CHT/HA]₇₅; (B) Formulation 2: [CHT/HA-DN/CHT/HA-DN]₇₅; (C) Formulation 3: [CHT/HA/CHT/Ag-BG-NPs]₇₅; (D) Formulation 4: [CHT/HA-DN/CHT/Ag-BG-NPs]₇₅.

Through the analysis of Figure 5.1, we can see that formulations 1 and 2 (without Ag-BG-NPs) are transparent, whereas LbL films of formulations 3 and 4 are opaque. The Ag-BG-NPs presence alters their optical properties [37]. Furthermore, it was observed that the crosslinked reaction with genipin changed the color of the LbL films. Genipin has been used as a crosslinker agent because it is a natural molecule [38], extracted from the gardenia fruit [39]. Moreover, genipin presents lower cytotoxicity [39, 40] when comparing with other crosslinking agents, such as formaldehyde [39], dialdehyde starch [39], epoxy components [39] and glutaraldehyde [39, 40].

5.5.1. FT-IR results

The FT-IR results of the crosslinked free-standing films and the control (native films) are shown in Figure 5.2.

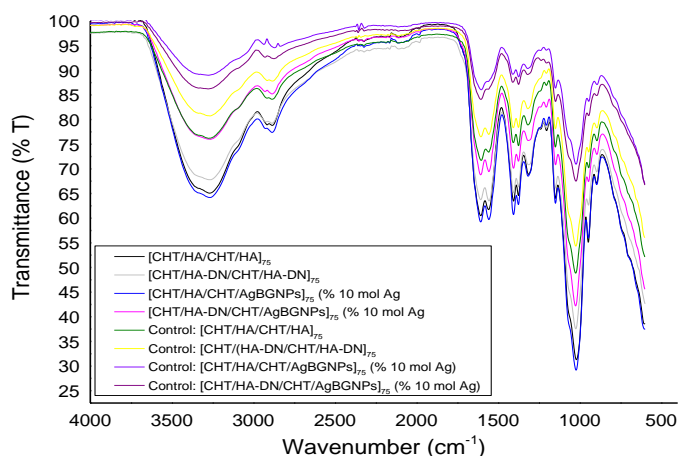


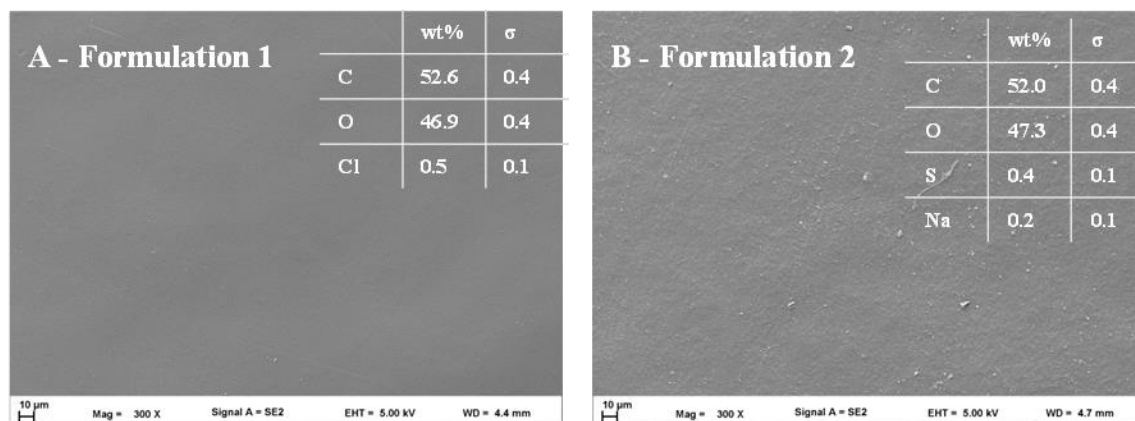
Figure 5. 2 - FT-IR results of the crosslinked free-standing films crosslinked with genipin (1 mg/mL) and the control (native film).

Chapter 5. Antibacterial Natural-Based Free-Standing Films Inspired by the Sea

Through the analysis of Figure 5.2, we can see the bands of chitosan (CHT). The band at 3267 cm^{-1} corresponds to the transmittance band of amine and hydroxyl group [40]. Furthermore, the band at 1392 and 1565 cm^{-1} corresponds to the amide II of CHT (O=C-N-H) [34]. At 926 cm^{-1} to 1151 cm^{-1} there are the vibrational bands of CHT [27, 40-42] and at 1281 , 1026 and 1078 cm^{-1} and they are attributed to the presence of OH-, C-O and C-N stretching, respectively [40]. At 1620 and 1660 cm^{-1} and around 1630 and 1700 cm^{-1} correspond to C=O bands and amide I of CHT [27, 42], respectively. The characteristic peaks of HA are detected at 3383 cm^{-1} , which corresponds to the -OH- of HA [43] which are detectable in a range of 3350 to 3250 cm^{-1} . The methylene group (CH_3) appears around 2940 and 2920 cm^{-1} and amide bonds stretching (C=O) are detectable in a range of 1700 to 1250 cm^{-1} . The peak on 1560 cm^{-1} corresponds to N-H groups and the peak on 1100 cm^{-1} corresponds to ethers groups (-C-O-C) [44]. Furthermore, the C-O and C-O-C stretching modes are detected at 1132 cm^{-1} [27]. Also, is possibly to identify various vibrational modes of Ag-BG-NPs, namely O-H stretching vibration at 3430 cm^{-1} and 1630 cm^{-1} due to the presence of water [45, 46]. Around 1045 and 1051 cm^{-1} there is the Si-O-Si asymmetric stretching vibration [45-48]. The spectrum of crosslinked films is different than the uncrosslinked ones [34], because there is an increase in transmission for crosslinked samples unlike the uncrosslinked ones, due to the interactions between the ester groups of genipin and the amine group (N-H) of CHT [34, 49]. These changes are detected in the characteristic bands of amide I and II of CHT, leading to the formation of amide bond [34]. Furthermore, at 1410 – 1560 cm^{-1} and 1575 cm^{-1} there is an increase in transmittance due to the formation of alkene groups [34, 49] and an increase of amine peak, detectable at 1575 cm^{-1} .

5.5.2. Analysis of the free-standing films morphology

Figure 5.3 shows the surface morphology and the elemental composition of the films.



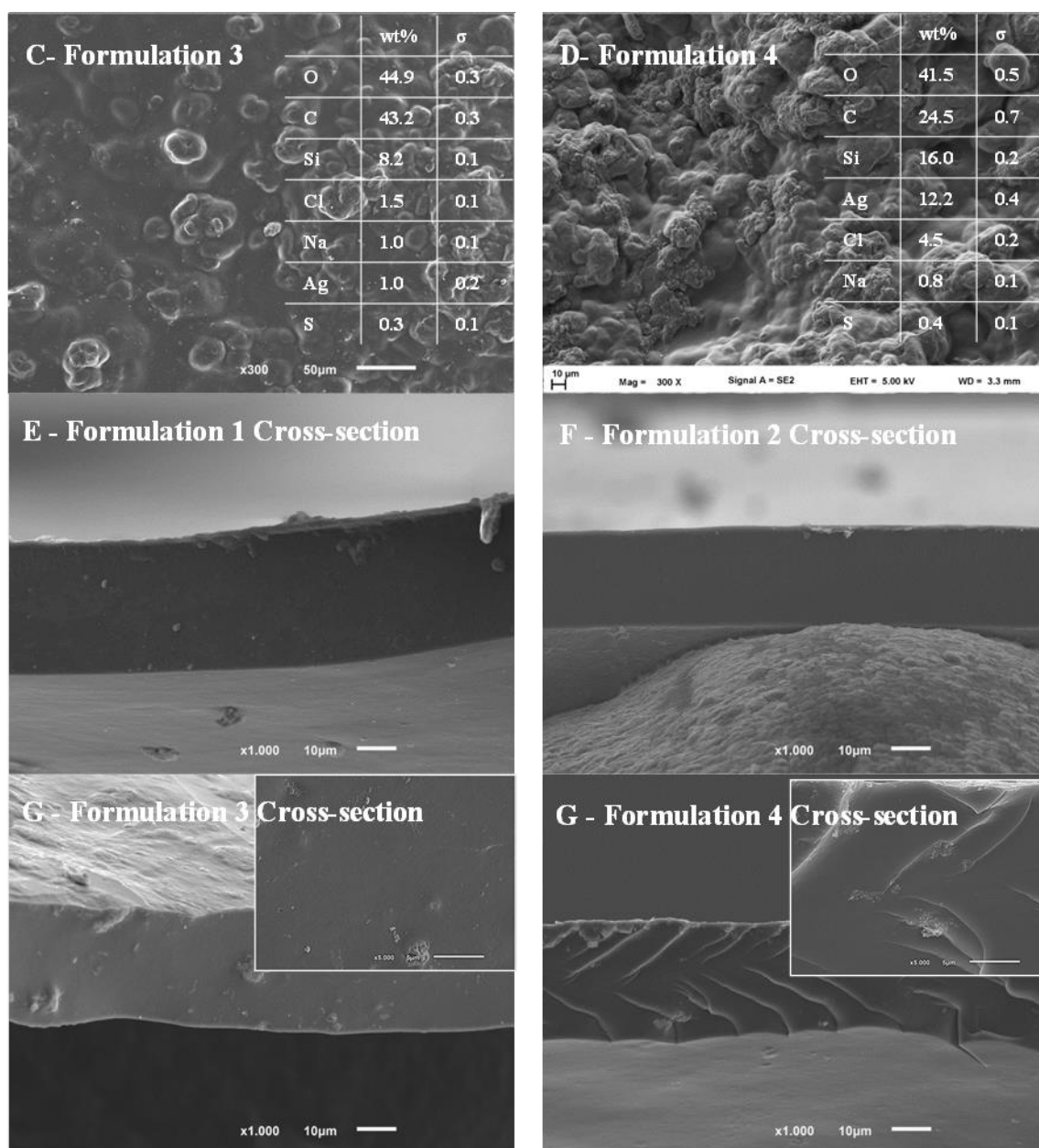
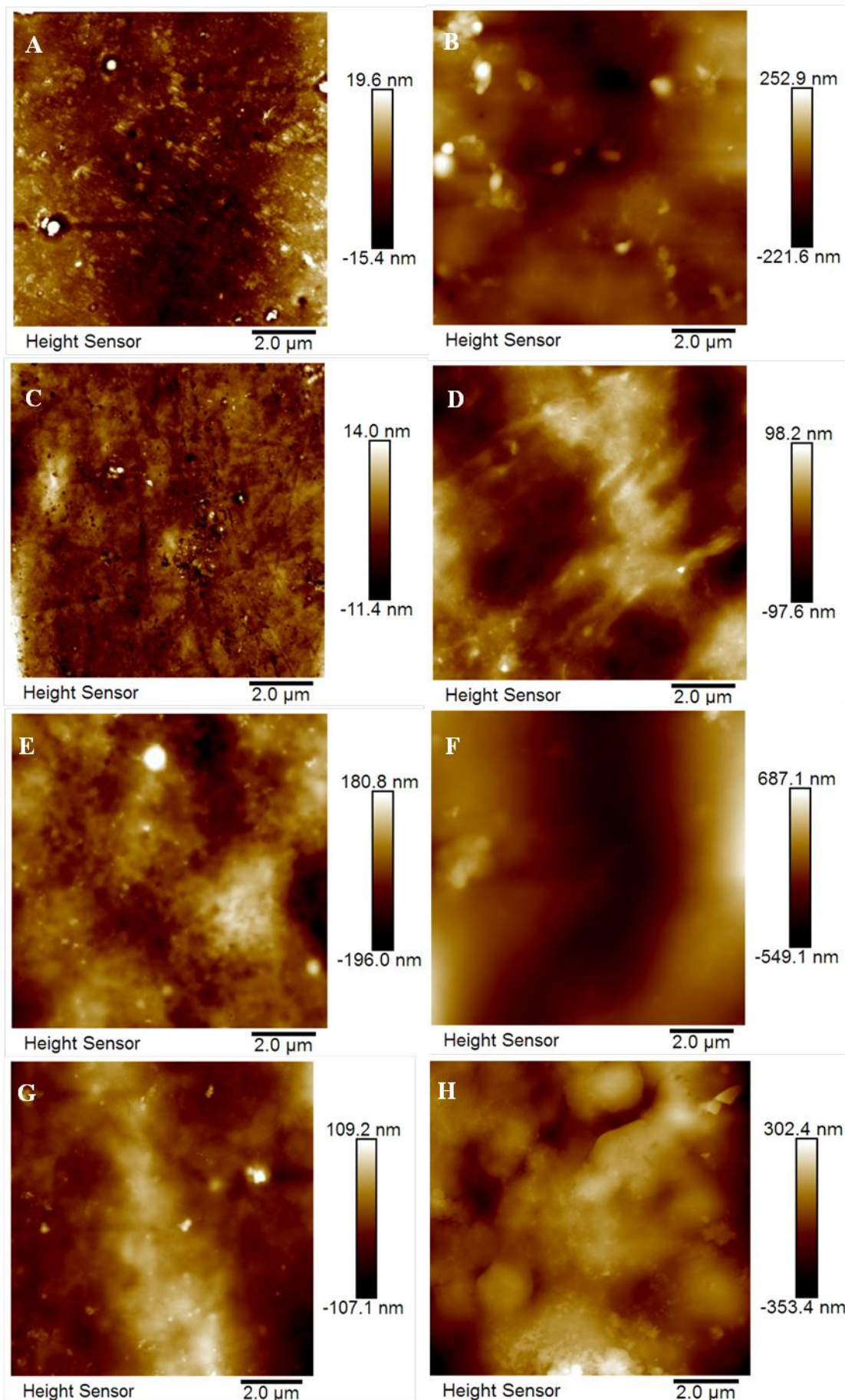


Figure 5. 3 - SEM-EDS micrographs. Top view of (A) Formulation 1: [CHT/HA/CHT/HA]₇₅; (B) Formulation 2: [CHT/HA-DN/CHT/HA-DN]₇₅; (C) Formulation 3: [CHT/HA/CHT/Ag-BG-NPs]₇₅; (D) Formulation 4: [CHT/HA-DN/CHT/Ag-BG-NPs]₇₅; Cross-section views of (E) Formulation 1: [CHT/HA/CHT/HA]₇₅; (F) Formulation 2: [CHT/HA-DN/CHT/HA-DN]₇₅; (G) Formulation 3: [CHT/HA/CHT/Ag-BG-NPs]₇₅ and (H) Formulation 4: [CHT/HA-DN/CHT/Ag-BG-NPs]₇₅.

Figures 5.3-A and B show a homogeneous and smooth surface. At Figures 5.3-C and D we can see the adsorption of nanoparticles in the end-layer and at Figures 5.3-E and H, it can be seen that there is the adsorption of Ag-BG-NPs across the films build-up. To better understand the films' topography at a micrometer level AFM imaging was performed and shown in Figure 5.4.

Chapter 5. Antibacterial Natural-Based Free-Standing Films Inspired by the Sea



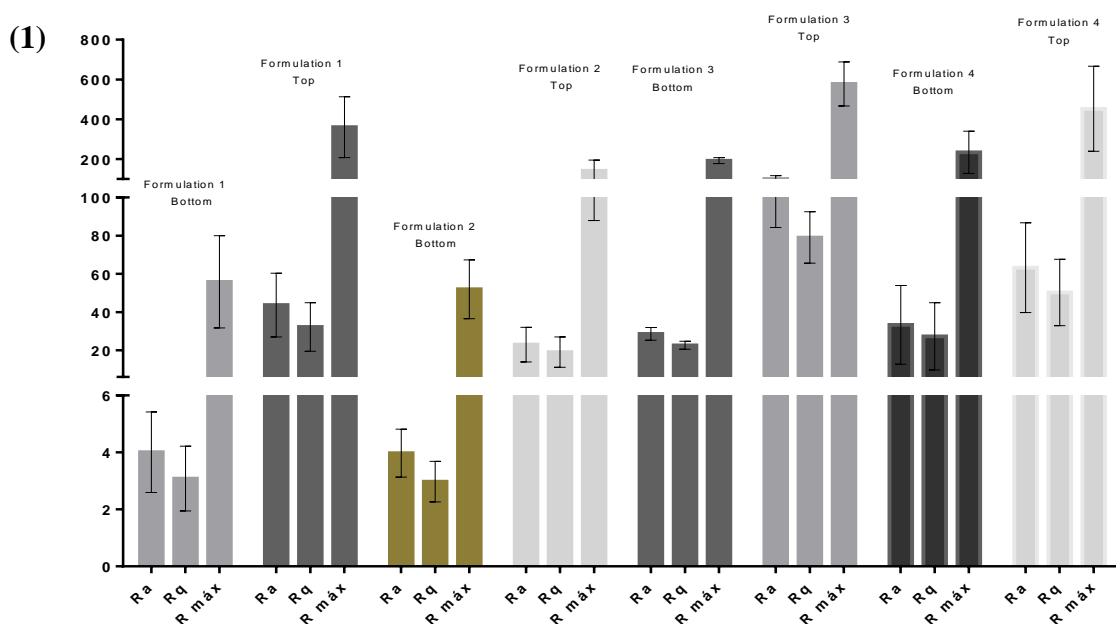


Figure 5. 4 - Atomic force microscopy (AFM) results (2D images). The bar next to all images is the Z-scale (nm). **(A)** Formulation 1: [CHT/HA/CHT/HA]₇₅ (bottom view); **(B)** Formulation 1: [CHT/HA/CHT/HA]₇₅ (top view); **(C)** Formulation 2: [CHT/HA-DN/CHT/HA-DN]₇₅ (bottom view); **(D)** Formulation 2: [CHT/HA-DN/CHT/HA-DN]₇₅ (top view); **(E)** Formulation 3: [CHT/HA/CHT/Ag-BG-NPs]₇₅ (bottom view); **(F)** Formulation 3: [CHT/HA/CHT/Ag-BG-NPs]₇₅ (top view); **(G)** Formulation 4: [CHT/HA-DN/CHT/Ag-BG-NPs]₇₅ (bottom view); **(H)** Formulation 4: [CHT/HA-DN/CHT/Ag-BG-NPs]₇₅ (top view); **(I)** Column graphic with root mean square (Rq), average roughness (Ra) values and maximum roughness (Rmax), n = 3. Representative images four different free-standing films formulations: top and bottom views (10 μ m x10 μ m).

Through the analysis of the graphic present in Figure 5.4-1, it can be seen that comparing the root mean square (Rq), average roughness (Ra) and maximum roughness (Rmax) values, they are lower for the bottom side, in contact with the poly(propylene) substrate than the top surface. Also, when comparing all Rq, Ra and Rmax for the bottom surface of formulations 1 and 2, it can be noted that they have similar values due to the contact with the substrate. For the top side, the formulation 1 presents higher values when compared to formulation 2. The present data were corroborated in a previous work [8], where higher roughness was obtained for coatings with CHT and HA than for the ones with CHT and HA-DN. Regarding formulations 3 and 4, for the bottom side, we can see that the surface roughness is lower than the obtained values for the top side, as they are in contact with the substrate, but they present higher values than formulation 1 and 2, probably due to some diffusion processes. Regarding the top surface of formulations 3 and 4, it can be seen that they present higher Ra, Rq and Rmax values than the control ones (Figure 5.4-1). This can be justified by the presence of Ag-BG-NPs in the end-layer which can lead to a higher roughness. Furthermore, the texture present in the top side of formulation 4- Figure 5.4-H, is consistent with Ag-BG-NPs agglomerates. Additionally,

formulation 3 presents higher Ra and Rq values when compared with formulation 4. In fact, the top surface in formulation 3 presents nanoparticles' agglomerates, meaning that these nanoparticles aren't uniformly distributed on its surface, implying that formulation 3 is more heterogeneous than formulation 4. A rough surface is useful for cell adhesion, because there are more anchor points and more available surface area for protein adsorption [50].

5.5.3. Thermogravimetric analysis

TGA analysis was conducted to quantify the relative quantity of Ag-BG-NPs present in formulations 3 and 4, as it can be seen in Figure 5.5.

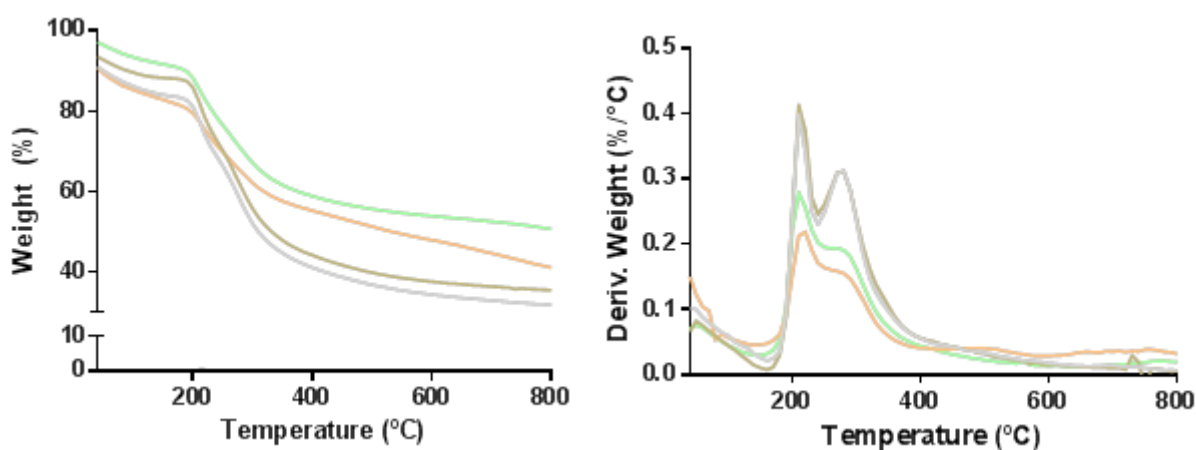


Figure 5.5 - Representative TGA results. Gray curve: Formulation 1-[CHT/HA/CHT/HA]₇₅; Dark yellow: Formulation 2-[CHT/HA-DN/CHT/HA-DN]₇₅; Orange curve: Formulation 3: [CHT/HA/CHT/Ag-BG-NPs]₇₅ (% 10 mol Ag); Green curve: Formulation 4: [CHT/HA-DN/CHT/Ag-BG-NPs]₇₅ (% 10 mol Ag).

Through the analysis of Figure 5.5 for formulation 3, the percentage of mineral charge incorporated in the film was near to 41%. For formulation 4, the percentage of nanoparticle incorporation was near 50%. The thermal degradation of CHT and HA takes place at a lower temperature than that of HA and CHT by themselves [51]. Furthermore, HA degrades at 220°C and CHT degrades at 290°C. The obtained results are around 213 °C for HA and 278 °C for CHT. The TGA thermograms show that around 60°C to 80 °C there is a weight loss [31]. This is related to the release of water and alcohol. Moreover, around 540°C and 550°C there is the decomposition of the unreacted Ca(NO₃)₂ [31]. For formulation 1 and 2, we can see the same decomposition steps. Discounting the final percentage of waste at 800°C for formulation 3 and 4 and the control ones (formulation 1 and 2), respectively, the incorporation of Ag-BG-NPs was 15% for formulation 3 and 16% for formulation 4. These results are quite satisfactory, since the Ag-BG-NPs suspensions were put on each LbL cycle in the sonicator to avoid the nanoparticle's

agglomeration and precipitation in order to maximize the Ag-BG-NPs adsorption. These results are similar to a previous work of our group [37].

5.5.4. Mechanical properties of the crosslinked free-standing films

The mechanical properties are important to understand if a biomaterial can be used in biomedical applications, i.e., if it is able to resist in biological environments [52]. The tensile mechanical properties shown in Figures 5.6 and 5.7 correspond to the values obtained for the samples in dry and wet state, respectively.

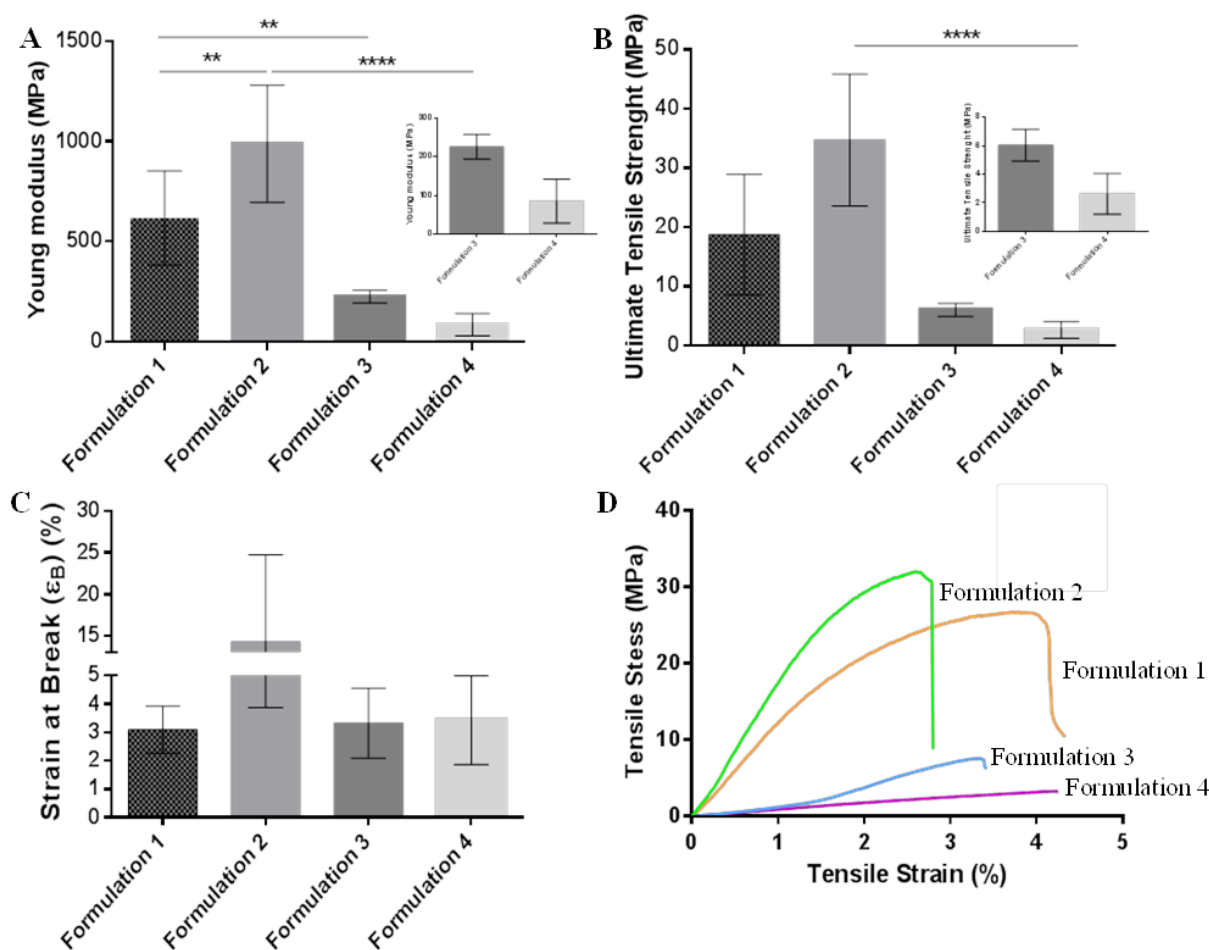


Figure 5. 6 - Mechanical Properties-Dry samples. The data is presented as Mean \pm SD, n = 5. (A) Tensile Young modulus (MPa) (one-way ANOVA, p < 0.01 [**], p < 0.0001 [****]) (B) Ultimate tensile strength (MPa) (non-parametric tests, Kruskal-Wallis statics), (C) Strain at break (%) (Non-parametric tests, Kruskal-Wallis statics), (D) Tensile stress (MPa) vs. tensile strain (%) - representative curves for each formulation.

We can see that the Young modulus, in Figure 5.6-A, present higher values for formulation 1 and 2, than for the formulations with addition of Ag-BG-NPs. In fact, formulation 3 and 4 show a brittle structure, because instead of increasing the strength of the film, they disrupt the structure, leading to the premature failure of the film. Moreover,

the mechanical tests were performed in wet conditions, shown in Figure 5.7 because it simulates the physiological environment [52].

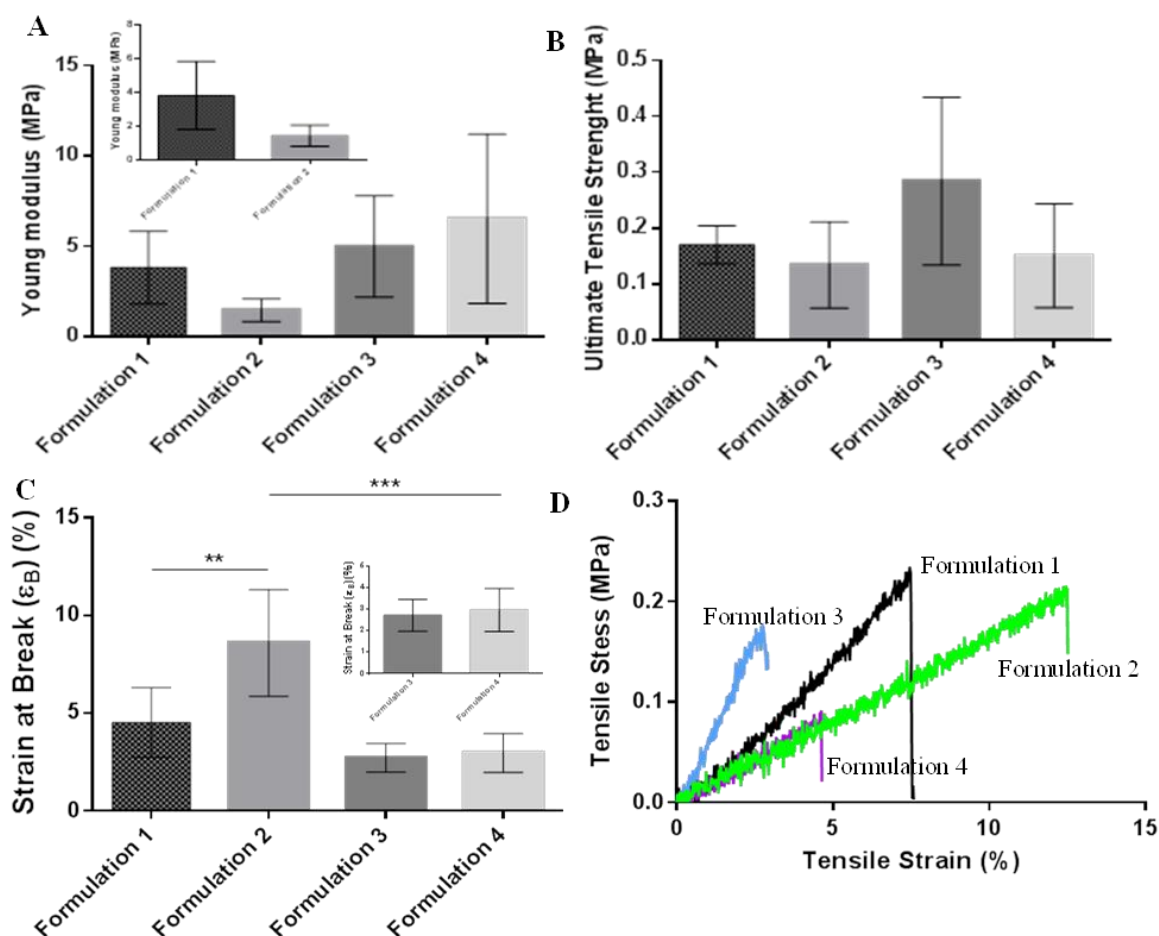


Figure 5. 7 - Mechanical Properties-Wet samples. The data is presented as Mean ± SD. Formulation 1: [CHT/HA/CHT/HA]₇₅, Formulation 2: [CHT/HA-DN/CHT/HA-DN]₇₅, Formulation 3: [CHT/HA/CHT/Ag-BG-NPs]₇₅ and Formulation 4: [CHT/HA-DN/CHT/Ag-BG-NPs]₇₅. (A) Tensile Young modulus (MPa) (one-way ANOVA) (B) Ultimate tensile strength (MPa) (one-way ANOVA) (C) Strain at break (%) for (one-way ANOVA, p < 0.01 [**], p < 0.001 [***]) (D) Tensile stress (MPa) vs. tensile strain (%) curves for one of the representative curve for each formulation.

The Young's modulus values in wet conditions showed the opposite values than the mechanical tests performed in dry conditions. This is justified by the plasticizing effect of PBS [52]. The UTS and E values decreased in wet conditions comparing to the dry ones, which are in accordance with Mota and co-workers' [53] results. However, the strain at break showed similar results, which wasn't expected (Figure S 5.1). Analyzing the tensile tests performed in wet conditions we can see higher Young modulus for the formulations with incorporation of Ag-BG-NPs, but for the strain at break (ε_B) they presented lower values than the control ones. These values are, once again, according to Mota and co-workers' [53] results. Regarding the strain at break in wet conditions, formulation 1 and 2, which are composed only by polymers, they are more ductile,

presenting higher strain values, but they present lower stiffness, implying lower Young modulus values. In a recent work developed by Neto and co-workers [54], they studied the effect of the crosslinking of [CHT/HA]_{5,10} and ₁₅, [CHT/HA-DN]_{5,10} and ₁₅ bi-layers with genipin. The results reveal that they are stiffer than the uncrosslinked ones.

Adhesion tests were also conducted to analyse the influence of the end-layer in the adhesive character of the developed films, shown in Figure 5.8.

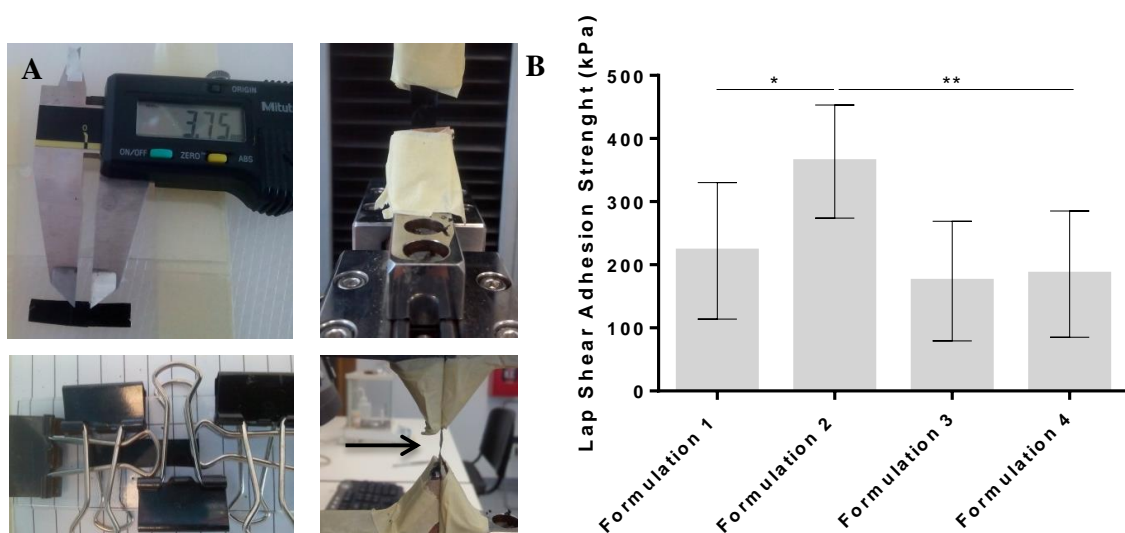


Figure 5. 8 - (A) All steps followed to prepare the samples to perform the adhesion tests, according to ASTM D1002 standard, as described in section Materials and Methods. **(B)** Adhesive strength of the free-standing films. Data shown is represented as Mean \pm Standard Deviation (SD), n=5 at least. Statistical analysis performed using One-way ANOVA). Formulation 1-[CHT/HA/CHT/HA]₇₅; Formulation 2-[CHT/HA-DN/CHT/HA-DN]₇₅; Formulation 3: [CHT/HA/CHT/Ag-BG-NPs]₇₅; Formulation 4: [CHT/HA-DN/CHT/Ag-BG-NPs]₇₅.

In fact, the free-standing films have three different end-layers, namely HA, HA-DN and Ag-BG-NPs. It can be seen, through analysis of Figure 5.8-B, that the higher lap-shear adhesion strength was obtained for formulation 2: [CHT/HA-DN/CHT/HA-DN]₇₅, which has HA-DN, when compared with the control, i.e. formulation 1: [CHT/HA/CHT/HA]₇₅. In previous works of our group, it was studied the adhesion behavior of coatings with and without HA-DN [8], the same biopolymers with ternary bioglass nanoparticles [33] and more recently, CHT, HA, HA-DN and Ag-BG-NPs [32]. Neto and co-workers [8] showed that the adhesive strength for films with HA-DN was higher when compared with the control one. Furthermore, the same author showed that the adhesive strength increased for films with higher concentrations of catechol groups, and the coatings made with CHT/HA-DN present higher adhesive strength than the control ones (CHT/HA). It was found that the adhesive force increased as the number of bi-layers increased also [54]. Coatings containing BG-NPs and HA-DN, presented higher adhesive strength, unlike the

control group [33]. Although the adhesive strength is lower for coatings with BG-NPs when comparing to the control ones (the same thing happens comparing the results for formulations 2 versus 4), the presence of HA-DN allows better results comparing with the control ones [33, 37]. Comparing the results for formulation 3: [CHT/HA-DN/CHT/Ag-BG-NPs]₇₅ and formulation 4: [CHT/HA-DN/CHT/Ag-BG-NPs]₇₅, there was no statistical difference between them, which wasn't expected [37]. In fact, formulation 3 presented in its constitution HA and formulation 4 HA-DN and both presented Ag-BG-NPs in the end-layer. Comparing these results with a recent work of our group [37], it can be seen that the results present the same order of magnitude (kPa), but are higher than the previous work. Moreover, films with HA-DN presented higher adhesive strength, unlike the control formulation, which is according with the Rodrigues and co-workers' [37] findings.

5.5.5. Bioactivity tests

In order to investigate if the developed free-standing films present a bioactive character they were immersed in SBF during 14 days, shown in Figure 5.9.

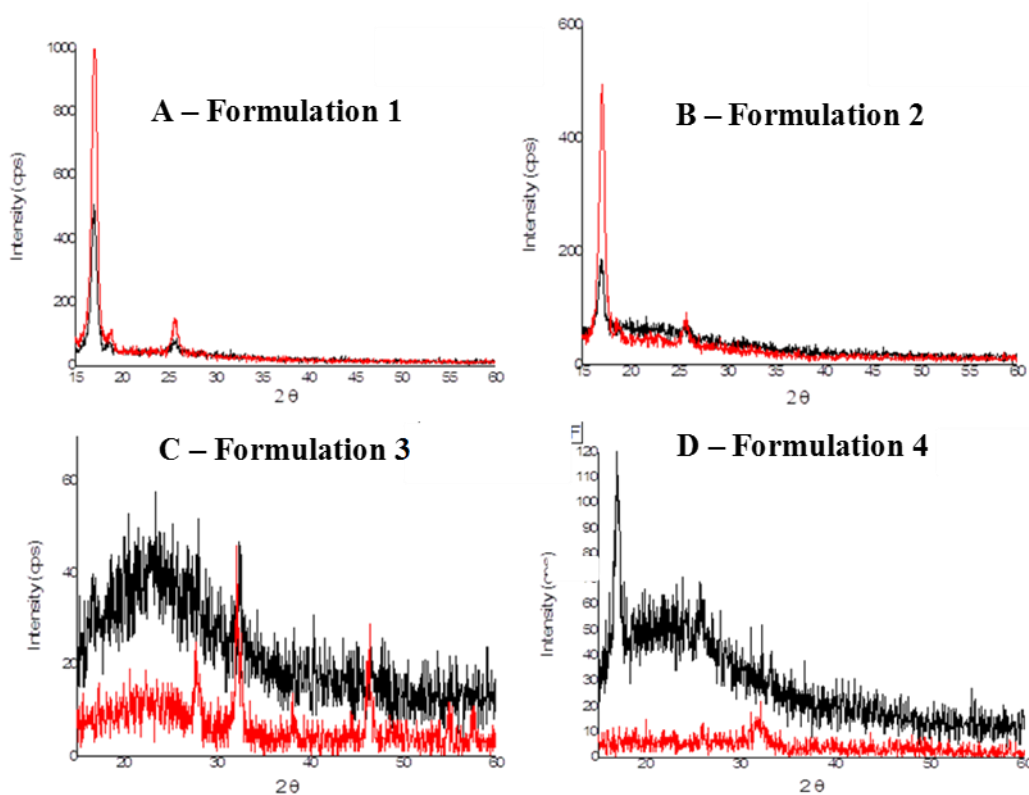


Figure 5. 9- XRD diffractograms. The black line corresponds to the XRD pattern before immersion in SBF solution (0 days) and the red line corresponds to the XRD pattern after immersion in SBF solution during 14 days.

Chapter 5. Antibacterial Natural-Based Free-Standing Films Inspired by the Sea

Through the analysis of Figure 5.9, we can see four different X-ray diffraction patterns that correspond to the four different formulations of free-standing films with and without immersion in SBF solution. The results showed that after immersion in SBF, for formulation 1 and 2, there was no formation of hydroxyapatite on its surface, as expected [55]. However, for formulation 3 and 4 (0 days- Figure 5.9-A and B) the samples correspond to an amorphous material, because they contained no long-range order. Moreover, we observed in the two X-ray patterns a characteristic halo of the amorphous materials in the 2θ region from 15 to 35° . For the samples immersed during 14 days (Figure 5.9-C and D) crystalline peaks appeared, $2\theta=15^\circ$ to 35° , there are identified as hydroxyapatite ($\text{Ca}_5(\text{PO}_4)_3(\text{OH})$, Hexagonal, pattern: 01-089-4405). The strongest line is present at $2\theta = 31.7^\circ$. These results are similar to other works developed in our group [32, 33] and demonstrate the capacity of these free-standing films, incorporated with Ag-BG-NPs to induce the creation of a hydroxyapatite layer on its surface. SEM micrographs, shown in Figure 5.10, corroborated this bioactive character.

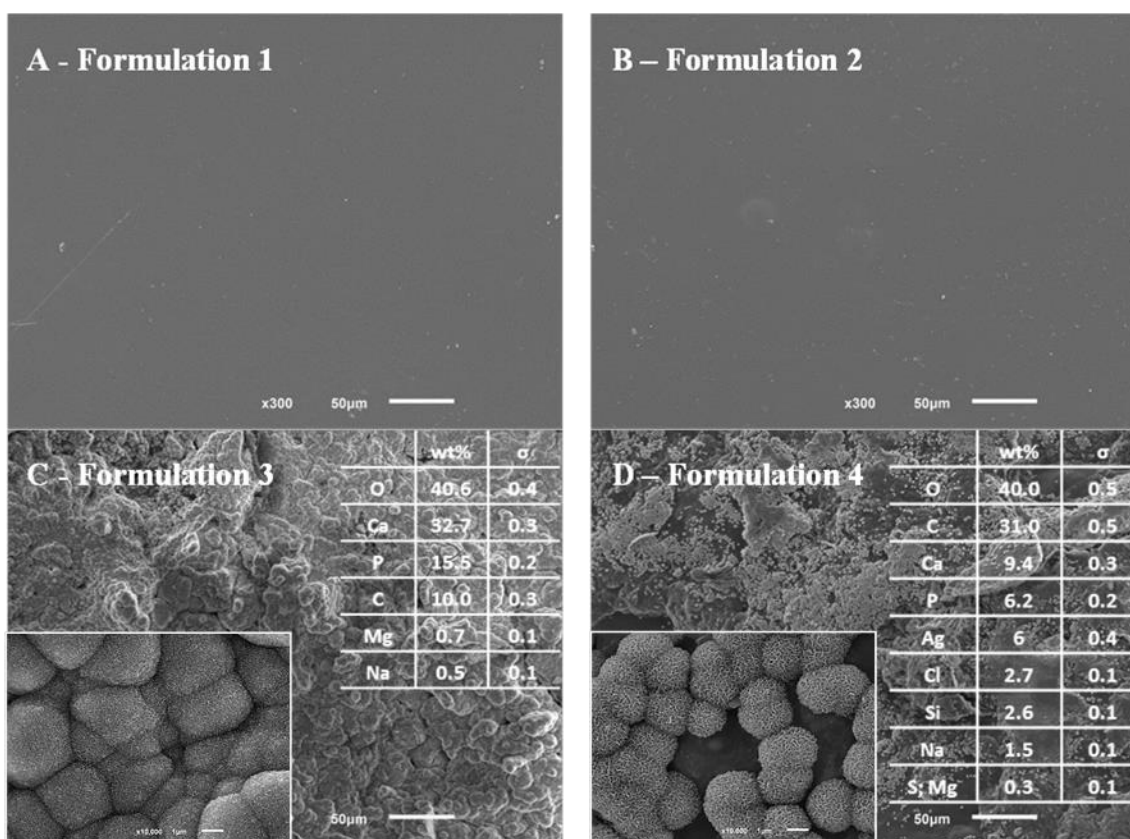


Figure 5. 10 - SEM-EDS micrographs of the surface morphology of the free-standing films after, 14 days, of immersion in SBF solution.

Through the analysis of Figure 5.10, we can see that after 14 days there is the formation of a calcium phosphate (Ca-P) layer on its surface, which corroborates the XRD pattern

shown in Figure 5.9 and demonstrate the bioactive character of this multilayer films, for formulations 3 and 4 and there is no Ca-P layer for formulations 1 and 2 (Figures 5.10 – A and B), as was expected [55]. The EDS spectra showed the presence of carbon (C), oxygen (O), sodium (Na) and chloride (Cl) due to the presence of washing solutions in the washing steps during the LbL assembly creation. Moreover, high amounts of calcium (Ca) and phosphorous (P) due to the formation of a calcium-phosphate layer (Ca-P) for formulations 3 and 4 – see Figures 5.10 – C and D and insets, and a decreased of silicon (Si), due to the dissolution of Ag-BG-NPs. These results are in agreement with a previous work [32].

5.5.6. Water contact angle measurements of the crosslinked free-standing films

The water contact angle (WCA) analysis, shown in Figure 5.11, is used to measure the hydrophobicity or hydrophilicity of materials.

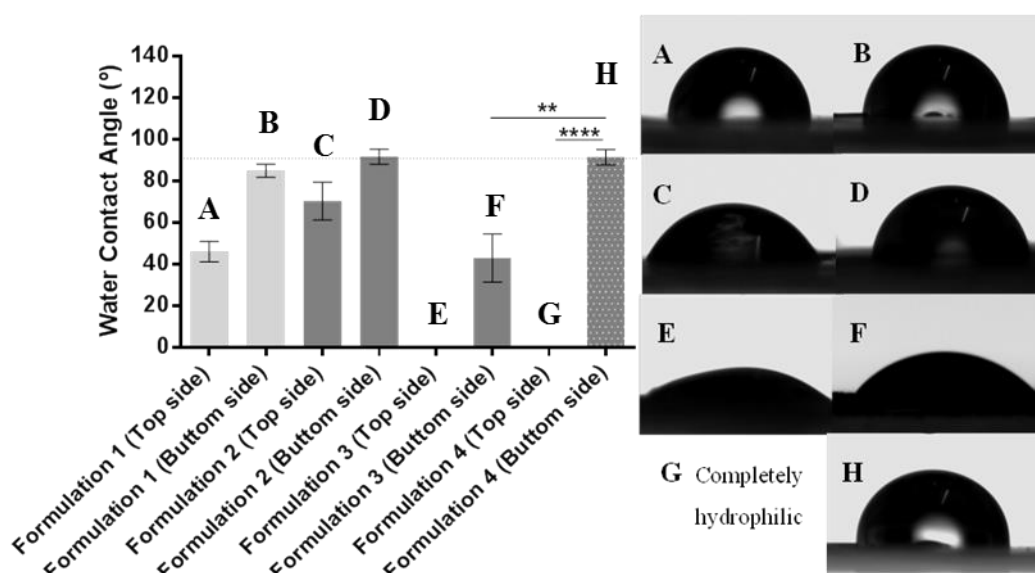


Figure 5. 11 - Water contact angle analysis of the free-standing films, top and bottom side. The top side corresponds to the hyaluronic acid (HA), hyaluronic acid dopamine conjugate (HA-DN) or silver doped bioglass nanoparticles (Ag-BG-NPs) and the bottom side corresponds to the layer composed by chitosan (CHT). Formulation 1: [CHT/HA/CHT/HA]₇₅; Formulation 2: [CHT/HA-DN/CHT/HA-DN]₇₅; Formulation 3: [CHT/HA/CHT/Ag-BG-NPs]₇₅ and Formulation 4: [CHT/HA-DN/CHT/Ag-BG-NPs]₇₅. The data is presented as Mean ± SD (non-parametric tests, Kruskal-Wallis test, p-value < 0,0001 [****]).

Hydrophilic materials imply smaller water contact angles, i.e., angles below 90°. On the other hand, hydrophobic materials present contact angles higher than 90° [56]. Overall, we observed that the contact angle values were higher for the side of the films that was in contact with the substrate, poly(propylene) and smaller for the top side of the film. In this case, the obtained results were for formulation 1, top side, 44.36° ± 4.629°, and for formulation 2, top side, 64.98° ± 3.389°. According to Neto and co-workers [8], the values

of WCA for [CHT/HA]₁₀ and [CHT/HA-DN]₁₀ were 77.36°±1.44° and 73.34°±1.82°, respectively. These two results are lower than the ones obtained in previous works [8,54], and could be justified by the crosslinking process that reduces the WCA values [54]. CHT, bottom side, presents hydrophobicity, i.e., has WCA above 90° [34]. The obtained results are overall near or above 90°, except for formulation 3, which had a WCA equal to 51.60° ± 9.327°. As far as the top sides of formulations 3 and 4 are concerned, the obtained values revealed that the surfaces are hydrophilic and for formulation 4 it is completely hydrophilic (WCA = 0°). The probable explanation for the difference between the WCA values for the top sides of formulations 3 and 4 is the higher concentration of Ag-BG-NPs on the surface of the last one which implies a decrease in WCA value. Roohani-Esfahani and co-workers [57] developed a nanocomposite made by biphasic calcium phosphates, poly-ε-caprolactone and bioactive glass nanoparticles. Pure PCL showed a WCA value of 109.2° that became more hydrophilic with the addition of bioglass nanoparticles (WCA decreased to 54.7°) [57]. In fact, overall WCA values decreased with the presence of bioglass nanoparticles, which are coincident with Roohani-Esfahani and co-workers' results.

5.4.3.7. Swelling behavior

The wettability were assessed by swelling analysis at $t = 0, 5 \text{ min}, 15 \text{ min}, 30 \text{ min}$ and 1 h to 7 h , shown in Figure 5.12.

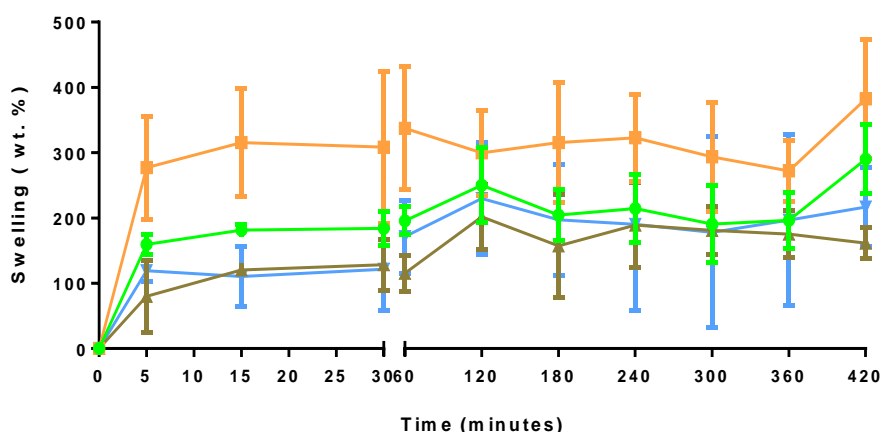


Figure 5. 12 - Swelling behavior of free-standing films when immersed in phosphate buffered saline (PBS) solution during different time-points. Formulation 1: [CHT/HA/CHT/HA]₇₅ (green line); Formulation 2: [CHT/HA-DN/CHT/HA-DN]₇₅ (orange line); Formulation 3: [CHT/HA/CHT/Ag-BG NPs]₇₅ (dark yellow line) and Formulation 4: [CHT/HA-DN/CHT/Ag-BG-NPs]₇₅ (blue line). The data is presented as Mean ± SD, n = 3.

The films swelled rapidly in the first 5 min and then stabilized reaching the equilibrium ($t = 30 \text{ min}$). This result is according to Kim and co-workers' [58] results. Formulations

1 and 2 swelled around 150 to 300%, but formulation 3 and 4, with the addition of Ag-BG-NPs, showed a swelling lower than the control ones, around 100 to 150%. The free-standing films crosslinked with genipin present lower swelling values than the uncrosslinked ones [34, 59], because the incorporation of a crosslinker reduces the intermolecular space between the polyelectrolyte chains [34]. One possible reason to explain the lower swelling percentage of formulations with addition of nanoparticles is that with the addition of nanoparticles the space between the polyelectrolyte chains is lower than the controls ones, implying lower available space to the water presence.

5.5.7. Weight Loss (WL)

In order to determine the applicability of free-standing films for biomedical applications it is crucial to perform longer degradation studies, in order to analyze the stability and integrity of films along the time [60]. For that reason the degradation tests were performed during 28 days at 37°C, Figure 5.13, by immersion of films in a PBS solution, since it simulates the saline environment of the human body [60].

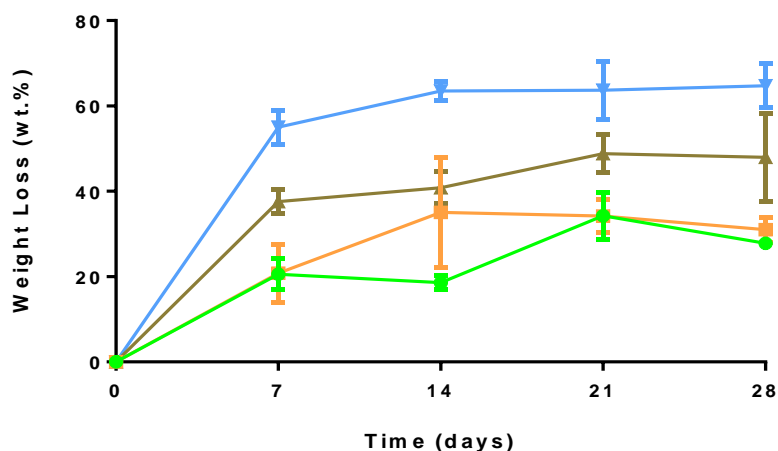


Figure 5. 13 - Weight loss behavior of free-standing films when immersed in PBS solution during different time-points at T=37°C. Formulation 1: [CHT/HA/CHT/HA]₇₅ (green line); Formulation 2: [CHT/HA-DN/CHT/HA-DN]₇₅ (orange line); Formulation 3: [CHT/HA/CHT/Ag-BG-NPs]₇₅ (dark yellow line) and Formulation 4: [CHT/HA-DN/CHT/Ag-BG-NPs]₇₅ (blue line). The data is presented as Mean ± SD, n = 3.

There was an increase of weight loss for all formulation until day 14 (except for formulation 1) and this is when it stabilizes reaching the equilibrium. Moreover, we can see that the formulations containing Ag-BG-NPs presented higher weigh loss rates, when compared with the control ones. Goh and co-workers [46] studied the change of pH over time for different formulations of bioglass nanoparticles immersed in PBS solution. The results showed a pH increase over time. This pH increase is due to the Ca²⁺ ions released with H⁺ ions present in the PBS solution. Probably, this high pH and the silver ions (Ag⁺)

released to the PBS solution are probably at fault for the acceleration of the degradation behavior for formulations 3 and 4.

5.5.8. Microbiological analysis

Finally, the antimicrobial vulnerability of the produced films was investigated. The results are present in Figure 5.14.

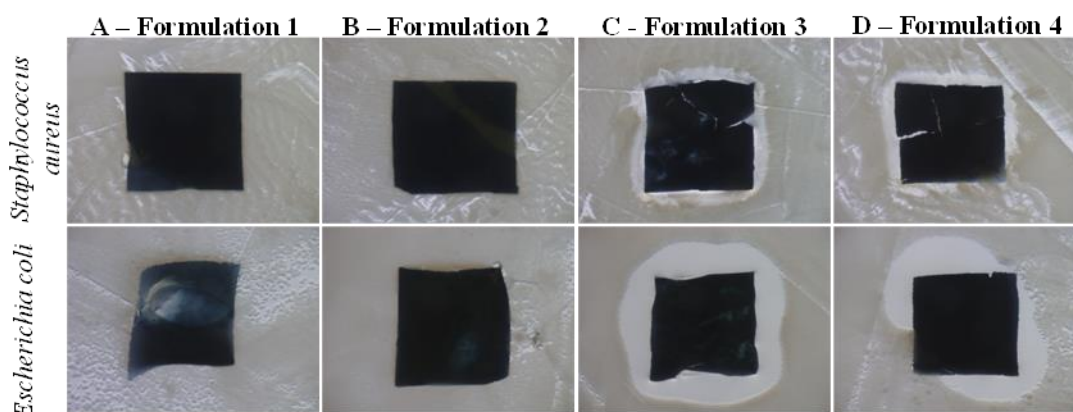


Figure 5. 14 - Photograph of free-standing films after 16 hours after being placed on top of a Mueller-Hinton agar plate with gram-negative *E. coli* and gram-positive *S. aureus* (1.5×10^8 CFU) incubated at 37 °C. The antimicrobial behavior of the LbL coatings is demonstrated by the formation of an inhibitory zone surrounding of Formulation 3: [CHT/HA/CHT/AgBG-NPs]₇₅ and Formulation 4: [CHT/HA-DN/CHT/AgBG-NPs]₇₅.

When the bioglass nanoparticles are immersed in PBS solution there is an increase of the pH over time [46]. According to the same author, the antibacterial performance of Ag-BG-NPs is due to the pH increase. Furthermore, silver doped bioglass nanoparticles obtained through the sol-gel methodology showed excellent antibacterial results [46]. Comparing silver doped bioglass nanoparticles with copper (Cu) doped bioglass nanoparticles, the first ones showed quick ions release for the medium, proving to be a faster bacteria-killing agent [46]. The antibacterial performance of silver doped bioglass nanoparticles is due to the silver ions released to the medium [61]. Silver ions react with bacterial nucleophilic amino acid residues present in proteins [61], inhibiting the bacterial cell wall creation, DNA and RNA synthesis [61], causing protein denaturation [61] and promoting the metabolic pathway disorder [46]. Bellantone and co-workers [62], produced SiO₂-CaO-P₂O₅ with 3% of Ag₂O and the results showed that silver doped bioglass nanoparticles had a bacteriostatic effect in liquid culture medium and PBS solution, whereas bioglass-free Ag₂O didn't show such effect. In a previous work of our group [32], an antibacterial performance for coatings with Ag-BG-NPs was also detected. The inhibition zone is not regular possibly because the sample is not flat and not placed right on the agar plate. However, in Figures 5.14-C and D there is a clear inhibition zone

surrounding the formulation 3 and 4 (with Ag-BG-NPs), whereas for formulation 1 and 2, Figure 5.14 A and B, there is no inhibition zone.

5.6. Conclusions

Four different LbL free-standing films based on CHT, HA, HA-DN and Ag-BG-NPs were successfully developed. In fact, handleable films were created. The incorporation of Ag-BG-NPs induced the formation of a calcium-phosphate layer on its surface. Furthermore, adhesion tests revealed that the presence of catechol groups led to an increase of adhesion strength, as it can be seen for formulation 2: [CHT/HA-DN/CHT/HA-DN]₇₅ versus formulation 1: [CHT/HA/CHT/HA]₇₅ as well as for formulation 4: [CHT/HA-DN/CHT/AgBGNPs]₇₅ versus formulation 3: [CHT/HA/CHT/AgBGNPs]₇₅ because it presents a higher lap shear adhesive strength value. Microbiological studies were performed and revealed that formulations which contain silver doped nanoparticles showed an antibacterial performance. Besides their ability to induce hydroxyapatite on its surface, after immersion in SBF solution during 14 days, they presented an effective antibacterial activity against *E. coli* and *S. aureus* bacteria after 16 hours. Based on the results, formulation 4: [CHT/HA-DN/CHT/AgBGNPs]₇₅ revealed to be the best configuration, because it combines three relevant functionalities, bioactivity, adhesive and antibacterial properties which could be useful to the orthopedic or dental area.

Acknowledgements:

The authors acknowledge the Portuguese Foundation for Science and Technology (FCT) and the European program FEDER/COMPETE for the financial support through project LA ICVS/3Bs - 2015-2017.

5.7. References:

- [1] P. Podsiadlo, Z. Q. Liu, D. Paterson, P. B. Messersmith, and N. A. Kotov, "Fusion of seashell nacre and marine bioadhesive analogs: High-strength nanocomposite by layer-by-layer assembly of clay and L-3,4-dihydroxyphenylalanine polymer," (in English), *Advanced Materials*, Article vol. 19, no. 7, pp. 949-+, Apr 2007.
- [2] H. Lee, N. F. Scherer, and P. B. Messersmith, "Single-molecule mechanics of mussel adhesion," (in English), *Proceedings of the National Academy of Sciences of the United States of America*, Article vol. 103, no. 35, pp. 12999-13003, Aug 2006.
- [3] H. G. Silverman and F. F. Roberto, "Understanding marine mussel adhesion," (in English), *Marine Biotechnology*, Review vol. 9, no. 6, pp. 661-681, Dec 2007.

Chapter 5. Antibacterial Natural-Based Free-Standing Films Inspired by the Sea

- [4] S. K. Madhurakkat Perikamana et al., "Materials from Mussel-Inspired Chemistry for Cell and Tissue Engineering Applications," *Biomacromolecules*, vol. 16, no. 9, pp. 2541-55, 2015-Sep-14 2015.
- [5] Y. C. Choi, J. S. Choi, Y. J. Jung, and Y. W. Cho, "Human gelatin tissue-adhesive hydrogels prepared by enzyme-mediated biosynthesis of DOPA and Fe³⁺ ion crosslinking," (in English), *Journal of Materials Chemistry B*, Article vol. 2, no. 2, pp. 201-209, 2014.
- [6] M. Cencer, Y. Liu, A. Winter, M. Murley, H. Meng, and B. P. Lee, "Effect of pH on the Rate of Curing and Bioadhesive Properties of Dopamine Functionalized Poly(ethylene glycol) Hydrogels," (in English), *Biomacromolecules*, Article vol. 15, no. 8, pp. 2861-2869, Aug 2014.
- [7] Y. Lee et al., "Thermo-sensitive, injectable, and tissue adhesive sol-gel transition hyaluronic acid/pluronic composite hydrogels prepared from bio-inspired catechol-thiol reaction," (in English), *Soft Matter*, Article vol. 6, no. 5, pp. 977-983, 2010.
- [8] A. I. Neto et al., "Nanostructured Polymeric Coatings Based on Chitosan and Dopamine-Modified Hyaluronic Acid for Biomedical Applications," (in English), *Small*, Article vol. 10, no. 12, pp. 2459-2469, Jun 2014.
- [9] J. J. Wilker, "The Iron-Fortified Adhesive System of Marine Mussels," (in English), *Angewandte Chemie-International Edition*, Editorial Material vol. 49, no. 44, pp. 8076-8078, 2010.
- [10] S. A. Burke, M. Ritter-Jones, B. P. Lee, and P. B. Messersmith, "Thermal gelation and tissue adhesion of biomimetic hydrogels," (in English), *Biomedical Materials*, Article vol. 2, no. 4, pp. 203-210, Dec 2007.
- [11] N. M. Alves and J. F. Mano, "Chitosan derivatives obtained by chemical modifications for biomedical and environmental applications," (in English), *International Journal of Biological Macromolecules*, Review vol. 43, no. 5, pp. 401-414, Dec 2008.
- [12] M. Rinaudo, "Chitin and chitosan: Properties and applications," (in English), *Progress in Polymer Science*, Review vol. 31, no. 7, pp. 603-632, Jul 2006.
- [13] D. S. Couto, Z. K. Hong, and J. F. Mano, "Development of bioactive and biodegradable chitosan-based injectable systems containing bioactive glass nanoparticles," (in English), *Acta Biomaterialia*, Article vol. 5, no. 1, pp. 115-123, Jan 2009.
- [14] C. Shi, Y. Zhu, X. Ran, M. Wang, Y. Su, and T. Cheng, "Therapeutic Potential of Chitosan and Its Derivatives in Regenerative Medicine1," *Journal of Surgical Research*, vol. 133, no. 2, pp. 185-192, 6/15/ 2006.
- [15] M. Dash, F. Chiellini, R. M. Ottenbrite, and E. Chiellini, "Chitosan-A versatile semi-synthetic polymer in biomedical applications," *Progress in Polymer Science*, vol. 36, no. 8, pp. 981-1014, Aug 2011.
- [16] M. Morra, "Engineering of biomaterials surfaces by hyaluronan," (in English), *Biomacromolecules*, Review vol. 6, no. 3, pp. 1205-1223, May-Jun 2005.
- [17] P. Kujawa, P. Moraille, J. Sanchez, A. Badia, and F. M. Winnik, "Effect of molecular weight on the exponential growth and morphology of hyaluronan/chitosan multilayers: A surface plasmon resonance spectroscopy and

- atomic force microscopy investigation," (in English), *Journal of the American Chemical Society*, Article vol. 127, no. 25, pp. 9224-9234, Jun 2005.
- [18] J. F. Mano et al., "Natural origin biodegradable systems in tissue engineering and regenerative medicine: present status and some moving trends," (in English), *Journal of the Royal Society Interface*, Review vol. 4, no. 17, pp. 999-1030, Dec 2007.
- [19] J. R. E. Fraser, T. C. Laurent, and U. B. G. Laurent, "Hyaluronan: Its nature, distribution, functions and turnover," (in English), *Journal of Internal Medicine*, Article vol. 242, no. 1, pp. 27-33, Jul 1997.
- [20] W. G. Pitt, R. N. Morris, M. L. Mason, M. W. Hall, Y. Luo, and G. D. Prestwich, "Attachment of hyaluronan to metallic surfaces," (in English), *Journal of Biomedical Materials Research Part A*, Article vol. 68A, no. 1, pp. 95-106, Jan 2004.
- [21] J. M. Silva, A. R. C. Duarte, S. G. Caridade, C. Picart, R. L. Reis, and J. F. Mano, "Tailored Freestanding Multi layered Membranes Based on Chitosan and Alginate," (in English), *Biomacromolecules*, Article vol. 15, no. 10, pp. 3817-3826, Oct 2014.
- [22] G. V. Martins, J. F. Mano, and N. M. Alves, "Nanostructured self-assembled films containing chitosan fabricated at neutral pH," (in English), *Carbohydrate Polymers*, Article vol. 80, no. 2, pp. 570-573, Apr 2010.
- [23] J. Borges and J. F. Mano, "Molecular Interactions Driving the Layer-by-Layer Assembly of Multilayers," (in English), *Chemical Reviews*, Review vol. 114, no. 18, pp. 8883-8942, Sep 2014.
- [24] P. T. Hammond, "Engineering Materials Layer-by-Layer: Challenges and Opportunities in Multilayer Assembly," (in English), *Aiche Journal*, Editorial Material vol. 57, no. 11, pp. 2928-2940, Nov 2011.
- [25] L. Han et al., "Mussel-inspired adhesive and transferable free-standing films by self-assembling dexamethasone encapsulated BSA nanoparticles and vancomycin immobilized oxidized alginate," (in English), *Colloids and Surfaces B-Biointerfaces*, Article vol. 126, pp. 452-458, Feb 2015.
- [26] M. Kohri et al., "Facile Synthesis of Free-Standing Polymer Brush Films Based on a Colorless Polydopamine Thin Layer," (in English), *Macromolecular Rapid Communications*, Article vol. 34, no. 15, pp. 1220-1224, Aug 2013.
- [27] S. G. Caridade, C. Monge, F. Gilde, T. Boudou, J. F. Mano, and C. Picart, "Free-Standing Polyelectrolyte Membranes Made of Chitosan and Alginate," (in English), *Biomacromolecules*, Article vol. 14, no. 5, pp. 1653-1660, May 2013.
- [28] A. L. Larkin, R. M. Davis, and P. Rajagopalan, "Biocompatible, Detachable, and Free-Standing Polyelectrolyte Multilayer Films," (in English), *Biomacromolecules*, Article vol. 11, no. 10, pp. 2788-2796, Oct 2010.
- [29] S. G. Caridade et al., "Myoconductive and osteoinductive free-standing polysaccharide membranes," *Acta Biomaterialia*, vol. 15, pp. 139-149, 3/15/2015.
- [30] X. M. Zhang, Z. Y. Li, X. B. Yuan, Z. D. Cui, and X. J. Yang, "Fabrication of dopamine-modified hyaluronic acid/chitosan multilayers on titanium alloy by

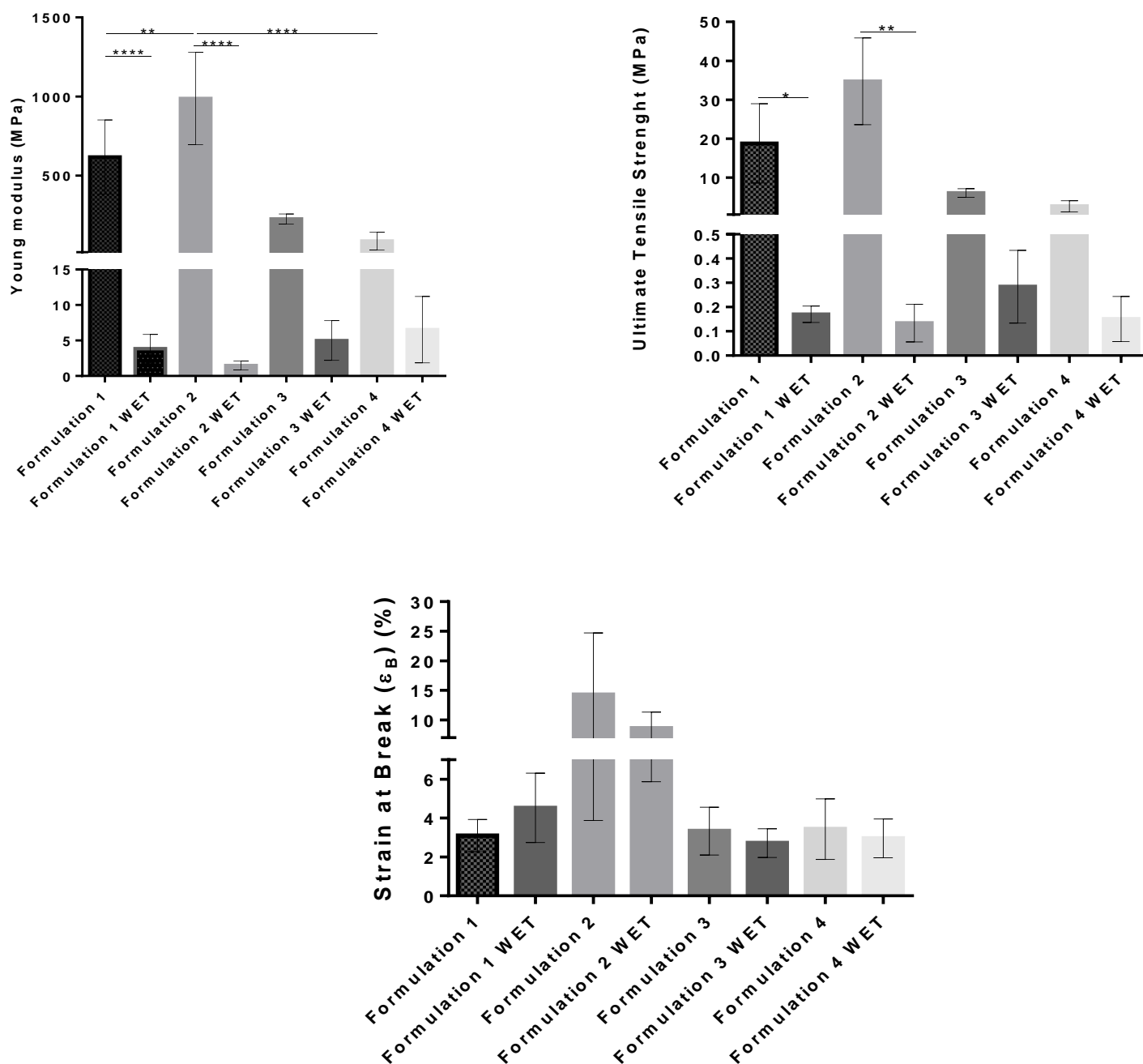
- layer-by-layer self-assembly for promoting osteoblast growth," (in English), *Applied Surface Science*, Article vol. 284, pp. 732-737, Nov 2013.
- [31] A. Vulpoi, L. Baia, S. Simon, and V. Simon, "Silver effect on the structure of SiO₂-CaO-P₂O₅ ternary system," (in English), *Materials Science & Engineering C-Materials for Biological Applications*, Article vol. 32, no. 2, pp. 178-183, Mar 2012.
- [32] A. L. Carvalho et al., "Antibacterial bioadhesive layer-by-layer coatings for orthopedic applications," *Journal of Materials Chemistry B*, 10.1039/C6TB00841K 2016.
- [33] S. J. Rego, A. C. Vale, G. M. Luz, J. F. Mano, and N. M. Alves, "Adhesive Bioactive Coatings Inspired by Sea Life," (in English), *Langmuir*, Article vol. 32, no. 2, pp. 560-568, Jan 2016.
- [34] J. M. Silva, S. G. Caridade, N. M. Oliveira, R. L. Reis, and J. F. Mano, "Chitosan-alginate multilayered films with gradients of physicochemical cues," *Journal of Materials Chemistry B*, vol. 3, no. 22, pp. 4555-4568, 2015 2015.
- [35] A. Oyane, H. M. Kim, T. Furuya, T. Kokubo, T. Miyazaki, and T. Nakamura, "Preparation and assessment of revised simulated body fluids," *Journal of Biomedical Materials Research Part A*, vol. 65A, no. 2, pp. 188-195, May 1 2003.
- [36] A. Oyane, K. Onuma, A. Ito, H. M. Kim, T. Kokubo, and T. Nakamura, "Formation and growth of clusters in conventional and new kinds of simulated body fluids," *Journal of Biomedical Materials Research Part A*, vol. 64A, no. 2, pp. 339-348, Feb 1 2003.
- [37] J. R. Rodrigues, N. M. Alves, and J. F. Mano, "Biomimetic polysaccharide/bioactive glass nanoparticles multilayer membranes for guided tissue regeneration," *Rsc Advances*, vol. 6, no. 79, pp. 75988-75999, 2016.
- [38] M. Mekhail, K. Jahan, and M. Tabrizian, "Genipin-crosslinked chitosan/poly-L-lysine gels promote fibroblast adhesion and proliferation," *Carbohydrate Polymers*, vol. 108, pp. 91-98, 8/8/ 2014.
- [39] A. L. Hillberg, C. A. Holmes, and M. Tabrizian, "Effect of genipin cross-linking on the cellular adhesion properties of layer-by-layer assembled polyelectrolyte films," *Biomaterials*, vol. 30, no. 27, pp. 4463-4470, 9// 2009.
- [40] L. Cui, J. Jia, Y. Guo, Y. Liu, and P. Zhu, "Preparation and characterization of IPN hydrogels composed of chitosan and gelatin cross-linked by genipin," *Carbohydrate Polymers*, vol. 99, pp. 31-38, 1/2/ 2014.
- [41] S. Gorgieva and V. Kokol, "Preparation, characterization, and in vitro enzymatic degradation of chitosan-gelatin hydrogel scaffolds as potential biomaterials," *Journal of Biomedical Materials Research Part A*, vol. 100A, no. 7, pp. 1655-1667, Jul 2012.
- [42] M. L. Duarte, M. C. Ferreira, M. R. Marvao, and J. Rocha, "An optimised method to determine the degree of acetylation of chitin and chitosan by FTIR spectroscopy," (in English), *International Journal of Biological Macromolecules*, Article vol. 31, no. 1-3, pp. 1-8, Dec 2002, Art. no. Pii s0141-8130(02)00039-9.
- [43] U. Manna, S. Bharani, and S. Patil, "Layer-by-Layer Self-Assembly of Modified Hyaluronic Acid/Chitosan Based on Hydrogen Bonding," *Biomacromolecules*, vol. 10, no. 9, pp. 2632-2639, Sep 2009.

- [44] S. Hong et al., "Hyaluronic Acid Catechol: A Biopolymer Exhibiting a pH-Dependent Adhesive or Cohesive Property for Human Neural Stem Cell Engineering," (in English), *Advanced Functional Materials*, Article vol. 23, no. 14, pp. 1774-1780, Apr 2013.
- [45] Z. K. Hong et al., "Mono-dispersed bioactive glass nanospheres: Preparation and effects on biomechanics of mammalian cells," (in English), *Journal of Biomedical Materials Research Part A*, Article vol. 95A, no. 3, pp. 747-754, Dec 2010.
- [46] Y.-F. Goh, A. Z. Alshemary, M. Akram, M. R. A. Kadir, and R. Hussain, "Bioactive Glass: An In-Vitro Comparative Study of Doping with Nanoscale Copper and Silver Particles," *International Journal of Applied Glass Science*, vol. 5, no. 3, pp. 255-266, Sep 2014.
- [47] A. M. El-Kady, A. F. Ali, R. A. Rizk, and M. M. Ahmed, "Synthesis, characterization and microbiological response of silver doped bioactive glass nanoparticles," (in English), *Ceramics International*, Article vol. 38, no. 1, pp. 177-188, Jan 2012.
- [48] A. Vulpoi et al., "Bioactivity and protein attachment onto bioactive glasses containing silver nanoparticles," *Journal of Biomedical Materials Research Part A*, vol. 100A, no. 5, pp. 1179-1186, May 2012.
- [49] C. Chaubaroux et al., "Collagen-Based Fibrillar Multilayer Films Cross-Linked by a Natural Agent," *Biomacromolecules*, vol. 13, no. 7, pp. 2128-2135, Jul 2012.
- [50] T. Nardo, V. Chiono, G. Ciardelli, and M. Tabrizian, "PolyDOPA Mussel-Inspired Coating as a Means for Hydroxyapatite Entrapment on Polytetrafluoroethylene Surface for Application in Periodontal Diseases," (in English), *Macromolecular Bioscience*, Article vol. 16, no. 2, pp. 288-298, Feb 2016.
- [51] S. B. Lee, Y. M. Lee, K. W. Song, and M. H. Park, "Preparation and properties of polyelectrolyte complex sponges composed of hyaluronic acid and chitosan and their biological behaviors," *Journal of Applied Polymer Science*, vol. 90, no. 4, pp. 925-932, Oct 24 2003.
- [52] M. N. Rodrigues, M. B. Oliveira, R. R. Costa, and J. F. Mano, "Chitosan/Chondroitin Sulfate Membranes Produced by Polyelectrolyte Complexation for Cartilage Engineering," (in English), *Biomacromolecules*, Article vol. 17, no. 6, pp. 2178-2188, Jun 2016.
- [53] J. Mota et al., "Chitosan/bioactive glass nanoparticle composite membranes for periodontal regeneration," (in English), *Acta Biomaterialia*, Article vol. 8, no. 11, pp. 4173-4180, Nov 2012.
- [54] A. I. Neto, N. L. Vasconcelos, S. M. Oliveira, D. Ruiz-Molina, and J. F. Mano, "High-Throughput Topographic, Mechanical, and Biological Screening of Multilayer Films Containing Mussel-Inspired Biopolymers," *Advanced Functional Materials*, vol. 26, no. 16, pp. 2745-2755, Apr 2016.
- [55] N. M. Alves, I. B. Leonor, H. S. Azevedo, R. L. Reis, and J. F. Mano, "Designing biomaterials based on biomineralization of bone," (in English), *Journal of Materials Chemistry*, Article vol. 20, no. 15, pp. 2911-2921, 2010.
- [56] Y. L. Cui et al., "Biomimetic surface modification of poly(l-lactic acid) with chitosan and its effects on articular chondrocytes in vitro," *Biomaterials*, vol. 24, no. 21, pp. 3859-3868, 9// 2003.

Chapter 5. Antibacterial Natural-Based Free-Standing Films Inspired by the Sea

- [57] S. I. Roohani-Esfahani, S. Nouri-Khorasani, Z. F. Lu, R. C. Appleyard, and H. Zreiqat, "Effects of bioactive glass nanoparticles on the mechanical and biological behavior of composite coated scaffolds," *Acta Biomaterialia*, vol. 7, no. 3, pp. 1307-1318, 3// 2011.
- [58] S. J. Kim, S. R. Shin, K. B. Lee, Y. D. Park, and S. I. Kim, "Synthesis and characteristics of polyelectrolyte complexes composed of chitosan and hyaluronic acid," *Journal of Applied Polymer Science*, vol. 91, no. 5, pp. 2908-2913, Mar 2004.
- [59] J. M. Silva, S. G. Caridade, R. L. Reis, and J. F. Mano, "Polysaccharide-based freestanding multilayered membranes exhibiting reversible switchable properties," *Soft Matter*, vol. 12, no. 4, pp. 1200-1209, 2016.
- [60] M. J. Cardoso, S. G. Caridade, R. R. Costa, and J. F. Mano, "Enzymatic Degradation of Polysaccharide-Based Layer-by-Layer Structures," *Biomacromolecules*, vol. 17, no. 4, pp. 1347-1357, Apr 2016.
- [61] A. A. Ahmed, A. A. Ali, D. A. R. Mahmoud, and A. M. El-Fiqi, "Study on the preparation and properties of silver-doped phosphate antibacterial glasses (Part I)," *Solid State Sciences*, vol. 13, no. 5, pp. 981-992, 5// 2011.
- [62] M. Bellantone, H. D. Williams, and L. L. Hench, "Broad-spectrum bactericidal activity of Ag₂O-doped bioactive glass," (in English), *Antimicrobial Agents and Chemotherapy*, Article vol. 46, no. 6, pp. 1940-1945, Jun 2002.

Supporting information (SI)



S 5. 1 - Comparison between (A) Tensile Young modulus (MPa) for the tensile tests performed in dry and wet conditions (n = 5, one-way ANOVA, p-value < 0.0001 [, ****]), (B) Ultimate tensile strength (MPa) for the tensile tests performed in dry and wet conditions (n = 5, non-parametric tests, Kruskal-Wallis statics, p-value < 0.0001, [****]) (C) Strain at break (%) for the tensile tests performed in dry and wet conditions (n = 5, non-parametric tests, Kruskal-Wallis statics).

CHAPTER 6

HYDROGELS

**DEVELOPMENT BASED ON NATURAL
POLYMERS AND INSPIRED BY THE SEA**

6. HYDROGELS DEVELOPMENT BASED ON NATURAL POLYMERS AND INSPIRED BY THE SEA

Abstract:

Hydrogels are used in the biomedical field. They have in their constitution high contents of water and they present a structure similar to the extracellular matrix (ECM) of the cells. However, their poor mechanical properties constitute a great disadvantage that limits their use. Hydrogels based on natural polymers, such as chitosan (CHT) with and without the addition of bioglass nanoparticles (BG-NPs), crosslinked with genipin were produced in this work. The results revealed that the addition of bioglass nanoparticles in the hydrogel network improved their mechanical properties as well as their capacity to dissipate energy.

Moreover, it was shown that it is possible to successfully modify chitosan with the adhesive catechol groups found in marine mussel adhesive proteins (MAPs).

Keywords: Chitosan, genipin, bioglass nanoparticles, chitosan-catechol conjugate, biomedical field.

6.1. Introduction

Hydrogels are used in biomedical applications [2], namely tissue engineering [8, 13], regenerative medicine [3, 10] and it is used in wound [13] drug [13], cells therapies [3], cancer researches [3] gene delivery systems [3] and separation of cells and biomolecules [10]. Furthermore, hydrogels have rubbery behavior comparable to tissues [2]. Their capability for these applications depends largely on their bulk structures. Some parameters are important to take into account to evaluate the structure network, namely the molecular weight between two crosslinked points, mesh size and the polymer volume fraction [1]. The first allows us to know the degree of crosslinking, the second, the distance between two crosslinked points and the last parameter allows us to know how much fluid is present in hydrogel [1] structure. Hydrogels are used for many reasons, namely because they are biocompatible [3-5], present versatility [3], flexibility [4], softness [4], chemical, biological and physical properties [3], high porosity [6] and have extracellular matrix (ECM) likeness [3, 7, 8]. Hydrogels are constituted by hydrophilic polymers [6]. Furthermore, they can swell in contact with body fluids or water [3, 7, 9-11] and they have a three-dimensional structure [3, 6, 7, 9-11].

To create a hydrogel, it is indispensable to crosslink it by physical and chemical way [3, 4]. For chemical crosslinking, chemical bonds are created [9], but for physical crosslinking there are chain interconnections [9], crystallite development [9] or secondary forces acting [9]. According to Yu and Ding [11], if covalent bonds are responsible for the three-dimensional gel structure it is called a chemical gel, whereas if physical associations were responsible for gel formation, the created gel is called a physical gel [11]. Furthermore, in the last crosslinking process, it is not necessary the use of monomers or initiators and their biocompatibility is ensured by the absence of these residues [11].

Changes in environmental factors can alter the swelling behavior of hydrogels [2], such as changes in pH [2, 3, 10, 11], ionic strength [2, 10], ionic interactions [3], ionic concentration [11], light exposure [3], electromagnetic radiation [2], salt [11], electric field action [11] and temperature [2, 3, 10, 11]. Furthermore, the swelling behavior is also changed by physicochemical interactions, namely hydrogen bonds [3, 10], proteins interactions [3], hydrophobic interactions [10], supramolecular chemistry [10], charge condensation [10] and stereocomplexion [10].

Hydrogels based on distinct materials have been proposed, for example, on cellulose [9], chitosan [3, 7, 9], heparin [3], collagen [3, 5, 7, 12], dextran [7, 9], gelatin [3, 9, 12], fibrin

[5, 7, 12], hyaluronic acid [3, 5, 7, 12], alginate [3, 5, 7, 12], elastin [3, 7], chondroitin sulfate [3] and agarose [5, 7, 12]. The main drawbacks of hydrogels are the poor mechanical properties, the incapacity to control its structure, degradation and the risk of presenting immunogenicity [3]. Hydrogels that respond to environmental stimulus are called responsive hydrogels [3]. Hydrogels can be neutral or ionic [2]. If the hydrogel is pH-dependent [2], in the presence of acidic or basic solutions, the swelling behavior of hydrogels is different. If the gel has acidic or basic groups, and if the pH of solution increases, the equilibrium degree of swelling also increases and if the pH decreases the swelling increases, respectively [3]. Also, hydrogels can be obtained by changing the temperature [6].

Marine mussels present specific proteins which can be used to stick/adhere in various substrates in wet and saline environment [14, 15]. These marine mussel adhesive proteins (MAPs) contain an unusual amino acid, known as 3, 4-dihydroxy-L-phenylalanine (DOPA) [15-24], which is used for adhesion to various substrates [15, 16, 18, 23-26]. According to Cencer and co-workers [15], catechol groups can form complexation bonds with metals, oxides and covalent bonds when it is oxidized [15], such as catechol oxidase enzymes (tyrosinase and periodate).

Hong and co-workers [27] proved that in alkaline conditions, hyaluronic acid-dopamine conjugate (HA-DN) shown cohesive properties useful for hydrogels formation [27]. Gels made by complexion with Fe^{3+} -DOPA and covalent bonds with DOPA-quinone were also reported in the literature [28]. To understand the adherence to tissues depending on the change of pH, Cencer [15] developed a hydrogel made of poly(ethylene glycol) (PEG) end-capped with dopamine and the results showed that the curing rate is affected by pH changes. A pH equal to 7.4 showed a good equilibrium with curing rate, mechanical and binder properties [15]. Lee and co-workers [29] developed a hydrogel with alginate conjugated with catechol groups. For the hydrogel production, the pH was adjusted to basic conditions and was used with sodium periodate as a crosslinker agent because the groups demonstrated cohesive properties with quinone formation. The results showed that this hydrogel demonstrated no cytotoxicity and low immunogenicity. Fullenkamp and co-workers [30] developed a hydrogel based on branched catechol-derivatized PEG and silver (Ag) ions. Silver ions allow hydrogel creation by crosslinking of catechol oxidation made by silver ions. Increasing the $[\text{Ag}^+]/[\text{catechol}]$ ratio there is a decreasing of gelation time and an increase of hydrogel rigidity. The addition of silver in bioglass nanoparticles allows a controlled release of antibacterial agents [30, 31]. Furthermore, it is possible, the

addition of bioglass nanoparticles in the hydrogel [32]. Bioglass nanoparticles are used due to its angiogenic properties, enhancing osteogenic cell differentiation and proliferation and bone-like apatite formation [33] after immersion in simulated body fluid (SBF). Furthermore, and according to Nardo and co-workers [34], bioactive glasses are used because it induces the creation of regenerative materials physicochemical similar to bone tissue. Moreover, and according to the same author [34], hydroxyapatite crystals have the same chemical composition than the mineral component of bone. Oliveira and co-workers [35] developed different formulations of hydrogels, using chitosan, ternary bioglass nanoparticles formulation and different concentrations of genipin. The results showed that the storage modulus of the hydrogel was mostly affected by chitosan concentration and secondly by incorporation of bioglass nanoparticles. Genipin also, revealed to have an impact in the storage modulus. Furthermore, in the presence of MC3T3-E1 pre-osteoblast, the results showed that the cell proliferation was better for formulation that contains 12.5% of bioglass nanoparticles, 2% (w/v) of chitosan and 2.5% (w/v) of genipin.

Herein, hydrogels based on natural polymers with and without addition of bioglass nanoparticles were produced. Regarding chitosan, it is a linear polysaccharide [1, 36] that it is constituted by glucosamine and N-acetyl glucosamine units linked by β -(1-4) glycosidic bonds [36] and has chemical composition similar to glycosaminoglycans (GAGs) [8]. As already mentioned, chitosan can be processed into hydrogels [37-40] and it is useful for many biomedical applications [1]. A ternary formulation of bioglass nanoparticles with a thermal treatment of 3 hours at 700°C obtained through the sol-gel methodology was chosen for the development of the nanoparticles-chitosan hybrid system. This thermal treatment was chosen because the same formulation was studied in previous works and this heat treatment allows the maximum of bioglass bioactivity character [42, 43]. Moreover, chitosan with catechol groups (CHT-c) was successfully synthesized. This modified chitosan will be combined in the future with the above mentioned nanoparticles in order to obtain a hydrogel with both enhanced mechanical and adhesive properties.

6.2. Experimental section

6.2.1. Methods

6.2.1.1. Synthesis of ternary bioglass nanoparticles (BG-NPs)

BG-NPs were prepared using the protocol present in [42], using the sol–gel method. This method is optimized to obtain the ternary system of BG ($\text{SiO}_2/\text{CaO}/\text{P}_2\text{O}_5$ (mol %) = 50:45:5). Briefly, to produce the solution A, at room temperature, 7.639 g of calcium nitrate tetrahydrate was dissolved in 120 mL of dissolved water. After that, 60 mL of ethanol absolute and 9.8353 mL of tetraethyl orthosilicate were added to the calcium nitrate solution. The pH was adjusted to 2 with a citric acid solution (30 mL, 10%), and the reaction was left to agitate for 3 h. For the solution B, 1.078 g of ammonium phosphate dibasic was dissolved in deionized water, and ammonium hydroxide solution was used to adjust the pH to 11.5. Then, solution A was added drop-by-drop to solution B. Ammonium hydroxide solution was used to maintain at 11.5. This mixture was left to dissolve under magnetic stirring during 48 h and then a resting period of 24 h followed. The precipitate was washed three times with distilled water and was stored for 24 h at the ultra-low freezer ($T = -80^\circ\text{C}$). The precipitate was subsequently freeze dried for 7 days. To the purpose of obtaining bioglass nanoparticles, the gel was calcinated at 700°C during 3 h.

6.2.1.2. Production of a poly(dimethylsiloxane) (PDMS) mold

In order to create a poly(dimethylsiloxane) (PDMS) mold, Sylgard(r) 184 silicone elastomer kit was purchased from Dow Corning (Seneffe, Belgium). The curing agent was added to the silicone in a proportion of 1:9. After mixing vigorously the resultant mixture was put into Petri dishes. Then, the samples were stored under vacuum for 30 minutes in order to remove the air bubbles. Finally, to accelerate the gelation of the PDMS mold, the samples were left at 60°C until complete crosslinking. After that, the PDMS mold was punched (5 mm of diameter and 4 mm of height).

6.2.1.3. Synthesis of chitosan and chitosan plus BG-NPs incorporation hydrogels

Based on Oliveira and co-workers [35] protocol, solutions of medium molecular weight CHT (Sigma-Aldrich) were prepared in acetic acid (2% v/v) in concentrations of 2% (w/v). Also, 12.5% w/v of bioglass nanoparticles relative to the total mass of CHT were incorporated. 80 μL of each solution was dropped in a PDMS mold well (5 millimeters

of diameter and 4 millimeters of height). 40 μL of genipin with concentrations of 1 v/v % and dissolved in a 10 ethanol–90 water mixture were dropped on the top of each well. The crosslinking reaction occurred overnight at 37 °C and it was stopped by immersing the hydrogels in ethanol (to clean the genipin residues), and afterwards in PBS at 37 °C for 1 hour.

6.2.1.4. Synthesis of chitosan-catechol conjugate (CHT-c)

Chitosan chemically modified with catechol groups (CHT-cat) was synthesized using EDC chemistry, where the catechols were conjugated with the amine groups of chitosan, based on the procedure proposed by Ryu and co-workers [41]. Briefly, 60 mL of 1% (w/v) medium molecular weight CHT solution was prepared in hydrochloric acid (HCl) at pH 2.5. Then, 0.145 g of hydrocaffeic acid (HCA) was dissolved in 15 mL of ethanol to prevent precipitation and 0.356 g of EDC was dissolved in 15 mL of deionized water. These two solutions were mixed and added to CHT solution under intensive stirring at room temperature for 18 h and the pH of the reaction solution was adjusted to 5.5. The resulting products were purified by dialysis in acidic deionized water solution (pH 5.0, HCl) during 2 days, in PBS buffer during 4 h and in deionized water during 4 h. The final product was lyophilized and kept in a moisture-free desiccator before use.

6.2.2. Characterization techniques

6.2.2.1. Zeta potential analysis

The synthesized BG-NPs with a thermal treatment of 700°C during 3 hours were analyzed using a concentration of 0.3 mg/mL. They were suspended in ultra-pure water (UPW) under magnetic stirring and further ultrasonic dispersion at 25°C during 15 minutes. Moreover, the Zetasizer equipment (Nano ZS) from Malvern Instruments with a Dispersion Technology Software (DTS) was used to perform this analysis.

6.2.2.2. Ultraviolet-visible (UV-vis) spectroscopy

Characterization of the conjugate was performed using the UV-vis spectrophotometry in order to confirm the successful modification of chitosan with the catechol groups and also to determine the degree of substitution of catechol group present in the modified chitosan. Two different solutions were made with four different concentrations each. 0.5 mg/mL, 1 mg/mL, 1.5 mg/mL and 2 mg/mL of chitosan dissolved in DW plus three drops of acetic acid and 0.5 mg/mL, 1 mg/mL, 1.5 mg/mL and 2 mg/mL of CHT-catechol were analyzed.

1 cm quartz cells were used (because quartz cells are transparent to UV light). The UV-vis spectrophotometer (Shimadzu UV- 1601) was used to perform this analysis.

6.2.2.3. Scanning electron microscopy coupled with energy dispersive X-ray (SEM-EDS) spectroscopy

The High-Resolution Field Emission Scanning Electron Microscope with Focused Ion Beam (FIB–SEM) (AURIGA COMPACT, ZEISS) equipment was used to evaluate the surface morphology and detect the chemical elements present on its surface. All samples were coated with a conductive layer of sputtered platinum.

6.2.2.4. Bioactivity tests

To investigate if the produced hydrogels with chitosan and bioglass nanoparticles induce the of hydroxyapatite formation on its surface after immersion in modified-simulated body fluid, in vitro bioactivity tests were performed. This solution was prepared according to Oyane and co-workers [44] and Oyane and co-workers [45] procedures. Dissolving sodium chloride (NaCl, Merck), sodium sulphate (Na₂SO₄, Panreac), magnesium chloride hexahydrate (MgCl₂.6H₂O, Merck), di-Potassium hydrogen phosphate trihydrate (K₂HPO₄.3H₂O, Merck), calcium chloride (CaCl₂, Merck), potassium chloride (KCl, Merck), sodium hydrogen carbonate (NaHCO₃, Merck), sodium carbonate (Na₂CO₃, Merck), sodium hydroxide (NaOH, Panreac) and 2-(4-(2-hydroxyethyl)-1-piperazinyl) ethanesulfonic acid (HEPES, C₈H₁₈N₂O₄S, Sigma) in ultra-pure water (UPW) at 36.5°C. The final pH was adjusted to 7.4. The bioactivity tests were performed during 3, 7 and 14 days. This solution simulates the concentration of different ionic species in human blood plasma. Each hydrogel was immersed in 25 mL of SBF solution during 0 (control), 3, 7 and 14 days at 37 °C. Upon removing from SBF, the hydrogels were rinsed with distilled water, put in the ultra-low freezer at T= - 80 °C during 24 h and then lyophilized. They were analyzed by SEM-EDS analysis to confirm their bioactivity character.

6.2.2.5. Dynamic mechanical analysis (DMA)

Chitosan crosslinked with genipin (CHT + genipin) and chitosan hydrogel with bioglass nanoparticles incorporation and genipin (CHT + BG-NPs + genipin) were studied using the TRITEC 2000 DMA equipment (Trinton Technology, UK), using a range of frequencies scan between 0.1 and 20 Hz. For that, the studied hydrogels were immersed

in phosphate buffered saline (PBS) solution at 37°C placed in a Teflon reservoir with a displacement equal to 0.050 mm. Data shown represented the Mean \pm Standard Deviation with a population of n = 5.

6.3. Results and Discussion

6.3.1. Bioglass nanoparticles (BG-NPs) production and characterization

BG-NPs were produced according to the condition described at the experimental section. Therafter, in order to assess the bioactivity properties/character of bioglass nanoparticles with a ternary formulation, *in vitro* bioactivity tests were performed during 7 days. Also, the potential zeta was measured. The results are shown below-Figure 6.1.

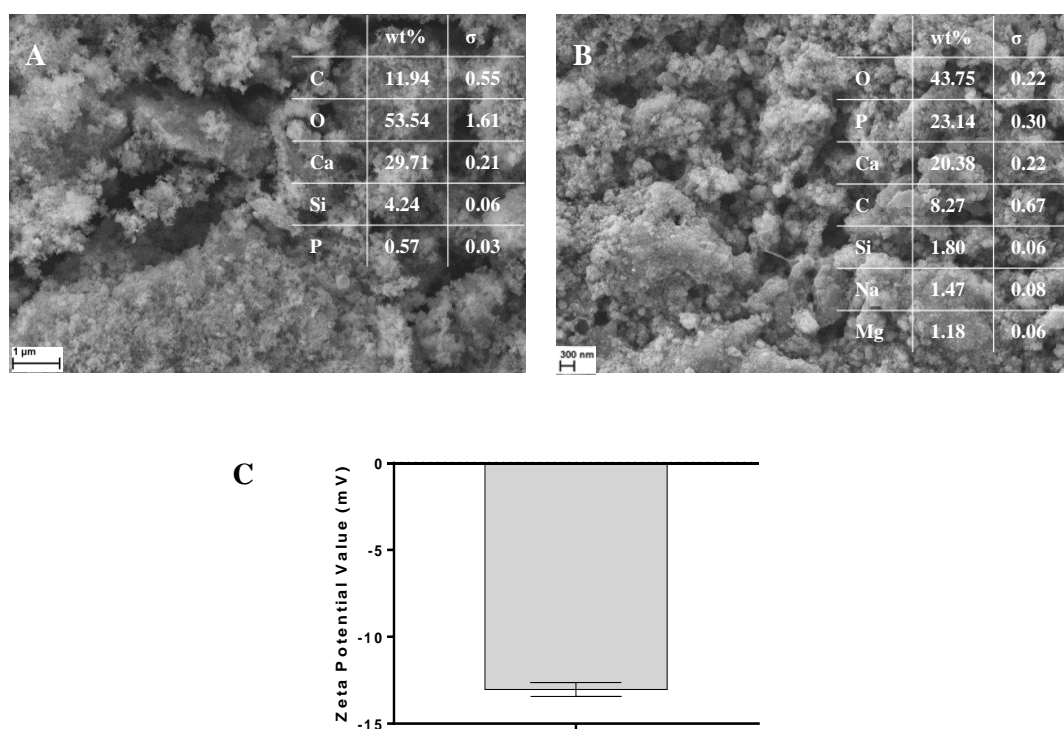


Figure 6. 1 - SEM-EDS micrographs of the surface of the ternary bioglass nanoparticles. (A) BG-NPs before immersion in SBF solution; (B) BG-NPs after immersion SBF solution during 7 days and (C) Zeta potential value for BG-NPs with a thermal treatment at 700°C during 3 hours (n = 3).

Through analysis of Figure 6.1, it can be seen that there was a decrease of silicon and an increase of phosphorus percentage due to nanoparticles dissolution [43]. These results corroborated the bioactivity performance of these bioglass nanoparticles. The zeta size measurement performed with ultra-pure water (UPW) revealed that the BG-NPs had a negative value (-13.03 ± 0.40 mV), which is consistent with previous works [43]. This result also revealed that these nanoparticles have tendency to aggregate in solution because its zeta-potential value is higher than -30 mV [46].

6.3.2. Hydrogels production and characterization

Figure 6.2 shows the cross-section morphology of hydrogels made with chitosan crosslinked with genipin (Figure 6.2-A), and the hydrogels made with the same system, but with the addition of BG-NPs (Figure 6.2-B).

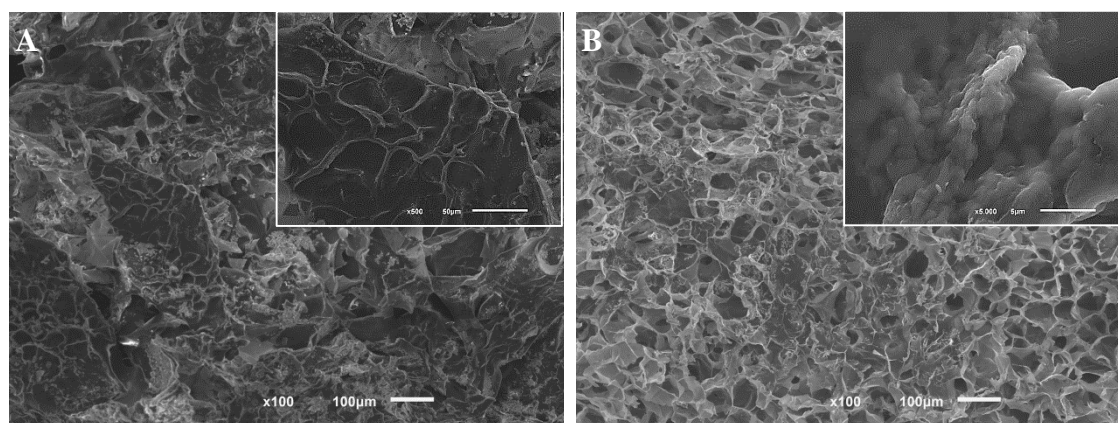
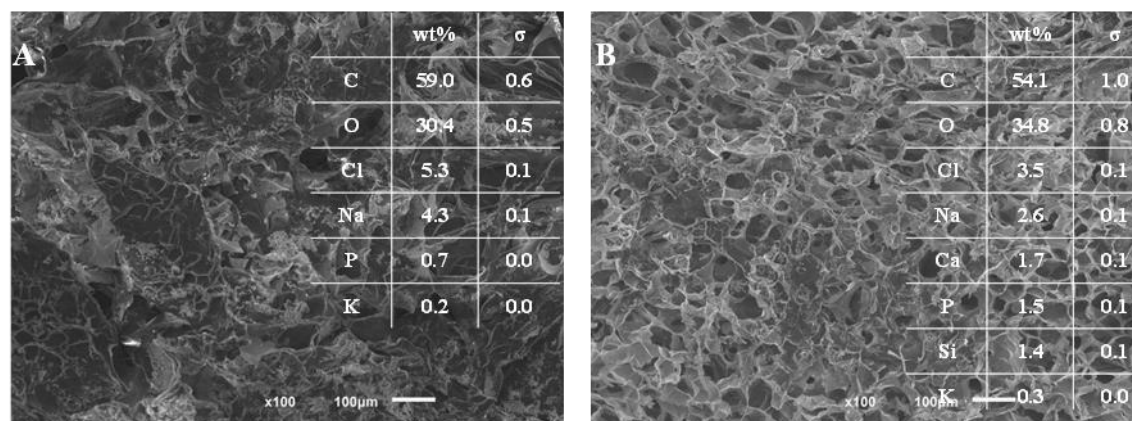


Figure 6. 2 – Representative SEM micrographs of hydrogels production. (A) CHT hydrogel crosslinked with genipin, (B) CHT + BG-NPs hydrogel crosslinked with genipin. The inset images are SEM micrographs with higher magnifications.

Through the analysis of Figure 6.2, it can be seen both surfaces are similar and present a porous structure due to the lyophilization process. However, by looking at Figure 6.2-B (magnified image) the surface is rougher which is probably caused by the presence of clusters of bioglass nanoparticles between the polymeric matrix. The same surface morphology, i.e., the presence of clusters of bioglass nanoparticles in the polymeric matrix, was found in a previous work of our group [47].

In order to study the bioactivity performance of the produced hydrogel (CHT+BG-NPs), in vitro bioactivity tests were performed. For that, the hydrogel was soaked in SBF during distinct time periods. Also, the same procedure was done for the control hydrogel (CHT crosslinked with genipin). The results are shown in Figure 6. 3.



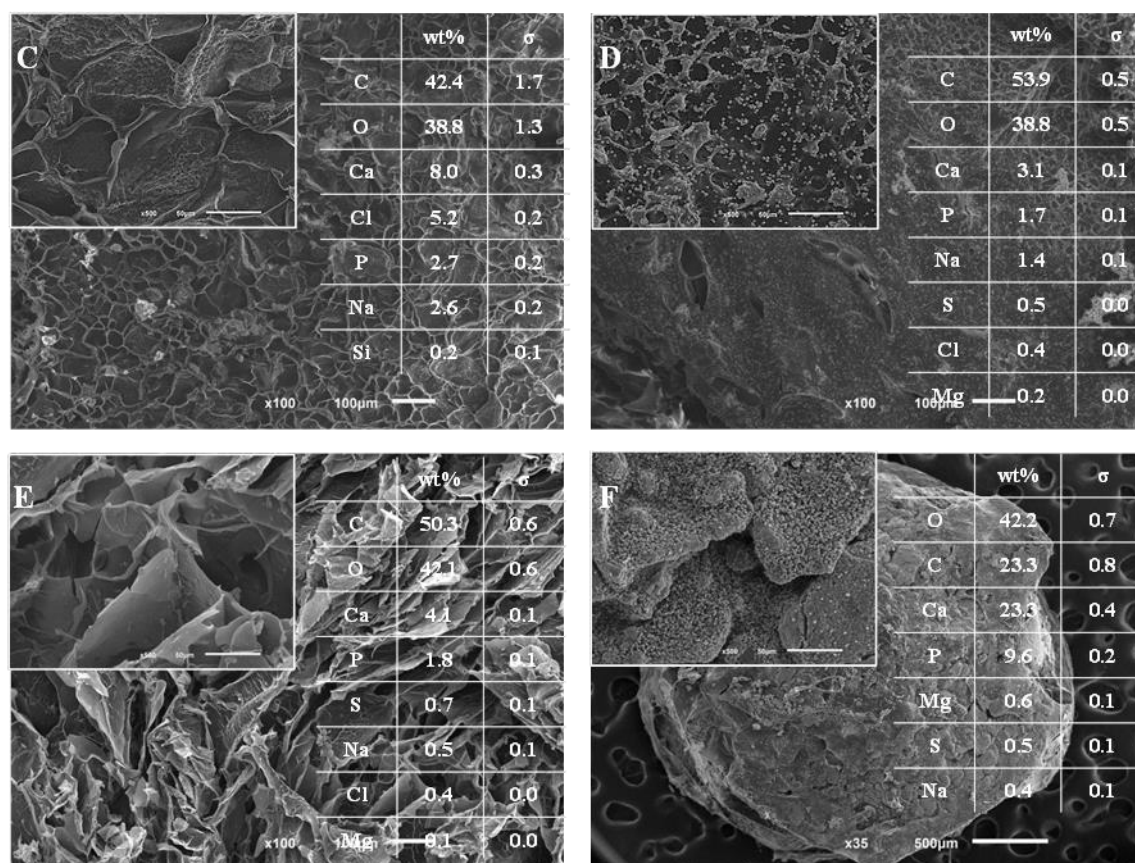


Figure 6. 3 – SEM-EDS micrographs for hydrogels soaked in SBF solution for different time-points. (A) Cross-section view of CHT hydrogel crosslinked with genipin – 0 days (control), (B) Cross-section view of CHT+ BG-NPs hydrogel crosslinked with genipin – 0 days (control), (C) Cross-section view of CHT+BG-NPs hydrogel crosslinked with genipin – 3 days, (D) Cross-section view of CHT+BG-NPs hydrogel crosslinked with genipin – 7 days, (E) Cross-section view of CHT+BG-NPs hydrogel crosslinked with genipin – 14 days and (F) SEM-EDS micrographs for the bottom side of CHT+BG-NPs – 14 days.

It can be seen that for the control one (Figure 6.3-A), the EDS spectrum revealed the presence of carbon (C), oxygen (O), sodium (Na) and chloride (Cl) due to the drying process. In Figure 6.2-B, the EDS spectrum revealed the presence of silicon (Si), calcium (Ca) and phosphorus (P), which corroborates the presence of bioglass nanoparticles. Along the time-experience it can be seen that there was the formation of a calcium-phosphate (Ca-P) layer (hydroxyapatite) onto the hydrogels surface glued between the polymeric matrix-see Figure 6.3-C to E. This Ca-P layer is also present on the bottom surface of CHT+BG-NPs hydrogel crosslinked with genipin, Figure 6.3-F. These results revealed that the bioglass nanoparticles are well-dispersed on the hydrogel network (top, cross-section and bottom sides).

The mechanical properties of the created hydrogels were studied by Dynamic Mechanical Analysis (DMA) under physiological conditions (pH = 7.4 and T = 37°C) – see Figure 6.4. According to Oliveira and co-workers [35] the bone tissue has a viscoelastic behavior, implying energy dissipation and time-dependent properties [35, 48]. Dynamic

mechanical analysis is a non-destructive technique which allows to study the mechanical properties under simulated physiological conditions [49] with a frequency or temperature range.

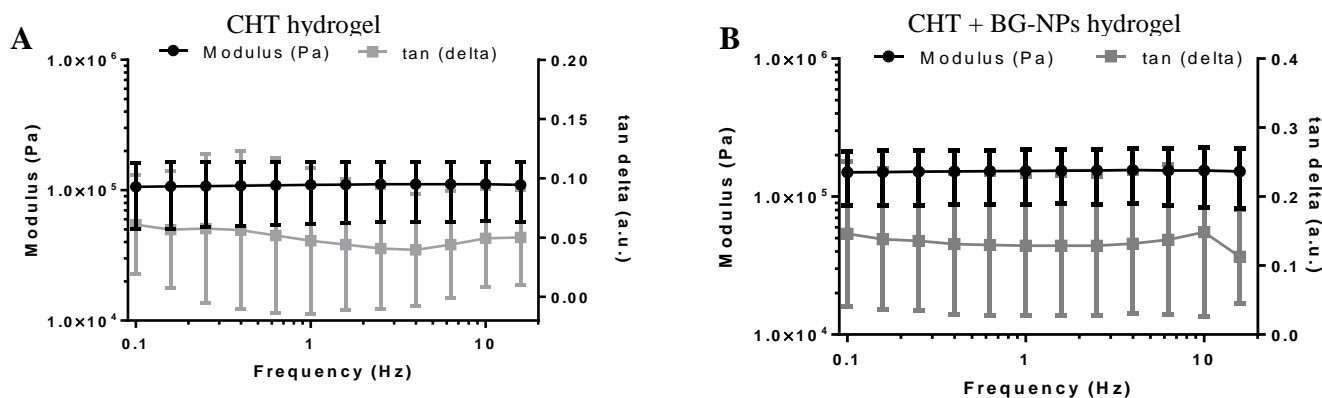


Figure 6. 4- Dynamic mechanical analysis (DMA) results. (A) Modulus and tan (δ) results of the CHT hydrogel crosslinked with genipin; (B) Modulus and tan (δ) of the CHT + BG-NPs hydrogel crosslinked with genipin.

The results present in this figure were obtained at 37°C and the frequency ranged between 0.1 and 20 Hz. These values were chosen because human beings in their daily activities show frequency ranges from 0.1 to 20 Hz. It was chosen the BG-NPs content of 12.5 % relative to the total mass of CHT because according to a previous work of our group [35] hydrogels containing 12.5% of bioglass nanoparticles, the same concentration of CHT, but higher percentage of genipin revealed better cell proliferation. In our case, we maintained all components but the same concentration of crosslinker agent tested on free-standing films (1 % v/v.) - see Chapter 5. Figure 6.4-A shows the storage modulus (E') and the loss factor ($\tan \delta$) of hydrogels made only of chitosan and crosslinked with genipin. Through the analysis of Figure 6.4-A, we can see an increase of E' and a decrease of the loss factor along the frequencies range. Moreover, for the control hydrogel, the E' value was 109.7 ± 54.7 kPa for a frequency of 1 Hz. For hydrogels made with chitosan plus bioglass nanoparticles incorporation, crosslinked with genipin, shown in Figure 6.4-B, it can be seen that the storage modulus (E') increased along the frequencies range (from 0.1 to 15.849 Hz). The hydrogel made with chitosan plus bioglass nanoparticles incorporation showed an E' value of 153.5 ± 65.3 kPa for 1.0 Hz. Regarding the loss factor, there was a decrease from 0.1 Hz to 15.849 Hz. Regarding E' , the CHT + BG-NPs + genipin hydrogel had twice the value obtained for the control one. For the loss factor, CHT + BG-NPs + genipin hydrogels present a value that is nearly 2.6 times higher than the control one. According to Caridade and co-workers [50], high loss factor values

implies higher capacity to dissipate energy. The same authors produced a film with chitosan and micro- and nano-sized bioglass nanoparticles. Better mechanical properties were achieved for nano-sized BG due to large interface area between the polymer matrix and the bioglass nanoparticles [50]. Comparing the obtained values with Oliveira and co-workers [35] results, it can be seen that the addition or not of bioglass nanoparticles, overall at lower concentrations of chitosan slightly increased the storage modulus. In our case the addition of BG-NPs led to a big increase of E' , as it is said and shown above.

6.3.3. Chitosan modified with catechol groups (CHT-cat) conjugate synthesis and characterization:

The synthesis of chitosan-catechol conjugate was based on the procedure proposed by Kim and co-workers [40] and Ryu and co-workers [41]. In order to understand if this synthesis was successful the UV-vis spectrophotometry characterization technique was performed- Figure 6.5. According to the literature this substitution implies the appearance of a peak in at nearly 280 nm of maximum absorbance, λ_{\max} [40, 51]. It can be seen in Figure 6.5 that the synthesized conjugate presents the referred characteristic peak at 280 nanometers (nm), which demonstrates the presence of catechol groups present in chitosan backbone. Moreover, the control spectrum did not show this peak. Also, the appearance of a peak at 220 nm allows to infer the presence of amine and hydroxyl groups [40]. Three different formulations were done, namely as it can be seen in Table 6.1 and Figures 6.5-A to D. The concentration of chitosan was the same to guarantee similar free-amines groups present in the chitosan backbone that could be substituted by ortho-dihydroxyphenyl groups as well as the activate component (EDC) was the same. The HCA concentration increased, implying higher content of available catechol groups that could react with the free-amines present in the chitosan backbone. By analysis of Figures 6.5-A to D, it can be said that the better degree of substitution was achieved for Formulation 3, shown in Figure 6.5-C. Furthermore, 13.23%, 12.88% and 25.18% are the substitution degrees of ortho-dihydroxyphenyl groups in chitosan and 0.1323, 0.0644 and 0.2518 mM are the concentrations of catechol present in chitosan (CHT) backbone for condition 1, 2 and 3, respectively. Figure 6.5 also shows that, with an increase of catechol group concentrations there is an increase in the absorbance, because there are higher catechol groups present in the conjugate backbone.

Table 6. 1 - Different formulations tested to produce chitosan-catechol (CHT-c) conjugate

Experiences			
Formulation	CHT	HCA (mg/3 mL)	EDC (mg/3 mL)
(A) - 1	1% w/v	295	71.2
(B) - 2	1% w/v	29	71.2
(C) - 3	1% w/v	592	71.2

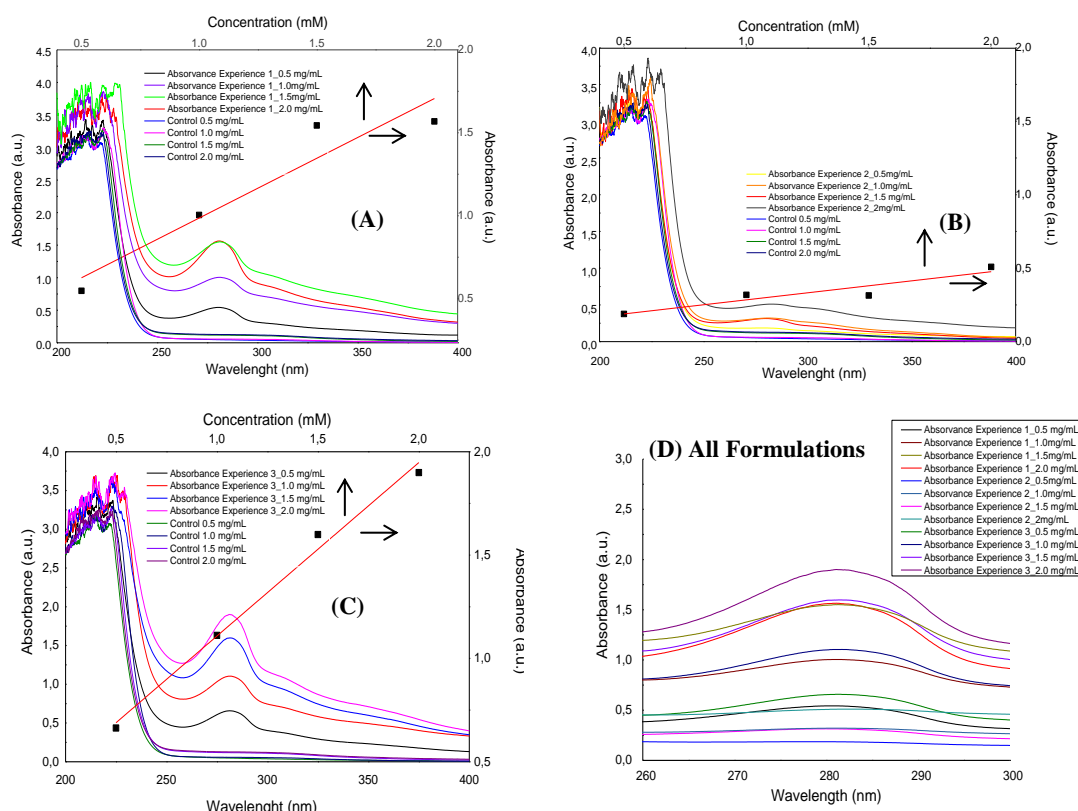


Figure 6. 5 - (A) UV-vis spectrum of CHT (control) and CHT-catechol for Formulation 1, (B) UV-vis spectrum of CHT (control) and CHT-catechol for Formulation 2, (C) UV-vis spectrum of CHT (control) and CHT-catechol for Formulation 3 and (D) Overlay.

6.4. Conclusions and future work:

It can be concluded that hydrogels containing chitosan crosslinked with genipin as well as with the addition of bioglass nanoparticles were successfully developed. SEM micrographs showed its surface morphology. It was concluded that freezing the hydrogels in the ultra-low freezer led to a change on its surface morphology. Also, the hydrogels presented a bioactive character after immersion in SBF during 3, 7 and 14 days. Dynamic mechanical analysis showed that the addition of bioglass nanoparticles in the hydrogel

network improved their mechanical properties as well as their capacity to dissipate energy.

Characterization of the chitosan-catechol conjugate (CHT-cat) was performed by UV-vis spectrophotometry in order to confirm the successful modification of chitosan with the catechol groups and also to determine the degree of substitution of catechol groups present in the modified chitosan. The obtained results were satisfactory because it is the first time that this conjugate is produced in our group. It was tried the production of chitosan-catechol-based hydrogels following the Kim and co-workers [40] procedure, but unfortunately they need more optimization.

For future work silver doped bioglass nanoparticles could be incorporated in the chitosan crosslinked with genipin formulation in order to study the antibacterial effect of silver doped bioglass nanoparticles, namely the Ag-BG-NPs heat-treated during 2 hours at 90°C and ½ hour at 100°C (the best thermal treatment - see Chapter 4). Moreover, after optimization, chitosan-catechol conjugate hydrogels development could be tried with or without addition of bioglass nanoparticles as well as with silver doped bioglass nanoparticles. The production of such hybrid systems could be tried with the addition of iron ions (formation of stereo-complexes) or base addition (NaOH: there is the formation of reactive species (ortho-quinones) responsible for the crosslinking between the catechol groups and the formation of a 3D network). It is expected that these hydrogels, besides their enhanced mechanical properties, would have superior adhesive properties due to the presence of catechol groups.

6.5. References:

- [1] N. A. Peppas, J. Z. Hilt, A. Khademhosseini, and R. Langer, "Hydrogels in biology and medicine: From molecular principles to bionanotechnology," *Advanced Materials*, vol. 18, no. 11, pp. 1345-1360, 2006.
- [2] R. Langer and N. A. Peppas, "Advances in biomaterials, drug delivery, and bionanotechnology," *Aiche Journal*, vol. 49, no. 12, pp. 2990-3006, 2003.
- [3] N. Annabi et al., "25th Anniversary Article: Rational Design and Applications of Hydrogels in Regenerative Medicine," *Advanced Materials*, vol. 26, no. 1, pp. 85-124, 2014.
- [4] E. Caló and V. V. Khutoryanskiy, "Biomedical applications of hydrogels: A review of patents and commercial products," *European Polymer Journal*, vol. 65, pp. 252-267, 2015.
- [5] J. B. Park, "The use of hydrogels in bone-tissue engineering," (in English), *Medicina Oral Patologia Oral Y Cirugia Bucal*, Article vol. 16, no. 1, pp. E115-E118, 2011.

- [6] L. Gasperini, J. F. Mano, and R. L. Reis, "Natural polymers for the microencapsulation of cells," (in English), *Journal of the Royal Society Interface*, Article vol. 11, no. 100, p. 19, 2014, Art. no. Unsp 20140817.
- [7] N. Annabi, S. M. Mithieux, E. A. Boughton, A. J. Ruys, A. S. Weiss, and F. Dehghani, "Synthesis of highly porous crosslinked elastin hydrogels and their interaction with fibroblasts in vitro," *Biomaterials*, vol. 30, no. 27, pp. 4550-4557, 2009.
- [8] J. L. Drury and D. J. Mooney, "Hydrogels for tissue engineering: scaffold design variables and applications," (in English), *Biomaterials*, Review vol. 24, no. 24, pp. 4337-4351, 2003.
- [9] L. Klouda and A. G. Mikos, "Thermoresponsive hydrogels in biomedical applications," *European Journal of Pharmaceutics and Biopharmaceutics*, vol. 68, no. 1, pp. 34-45, 2008.
- [10] T. R. Hoare and D. S. Kohane, "Hydrogels in drug delivery: Progress and challenges," (in English), *Polymer*, Review vol. 49, no. 8, pp. 1993-2007, 2008.
- [11] L. Yu and J. Ding, "Injectable hydrogels as unique biomedical materials," *Chemical Society Reviews*, vol. 37, no. 8, pp. 1473-1481, 2008.
- [12] K. Y. Lee and D. J. Mooney, "Hydrogels for tissue engineering," *Chemical Reviews*, vol. 101, no. 7, pp. 1869-1879, 2001.
- [13] K. Pal, A. K. Banthia, and D. K. Majumdar, "Polymeric Hydrogels: Characterization and Biomedical Applications," *Designed Monomers and Polymers*, vol. 12, no. 3, pp. 197-220, 2009.
- [14] M. E. Yu, J. Y. Hwang, and T. J. Deming, "Role of L-3,4-dihydroxyphenylalanine in mussel adhesive proteins," (in English), *Journal of the American Chemical Society*, Article vol. 121, no. 24, pp. 5825-5826, 1999.
- [15] M. Cencer, Y. Liu, A. Winter, M. Murley, H. Meng, and B. P. Lee, "Effect of pH on the Rate of Curing and Bioadhesive Properties of Dopamine Functionalized Poly(ethylene glycol) Hydrogels," (in English), *Biomacromolecules*, Article vol. 15, no. 8, pp. 2861-2869, 2014.
- [16] H. Lee, N. F. Scherer, and P. B. Messersmith, "Single-molecule mechanics of mussel adhesion," (in English), *Proceedings of the National Academy of Sciences of the United States of America*, Article vol. 103, no. 35, pp. 12999-13003, 2006.
- [17] H. G. Silverman and F. F. Roberto, "Understanding marine mussel adhesion," (in English), *Marine Biotechnology*, Review vol. 9, no. 6, pp. 661-681, 2007.
- [18] P. Podsiadlo, Z. Q. Liu, D. Paterson, P. B. Messersmith, and N. A. Kotov, "Fusion of seashell nacre and marine bioadhesive analogs: High-strength nanocomposite by layer-by-layer assembly of clay and L-3,4-dihydroxyphenylalanine polymer," (in English), *Advanced Materials*, Article vol. 19, no. 7, pp. 949-+, 2007.
- [19] S. K. Madhurakkat Perikamana et al., "Materials from Mussel-Inspired Chemistry for Cell and Tissue Engineering Applications," *Biomacromolecules*, vol. 16, no. 9, pp. 2541-55, 2015.
- [20] Y. C. Choi, J. S. Choi, Y. J. Jung, and Y. W. Cho, "Human gelatin tissue-adhesive hydrogels prepared by enzyme-mediated biosynthesis of DOPA and Fe³⁺ ion crosslinking," (in English), *Journal of Materials Chemistry B*, Article vol. 2, no. 2, pp. 201-209, 2014.

- [21] Y. Lee et al., "Thermo-sensitive, injectable, and tissue adhesive sol-gel transition hyaluronic acid/pluronic composite hydrogels prepared from bio-inspired catechol-thiol reaction," (in English), *Soft Matter*, Article vol. 6, no. 5, pp. 977-983, 2010.
- [22] B. P. Lee, J. L. Dalsin, and P. B. Messersmith, "Synthesis and gelation of DOPA-Modified poly(ethylene glycol) hydrogels," (in English), *Biomacromolecules*, Article vol. 3, no. 5, pp. 1038-1047, 2002.
- [23] S. A. Burke, M. Ritter-Jones, B. P. Lee, and P. B. Messersmith, "Thermal gelation and tissue adhesion of biomimetic hydrogels," (in English), *Biomedical Materials*, Article vol. 2, no. 4, pp. 203-210, 2007.
- [24] Y. Ai, J. Nie, G. Wu, and D. Yang, "The DOPA-Functionalized Bioadhesive with Properties of Photocrosslinked and Thermoresponsive," *Journal of Applied Polymer Science*, vol. 131, no. 22, 2014, Art. no. 41102.
- [25] A. I. Neto et al., "Nanostructured Polymeric Coatings Based on Chitosan and Dopamine-Modified Hyaluronic Acid for Biomedical Applications," (in English), *Small*, Article vol. 10, no. 12, pp. 2459-2469, 2014.
- [26] J. J. Wilker, "The Iron-Fortified Adhesive System of Marine Mussels," (in English), *Angewandte Chemie-International Edition*, Editorial Material vol. 49, no. 44, pp. 8076-8078, 2010.
- [27] S. Hong et al., "Hyaluronic Acid Catechol: A Biopolymer Exhibiting a pH-Dependent Adhesive or Cohesive Property for Human Neural Stem Cell Engineering," (in English), *Advanced Functional Materials*, Article vol. 23, no. 14, pp. 1774-1780, 2013.
- [28] B. J. Kim et al., "Mussel-Mimetic Protein-Based Adhesive Hydrogel," (in English), *Biomacromolecules*, Article vol. 15, no. 5, pp. 1579-1585, 2014.
- [29] C. Lee et al., "Bioinspired, Calcium-Free Alginate Hydrogels with Tunable Physical and Mechanical Properties and Improved Biocompatibility," *Biomacromolecules*, vol. 14, no. 6, pp. 2004-2013, 2013.
- [30] D. E. Fullenkamp et al., "Mussel-inspired silver-releasing antibacterial hydrogels," (in English), *Biomaterials*, Article vol. 33, no. 15, pp. 3783-3791, 2012.
- [31] A. Vulpoi et al., "Bioactivity and protein attachment onto bioactive glasses containing silver nanoparticles," *Journal of Biomedical Materials Research Part A*, vol. 100A, no. 5, pp. 1179-1186, 2012.
- [32] A. K. Gaharwar, N. A. Peppas, and A. Khademhosseini, "Nanocomposite Hydrogels for Biomedical Applications," *Biotechnology and Bioengineering*, vol. 111, no. 3, pp. 441-453, 2014.
- [33] U. Rottensteiner et al., "In vitro and in vivo Biocompatibility of Alginate Dialdehyde/Gelatin Hydrogels with and without Nanoscaled Bioactive Glass for Bone Tissue Engineering Applications," (in English), *Materials*, Article vol. 7, no. 3, pp. 1957-1974, 2014.
- [34] T. Nardo, V. Chiono, G. Ciardelli, and M. Tabrizian, "PolyDOPA Mussel-Inspired Coating as a Means for Hydroxyapatite Entrapment on Polytetrafluoroethylene Surface for Application in Periodontal Diseases," (in English), *Macromolecular Bioscience*, Article vol. 16, no. 2, pp. 288-298, 2016.

- [35] M. B. Oliveira, G. M. Luz, and J. F. Mano, "A combinatorial study of nanocomposite hydrogels: on-chip mechanical/viscoelastic and pre-osteoblast interaction characterization," (in English), *Journal of Materials Chemistry B*, Article vol. 2, no. 34, pp. 5627-5638, 2014.
- [36] N. M. Alves and J. F. Mano, "Chitosan derivatives obtained by chemical modifications for biomedical and environmental applications," (in English), *International Journal of Biological Macromolecules*, Review vol. 43, no. 5, pp. 401-414, 2008.
- [37] R. Jayakumar, M. Prabakaran, P. T. S. Kumar, S. V. Nair, and H. Tamura, "Biomaterials based on chitin and chitosan in wound dressing applications," *Biotechnology Advances*, vol. 29, no. 3, pp. 322-337, 2011.
- [38] F. Croisier and C. Jerome, "Chitosan-based biomaterials for tissue engineering," *European Polymer Journal*, vol. 49, no. 4, pp. 780-792, 2013.
- [39] M. Dash, F. Chiellini, R. M. Ottenbrite, and E. Chiellini, "Chitosan-A versatile semi-synthetic polymer in biomedical applications," *Progress in Polymer Science*, vol. 36, no. 8, pp. 981-1014, 2011.
- [40] K. Kim, J. H. Ryu, D. Y. Lee, and H. Lee, "Bio-inspired catechol conjugation converts water-insoluble chitosan into a highly water-soluble, adhesive chitosan derivative for hydrogels and LbL assembly," (in English), *Biomaterials Science*, Article vol. 1, no. 7, pp. 783-790, 2013.
- [41] J. H. Ryu, Y. Lee, W. H. Kong, T. G. Kim, T. G. Park, and H. Lee, "Catechol-Functionalized Chitosan/Pluronic Hydrogels for Tissue Adhesives and Hemostatic Materials," (in English), *Biomacromolecules*, Article vol. 12, no. 7, pp. 2653-2659, 2011.
- [42] G. M. Luz and J. F. Mano, "Chitosan/bioactive glass nanoparticles composites for biomedical applications," (in English), *Biomedical Materials*, Article vol. 7, no. 5, p. 9, 2012, Art. no. 054104.
- [43] G. M. Luz and J. F. Mano, "Preparation and characterization of bioactive glass nanoparticles prepared by sol-gel for biomedical applications," (in English), *Nanotechnology*, Article vol. 22, no. 49, p. 11, 2011, Art. no. 494014.
- [44] A. Oyane, H. M. Kim, T. Furuya, T. Kokubo, T. Miyazaki, and T. Nakamura, "Preparation and assessment of revised simulated body fluids," *Journal of Biomedical Materials Research Part A*, vol. 65A, no. 2, pp. 188-195, 2003.
- [45] A. Oyane, K. Onuma, A. Ito, H. M. Kim, T. Kokubo, and T. Nakamura, "Formation and growth of clusters in conventional and new kinds of simulated body fluids," *Journal of Biomedical Materials Research Part A*, vol. 64A, no. 2, pp. 339-348, 2003.
- [46] G. M. Luz and J. F. Mano, "Nanoengineering of bioactive glasses: hollow and dense nanospheres," (in English), *Journal of Nanoparticle Research*, Article vol. 15, no. 2, p. 11, 2013, Art. no. 1457.
- [47] D. S. Couto, Z. K. Hong, and J. F. Mano, "Development of bioactive and biodegradable chitosan-based injectable systems containing bioactive glass nanoparticles," (in English), *Acta Biomaterialia*, Article vol. 5, no. 1, pp. 115-123, 2009.

- [48] S. Ghosh et al., "Dynamic mechanical behavior of starch-based scaffolds in dry and physiologically simulated conditions: Effect of porosity and pore size," *Acta Biomaterialia*, vol. 4, no. 4, pp. 950-959, 2008.
- [49] J. M. Silva, A. R. C. Duarte, S. G. Caridade, C. Picart, R. L. Reis, and J. F. Mano, "Tailored Freestanding Multi layered Membranes Based on Chitosan and Alginate," (in English), *Biomacromolecules*, Article vol. 15, no. 10, pp. 3817-3826, 2014.
- [50] S. G. Caridade, E. G. Merino, N. M. Alves, V. d. Z. Bermudez, A. R. Boccaccini, and J. F. Mano, "Chitosan membranes containing micro or nano-size bioactive glass particles: evolution of biomineralization followed by in situ dynamic mechanical analysis," *Journal of the Mechanical Behavior of Biomedical Materials*, vol. 20, pp. 173-183, 2013.
- [51] J. H. Ryu, S. Hong, and H. Lee, "Bio-inspired adhesive catechol-conjugated chitosan for biomedical applications: A mini review," (in English), *Acta biomaterialia*, ; Review vol. 27, pp. 101-15, 2015.

CHAPTER 7

CONCLUSIONS AND

FUTURE WORK

7. CONCLUSIONS AND FUTURE WORK

The work developed in this thesis was inspired in the fact that marine mussels present an unusual amino acid, 3, 4-dihydroxi-L-phenilalanine (DOPA) that can be used as a glue to stick in wet environment. This amino acid can be used in the biomaterials area to improve the adhesion to various substrates, either in inorganic or organic surfaces. The layer-by-layer (LbL) technique was also chosen to produce some of the materials developed in this thesis because allows the production of various coatings, free-standing films, among others as it is a simple, cheap, versatile and an efficient technique. So, the LbL technique using biomaterials based on DOPA is a resource with enormous potential in the biomedical field, as evidenced in the present work.

An optimization work about silver doped bioglass nanoparticles obtained through sol-gel technique was conducted in this thesis. Eight different thermal treatments were studied. It should be pointed that, as far as we know, this is the first time that a systematic study of the effect of the chosen thermal treatment on the properties of the Ag-doped bioglass nanoparticles was analysed. The results revealed the successful incorporation of silver corroborated by EDS analysis. Moreover, the produced nanoparticles induced the formation of hydroxyapatite after immersion in SBF after 7 days, corroborated by SEM-EDS and XRD analysis. In conclusion, it's preferable the Ag-BG-NPs thermally treated with higher temperatures, namely 2 hours at 90°C plus ½ hour at 100°C, 100°C/h plus ½ h at 400°C, 500°C, 580°C and 700°C, because the zeta potential values were higher, implying better stability in solution. Furthermore, hydroxyapatite formation is engaged by negative surfaces. Summarizing, the results revealed that these nanoparticles are useful in the biomedical field, namely in the orthopedic area and dental applications.

In this thesis, free-standing films based on natural-based materials such as chitosan, hyaluronic acid and hyaluronic acid-dopamine conjugate were developed. The modification with dopamine was done in order to improve adhesive properties. Different crosslinker agents were tried with different concentrations using EDC/NHS and genipin. The results revealed that these free-standing films were handleable after crosslinked with genipin, with a concentration of 1mg/mL. Moreover, FT-IR analysis in ATR mode, TGA and SEM-EDS analysis allowed infer the nanoparticles adsorption across and on the top the films for formulation 3 ([CHT/HA/CHT/Ag-BG-NPs]₇₅) and formulation 4 ([CHT/HA-DN/CHT/Ag-BG-NPs]₇₅). Fifteen percent of Ag-BG-NPs were adsorbed in

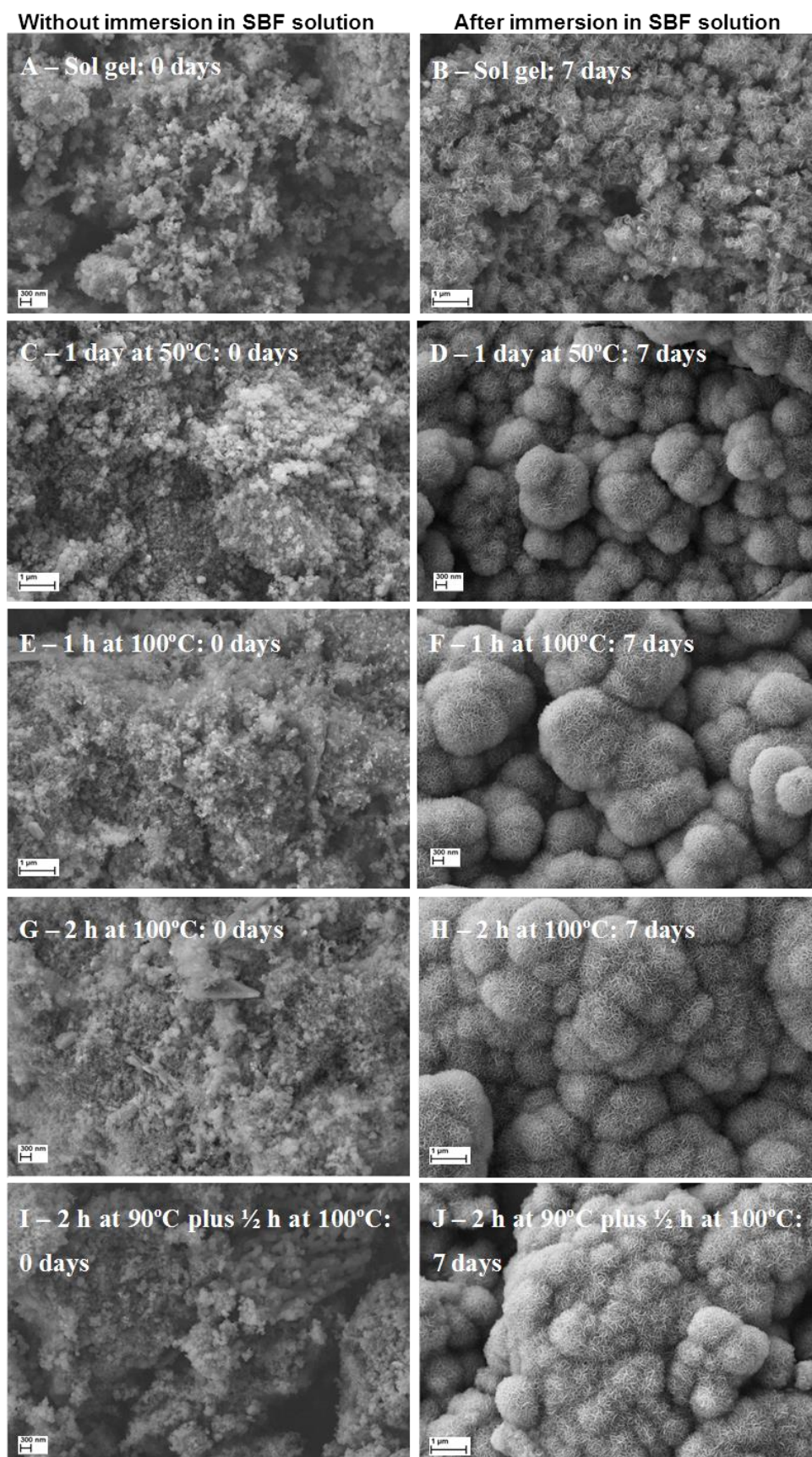
the LbL build-up. These results are quite satisfactory, since the nanoparticle solutions were put on each LbL cycle in the sonicator to avoid the nanoparticle's agglomeration and precipitation in order to maximize the nanoparticles adsorption. After immersion in SBF they revealed the formation of hydroxylapatite on its surface and showed an improved antibacterial performance against *E. coli* and *S. aureus*. In summary, comparing formulation 3, built-up with chitosan, hyaluronic acid and Ag-BG-NPs with 75 tetralayers ([CHT/HA/CHT/Ag-BG-NPs]₇₅) and formulation 4 ([CHT/HA-DN/CHT/Ag-BG-NPs]₇₅), the last one presents higher adhesive property, being available to use in the orthopedic area and dental applications because it is tissue-adhesive, promotes the formation of a calcium-phosphate layer (mandatory to be used in the envisaged application) and demonstrates antibacterial performance.

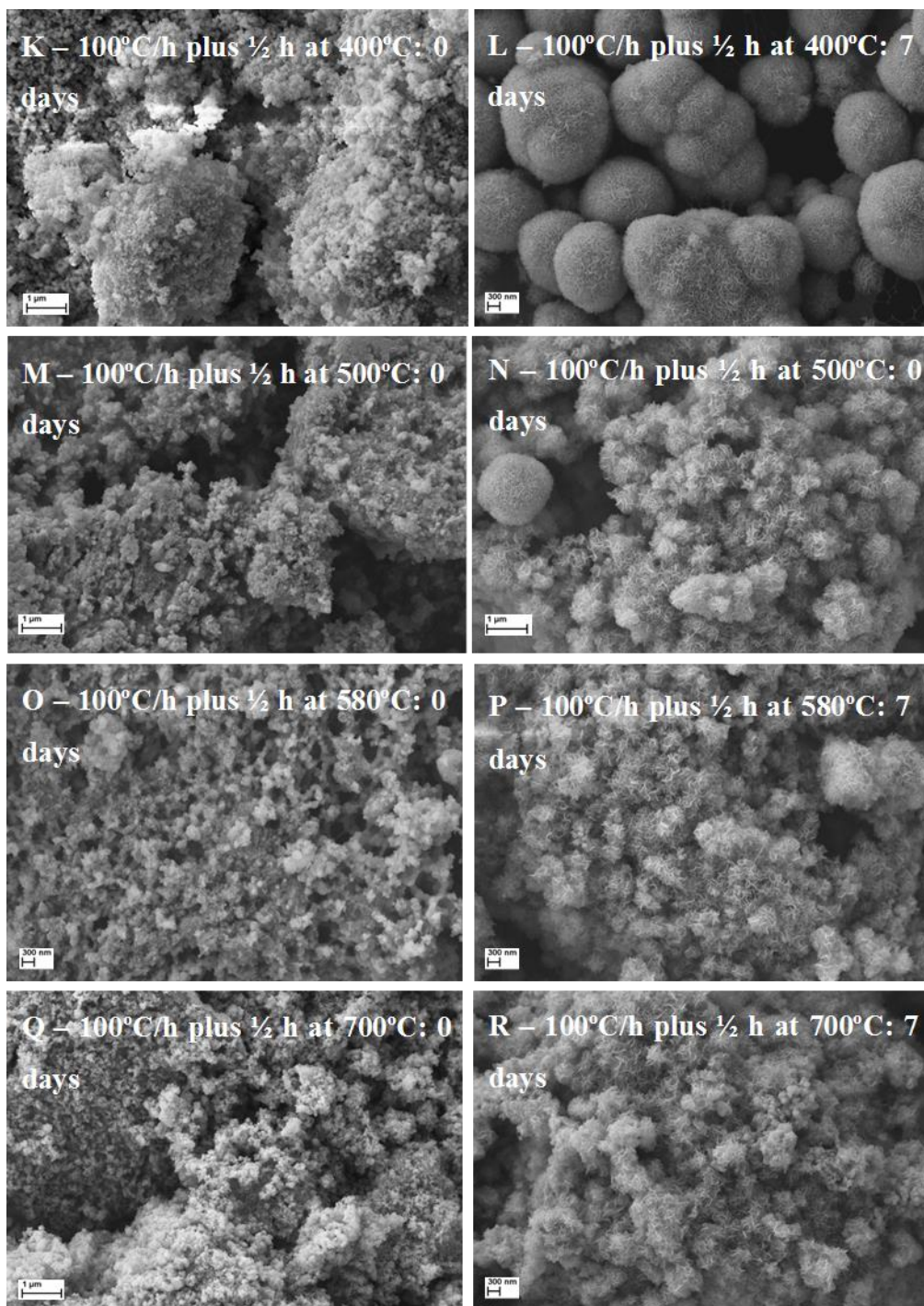
Finally, hydrogels either with chitosan or chitosan plus bioglass nanoparticles incorporation were produced. Both hydrogels were successfully crosslinked with genipin. The DMA results showed that the addition of nanoparticles allowed enhanced damping and stiffness properties. Also, the successful modification of chitosan with the adhesive groups present in DOPA groups was done.

For future work, bioglass and silver doped bioglass nanoparticles with an optimized thermal treatment should be incorporated in the chitosan hydrogel network, in order to study its antibacterial properties. Moreover, hydrogels that combine other natural polymers with the adhesive groups of DOPA could be developed in order to obtain materials with superior adhesive properties and improved cell response.

APPENDIX

In Appendix 1, the Ag-BG-NPs surface morphologies before and after immersion in SBF solution is shown. In Appendixes 2.1 to 2.3, UV-vis results of the hyaluronic acid modified with dopamine conjugate synthesis are shown. Regarding Appendixes 3 and 4, TGA thermograms and AFM results (2D images 5 μm x 5 μm) are shown, respectively. In Appendix 5, the analysis of the free-standing films' surfaces after immersion in SBF solution during 14 days is shown. Appendix 6, presents the SEM-EDS micrographs and FT-IR spectras of the native and crosslinked (with EDC/NHS) LbL free-standing films.

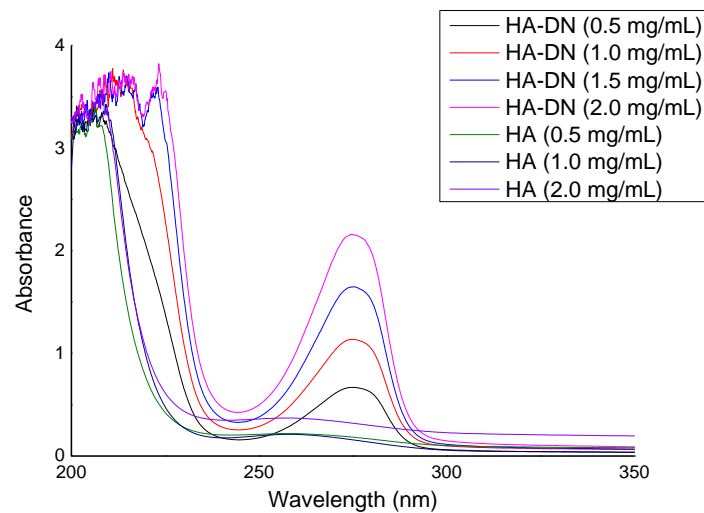
Appendix 1 - SEM-EDS micrographs before and after immersion in SBF solution (0 days and 7 days)



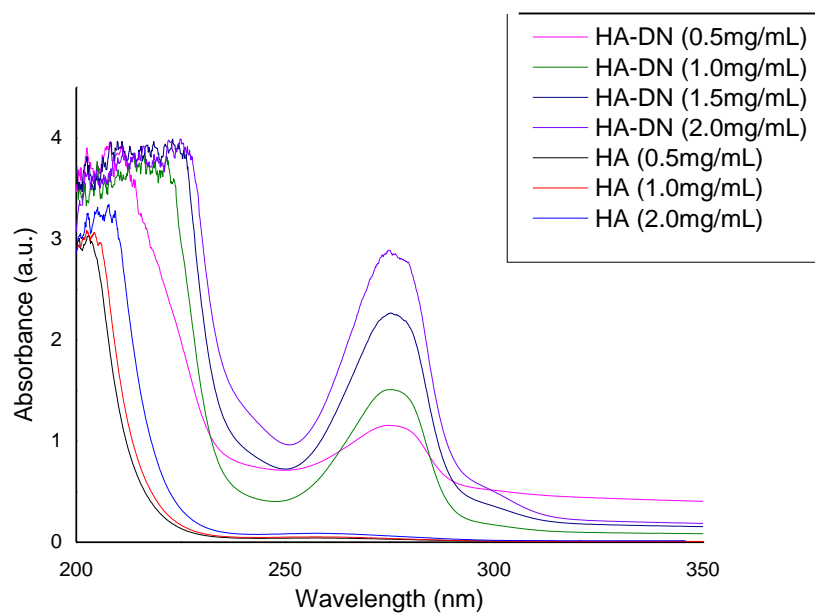
Appendix 1 - SEM-EDS micrographs before and after immersion in SBF solution (0 days and 7 days).

Appendix 2 - Hyaluronic acid modified with dopamine (HA-DN) conjugate synthesis and characterization: UV-vis results

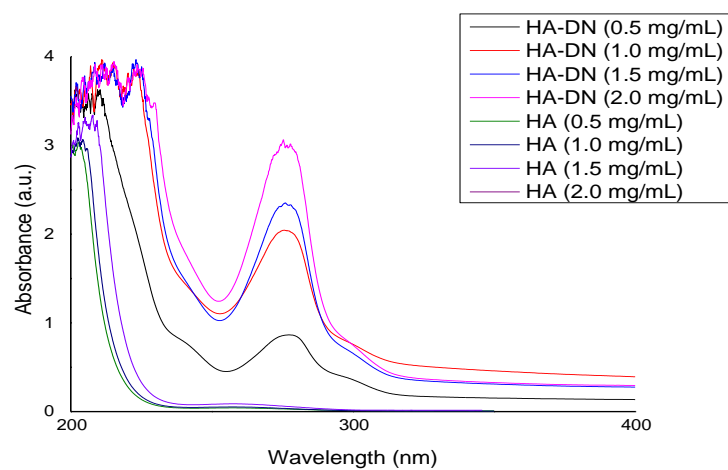
In order to understand if the modification of hyaluronic acid (HA) was correctly done, an UV-vis spectrophotometry was performed. Appendixes 2.1 to 2.3 show a peak at nearly 280 nm for HA-DN, whereas HA (control) does not present the same peak. According to the literature, HA-DN presents a characteristic band at 280 nm and nonappearance of peaks at 300 nm showed that catechol groups were not oxidized [1-4]. The degree of substitution was $21.77\% \pm 8.59\%$ ($n = 3$).



Appendix 2. 1 - Representative UV-vis spectra of HA (control) and HA-DN with different concentrations.

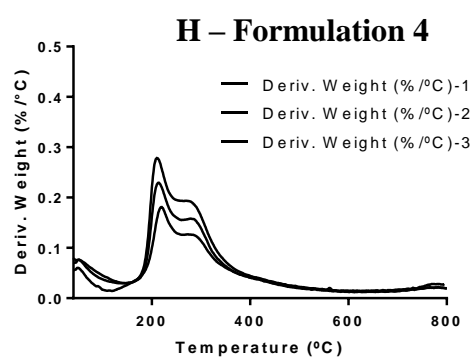
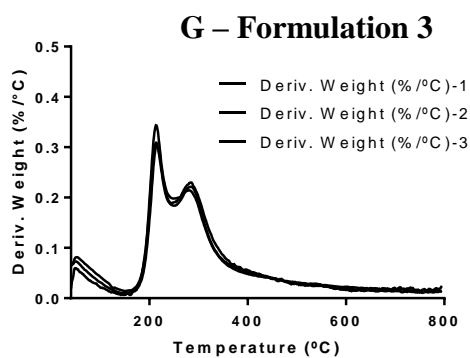
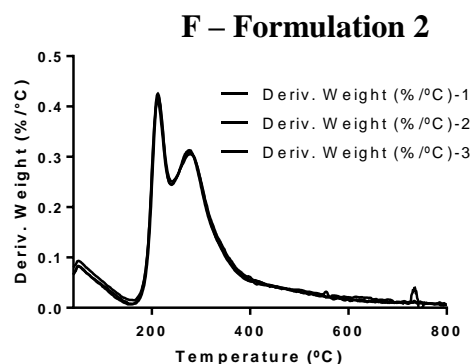
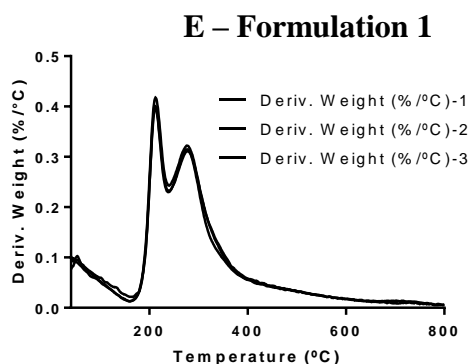
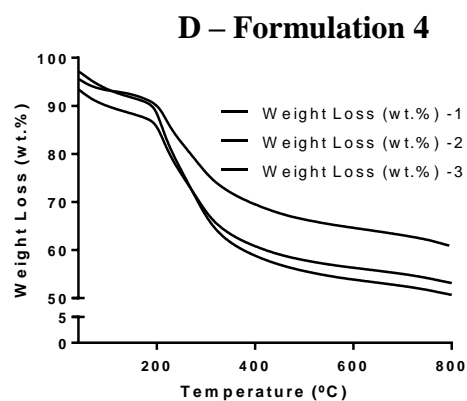
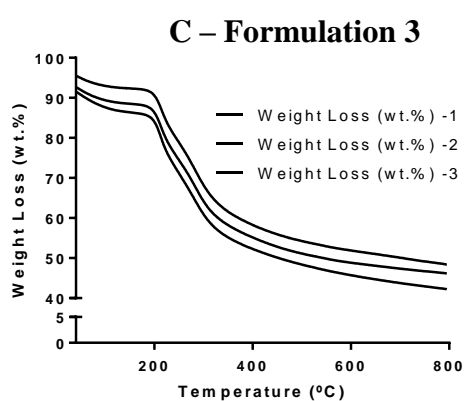
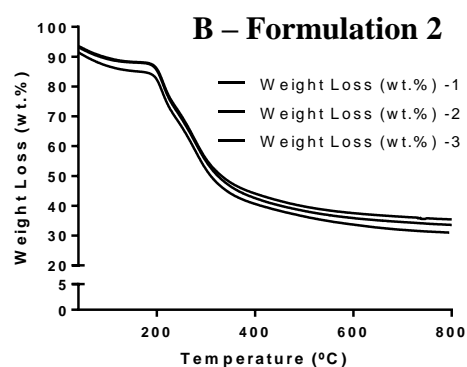
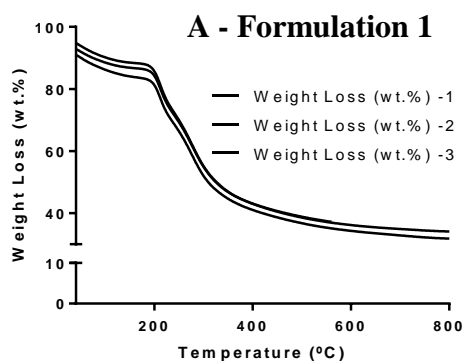


Appendix 2. 2 - UV-vis spectra of HA (control) and HA-DN solutions with different concentrations.



Appendix 2. 3 - UV-vis spectra of HA (control) and HA-DN solutions with different concentrations.

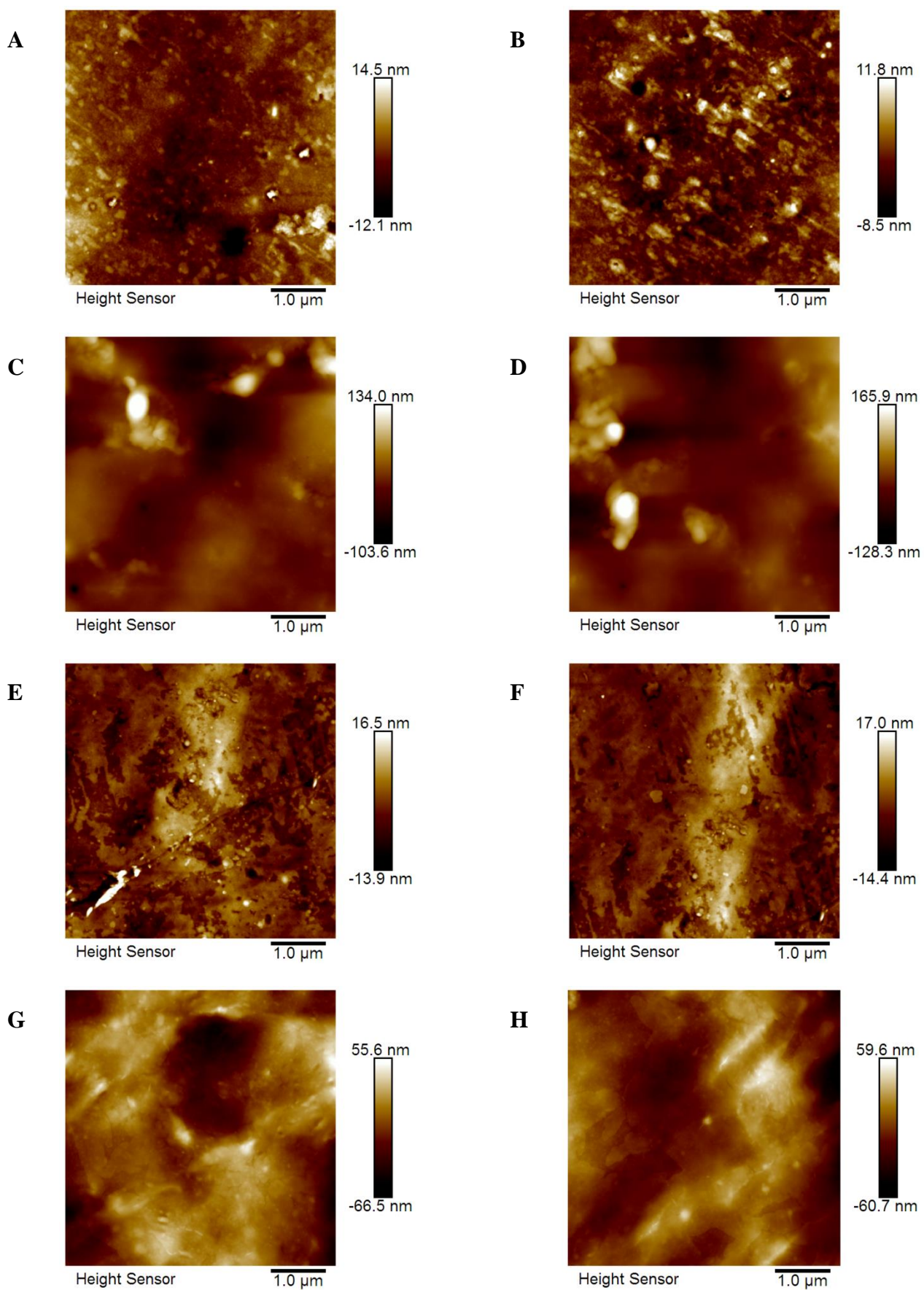
Appendix 3 - TGA results

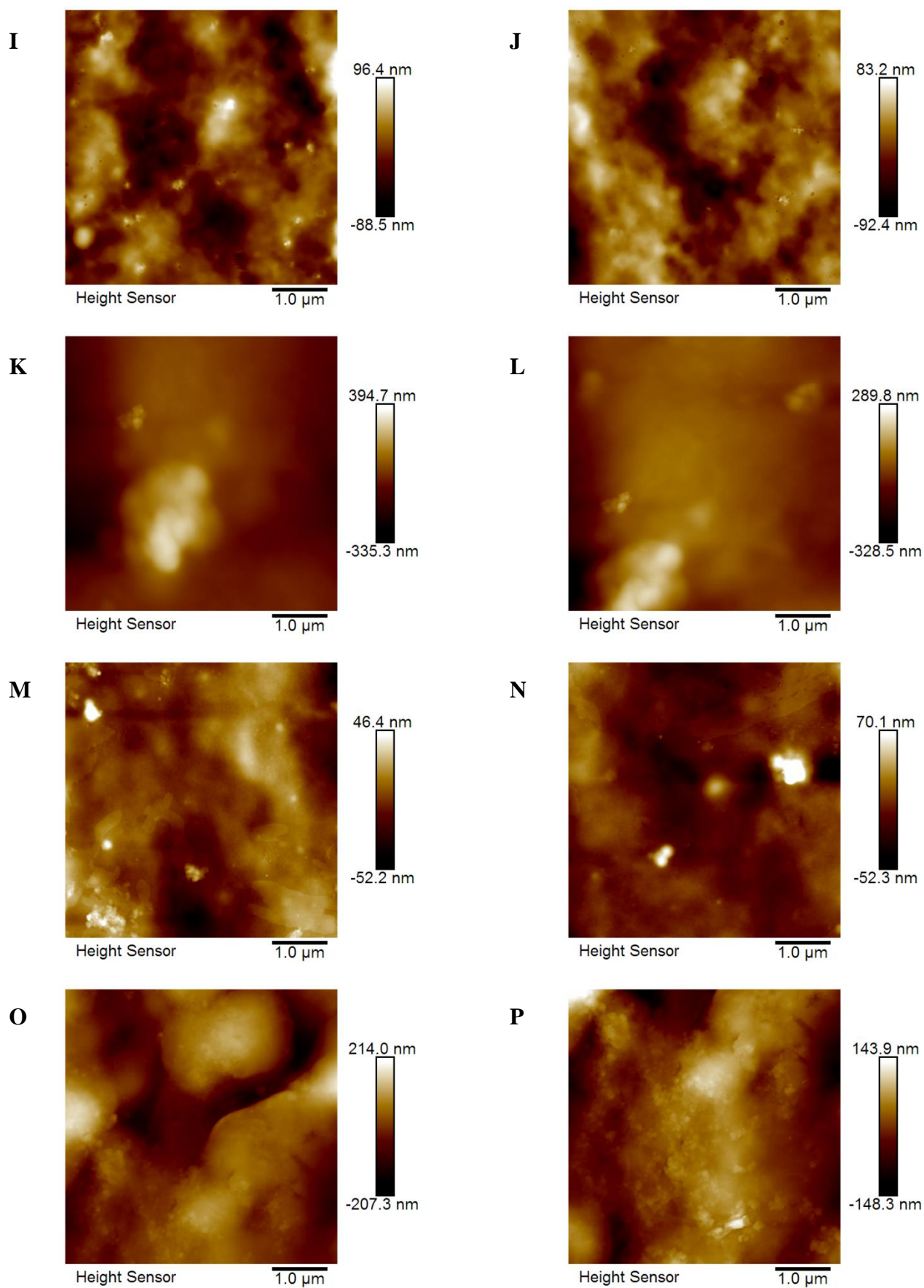


Appendix 3 - TGA results (n = 3). (A) Weight loss (wt.%) for Formulation 1-[CHT/HA/CHT/HA]₇₅, (B) Weight loss (wt.%) for Formulation 2-[CHT/HA-DN/CHT/HA-DN]₇₅, (C) Weight loss (wt.%) for Formulation 3: [CHT/HA/CHT/Ag-BG-NPs]₇₅ (%10 mol Ag), (D) Weight loss (wt.%) for Formulation 4: [CHT/HA-DN/CHT/Ag-BG-NPs]₇₅ (%10 mol Ag), (E) Deriv. Weight (%/°C) for Formulation 1-

[CHT/HA/CHT/HA]₇₅, **(F)** Deriv. Weight (%/°C) for Formulation 2-[CHT/HA-DN/CHT/HA-DN]₇₅, **(G)** Deriv. Weight (%/°C) for Formulation 3: [CHT/HA/CHT/Ag-BG-NPs]₇₅ (%10 mol Ag), **(H)** Deriv. Weight (%/°C) for Formulation 4: [CHT/HA-DN/CHT/Ag-BG-NPs]₇₅ (%10 mol Ag).

Appendix 4 - AFM results

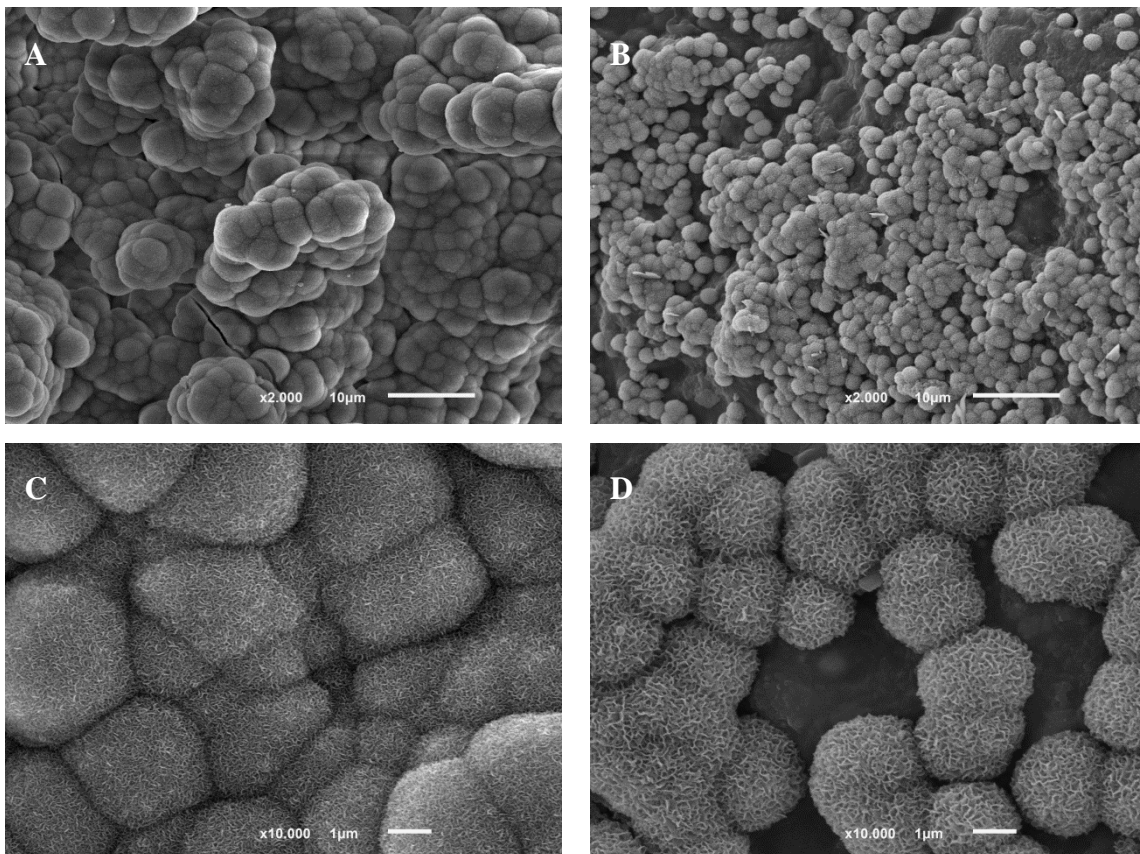




Appendix 4 - Atomic force microscopy (AFM) results: top and bottom 2D views (5 μm x 5 μm). The bar next to all images is the Z-scale (nm). (A) Formulation 1: [CHT/HA/CHT/HA]₇₅ (2D-image, bottom view);

(B) Formulation 1: [CHT/HA/CHT/HA]₇₅ (bottom view); (C) Formulation 1: [CHT/HA/CHT/HA]₇₅ (top view); (D) Formulation 1: [CHT/HA/CHT/HA]₇₅ (top view); (E) Formulation 2: [CHT/HA-DN/CHT/HA-DN]₇₅ (bottom view); (F) Formulation 2: [CHT/HA-DN/CHT/HA-DN]₇₅ (bottom view); (G) Formulation 2: [CHT/HA-DN/CHT/HA-DN]₇₅ (top view); (H) Formulation 2: [CHT/HA-DN/CHT/HA-DN]₇₅ (top view); (I) Formulation 3: [CHT/HA/CHT/Ag-BG-NPs]₇₅ (bottom view); (J) Formulation 3: [CHT/HA/CHT/Ag-BG-NPs]₇₅ (bottom view); (K) Formulation 3: [CHT/HA/CHT/Ag-BG-NPs]₇₅ (top view); (L) Formulation 3: [CHT/HA/CHT/Ag-BG-NPs]₇₅ (top view); (M) Formulation 4: [CHT/HA-DN/CHT/Ag-BG-NPs]₇₅ (bottom view); (N) Formulation 4: [CHT/HA-DN/CHT/Ag-BG-NPs]₇₅ (bottom view); (O) Formulation 4: [CHT/HA-DN/CHT/Ag-BG-NPs]₇₅ (top view); (P) Formulation 4: [CHT/HA-DN/CHT/Ag-BG-NPs]₇₅ (top view);

Appendix 5 - Analysis of the films morphology



Appendix 5 - Analysis of the free-standing films surfaces after immersion in SBF solution during 14 days. (A) Formulation 3: [CHT/HA/CHT/Ag-BG-NPs]₇₅ (mag. 2000 x); (B) Formulation 4: [CHT/HA-DN/CHT/Ag-BG-NPs]₇₅ (mag. 2000 x); (C) Formulation 3: [CHT/HA/CHT/Ag-BG-NPs]₇₅ (mag. 10 000 x) and (D) Formulation 4: [CHT/HA-DN/CHT/Ag-BG-NPs]₇₅ (mag. 10 000 x).

Appendix 6 – Optimization work

1.1. Native films

1.1.1. FT-IR analysis of the native LbL free-standing films

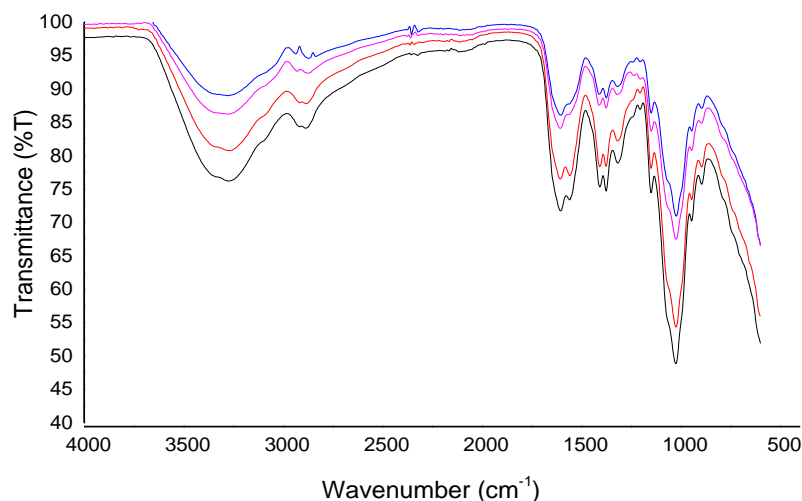


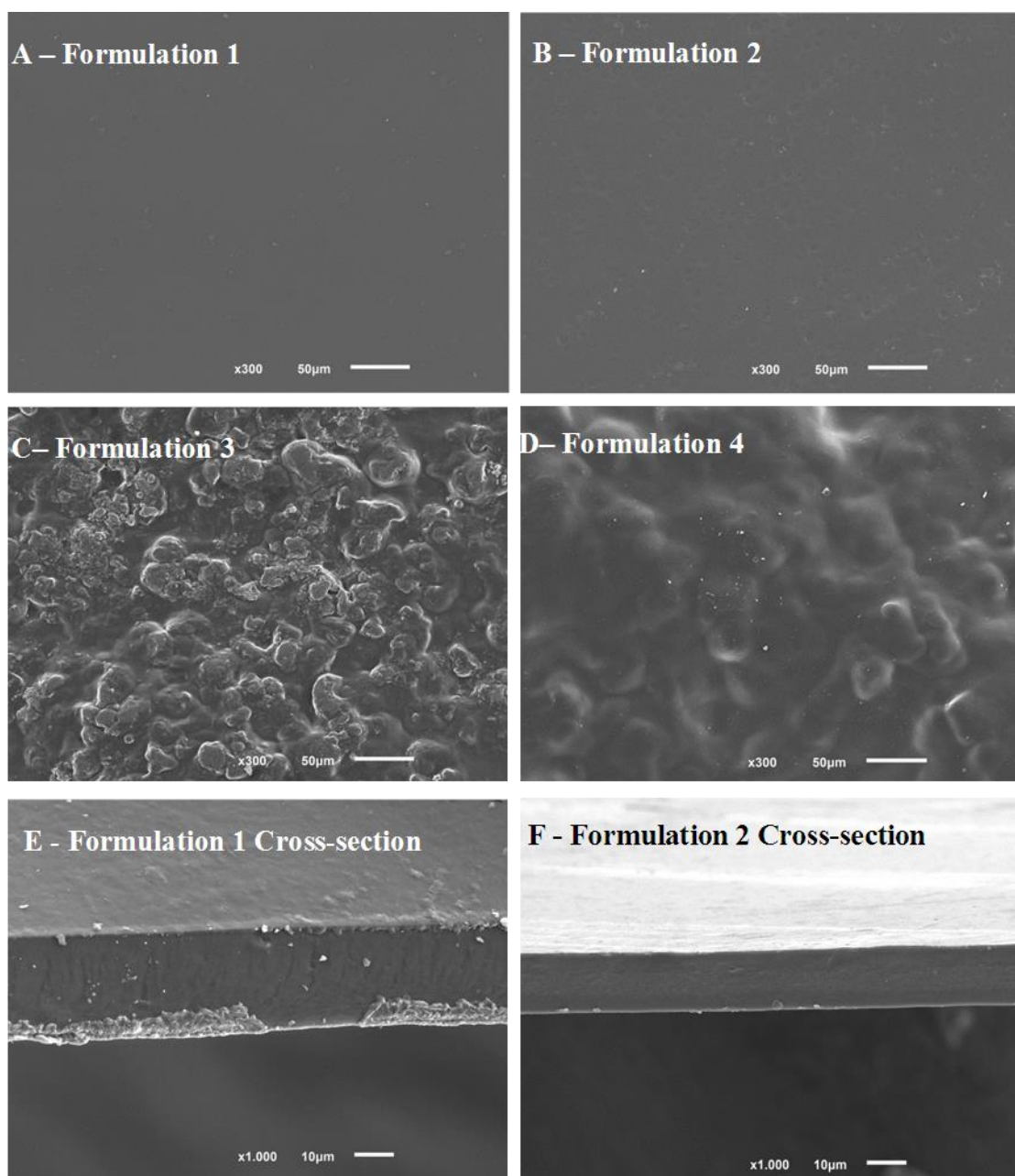
Figure 1.1 - FT-IR results of the native LbL free-standing films for all formulations. Formulation 1: [CHT/HA/CHT/HA]₇₅ (black curve); Formulation 2: [CHT/HA-DN/CHT/HA-DN]₇₅ (red curve); Formulation 3: [CHT/HA/CHT/Ag-BG-NPs]₇₅ (blue curve) and Formulation 4: [CHT/HA-DN/CHT/Ag-BG-NPs]₇₅ (purple curve).

According to Caridade and co-workers [5] and Duarte co-workers [6], the peak around 1000 cm^{-1} corresponds to polysaccharide peaks of chitosan (CHT) [5] and hyaluronic acid (HA), namely the peak at 1132 cm^{-1} , that correspond to C-O and C-O-C stretching [5]. The region between 1400 and 1500 cm^{-1} is due to the presence of amine II groups (O=C-N-H) present in chitosan, as can be corroborated by looking at Figure 1.1 in a range of 1392 and 1565 cm^{-1} , 1620 and 1660 cm^{-1} and around 1630 and 1700 cm^{-1} corresponding to C=O bands and amide I of chitosan [5, 6], respectively. With regard to the peaks between 2000 cm^{-1} and 2500 cm^{-1} it is due to the presence of CO₂. According to Hong and co-workers [2], the methylene group, around 2940 and 2920 cm^{-1} of hyaluronic acid (HA) and amide bonds, i.e., C=O stretching detectable in a range of 1700 and 1250 cm^{-1} . The peak on 1565 cm^{-1} corresponds to NH groups and the one on 1100 cm^{-1} corresponds to ethers groups (-C-O-C). Hydroxyls groups, -OH-, are detectable in a range of 2973 and 3700 cm^{-1} , and it is in accordance to Hong and co-workers [2] results (3350 and 3250 cm^{-1}). The results show that unmodified and modified spectras are very similar, however, and according to the same author, presence of amide and nitrogen groups corroborates the successful synthesis of HA-DN. In a range of 2900 cm^{-1} and 3700 cm^{-1} there is a

difference in transmittance in two curves. This difference can be explained by the presence of OH- groups in dopamine [2]. It's also possible to identify various vibrational modes of nanoparticles, namely O-H stretching vibration at 3326 cm^{-1} , Si-O-Si asymmetric stretching detectable in a range of $1200\text{-}1000\text{ cm}^{-1}$ [7-9].

1.1.2. Analysis of the native LbL free-standing films morphology

Figure 1.2 shows the SEM-EDS micrographs of all formulations, and, also their cross-section views.



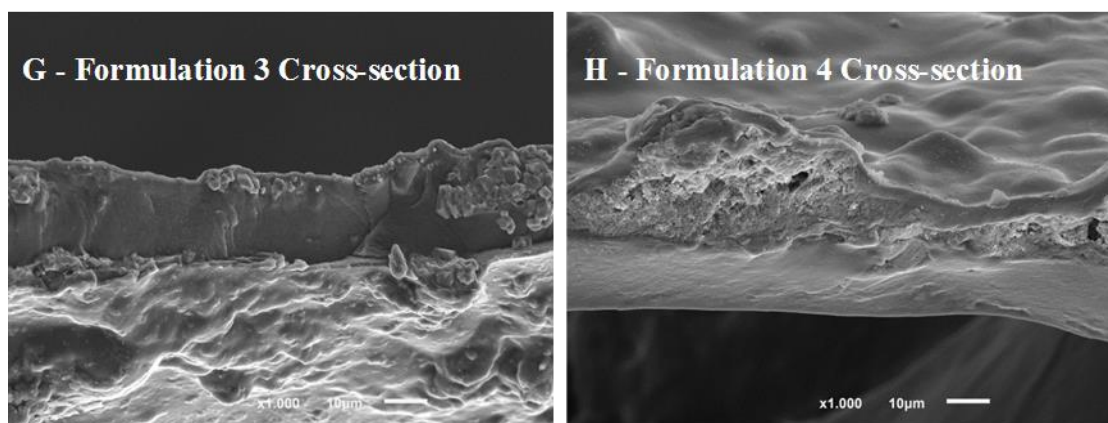


Figure 1. 2 - SEM-EDS micrographs of the native LbL free-standing films, top and cross-section views. (A) Formulation 1: [CHT/HA/CHT/HA]₇₅; (B) Formulation 2: [CHT/HA-DN/CHT/HA-DN]₇₅; (C) Formulation 3: [CHT/HA/CHT/Ag-BG-NPs]₇₅; (D) Formulation 4: [CHT/HA-DN/CHT/Ag-BG-NPs]₇₅; (E) Cross-section view of Formulation 1: [CHT/HA/CHT/HA]₇₅; (F) Cross-section view of Formulation 2: [CHT/HA-DN/CHT/HA-DN]₇₅; (G) Cross-section view of Formulation 3:[CHT/HA/CHT/Ag-BG-NPs]₇₅ and (H) Cross-section view of Formulation 4: [CHT/HA-DN/CHT/Ag-BG-NPs]₇₅.

Figures 1.2-A and B show the top view of [CHT/HA/CHT/HA]₇₅ and [CHT/HA-DN/CHT/HA-DN]₇₅, respectively. The micrographs showed that they have a uniform surface and no difference in morphology can be detected. In Figures 1.2-C, [CHT/HA/CHT/Ag-BG-NPs]₇₅, nanoparticles agglomerations on its surface, corroborating the adsorption of nanoparticles in the end-layer. The same thing happens to [CHT/HA /CHT/Ag-BG-NPs]₇₅ (present in Figure 1.2-D). Figures 1.2-E to H allows us to know the dry-thickness of the film, and it seems that the thickness of [CHT/HA/CHT/Ag-BG-NPs]₇₅ film is higher than [CHT/HA-DN/CHT/Ag-BG-NPs]₇₅ one. Although these images do not allow us to understand the nanostructure of the film layers, when the sample preparation took place it was put in liquid nitrogen (T = - 80°C). To be able to visualize this nanostructure, it would be necessary for a fragile break to occurred, but in this case it occurred a plastic deformation. Moreover, through analysis of Figures 1.2 - G and H we can corroborate that the incorporation of silver doped bioglass nanoparticles over the film took place.

1.2. Crosslinked LbL free-standing films with EDC and NHS

According to Zhou and co-workers [10], the nanoparticles incorporation in the composites structure results in lower stability, because there aren't sufficient entanglements between the adjacent layers. According to Alves, Picart and Mano [11], crosslinked films present better mechanical properties and are more rigid than uncrosslinked films. Moreover, the crosslinking process does not compromise their biodegradability. So, to improve their stability it is needed the incorporation of a crosslinking agent. Firstly, the crosslinker process with 1-(3-dimethylaminopropyl)-3-

ethylcarbodiimide (EDC) and N-hydroxysuccinimide (NHS) was tried as it is shown the following point. To avoid the degradation of films in ultra-pure water and phosphate buffered saline solution (PBS), i.e., to ensure their stability a crosslinking process was used. In order to do that, 1-(3-dimethylaminopropyl)-3-ethylcarbodiimide (EDC), with a concentration of 30 mg/mL of EDC and 11 mg/mL of NHS (is fix) (ratio EDC/NHS=2.(72)) was used. The crosslinking process is based on the reaction of primary amine groups with activated carboxylic sites [12]. The results showed that these films were stable in the osmotized water, but they cracked while going through the drying step. For that reason this concentration was eliminated. Also, another concentration of 50 mg/mL of EDC, and N-hydroxysuccinimide (NHS), with a concentration of 11 mg/mL (ratio EDC/NHS=4. (54)) was tried and the results of it are shown below.

1.2.1. FT-IR analysis of the crosslinked LbL free-standing films

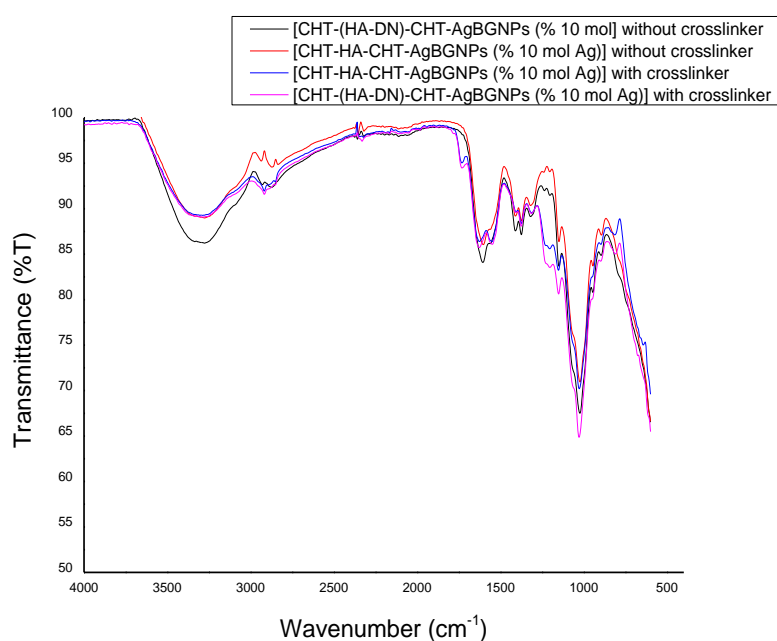


Figure 1. 3 - Comparison between the FT-IR results for formulation 3 and 4 crosslinked with 50 mg/mL EDC and 11 mg/mL of NHS and formulation 3 and 4 uncrosslinked (native LbL films).

According to Caridade and co-workers [5], Duarte co-workers [6] and Gorgieva and V. Kokol [13], the peak around 1000 cm^{-1} corresponds to polysaccharide peaks of chitosan (CHT) [5, 6, 13] and hyaluronic acid (HA), namely the peak at 1132 cm^{-1} , that correspond to C-O and C-O-C stretching [5]. The region between 1400 and 1500 cm^{-1} is due to the presence of amine II groups (O=C-N-H) present in chitosan, as can be corroborated by analyzing of Figure 1.3 in a range of 1392 and 1565 cm^{-1} , 1620 and 1660 cm^{-1} and around 1630 and 1700 cm^{-1} correspond to C=O bands and amide I of chitosan [5, 6], respectively. With regards to the peaks between 2000 cm^{-1} and 2500 cm^{-1} , they are due to the presence

of noise in the equipment (CO_2 presence). CHT also presents, and according to Gorgieva and co-worker [13], absorption of IR light around $3200\text{--}3500\text{ cm}^{-1}$ attributed to N-H stretching, and hyaluronic acid presents hydroxyls groups, -OH-, which are detectable in a range of 2973 and 3700 cm^{-1} , and this it is in accordance with Hong and co-workers [2] results (3350 and 3250 cm^{-1}). According to Hong and co-workers [2], the methylene group appears around 2940 and 2920 cm^{-1} of hyaluronic acid (HA) and amide bonds, i.e., C=O stretching detectable in a range of 1700 and 1250 cm^{-1} . The peak on 1560 cm^{-1} corresponds to NH groups and 1100 cm^{-1} corresponds to ethers groups (-C-O-C). According to the same author, the presence of amide and nitrogen groups corroborates the successful synthesis of HA-DN. In a range of 2900 cm^{-1} and 3700 cm^{-1} it's possible to verify that there is also a difference in the two curves. This difference can possibly be explained by the OH- groups present in dopamine. It's also possible also, to identify various vibrational modes of nanoparticles doped with silver, specifically O-H stretching vibration at 3326 cm^{-1} , Si-O-Si asymmetric stretching detectable in a range of $1200\text{--}1000\text{ cm}^{-1}$ [7-9]. Furthermore, the presence of crosslinking EDC and NHS, and according to Dahoumane co-workers [14], suggest an existence of two new bands centered at 1539 and 1650 cm^{-1} . These peaks, in the present results, appear in 1628 and 1547 cm^{-1} . According to the same author, they used in their work a concentration equal to ours (50 mM) of EDC, but the double of NHS, which implies a presence of more anhydride peaks at 1740 , 1780 and 1815 cm^{-1} . These peaks appear on this spectrum on 1732 cm^{-1} and 1781 , but not in 1815 cm^{-1} [14]. This spectrum shows very similar results between all spectra. However, and according to Dahoumane and co-workers [14], NHS and EDC existence implies an appearance of two new bands centered at 1539 and 1650 cm^{-1} . These peaks, in the present results, appear in 1628 and 1547 cm^{-1} . Moreover, anhydride peaks appears at 1740 , 1780 and 1815 cm^{-1} . These peaks appear on this spectrum on 1730 cm^{-1} and 1781 cm^{-1} , but not in 1815 cm^{-1} [14].

1.2.2. Analysis of the crosslinked LbL free-standing films morphology

In order to investigate differences in the surface morphology after crosslinking, the SEM was used, as it can be seen below (Figure 1.4).

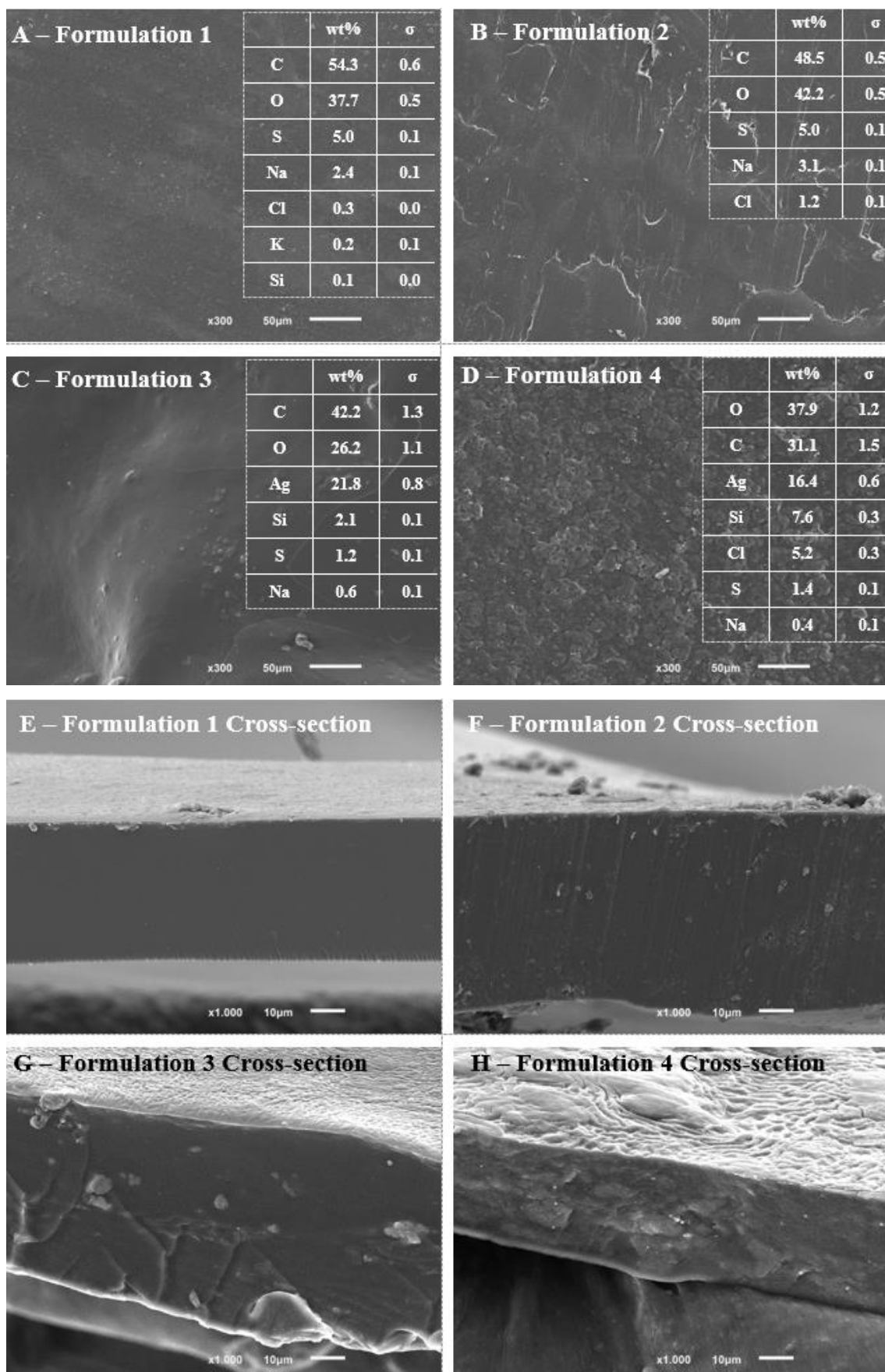


Figure 1. 4 - SEM-EDS micrographs of crosslinked LbL free-standing films (50 mg/mL EDC and 11 mg/mL of NHS). (A) Formulation 1: [CHT/HA/CHT/HA]₇₅ (top view), (B) Formulation 2: [CHT/HA-

DN/CHT/HA-DN]₇₅ (top view), (C) Formulation 3: [CHT/HA/CHT/Ag-BG-NPs]₇₅ with crosslinker (top view), (D) Formulation 4: [CHT/HA-DN/CHT/Ag-BG-NPs]₇₅ (top view), (E) Cross-section view of Formulation 1: [CHT/HA/CHT/HA]₇₅, (F) Cross-section view of Formulation 2: [CHT/HA-DN/CHT/HA-DN]₇₅, (G) Cross-section view of Formulation 3: [CHT/HA/CHT/Ag-BG-NPs]₇₅ and (H) Cross-section view of Formulation 4: [CHT/HA-DN/CHT/Ag-BG-NPs]₇₅.

Analyzing Figure 1.4 we can see in Figure 1.4-A ([CHT/HA/CHT/HA]₇₅) and in Figure 1.4-B ([CHT/HA-DN/CHT/HA-DN]₇₅) homogeneous surfaces. Comparing both micrographs with the micrographs of the samples without crosslinking process, it can be seen that no morphology changes can be detected. The EDS spectrum shows the presence of carbon (C) and oxygen (O) from the organic samples, but also the presence of sodium (Na), chlorine (Cl), which can be explained by the drying process of the free-standing films after production that led to salt precipitation. Regarding Figure 1.4-C ([CHT/HA/CHT/Ag-BG-NPs]₇₅) and D ([CHT/HA-DN/CHT/Ag-BG-NPs]₇₅) the successful adsorption of silver doped bioglass nanoparticles Ag-BG-NPs (% 10 mol Ag) in the top of film can be seen. The EDS spectrum is coherent with the micrographs, because it reveals the presence of silicon (Si) and silver (Ag). Note that on 1.4-C the percentage of silver was analyzed exclusively on point 1, whereas in Figure 1.4-D the analysis was done on all surface area. As far as the cross-sections micrographs are concerned, it can be seen in Figures 5.5-E to H the dry-thickness of films. In Figures 1.4-E and F we can see a homogeneous structure showing that chitosan (CHT), hyaluronic acid (HA) and hyaluronic acid dopamine conjugate (HA-DN) present a good compatibility. In Figures 1.4-G and H we can see the adsorption of silver doped bioglass nanoparticles through the film. These images do not allow us to understand the nanostructure of the films as it happened on the previous SEM micrographs (Figure 1.2).

Conclusions

Although the build-up of LbL free-standing films was correctly done, the films were not stable. For that reason, the crosslinking process with EDC and NHS was tried, but their concentration was very high which led the LbL films to crack. A different crosslinker was tried in order to ensure the stability of the films, namely genipin -see Chapter 5.

References

- [1] A. I. Neto et al., "Nanostructured Polymeric Coatings Based on Chitosan and Dopamine-Modified Hyaluronic Acid for Biomedical Applications," (in English), *Small*, Article vol. 10, no. 12, pp. 2459-2469, 2014.
- [2] S. Hong et al., "Hyaluronic Acid Catechol: A Biopolymer Exhibiting a pH-Dependent Adhesive or Cohesive Property for Human Neural Stem Cell

- Engineering," (in English), *Advanced Functional Materials*, Article vol. 23, no. 14, pp. 1774-1780, 2013.
- [3] J. X. Sun, C. Su, X. J. Zhang, W. J. Yin, J. Xu, and S. G. Yang, "Reversible Swelling-Shrinking Behavior of Hydrogen-Bonded Free-Standing Thin Film Stabilized by Catechol Reaction," (in English), *Langmuir*, Article vol. 31, no. 18, pp. 5147-5154, 2015.
- [4] M. E. Yu and T. J. Deming, "Synthetic polypeptide mimics of marine adhesives," (in English), *Macromolecules*, Article vol. 31, no. 15, pp. 4739-4745, 1998.
- [5] S. G. Caridade, C. Monge, F. Gilde, T. Boudou, J. F. Mano, and C. Picart, "Free-Standing Polyelectrolyte Membranes Made of Chitosan and Alginate," (in English), *Biomacromolecules*, Article vol. 14, no. 5, pp. 1653-1660, 2013.
- [6] M. L. Duarte, M. C. Ferreira, M. R. Marvao, and J. Rocha, "An optimised method to determine the degree of acetylation of chitin and chitosan by FTIR spectroscopy," (in English), *International Journal of Biological Macromolecules*, Article vol. 31, no. 1-3, pp. 1-8, 2002, Art. no. Pii s0141-8130(02)00039-9.
- [7] T. Srikumar et al., "Photostimulated optical effects and some related features of CuO mixed Li₂O-Nb₂O₅-ZrO₂-SiO₂ glass ceramics," *Ceramics International*, vol. 37, no. 7, pp. 2763-2779, 2011.
- [8] A. Vulpoi et al., "Bioactivity and protein attachment onto bioactive glasses containing silver nanoparticles," *Journal of Biomedical Materials Research Part A*, vol. 100A, no. 5, pp. 1179-1186, 2012.
- [9] Z. K. Hong et al., "Mono-dispersed bioactive glass nanospheres: Preparation and effects on biomechanics of mammalian cells," (in English), *Journal of Biomedical Materials Research Part A*, Article vol. 95A, no. 3, pp. 747-754, 2010.
- [10] Y. Zhou, M. J. Cheng, X. Q. Zhu, Y. J. Zhang, Q. An, and F. Shi, "A facile method for the construction of stable polymer-inorganic nanoparticle composite multilayers," (in English), *Journal of Materials Chemistry A*, Article vol. 1, no. 37, pp. 11329-11334, 2013.
- [11] N. M. Alves, C. Picart, and J. F. Mano, "Self Assembling and Crosslinking of Polyelectrolyte Multilayer Films of Chitosan and Alginate Studied by QCM and IR Spectroscopy," (in English), *Macromolecular Bioscience*, Article vol. 9, no. 8, pp. 776-785, 2009.
- [12] L. Richert et al., "Improvement of stability and cell adhesion properties of polyelectrolyte multilayer films by chemical cross-linking," *Biomacromolecules*, vol. 5, no. 2, pp. 284-294, 2004.
- [13] S. Gorgieva and V. Kokol, "Preparation, characterization, and in vitro enzymatic degradation of chitosan-gelatine hydrogel scaffolds as potential biomaterials," *Journal of Biomedical Materials Research Part A*, vol. 100A, no. 7, pp. 1655-1667, 2012.
- [14] S. A. Dahoumane, M. N. Nguyen, A. Thorel, J.-P. Boudou, M. M. Chehimi, and C. Mangeney, "Protein-Functionalized Hairy Diamond Nanoparticles," *Langmuir*, vol. 25, no. 17, pp. 9633-9638, 2009.